

# Spatio-temporal dynamic of soil organic matter in fire affected land using spectroscopy and remote sensing

---

Hrelja, Iva

Doctoral thesis / Disertacija

2024

Degree Grantor / Ustanova koja je dodijelila akademski / stručni stupanj: **University of Zagreb, Faculty of Agriculture / Sveučilište u Zagrebu, Agronomski fakultet**

Permanent link / Trajna poveznica: <https://um.nsk.hr/um:nbn:hr:204:449642>

Rights / Prava: [In copyright](#) / [Zaštićeno autorskim pravom.](#)

Download date / Datum preuzimanja: **2025-04-02**



Repository / Repozitorij:

[Repository Faculty of Agriculture University of Zagreb](#)





University of Zagreb

FACULTY OF AGRICULTURE

Iva Hrelja

**SPATIO-TEMPORAL DYNAMIC OF SOIL  
ORGANIC MATTER IN FIRE AFFECTED  
LAND USING SPECTROSCOPY AND  
REMOTE SENSING**

DOCTORAL THESIS

Zagreb, 2024



Sveučilište u Zagrebu

AGRONOMSKI FAKULTET

Iva Hrelja

**PROSTORNO-VREMENSKA DINAMIKA  
ORGANSKE TVARI TLA NA  
OPOŽARENOM ZEMLJIŠTU  
PRIMJENOM SPEKTROSKOPIJE I  
DALJINSKOG ISTRAŽIVANJA**

DOKTORSKI RAD

Zagreb, 2024



University of Zagreb

FACULTY OF AGRICULTURE

IVA HRELJA

**SPATIO-TEMPORAL DYNAMIC OF SOIL  
ORGANIC MATTER IN FIRE AFFECTED  
LAND USING SPECTROSCOPY AND  
REMOTE SENSING**

DOCTORAL THESIS

Supervisors:

Assoc. Prof. Ivana Šestak, PhD

Assoc. Prof. Igor Bogunović, PhD

Zagreb, 2024



Sveučilište u Zagrebu

AGRONOMSKI FAKULTET

Iva Hrelja

**PROSTORNO-VREMENSKA DINAMIKA  
ORGANSKE TVARI TLA NA  
OPOŽARENOM ZEMLJIŠTU  
PRIMJENOM SPEKTROSKOPIJE I  
DALJINSKOG ISTRAŽIVANJA**

DOKTORSKI RAD

Mentori:

izv. prof. dr. sc. Ivana Šestak

izv. prof. dr. sc. Igor Bogunović

Zagreb, 2024

Bibliographic data:

- Scientific field: Biotechnical sciences
- Scientific field: Agriculture (agronomy)
- Scientific branch: Ecology and environmental protection
- Institution: University of Zagreb Faculty of Agriculture, Department of General Agronomy
- Supervisors of the doctoral thesis: Assoc. prof. dr.sc. Ivana Šestak and Assoc. prof. dr.sc. Igor Bogunović
- Number of pages: 149 pages
- Number of figures: 47
- Number of tables: 17
- Number of appendixes: 1
- Number of references: 249
- Date of defence of the doctoral thesis: \_\_/\_\_/\_\_\_\_.
- Doctoral thesis defence committee:  
President: Prof. Ivica Kisić, Ph.D.  
Member: Prof. Renata Pernar, Ph.D.  
Member: Assoc. Prof. Monika Zovko, Ph.D.

The thesis is stored in:

National and University Library in Zagreb, Ulica Hrvatske bratske zajednice 4 p.p. 550, 10 000 Zagreb, Library of the University of Zagreb, Faculty of Agriculture, Svetošimunska cesta 25, 10 000 Zagreb.

The topic of the thesis was accepted at the session of the Faculty Council of the Faculty of Agriculture, University of Zagreb, held on March 3, 2020, and approved at the session of the Senate of the University of Zagreb, held on September 15, 2020.

UNIVERSITY OF ZAGREB  
FACULTY OF AGRICULTURE

**STATEMENT OF ORIGINALITY**

I, **Iva Hrelja**, declare that I wrote solely by myself the thesis titled:

**SPATIO-TEMPORAL DYNAMIC OF SOIL ORGANIC MATTER IN FIRE AFFECTED  
LAND USING SPECTROSCOPY AND REMOTE SENSING**

With my signature I guarantee:

- that I am the sole author of this thesis;
- this thesis is an original report of my research, and due references have been provided on all supporting literatures and resources;
- that I am familiar with the provisions of the Code of Ethics of the University of Zagreb (Article 19).

Zagreb,

\_\_\_\_\_  
Doctoral student's signature

Dissertation was evaluated by Committee for dissertation assessment in the following composition:

1. Ivica Kisić, Ph.D.

*Full Professor, Faculty of Agriculture, University of Zagreb*

2. Renata Pernar, Ph.D.

*Full Professor, Faculty of Forestry and Wood Technology, University of Zagreb*

3. Monika Zovko, Ph.D.

*Associate Professor, Faculty of Agriculture, University of Zagreb*

Dissertation is defended on Faculty of Agriculture University of Zagreb, before the Committee on \_\_\_ \_\_ \_\_\_ in the following composition:

1. Ivica Kisić, Ph.D., \_\_\_\_\_

*Full Professor, Faculty of Agriculture, University of Zagreb*

2. Renata Pernar, Ph.D., \_\_\_\_\_

*Full Professor, Faculty of Forestry and Wood Technology, University of Zagreb*

3. Monika Zovko, Ph.D., \_\_\_\_\_

*Associate Professor, Faculty of Agriculture, University of Zagreb*



## INFORMATION ON MENTORS

### **Assoc. Prof. Ivana Šestak, PhD**

Associate Professor Ivana Šestak, PhD was born on December 1, 1979. in Sisak, where she finished primary and secondary school. She graduated from the University of Zagreb, Faculty of Agriculture on 18.12.2003. Since 2004, she has been employed as an assistant at the Faculty of Agriculture, University of Zagreb, at the Department of General Agronomy. She defended her doctoral thesis entitled "Use of Field Spectroscopy for Assessment of Nitrogen Use Efficiency in Winter Wheat" on 07.12.2011. at the University of Zagreb, Faculty of Agriculture in the scientific field of biotechnical sciences, the field of agriculture, branch of crop production. Employment and work experience timeline includes: 2004 - 2011: teaching assistant; 2011 - 2012: senior research assistant; 2012 - 2020: assistant professor; 2020 - now: associate professor.

Research interests and scientific work are focused on agroecology, sustainable agriculture, proximal soil and plant spectroscopy, remote sensing in agriculture, precision farming, GIS and geostatistics, multivariate statistics. As an author or co-author she has published 61 research and professional papers, of which 18 papers are a1 category (WoS). Bibliography (CROSBI) is available on:

<https://www.bib.irb.hr/pregled/znanstvenici/263291>;

and Google Scholar <https://scholar.google.hr/citations?user=lfSani4AAAAJ&hl=hr>

(N. citations: 287; h index: 10). She received scientific training and research experience at the University of Hohenheim, Stuttgart, Germany (2005, "Spatial Data Analysis with GIS" - TEMPUS), at the Analytical Spectral Devices Inc., Boulder, Colorado, USA (2008, "Chemometrics & Instrumentation Training" - field spectroscopy with qualitative and quantitative spectral data analysis), and at the Department of Agricultural and Biosystems Engineering, Iowa State University (ISU), Ames, Iowa, USA (2008 and 2010, field remote sensing techniques in agriculture), while teaching experience was achieved at the Malta College of Arts, Science and Technology (MCAST) - Institute of Agribusiness, Valletta, Malta (2012, development of curriculum: „Sustainable Land Use“).

She is a coordinator of the undergraduate study program of Agroecology on the Faculty of Agriculture, University of Zagreb, and as a course coordinator or associate she is involved in teaching courses on undergraduate level (Agroclimatology, Agriculture and

Environment); graduate level (Global Ecology, Agroclimatology and Climate Change, Modelling the energy crops production), and postgraduate level (Spectroscopic and Analytical Methods in Agroecosystem Research).

She has participated in 35 scientific (HZZ-Croatian Science Foundation, Ministry of Science and Education), expert (Ministry of Agriculture, business sector, administrative bodies, BICRO, EKONERG) and teaching (Erasmus+ Cooperation partnerships in higher education, Cooperation for innovation and the exchange of good practices, European Social Fund) projects (<https://www.agr.unizg.hr/hr/member/126>). As an author or co-author, she participated in more than 50 national and international scientific conferences. She is a member of the Croatian Society of Soil Science (HTD) and the Croatian Agrometeorological Society (HAgMD).

### **Assoc. Prof. Igor Bogunović, PhD**

Dr. Igor Bogunović is an Associate professor at the Faculty of Agriculture in the University of Zagreb. He is actively engaged in scientific research work and participates in performing lectures on a Bs (General Agronomy, Basics of agriculture), Ms Modules (Fertilizers and Fertilization, Urban Agriculture) and postgraduate study (modules: Agriculture and Environment; Analysis of time series, spatial and spatial-temporal data). He is fully acquainted with the module's objectives, detailed content and learning outcomes, as he has lectures, seminars and exercises and has been very active in conducting professional projects, and final and graduate theses. He became PhD at the Faculty of Agriculture after only 3 years of employment with a three-year research. Since the beginning of work at the Faculty, he has been involved in numerous researches related to soil management practices, land degradation, soil compaction, soil tillage, soil and water conservation, soil physics, fertilization, precision agriculture, geostatistics and GIS.

He is currently associated with 3 international (“InBestSoil - Monetary valuation of soil ecosystem services and creation of initiatives to invest in soil health: setting a framework for the inclusion of soil health in business and in the policy making process”; from 2023 to 2026., Horizon2020, Grant agreement ID: 101091099; “SHARInG-MeD - Soil Health and Agriculture Resilience through an Integrated Geographical information systems of Mediterranean Drylands”; from 2023 to 2026; PRIMA, Grant agreement ID: 2211; “Firelinks CA18135 - Fire in the Earth System: Science & Society”, from 2019. to 2023., WG and MC member; and 3 national Projects (Soil erosion and degradation in Croatia, project leader; Purchaser: Croatian Science Foundation, from 2018-2023); Can we save burned land? (Duration 2019 - 2021, project leader, purchaser: Adris Foundation); Impact of wildfires on soil and water quality, associate; purchaser: Croatian Science Foundation, from 2019-

2022). Until today, he published as an author or co-author of more than 200 papers, expertise and technical reports. A list of publications can be found in the Croatian Scientific Bibliography.

He has been on scientific visits and training at BOKU Vienna, Austria; University of Valencia, Valencia, Spain; and University of Durham, Durham, England where he gained knowledge about land use, degradation processes, and modified climate conditions. He is a member of the Croatian Society of Soil Science; Croatian Agrometeorological Society; Croatian Soil Tillage Research Organization; International Soil Tillage Research Organization; European Society for Soil Conservation; and the European Geoscience Union.

He is the author and editor of the book "Sustainable soil management measures in organic agriculture for climate conditions of Mediterranean Croatia" and 2 books by Springer: "Impact of Agriculture on Soil Degradation I - A European Perspective" and "Impact of Agriculture on Soil Degradation II - Perspectives from Africa, Asia, America and Oceania". He is the author of the 10 book chapters. During 2023, he mentored four doctoral students at the University of Zagreb, Faculty of Agriculture, while 1 PhD finished his dissertation under his supervision.

He is an Editorial board member of the Geography and Sustainability Journal by Elsevier Publishing House, Agriculture Journal by MDPI, and Columella - Journal of Agricultural and Environmental Sciences. He was a member of the organizing committee in several conferences. He received a National Science Award - Annual Award for Junior Researchers in 2017 and an award Mihovil Gračanin of the Croatian Soil Science Society in 2018. Faculty of Agriculture awarded him in 2020 with a medal to employees for exceptional contribution to scientific research, teaching, and professional activities, and in 2019 by award of the employees for exemplary work and special valuable contribution to the age of 35.

## ABSTRACT

Wildfires of low intensity and severity are part of the natural dynamics of the Mediterranean ecosystem. However, the recorded severe wildfires caused by anthropogenic influences and climate change have negative, often long lasting, effects on the environment and, in particular, on soils. Organic matter is an integral part of the soil and one of the most important indicators of soil quality. The changes in soils after a low-severity wildfire are often ephemeral and include decreased microbial respiration and enzyme activity, as well as the increase of soil pH and soil organic matter (SOM) content. High severity wildfires lead to soil degradation, such as volatilization of soil carbon (C), nitrogen (N), phosphorous (P) and sulphur (S) - the most vital soil nutrients. However, due to the heterogenous molecular nature of SOM it is difficult to draw straightforward conclusions regarding its post-fire dynamic and recovery in different environmental conditions.

The main purpose of the research was to apply soil spectroscopy, remote sensing and geostatistic methods in the pedological and climatic conditions of Mediterranean Croatia to test and develop an advanced, cost-effective and applicable methodology for monitoring of post-fire effects on SOM. The study was conducted in Zadar county, Croatia (44° 05' N; 15° 22' E; 72 m a.s.l.), on approximately 13.5 ha of wildfire affected mixed forest of *Quercus pubescens* Willd. and *Juniperus communis* L. The severity of the wildfire was medium to high, and the soil type was determined as chromic Cambisol. Soil samples were georeferenced which allowed for periodic soil sampling at the same microsite every 3 months. A total of 1080 samples were taken during the 2-year study period. Linear (PLSR) and non-linear (ANN) SOM prediction models based on spectral reflectance were developed and compared. Furthermore, geostatistical mapping of SOM was performed using two different interpolation methods. For univariate interpolation, ordinary kriging (OK) was used, and for multivariate interpolation, ordinary cokriging (OCK) was used. The covariates for OCK were soil pH, electrical conductivity (EC), and CaCO<sub>3</sub> content.

The results showed that high severity (HS) areas had a 35 to 48% increase in average SOM content, while medium severity (MS) areas did not record a significant change compared to unburned (C) areas. Spectral reflectance analysis indicated that soil reflectance is greatly influenced by changes in SOM content caused by different wildfire severities. Specifically, HS samples had the highest average SOM content, and therefore lowest average reflectance throughout the study period, whereas C areas had the lowest average SOM content causing highest average reflectance. The greatest spectral differences between C, MS and HS were found in green/yellow to red (500-700 nm) region, which indicates this region carries the majority of information on SOM that could be useful in developing universal models for estimating SOM in soils affected by wildfires.

ANN models generally proved to be superior to PLSR models (PLSR RPD = 1.35 to 2.29; ANN RPD = 1.74 to >2.5), thus confirming previous results that learning non-linear ANN algorithms are able to correlate complex spectral information with the target variable (SOM content), especially in the conditions of complex post-fire SOM dynamics.

Promising results were achieved in using ANN models and remotely sensed, multispectral data provided by ESA Sentinel-2 satellite sensors (Sentinel-2 ANN RPD = 1.48). In the future, freely available Sentinel-2 data could significantly reduce operational costs of future research. By comparing the accuracy and precision of univariate (OK) with multivariate spatial models (OCK), the results showed that univariate spatial models show lower spatial dependency than multivariate ones, which was assessed by interpreting nugget/sill ratio of the calculated experimental variograms (OK<sub>nugget/sill</sub>=10-74%, OCK<sub>nugget/sill</sub>=0.002-37%). Results obtained from this research provided the basis for understanding post-fire soil processes and the direction of SOM recovery and present the first step towards creation of a soil spectral database that will enhance post-fire soil survey in Mediterranean conditions.

**Key words:** spectroscopy, remote sensing, wildfire, soil reflectance, soil recovery, neural networks, linear modelling, non linear modelling, soil mapping, Sentinel-2

# Prostorno-vremenska dinamika organske tvari tla na opožarenom zemljištu primjenom spektroskopije i daljinskog istraživanja

Požari niskog intenziteta dio su prirodne dinamike mediteranskog ekosustava. Međutim, jaki požari uzrokovani antropogenim utjecajima i klimatskim promjenama imaju negativne, često dugotrajne učinke na okoliš, a posebice na tla. Organska tvar je sastavni dio i jedan od najvažnijih pokazatelja kakvoće tla. Promjene u tlu nakon požara manje jačine često su kratkotrajne i uključuju smanjenu mikrobiološku i enzimatsku aktivnost, kao i povećanje pH tla i sadržaja organske tvari (eng. SOM) u tlu. Jaki požari dovode do degradacije tla, kao što je volatilizacija ugljika (C), dušika (N), fosfora (P) i sumpora (S) - najvažnijih hranjivih tvari u tlu. Međutim, zbog heterogene molekularne prirode SOM teško je izvući jednostavne zaključke o njevoj dinamici nakon požara i oporavku u različitim okolišnim uvjetima. S obzirom na navedeno, iznimno je važno kontinuirano pratiti i stjecati nova saznanja o promjenama nakon požara, posebice u slučaju kvalitete tla, kako bi se prilagodili promjenjivim uvjetima okoliša i razvili održive prakse gospodarenja koje će ublažiti degradaciju tla. Praćenje i modeliranje oporavka okoliša na prirodne katastrofe omogućuje nam temeljitu analizu njihovih kratkoročnih, ali i dugoročnih posljedica.

Daljinska istraživanja u tloznanstvu relativno su novo područje istraživanja s velikim potencijalom za praćenje i kartiranje velikih površina. Daljinsko istraživanje tla može se provoditi sa zemlje, zraka ili svemira. Zemaljska daljinska istraživanja obično se provode pomoću ručnih senzora ili senzora montiranih na vozilo. Daljinska istraživanja iz zraka provode se sensorima montiranim u zrakoplovu. Daljinska istraživanja iz svemira provode se pomoću satelitskih senzora. Posljednjih godina ispituje se potencijal multispektralnih i hiperspektralnih podataka dobivenih putem satelitskih senzora (npr. Sentinel-2, Hyperion) i terenske spektroskopije u istraživanju tla, monitoringu i kartiranju, a podaci dobiveni takvim sensorima pružaju nam mogućnost analize, točnog predviđanja, klasificiranja i mapiranja različitih svojstava tla velikih područja korištenjem geostatističkih metoda. Kartiranje putem daljinskih istraživanja ključno je za razumijevanje prostorno-vremenske dinamike svojstava tla nakon požara. Do sada u pedološkim i klimatskim uvjetima Sredozemne Hrvatske nije provedeno praćenje prostorno-vremenskih promjena kvalitete tla nakon požara.

Glavna svrha ovog istraživanja je primjena spektroskopije tla, daljinskog istraživanja i geostatističkih metoda u pedološkim i klimatskim uvjetima Sredozemne Hrvatske za ispitivanje i razvoj napredne, isplative i primjenjive metodologije za praćenje učinaka požara na SOM tla. Glavni ciljevi istraživanja su: a) pratiti vremenski i prostorni raspored sadržaja organske tvari u tlu nakon požara, b) odrediti odnos spektralne refleksije i sadržaja organske tvari u tlu pomoću linearnih i nelinearnih kalibracijskih modela, c) usporediti točnost i preciznost hiperspektralnih modela predviđanja SOM usporedbom analitičkih i in-situ mjerenja te satelitskih slika i d) usporediti točnost i preciznost univarijatnih s multivarijatnim prostornim modelima.

Istraživanje je provedeno u Zadarskoj županiji (44° 05' N; 15° 22' E; 72 m n.v.) na približno 13,5 ha požarom zahvaćene mješovite šume *Quercus pubescens* Willd. i *Juniperus communis* L. Jačina požara bila je srednja do jaka, a tip tla utvrđen je kao smeđe na dolomitu i vapnencu (ili chromic Cambisol prema klasifikaciji WRB, 2015). Uzorci tla georeferencirani su što je omogućilo periodično uzorkovanje tla na istoj mikrolokaciji svaka 3 mjeseca. Tijekom dvogodišnjeg razdoblja istraživanja uzeto je ukupno 1080 uzoraka tla. Razvijeni su i uspoređeni linearni (parcijalna regresija najmanjih kvadrata - PLSR) i nelinearni (neuralne mreže - ANN) modeli predviđanja SOM temeljeni na podacima spektralne refleksije. Spektralni podaci dobiveni su putem spektroskopije tla i iz satelitskih snimaka preuzetih neposredno nakon požara. Nadalje, geostatičko kartiranje SOM provedeno je pomoću dvije različite metode interpolacije. Za univarijatnu interpolaciju korišten je obični kriging (OK), a za multivarijatnu interpolaciju korišten je obični kokriging (OCK). Kovarijable za OCK bile su pH tla, elektrovodljivost (EC) i sadržaj  $\text{CaCO}_3$ .

Rezultati su pokazali da je šumski požar visoke jačine (HS) uzrokovao povećanje prosječnog sadržaja SOM od 35 do 48%, dok požar srednje jačine (MS) nije uzrokovao značajnu promjenu u usporedbi s neizgorenim (C) područjima. Analiza spektralne refleksije pokazala je da na refleksiju tla uvelike utječu promjene u sadržaju SOM uzrokovane različitim jačinama požara. Konkretno, uzorci HS imali su najviši prosječni sadržaj SOM, a time i najmanju prosječnu refleksiju tijekom cijelog razdoblja istraživanja, dok su C uzorci imali najniži prosječni sadržaj SOM što je uzrokovalo najveću prosječnu refleksiju. Najveće spektralne razlike između C, MS i HS zabilježene su u zeleno/žutom do crvenom (500-700 nm) elektromagnetskom valnom području, što ukazuje da ovo područje nosi većinu informacija o SOM koje bi mogle biti korisne u razvoju univerzalnih modela za procjenu SOM u na opožarenim zemljištima.

ANN modeli pokazali su se općenito uspješnijima od PLSR modela (PLSR RPD = 1,35 do 2,29; ANN RPD = 1,74 do >2,5), čime se potvrđuju prethodni rezultati da učeći nelinearni ANN algoritmi mogu korelirati složene spektralne informacije s ciljnom varijablom (sadržaj SOM), posebno u uvjetima složene dinamike SOM nakon požara.

Obećavajući rezultati postignuti su upotrebom ANN modela i daljinski očitanih multispektralnih podataka proizašlih iz obrade satelitskih slika (Sentinel-2 ANN RPD = 1,48). Besplatno dostupni podaci Sentinela-2 mogli bi značajno smanjiti operativne troškove budućih istraživanja. Usporedbom točnosti i preciznosti univarijatnih (OK) s multivarijatnim prostornim modelima (OCK), rezultati su pokazali da univarijatni prostorni modeli pokazuju manju prostornu povezanost od multivarijatnih, što je procijenjeno interpretacijom omjera nugget/sill izračunatih eksperimentalnim variogramima ( $OK_{\text{nugget/sill}} = 10\text{-}74\%$ ,  $OCK_{\text{nugget/sill}} = 0,002\text{-}37\%$ ).

Rezultati dobiveni ovim istraživanjem dali su osnovu za razumijevanje procesa u tlu nakon požara i smjera oporavka organske tvari u tlu, te predstavljaju prvi korak prema stvaranju spektralne baze podataka tla koja će poboljšati istraživanje tla nakon požara u mediteranskim uvjetima.

**Ključne riječi:** spektroskopija, daljinska istraživanja, šumski požar, refleksija tla, obnavljanje tla, neuronske mreže, linearno modeliranje, nelinearno modeliranje, kartiranje tla, Sentinel-2

## CONTENTS

<b>1.INTRODUCTION</b> .....	<b>1</b>
1.1. Hypothesis and objectives of research .....	4
<b>2.BACKGROUND</b> .....	<b>5</b>
2.1. Wildfire impacts on soil organic matter (SOM).....	5
2.1.1. Impact of wildfire severity on SOM .....	5
2.1.2. Impact of vegetation species on SOM .....	9
2.1.3. Impact of time-after-fire on SOM.....	10
2.2. Wildfire impacts on soil chemical properties .....	11
2.2.1. Impact of wildfire severity and time-after-fire on soil pH, EC, and CaCO <sub>3</sub> ..	11
2.2.2. Impact of vegetation species on soil pH, EC, and CaCO <sub>3</sub> .....	12
2.3. Spectroscopy and remote sensing techniques for soil monitoring in post-fire period.....	14
2.3.1. Basic principles of soil spectroscopy .....	14
2.3.2. Soil spectroscopy for SOM research in post-fire period .....	16
2.3.3. Effect of soil moisture on predictive SOM modelling .....	18
2.3.4. The potential of remote sensing in research of post-fire SOM .....	19
2.4. Geostatistical methods of SOM monitoring.....	22
<b>3. MATERIALS AND METHODS</b> .....	<b>26</b>
3.1. Location and climate conditions .....	26
3.2. Experimental design.....	27
3.3. Laboratory analysis .....	31
3.3.1. Chemical and physical analysis .....	31
3.3.2. Measurement of soil reflectance .....	31
3.4. Satellite imagery acquisition and processing .....	32
3.5. Statistical analysis and predictive modelling.....	35
3.5.1. Descriptive statistics and variability of soil properties after the wildfire.....	35
3.5.2. Spectral data analysis and model development.....	35
3.6. Geostatistical univariate and multivariate modelling and mapping .....	39
<b>4. RESULTS</b> .....	<b>40</b>
4.1. Meteorological observations.....	40
4.2. Field observations of post-fire vegetation recovery and visual soil status report ..	43
4.3. Soil organic matter content after the wildfire .....	47
4.4. Other soil properties after the wildfire .....	54
4.5. Description of soil spectral data.....	63
4.6. Linear (PLSR) and non-linear (ANN) modelling of post-fire SOM .....	75
4.6.1. Comparison of PLSR and ANN models .....	75
4.6.2. Comparison of models obtained from in-situ and laboratory reflectance measurements .....	89
4.6.3. Comparison of models obtained from laboratory (hyperspectral) and satellite (multispectral) reflectance measurements .....	93
4.7. Geostatistical univariate and multivariate modelling and mapping of SOM .....	97
<b>5. DISCUSSION</b> .....	<b>105</b>
5.1. Soil organic matter content after the wildfire.....	105
5.2. Other soil properties .....	108

5.3. Wildfire influence on soil reflectance .....	110
5.4. Linear (PLSR) and non-linear (ANN) modelling of post-fire SOM .....	112
5.4.1. PLSR vs. ANN models .....	112
5.4.2. In-situ vs. laboratory reflectance measurements.....	114
5.4.3. Hyperspectral vs. multispectral reflectance measurements .....	115
5.5. Geostatistical univariate and multivariate modelling and mapping .....	117
<b>6. CONCLUSIONS .....</b>	<b>121</b>
<b>7. REFERENCES .....</b>	<b>123</b>
<b>CURRICULUM VITAE .....</b>	<b>145</b>
<b>8. APPENDIX .....</b>	<b>148</b>



**List of abbreviations:**

**ANN** – Artificial neural networks

**ANOVA** – Analysis of variance

**ASD** – **Advanced systems development Inc.**

**CA** – Correlation analysis

**EC** – Electrical conductivity

**EM** – Electromagnetic

**ESA** – European space agency

**MAF** – Months after fire

**PC/PCs** – Principal components

**PCA** – Principal component analysis

**PLSR** - Partial least square regression

**r** – Correlation coefficient

**R<sup>2</sup>** – Coefficient of determination

**RMSEC** – Root mean square error of calibration

**RMSEP** – Root mean square error of prediction

**RPD** – Ratio of performance to deviation

**RS** – Remote sensing

**SOM** – soil organic matter

**SWIR** – Short-wave infrared

**VIS-NIR** – Visible – near infrared (spectroscopy)

**$\lambda$**  – Wavelength

**$n\lambda$**  – refractive index

**List of tables:**

Table 2.1. Summary of recent research displaying the discrepancy of wildfire impact on C content

Table 3.1. General soil properties (0-10 cm) of the study area

Table 3.2. Summary of the sampling campaign with corresponding dates

Table 3.3. Summary of the analytical laboratory methods used in the study

Table 3.4. Information on Sentinel-2 wavelengths and bandwidths (Source: <https://sentinel.esa.int>)

Table 3.5. Summary description of the multispectral bands used in the study

Table 3.6. Classification system for model accuracy assessment determined by RPD value

Table 4.1. Meteorological data in the studied years and their deviation from the 30-year average

Table 4.2. Descriptive statistics of SOM content (%) for nine sampling times, three wildfire severity levels and two vegetation types

Table 4.3. Results of the factorial ANOVA and the mean values for the content of the SOM depending on the severity of the wildfire, time, vegetation and their interactions

Table 4.4. Descriptive statistics of soil pH, EC and CaCO<sub>3</sub> content for nine sampling times, three wildfire severity levels and two vegetation types

Table 4.5. Factorial ANOVA results and mean values for soil pH, EC and CaCO<sub>3</sub> content according to fire severity, time, vegetation, and their interactions

Table 4.6. PLSR and ANN Model performance at each individual sampling period as well as the entire reflectance dataset

Table 4.7. Average moisture (%) of the soil samples taken 3 and 15 months after the wildfire

Table 4.8. Model performance of laboratory (air dry) and in situ (field moist) spectroscopy

Table 4.9. Model performance of laboratory and Sentinel-2 reflectance data

Table 4.10. Model parameters fitted for semivariogram of SOM and cross-semivariograms between SOM and selected covariables

## List of figures:

Figure 2.1. Electromagnetic (EM) spectrum and approximate visible colour ranges in nanometers (nm). Adapted according to: Bruno and Svoronos (2005) and National Institute of Standards and Technology (<https://www.nist.gov>)

Figure 2.2. Typical spectral response characteristics of soil, water and vegetation; source: National Institute of Standards and Technology (downloaded from: <https://www.nist.gov>; 05.09.2022.)

Figure 2.3. Soil reflectance curves as a function of water content, (a) 5%, (b) 20%, and (c) 40% water content. Adapted according to: Ben-dor et al., 2008b and Stoner and Baumgardner, 1981

Figure 2.4. The difference between multispectral and hyperspectral sensors; source: GISGeography (downloaded from: <https://gisgeography.com>; 11.11.2022)

Figure 2.5. Semivariogram example. Adapted according to: Biswas and Cheng, 2013

Figure 3.1. Meteorological data of the study location based on the 30-year average.

Source: Zaninović et al., 2008

Figure 3.2. Sample division according to wildfire severity and vegetation type. A total of 120 samples were divided equally into control samples (C) and two wildfire categories: medium severity (MS) and high severity (HS). Each of the three severity categories was further subdivided into samples collected under *Quercus pubescens* Willd (Q) and *Juniperus communis* L. (J)

Figure 3.3. Study area and experimental design. Different shapes denote vegetation species (circles indicate samples under *Quercus pubescens* Willd.; triangles indicate samples under *Juniperus communis* L.) and different colours denote wildfire severity (green - C; orange - MS; red - HS)

Figure 3.4. Soil samples collected at three-month intervals at 120 marked locations, each time at a different part of the marked circle within a radius of approximately 0.5 m from the marker

Figure 3.5. Wildfire affected land photographed on 22<sup>nd</sup> August 2019

Figure 3.6. Laboratory measurement of soil reflectance on air dried samples using FieldSpec®3 spectroradiometer

Figure 3.7. Sentinel-2 image and multispectral reflectance curves obtained from image pixels

Figure 3.8. Schematic overview of spectral modelling procedure for comparison of hyperspectral and multispectral datasets. The procedure is similar when building models to compare in-situ and laboratory datasets

Figure 4.1. Monthly precipitation and temperature during the studied years in comparison with the 30-year average (1971-2020). The arrows indicate the dates on which sampling campaigns were carried out. *Graph data source: Croatian Meteorological and Hydrological Service (DHMZ)*

Figure 4.2. Soil condition on 22<sup>nd</sup> August 2019 (0 MAF): a) control, b) medium severity (MS), c) high severity (HS)

Figure 4.3. Soil condition on 28<sup>th</sup> February 2020 (6 MAF): a) control, b) medium severity (MS), c) high severity (HS)

Figure 4.4. Soil condition on 28<sup>th</sup> May 2020 (9 MAF): a) control, b) medium severity (MS), c) high severity (HS)

Figure 4.5. Charred material on the surface of the HS sampling area photographed on: a) 28<sup>th</sup> February 2020 (6 MAF), and b) 03<sup>rd</sup> March 2021 (18 MAF)

Figure 4.6. Soil condition on 25<sup>th</sup> May 2021 (21 MAF): a) control, b) medium severity (MS), c) high severity (HS)

Figure 4.7. Soil condition on 26<sup>th</sup> August 2021 (24 MAF): a) control, b) medium severity (MS), c) high severity (HS)

Figure 4.8. Histogram and Q-Q plot for SOM data before and after transformation (N=535).

Figure 4.9. Mean SOM content (%) according to the interaction of the wildfire severity and time-since-fire factors. Different letters represent significant differences between wildfire severities on each sampling date ( $p < 0.05$ )

Figure 4.10. Mean SOM content (%) according to the interaction of the wildfire severity, time-since-fire and vegetation factors. Whiskers represent 95% confidence intervals. Different letters indicate significant ( $p < 0.05$ ) differences between wildfire severities on each given date

Figure 4.11. Histogram and Q-Q plot for soil EC data before and after transformation (N=535)

Figure 4.12. Histogram and Q-Q plot for soil pH and CaCO<sub>3</sub> data (N=535)

Figure 4.13. Mean soil pH values ( $-\log[H^+]$ ) according to the interaction of the wildfire severity, time-since-fire and vegetation factors. Whiskers represent 95% confidence intervals. Different letters indicate significant ( $p < 0.05$ ) differences between wildfire severities on each given date

Figure 4.14. Mean soil EC values ( $\mu\text{S}/\text{cm}$ ) according to the interaction of the wildfire severity, time-since-fire and vegetation factors. Whiskers represent 95% confidence intervals. Different letters indicate significant ( $p < 0.05$ ) differences between wildfire severities on each given date

Figure 4.15. Mean soil CaCO<sub>3</sub> content (%) according to the interaction of the wildfire severity, time-since-fire and vegetation factors. Whiskers represent 95% confidence

intervals. Different letters indicate significant ( $p < 0.05$ ) differences between wildfire severities on each given date

Figure 4.16. Average raw (a) and first derivative (b) reflectance for control, medium severity and high severity samples taken under *Juniperus c.* vegetation immediately post-fire on 22<sup>nd</sup> of August 2019 (N=42). Wavelengths are expressed in nm

Figure 4.17. Average raw (a) and first derivative (b) reflectance for control, medium severity and high severity samples taken under *Quercus p.* vegetation immediately post-fire on 22<sup>nd</sup> of August 2019 (N=78). Wavelengths are expressed in nm

Figure 4.18. Average raw (a) and first derivative (b) reflectance for control, medium severity and high severity samples taken under *Juniperus c.* vegetation two years post-fire on 26<sup>th</sup> of August 2021 (N=42). Wavelengths are expressed in nm

Figure 4.19. Average raw (a) and first derivative (b) reflectance for control, medium severity and high severity samples taken under *Quercus p.* vegetation two years post-fire on 26<sup>th</sup> of August 2021 (N=78). Wavelengths are expressed in nm

Figure 4.20. Average raw (a) and first derivative (b) reflectance for control samples taken under *Juniperus c.* vegetation during the study period. Wavelengths are expressed in nm

Figure 4.21. Average raw (a) and first derivative (b) reflectance for control samples taken under *Quercus p.* vegetation during the study period. Wavelengths are expressed in nm

Figure 4.22. Average raw (a) and first derivative (b) reflectance for medium severity samples taken under *Juniperus c.* vegetation during the study period. Wavelengths are expressed in nm

Figure 4.23. Average raw (a) and first derivative (b) reflectance for medium severity samples taken under *Quercus p.* vegetation during the study period. Wavelengths are expressed in nm

Figure 4.24. Average raw (a) and first derivative (b) reflectance for high severity samples taken under *Juniperus c.* vegetation during the study period. Wavelengths are expressed in nm

Figure 4.25. Average raw (a) and first derivative (b) reflectance for high severity samples taken under *Quercus p.* vegetation during the study period. Wavelengths are expressed in nm

Figure 4.26. Comparative view of hyperspectral (a) and multispectral (b) reflectance data (N=28). Points on the graph below mark ten respective Sentinel-2 bands used in the study

Figure 4.27. PLSR models obtained from raw reflectance acquired at each individual sampling period as well as the entire reflectance dataset showing relationship between calibration and validation dataset

Figure 4.28. Score plots of PLSR models for the first 2 PCs explaining the most variance. Scores further out the scatter plot are extreme observations measured mostly in HS samples

Figure 4.29. Variable importance projection for PLSR models calibrated at each sampling period to predict SOM content. Dark blue indicates statistically significant wavelengths (nm)

Figure 4.30. Results of the PLSR model showing relationship between predicted and observed SOM content (%) using a) laboratory and b) in-situ raw reflectance data

Figure 4.31. Results of the PLSR model showing relationship between predicted and observed SOM content (%) using a) laboratory hyperspectral and b) Sentinel-2 multispectral reflectance data (N=28)

Figure 4.32. Variable importance projection for PLSR models calibrated from the same dataset at 0 MAF but measured with proximal (ASD) and satellite (Sentinel-2) sensors to predict SOM content. Dark blue indicates statistically significant wavelengths (nm)

Figure 4.33. Correlation matrix of the measured soil properties

Figure 4.34. Post-fire SOM content maps for the 2-year study period (0-24 MAF). Different shapes denote vegetation species (circles indicate samples under *Quercus pubescens* Willd.; triangles indicate samples under *Juniperus communis* L.) and different colours denote wildfire severity (green - C; orange - MS; red - HS)

# 1.INTRODUCTION

Throughout Earth's history, wildfires have been a universal phenomenon and driving force for change in terrestrial ecosystems (Vukomanović and Steelman, 2019; Keeley et al., 2011). For millennia, most ecosystems have depended on the established fire regime, i.e. – the frequency and intensity of wildfire occurrence over a long period of time, to prevent excessive fuel accumulation, and decrease the likelihood of larger, more severe fires. Forest fires are known to provide many regulatory ecosystem services, such as creating long-term carbon sinks during post-fire regeneration (Yue et al., 2016), and regulating water in the ecosystem by reducing vegetational water consumption, consequently increasing the availability of groundwater (Pausas and Keeley, 2019; Boisramé et al., 2017; Schmerbeck and Fiener, 2015). Flora and fauna are known to have evolved in parallel with the occurrence of wildfires and to have adapted to or even depended on wildfires to complete their reproductive cycles (Heim et al., 2022; Jhariya and Raj, 2014; Paula and Pausas, 2006). Moreover, the nutrient rich ash produced by wildfires, once incorporated into the soil, promotes the regrowth of young plants that benefit from the open, sunny habitats created by wildfires (Pausas and Keeley, 2019; Pavlek et al., 2017). These benefits are primarily associated with low and moderate-severity wildfires, which are often part of the established fire regime.

However, increasing problems at the global level such as unsustainable land management (land-use change, wetland drainage, lack of forest management) and climate change (more frequent weather extremes, higher temperatures, longer droughts) are leading to an increase in catastrophic wildfires (Kisić et al., 2023; Ali et al., 2022; Turco et al., 2014). Mediterranean ecosystems are one of the most vulnerable areas and are subject to a range of mostly negative processes leading to temporary and/or permanent change (Cramer et al., 2018; Ruffault et al., 2016). Although fires of low intensity and severity are part of the natural dynamics of the Mediterranean ecosystem and provide the before mentioned beneficial services, the recorded more severe wildfires caused by anthropogenic influences and climate change have negative, often long lasting, effects on the environment and, in particular, on soil (Grillakis et al., 2022; Pereira et al., 2018; Keeley et al., 2011). High severity wildfires can cause permanent environmental change, for example from high-value forests to shrubs, a process which is triggered by post-fire soil erosion (Francos et al., 2018a; Sheridan et al., 2018; Verma and Jayakumar, 2015). Additionally, long-term changes include disturbances in soil functions crucial for the survival of the biosphere, such as reduction of nutrient storage capacity, alterations of nutrient cycles, triggering the process of desertification, and modification of

organic matter – a key indicator of soil quality (Jiménez-González et al., 2016; Shakesby, 2011; DeBano et al., 1998). According to Pereira et al. (2018), the magnitude of changes in the soil depends on the components of the ecosystem (water, soil and vegetation type), the characteristics of the fire (intensity, severity) and other environmental factors (such as climate and geomorphology).

The coastal part of Croatia is characterised by a Mediterranean climate or Csa - Hot-summer Mediterranean under the Köppen-Geiger climate classification with hot and dry summers (Kottek et al., 2006). According to the Croatian Fire Brigade's 2022 report, Croatia experienced a 12.11% increase in burned area in 2021, with a total of 37,340 hectares burned, compared to the average from 2011 to 2020. Additionally, in the Mediterranean region of Croatia, the burned area index (the ratio of burned area to the number of fires) increased by 1.34% in the same year (Croatian Fire Brigade, 2022). The increase is in accordance with the general predictions that the higher temperatures and dryness caused by the variable climatic conditions in this area will create more favourable conditions for the emergence and rapid spread of forest fires in the future (DHMZ - Croatian Meteorological and Hydrological Service, 2013). Of course, the occurrence of wildfires is primarily influenced by weather conditions, and there have been years with fewer and less severe fires due to increased precipitation during the typically dry period between June and August. However, extreme weather is also one of the consequences of climate change across the Mediterranean, and it is likely that we will see more of the higher temperatures, prolonged drought periods, as well as precipitation extremes in the following decades - conditions in which severe environmental degradation is inevitable (Ali et al., 2022).

The negative effects of high severity wildfires on soils often include aggregate stability deterioration, and increase in bulk density (Francos et al., 2018b; Fernández et al., 2007). Increased soil bulk density can reduce the total soil porosity and permeability, and increase overland flow, which makes it easier for precipitation and wind to erode the soil, especially on sloped terrains (Carrión-Paladines et al., 2022). Soil erosion can lead to a loss of nutrients and a decline in the quality of the soil. The effects of soil depletion and erosion can be long-lasting, and in some cases, it can take years for the soil to recover (Francos et al., 2018a). Therefore, if not managed properly, wildfires can cause serious damage to the environment.

Considering the above, it is extremely important to continuously monitor and obtain new knowledge about post-fire changes, especially in the case of soil quality, in order to adapt to the changing environmental conditions and to develop sustainable management practices that will mitigate soil degradation. Monitoring and modelling environmental response to natural hazards in space and time allows us to thoroughly analyse their impacts in the short, as well as long-term.



Remote sensing in soil science has great potential for monitoring and mapping large areas of land from a distance. Soil remote sensing can be done from the ground, air, or space. Ground-based remote sensing is typically done with handheld or vehicle-mounted sensors. Airborne remote sensing is done with aircraft-mounted sensors. Spaceborne remote sensing is done with satellites.

In recent years, the potential of multispectral and hyperspectral data obtained via satellite sensors (e.g., Sentinel-2, Hyperion) and field spectroscopy has been explored in soil research, monitoring, and mapping (Vaudour et al., 2019; Gholizadeh et al., 2018a). The data obtained from such sensors provide us the ability to analyse, accurately predict, classify, and map various soil properties of large areas using geostatistical methods (Gholizadeh et al., 2018b; Shoshany et al., 2013). Mapping via remote sensing is vital for understanding the spatio-temporal dynamic of post-fire soil properties. So far, monitoring of spatio-temporal changes of post-fire soil quality has not been conducted in the pedological and climatic conditions of Mediterranean Croatia. The main purpose of the research was to apply soil spectroscopy, remote sensing and geostatistic methods in these conditions and test and develop an advanced, cost-effective and applicable methodology to provide a continuous quantitative assessment of post-fire effects on soil organic matter (SOM). Results obtained from this research will provide the basis for understanding post-fire soil processes and the direction of SOM recovery, as well as providing the first step towards creation of a soil spectral database that will enhance post-fire soil survey in Mediterranean conditions.

## 1.1. Hypothesis and objectives of research

### **Hypothesis:**

1. High intensity fires cause a decrease of soil organic matter content in the short term, while low to medium intensity fires cause an increase of the soil organic matter content.
2. Soil spectral reflectance calibration models can precisely predict soil organic matter content.
3. The accuracy of hyperspectral prediction models does not change with decreasing spatial and spectral resolution, whereas univariate spatial models show less spatial connectivity than multivariate ones.

### **Objectives:**

1. Monitor the temporal and spatial distribution of soil organic matter content after a fire.
2. Determine the relationship of spectral reflectance and soil organic matter content using linear and nonlinear calibration models.
3. Compare the accuracy and precision of hyperspectral prediction models by comparing analytical and in-situ measurements and satellite imagery.
4. Compare the accuracy and precision of univariate with multivariate spatial models.

## 2.BACKGROUND

### 2.1. Wildfire impacts on soil organic matter (SOM)

The socio-economic and land-use changes in the Mediterranean region (depopulation, abandonment of agricultural land, afforestation with flammable species) and climate change in the last decades has led to the increase in the number of catastrophic wildfires (Ferreira et al., 2022; Pausas et al., 2008). About 300-460 Mha are burned annually on Earth, which is about 4% of the surface (de la Rosa et al., 2019). Wildfires are a natural occurrence and drivers of change in most ecosystems (exceptions are some ecosystems of extreme climatic conditions, eg. deserts) (Keeley et al., 2011), which means they alter flora, fauna, and soil significantly.

Organic matter is an integral part of the soil, which consists of plant and animal detritus in various stages of decomposition, humus, microorganisms, meso- and macro-fauna of the soil and the products of their metabolism. Soil organic matter (SOM) is one of the most important indicators of soil quality - it participates in the circulation and retention of nutrients, improves soil structure, retains water, prevents erosion, absorbs and retains pollutants, and represents the main source, but also a global carbon (C) sink (FAO, 2020). Namely, soil organic carbon (SOC) makes up almost 58% of SOM (Heaton et al., 2016) and about 2/3 of the total C stored in the terrestrial ecosystem - about 2400 petagrams (Pg) C at a depth of up to 2 m (for comparison, the atmosphere contains about 830 Pg C) (Yousaf et al., 2017). Carbon is the central building block of living organisms and a key regulator of the global climate. It is also an important element in wildfires because it makes up almost 50% of the dry matter of all forms of vegetation (Ho, 1976).

#### 2.1.1. Impact of wildfire severity on SOM

The effects of wildfire on SOM are highly variable and depend on a number of factors, including the intensity and severity of the fire, the type of vegetation that was burned, the pre-fire soil conditions, and the post-fire management. The type, intensity and severity of the wildfire determine the degree of loss or increase because of the incorporation of partially burned plant mass into the soil (González-Pérez et al., 2004). Generally speaking, an increase in SOM was recorded in low- and medium-severity fires (Alcañiz et al., 2016; Inbar et al., 2014), and a decrease in high-severity fires (Moya et al., 2019), although there are some studies that report an increase of SOM even in high severity wildfires (see Table 2.1).

The reason for this discrepancy lies in the heterogeneous molecular structure of SOM in combination with external environmental factors (fuel type, soil type, wildfire severity etc.).

According to Cofer et al. (1997), the combustion of biomass can generate various compounds, such as carbon monoxide (CO), methane (CH<sub>4</sub>), and complex hydrocarbons, in addition to carbon dioxide (CO<sub>2</sub>), water (H<sub>2</sub>O), and minerals. Under the influence of high temperatures, this process creates new forms of carbon and alters existing forms, which are then present in the resulting ash. Ash created as a direct consequence of wildfires covers the soil surface in the immediate post-fire period. Its colour serves as a direct indicator of wildfire severity, in addition to the degree of foliage and tree trunks combustion, and aids researchers to classify and describe the fire-affected landscape. According to Pereira et al. (2019), black and dark grey ash and partial combustion of vegetation indicate low to moderate wildfire severity, while white ash and complete combustion of vegetation point to a high wildfire severity. The changes in soils after a low-severity wildfire are often ephemeral and include decreased microbial respiration and enzyme activity (Dove et al., 2020), as well as the increase of soil pH and SOM content (Moya et al., 2019), while high severity wildfires lead to severe soil degradation, such as volatilization of essential soil nutrients like soil C, nitrogen (N), phosphorous (P) and sulphur (S) - which are crucial for maintaining soil health (Delač et al., 2020; Delač et al., 2021; Hrelja et al., 2020; Hebel et al., 2009; Neary et al., 1999).

Due to the heterogeneous molecular nature of SOM it is difficult to draw straightforward conclusions regarding its post-fire dynamic and recovery in different environmental conditions. Previous studies stated that the impact of wildfire on SOM content and composition depends on temperatures reached, but also on soil properties. For example, soils with a higher proportion of clay contain more tightly bound organic C, which is more resistant to thermal decomposition (Santín and Doerr, 2019; Xue et al., 2014). Additionally, given that SOM combustion generally starts at temperatures above 200 °C, soil moisture can significantly impact its speed because it prevents the temperature in the soil from rising above 100 °C until all the water evaporates from the matrix (Santín et al., 2016a). Minor changes in organic matter begin at temperatures between 100 and 200°C, such as the condensation of volatile compounds, and a more significant impact begins at temperatures of 200-300 °C, when mineralization and loss of gases and aerosols occur (Santín and Doerr, 2016; González-Pérez et al., 2004).

Although previous research highlights the variability of the impact of fires on different soils (e.g. Alcaniz et al., 2018), it is generally considered that wildfires cause loss of soil nutrients through volatilization, erosion and leaching following a partial or complete burning of SOM (Agbeshie et al., 2022; Jiménez-Pinilla et al., 2016; Shakesby et al., 1993).

The recovery of SOM after wildfire is a complex process that is influenced by a number of factors. In general, however, it can take years for SOM to recover to its pre-fire levels (Mayer et al., 2020; Nave et al., 2011).

Table 2.1. Summary of recent research displaying the discrepancy of wildfire impact on C content

Location	Vegetation	Soil type	Post-fire sampling date	Fire severity	Form of C measured	Observed change in the soil	Reference
Russia	<i>Juniperus excelsa</i> , <i>Juniperus foetidissima</i> , <i>Pistacia mutica</i> , <i>Pinus brutia</i> var. <i>pityusa</i> , <i>Cotinus coggygria</i>	Cambisol	2 weeks post-fire	low	SOC	decreased	<i>Kazeev et al. (2022)</i>
				moderate		no change	
				high		increased	
China	Mixed coniferous forest	Light textured, shallow	Immediately post-fire	low	TOC	no change	<i>Ping et al. (2022)</i>
				moderate		increased	
				high		increased	
Croatia	<i>Olea europaea</i> L., grasses and maquis	Cambisol Rhodic	5 days, 3 months, 6 months, and 1 year after the wildfire	moderate	SOC	increased	<i>Šestak et al. (2022)</i>
				high		increased	
Portugal	<i>Pinus halepensis</i> Mill., <i>Macrochloa tenacissima</i> (L) Kunth, <i>Quercus coccifera</i> L., <i>Pistacia lentiscus</i> L.	Aridisols/ Lithic Haplocalcids	3 years post-fire	low/medium	SOC	no change	<i>Moya et al. (2019)</i>
				medium/high		decreased	
Poland	Mixed coniferous forest	Podzol	1 year post-fire	not discussed	SOC	decreased	<i>Majder-topatka et al. (2019)</i>
Spain	<i>Pinus pinaster</i> ssp.	Typic Haploxerept	18 years post-fire	low	SOM	decreased	<i>Francos et al. (2018a)</i>
		Lithic Haploxerept		high		decreased	
Spain	<i>Pinus halepensis</i> Miller, <i>Pinus nigra</i> Arnold and <i>Quercus ilex</i> L.	Fluventic Haploxerept	3 months post-fire	high	SOM	increased	<i>Francos et al. (2018b)</i>
Portugal	<i>Eucalyptus globulus</i> L., <i>Pinus pinaster</i>	Leptosols	2 weeks post-fire	low	SOC	decreased	<i>Otero et al. (2015)</i>
				high		decreased	
Israel	<i>Pinus halepensis</i> and <i>Pinus brutia</i>	Lithic Xerorthent	1 month post-fire	low/medium	SOM	increased	<i>Inbar et al. (2014)</i>

### 2.1.2. Impact of vegetation species on SOM

Immediately after a wildfire, there is a decrease in unstable organic compounds and an increase in aromatic compounds (i.e. char) resistant to chemical/thermal decomposition produced as byproducts of biomass burning and the formation of ash (Bodí et al., 2014). However, some studies suggest there is also an increase of unstable compounds in the case when there is incorporation of dead but unburnt biomass into the soil (Nocentini et al., 2010; Knicker et al., 1996). The key reason for this discrepancy is biomass composition that varies in different ecosystems and causes spatially heterogeneous effects on SOM in the small scale (Santín et al., 2016b).

In other words, the amount and chemical nature of the char and ash produced by wildfires vary greatly with type of biomass burned, which then greatly influences the soil properties as well, once they are incorporated into the soil profile via precipitation (Mastrolonardo et al., 2013).

For example, some studies have found that biomass with lower lignin content starts burning at lower temperatures, and creates less char and more ash than biomass with higher lignin content (Soucémariadin et al., 2013; Keiluweit et al., 2010; Nocentini et al., 2010). Combustion of biomass with lower lignin content also usually results in the formation of charred material that includes non-aromatic components, such as polysaccharides and N-heteroaromatic C derived from peptides, which are more heat resistant (Knicker et al., 1996; Nocentini et al., 2010). The lignin content in deciduous species is usually around 18–24%, in coniferous species 27–32%, in shrubs 6.5%, and in grasses 7–8% (Khviyuzov et al., 2020; Rahman et al., 2013; Heitner et al., 2010; Sosulski et al., 1960). Additionally, the combustion of grass plant material, rich in N, yields higher ash content than woody material (Nocentini et al., 2010; Knicker et al., 1996). Therefore, the type of biomass burned affects directly the post-wildfire SOM changes. Santín et al. (2012) found significant differences in the abundance of charred biomass in rainforest and eucalypt forests. Mastrolonardo et al. (2013) and McBeath et al. (2013) also observed that high variability in formation, amount and chemical properties of the charred biomass and ash depends on various differences in vegetation types and their composition.

### 2.1.3. Impact of time-after-fire on SOM

The recovery of soil organic matter after wildfire is a complex process that is influenced by a number of factors, such as wildfire severity, post-fire soil erosion processes, weather conditions and climate, or vegetation recovery. In general, however, it can take more than 10 years for SOM to recover to its pre-fire levels (Orumaa et al., 2022; Parro et al., 2019). On the other hand, other studies have shown that SOM can recover much faster, within one to two years (Bonilla et al., 2017).

Francos et al. (2018a) conducted a study of the impact of high severity wildfire on total C in the soil, and monitored its immediate increase in the soil after the wildfire, mostly due to the incorporation of ash, and a later (several years after the fire) decrease to a level lower than the control due to post-fire erosion and increased mineralization of SOM. However, 18 years after the fire, total C levels did not return to pre-fire levels, which was most likely related to the incomplete recovery of vegetation. The same study, when applied to fires of lower severity, confirmed only an immediate increase in total C after the fire (Francos et al., 2018a), and multi-year studies such as the one conducted by Alcaniz et al. (2018), revealed no significant changes in total C levels over time.

Given that SOM is one of the most important indicators of soil quality, an important reservoir of C at the global level, and about 4% of the Earth's surface suffers from the effects of fire annually, understanding post-fire soil processes is crucial for sustainable land management on fire-affected areas.



## 2.2. Wildfire impacts on soil chemical properties

This section deals mainly with the impacts of wildfire on soil pH and electrical conductivity (EC), as they represent important indicators of soil quality and play an important role in the soil capacity for performing environmental functions, as well as supporting agricultural production (Arshad and Martin, 2002). It also deals with the impact of wildfire on  $\text{CaCO}_3$  accumulation, as it can be an important indicator of temperatures reached during the wildfire and help characterise its severity (Francos et al., 2019; Dlapa et al., 2013).

### 2.2.1. Impact of wildfire severity and time-after-fire on soil pH, EC, and $\text{CaCO}_3$

Ash is an alkaline material characterised by high EC, and contains high levels of sulphates, oxides and carbonates of Ca, Mg and K, as well as other elements such as Al, Fe, Cu, Mn, Ni and Zn (Doufexi et al., 2022; Hrelja et al., 2020; Pereira et al., 2019). It is incorporated into the soil profile after the first precipitation event, and as water percolates through the ash, large quantities of base cations are leached into the soil, therefore causing changes in post-fire soil nutrient status, pH, and EC in the short and long-term (Pereira et al., 2019). In the immediate post-fire timeframe both soil pH and EC increase due to incorporation of ash into the soil, and the increased pH promotes the solubility of Ca, Mg, Na and K cations as a consequence of mineralization process, which can further change soil chemistry (Francos et al., 2018a; Pereira et al., 2015).

Soil pH and EC values are elevated in the short period and up to three years after the wildfire (Moya et al., 2019), mainly because of decreased competition for nutrients, which is dependent on the dynamic of vegetation recovery (Stavi, 2019). Additionally, the increase of both soil pH and EC was noted as ephemeral especially in low-severity wildfires that cause less disturbance in the environment, as reported by Pereira et al. (2017) and Zavala et al. (2014). According to Henig-Sever et al. (2001), higher temperatures achieved during moderate and high severity wildfires facilitate the increase of ash pH and the solubility of major cations, which can prolong the high pH soil status in the post-fire period. When severe wildfire occurs, it often causes serious and prolonged soil degradation, i.e. disruption of the stability of soil aggregates that leads to erosion and runoff on slopes after the fire, as well as volatilization of soil nutrients due to extreme temperatures during the fire (Pereira et al., 2018; Jordán et al., 2014; Jordán et al., 2011; Hebel et al., 2009).

In soils affected by low severity wildfires, the main changes are decreases in soil microbial community and enzyme activity, accompanied by increases in soil pH, EC and nutrient concentrations (Dove et al., 2020; Pereira et al., 2018).

According to Úbeda et al. (2009) calcite is one of the major inorganic constituents of ash that forms between 350 and 550 °C. Goforth et al. (2005) observed high CaCO<sub>3</sub> content in ash of lighter colours, originating from completely combusted organic matter, and concluded it contains more alkaline oxides able to form carbonates, unlike ash of darker colour which indicates the presence of organic C originating from incomplete combustion of organic matter. According to Ulery et al. (1993) the alkaline oxides in white ash produced by wildfires of a higher severity react with water vapour and CO<sub>2</sub> from the atmosphere and form carbonates and hydroxides over time. According to Dlapa et al. (2015), one of the hypotheses considering the origin of CaCO<sub>3</sub> in post-fire soil is the transformation of weatherable minerals into calcite during the burning process in high temperatures (>400°C). At temperatures above 580 °C the amount of carbonates decreases in favour of oxides, as CaCO<sub>3</sub> dissociates to CaO, as reported by Bodí et al. (2014). From the available literature, it would appear that CaCO<sub>3</sub> forms during high severity wildfires and is transformed over time into hydroxides in reaction with atmospheric water vapour and CO<sub>2</sub> due to its hydrophilic nature, as was observed by Dlapa et al. (2015), Pereira et al. (2012), Plante et al. (2009), and Echigo et al. (2005).

#### 2.2.2. Impact of vegetation species on soil pH, EC, and CaCO<sub>3</sub>

Vegetation species play a significant role in shaping soil pH, EC, and CaCO<sub>3</sub> dynamics. Certain coniferous trees (e.g., *Pinus*, *Piceoideae*) and heathland plants release organic acids, lowering pH over time, while some deciduous trees (e.g., *Populus*, *Quercus*) and grassland plants (e.g., *Poaceae*) release alkaline compounds, elevating pH (Dijkstra et al., 2001; Kesselmeier et al., 1997; Jalal and Read, 1983). Factors such as litter quality, root exudates, and nutrient uptake further modulate soil pH and EC by releasing soluble ions (Tavakkoli et al., 2015), enhancing ion solubility through root exudates (Lin et al., 2022), and resulting in the accumulation of ions by salt-tolerant species (Munns, 2002). Furthermore, water use patterns and organic matter input contribute to dynamic changes in soil EC (Wong et al., 2009; Mmolawa and Or, 2000). Similarly, in CaCO<sub>3</sub> dynamics, vegetation's root activity, organic matter input, and interactions with soil organisms influence CaCO<sub>3</sub> presence. Root exudates can dissolve or promote CaCO<sub>3</sub> formation (Ma et al., 2022), while plant-microbe interactions contribute to intricate changes in soil CaCO<sub>3</sub> content (Singh et al., 2020; Lambers et al., 2009). Local factors and feedback mechanisms add complexity to these interactions.

As wildfires occur, the combined effects of vegetation and fire severity shape the subsequent changes in soil pH, EC, and CaCO<sub>3</sub> content. Vegetation's role in post-fire recovery, nutrient cycling, and organic matter accumulation can either amplify or mitigate the impacts of wildfire on these soil parameters (Verma and Jayakumar, 2012; Neary et al., 1999). Studying these interactions with respect to vegetation species provides valuable insights into the complex dynamics of soil quality in ecosystems affected by wildfire.

## 2.3. Spectroscopy and remote sensing techniques for soil monitoring in post-fire period

### 2.3.1. Basic principles of soil spectroscopy

The main idea behind remote sensing research lies in the fact that information about objects of interest can be obtained by analysing data acquired via instruments that are not in close contact with the objects themselves (Lillesand et al., 2004). Soil spectroscopy in this context studies remotely sensed data measured proximally (usually up to 2 m away from the target) in-situ or in a controlled laboratory environment.

Spectroscopy is defined as the study of the interaction between matter and electromagnetic radiation. Electromagnetic (EM) radiation is a form of energy that travels through the air, or any other medium, in the form of a wave, and can be classified in terms of wavelength or frequency, which can be described in a following equation:

$$V = c / \lambda$$

where  $V$  is frequency (in seconds),  $c$  is the speed of light ( $3 \times 10^8 \text{ ms}^{-1}$ ) and  $\lambda$  is wavelength (in metres). Usually in VNIR spectroscopy, wavelength is expressed in nanometers (nm).

Additionally, the energy associated with EM radiation can be defined in the following equation:

$$E = h \times V$$

where  $E$  is energy (in Joules),  $h$  is Planck constant ( $6.62 \times 10^{-34} \text{ Js}$ ), and  $V$  is frequency (in seconds).

From these equations it is clear that frequency and wavelength are inversely related, and that radiation with shorter wavelength has higher frequency (and energy).

Visible and near-infrared radiation comprises only a small part of the EM spectrum that includes other forms of radiation, such as ultraviolet (UV), x-rays and gamma rays, as shown in Figure 2.1.

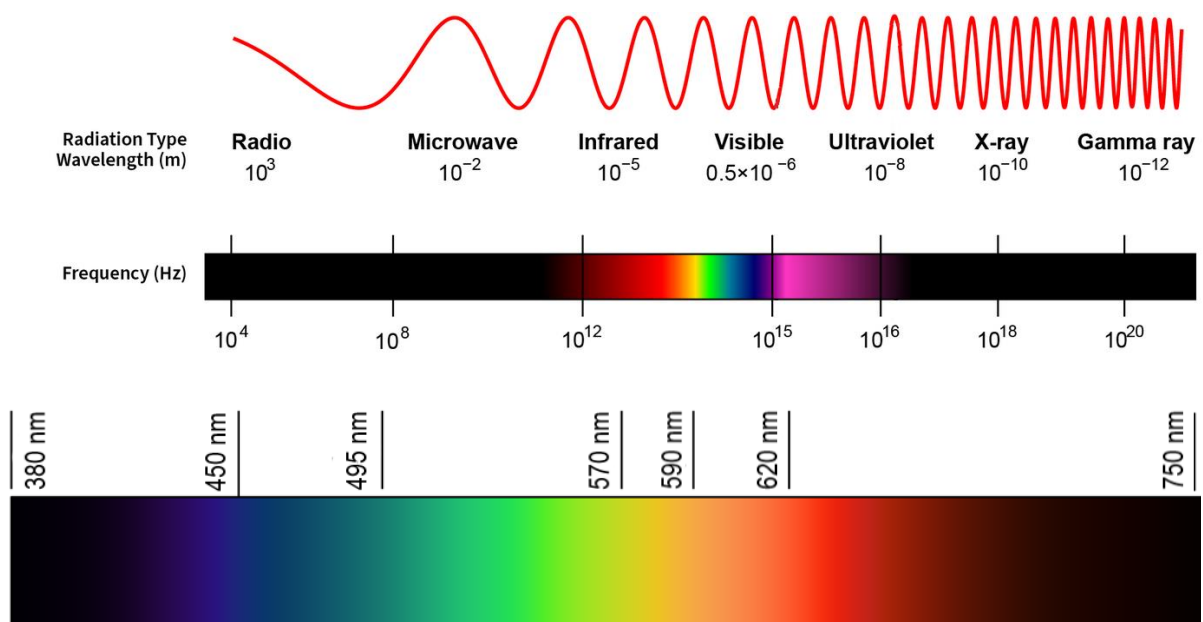


Figure 2.1. Electromagnetic (EM) spectrum and approximate visible colour ranges in nanometers (nm). Adapted according to: Bruno and Svoronos (2005) and National Institute of Standards and Technology (<https://www.nist.gov>)

When radiation interacts with matter, the processes of absorption, reflection, transmission, or emission of radiation can occur. When radiation interacts with a given matrix (or sample), the amount of radiation absorbed is the difference between the incident radiation and the transmitted radiation, and is expressed as either transmittance or absorbance, as expressed in the following equations:

$$T = (I / I_0) \times 100$$

or

$$A = -\log T,$$

where  $T$  is transmittance,  $A$  is absorbance,  $I_0$  is incident radiation and  $I$  is transmitted radiation.

Spectroradiometer is an instrument that generates EM radiation of a specific part of the spectrum and measures transmittance and absorbance of a given matrix. As the energy is inversely related to wavelength, the resulting spectrum produces a characteristic shape unique to each matrix type that can be used to further analyse the matrix properties (Miller, 2001). Figure 2.2 shows the typical spectral response of three different matrix types, soil, water and vegetation in the range from 500 to 2500 nm. Within this spectral region, specific zones of EM absorption by these matrices are known, and they are the result of interactions with the

vibrations of the chemical bonds on an atomic level. Because an EM wave is a form of energy, its absorption by the matrix causes the energy content of the molecules to increase.

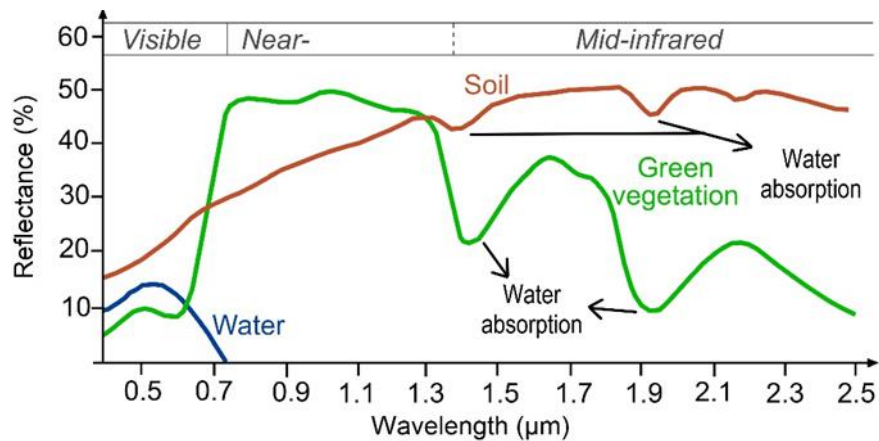


Figure 2.2. Typical spectral response characteristics of soil, water and vegetation; source: National Institute of Standards and Technology (downloaded from: <https://www.nist.gov>; 05.09.2022.)

Moreover, the literature refers to this type of spectroscopy as hyperspectral, because spectroradiometer instruments measure and record reflectance of a given matrix in a continuous spectral range. Contrary to hyperspectral, multispectral instruments measure and record a smaller number of wavelengths, usually referred to as bands. Multispectral imagery generally refers to 3 to 10 bands. More information on multispectral instruments is given in chapter 2.3.4.

### 2.3.2. Soil spectroscopy for SOM research in post-fire period

Soil spectroscopy is recognized as a fast, non-destructive and simple analytical method, and a tool for comprehensive soil research, which enables the simultaneous evaluation of many soil properties using hyperspectral data, multivariate statistical approaches and chemometric methods (Zovko et al., 2018; Viscarra Rossel et al., 2006).

In recent decades, the use of remote sensing data to monitor the recovery of SOM after wildfires has increased. This is due to the advantages of remote sensing, as well as the advances in technology. The development of new technology such as diffuse visible, near-infrared and shortwave-infrared (VNIR-SWIR) soil spectroscopy, allowed researchers to gather additional soil data and form complex databases whose information can be used to improve modelling and prediction of different soil properties, including organic matter (Rosero-Vlasova

et al., 2018; Makhamreh, 2006). VNIR-SWIR spectroscopy is a type of remote sensing that uses visible (V) and near-infrared (NIR), as well as short-wave infrared (SWIR) light, to measure the reflectance of the soil. The reflectance of the soil is dominantly affected by the amount of SOM in the soil, in addition to other soil properties that can affect reflectance, such as soil texture and moisture (Stenberg et al., 2010). For example, coarse-textured soils tend to reflect more light than fine-textured soils, because larger soil particles have larger pore spaces and less surface area per unit of soil, which reduces the amount of light that is absorbed and increases the amount that is reflected, while wet soils reflect less light than dry soils because water absorbs more light than soil particles (González-Teruel et al., 2020; Stenberg et al., 2010).

In general, by using spectroscopic methods the interaction of matter and EM radiation is detected and interpreted, and the intensity of the emitted, absorbed or scattered radiation is usually measured depending on its wavelength, i.e. frequency (Stenberg et al., 2010). In the last few decades, VNIR-SWIR calibrations have been used mostly to determine total C and SOC, as well as the content of clay and total N in soil (Šestak et al., 2022; Semella et al., 2022; dos Santos et al., 2020; Adeline et al., 2017; Stenberg et al., 2010).

Soils with a high SOM content tend to be darker in colour and have a lower reflectance than soils with a low SOM content, and according to Baumgardner et al. (1986), organic matter is the one of the most important property to explain reflectance differences in the VNIR spectral region, which arise due to stretching and bending of organic covalent bonds. This information can be used to monitor the recovery of SOM after wildfire.

According to Cozzolino and Morón (2006) the visible part of the spectrum (400-700 nm) affects C calibrations the most, because SOM reduces reflectance in the visible region. Additionally, in the NIR region (> 700 nm), wavelengths around 960 and 1100 nm tend to be absorbed by SOM (Francos et al., 2021; Daniel et al., 2004). Particularly the 690-700 and 788 nm impact calibrations of clay and silt bound C, while 700-800 nm region is thought to be associated with humic compounds derived from decomposition of SOM (Stevens et al., 2013; Cozzolino and Morón., 2006; Fidêncio et al., 2002; Daughtry, 2001). Moreover, according to Francos et al. (2021), the modelling of organic matter in soils with low content (< 0.6%) may lead to difficulties in its estimation. To improve the robustness of such models they propose conducting research by using samples at various SOM decomposition stages.

Overall, the use of laboratory spectroscopy in the VNIR-SWIR spectrum in combination with multivariate statistical methods such as PLSR has proven to be a precise technique for estimating not just soil C, but various other soil properties as well (Viscarra Rossel et al., 2006; Croft et al., 2012). Most commonly used chemometric models are principal component analysis (PCA), stepwise multiple linear regression (SMLR), partial least squares regression (PLSR), principal component regression (PCR), and artificial neural networks (ANN)

(Mohamed et al., 2018). Viscarra Rossel and Behrens (2010) compared different modelling algorithms to determine soil organic carbon content and found that significant wavelength selection techniques gave the best predictions if the ANN model based on the VNIR-SWIR (350–2500 nm) spectrum was used, mainly because ANNs can model complex nonlinear interactions in the data.

### 2.3.3. Effect of soil moisture on predictive SOM modelling

In addition to measuring SOM by spectroscopy under controlled laboratory conditions, field spectroscopy can also be used as a rapid method for monitoring changes in SOM, with a slight decrease in accuracy compared to laboratory measurements (Stevens et al., 2008). The decrease in accuracy in field measurements is caused mostly by soil conditions such as surface roughness, compaction level, temperature, and most importantly, soil moisture (Bendor et al., 2008a). Soil moisture drastically changes the refractive properties of soil.

Generally, a decrease of soil reflectance is observed with increased soil moisture, which is due to water-specific absorption characteristics defined by the Lambert-Beer law (Lobell and Asner, 2002). According to Oxford Reference (2022), the Lambert-Beer law demonstrates how “(...) *the intensity of light (or any other form of electromagnetic radiation) passing through a sample diminishes exponentially with the concentration and the thickness of the sample (for a given wave number)*” and expresses it through a formula:

$$\log(I/I_0) = -\epsilon[J]l,$$

where  $\epsilon$  is the molar absorption coefficient,  $I_0$  is incident radiation and  $I$  is transmitted radiation, and  $[J]$  is the molar concentration of the matrix.

Furthermore, EM radiation is more intensely scattered if it reaches the dry soil than wet soil particles. This is explained by the difference in refractive index ( $n\lambda$ ) between the mineral soil particles and the air or water surrounding them (Somers et al., 2010). In dry soils ( $n\lambda_{\text{soil}} \sim 1.5$ ) the particles are surrounded by air ( $n\lambda_{\text{air}} \sim 1.0$ ), and the difference in refractive indexes is relatively larger than if the particles are surrounded by water ( $n\lambda_{\text{water}} \sim 1.33$ ), effectively causing decreased scattering of incident light as the soil moisture increases (Bach and Mauser, 1994). Additionally, water absorption is detectable in the soil reflectance curve in the SWIR region of the spectrum (typically around 1400 and 1900 nm), and is marginal in the VNIR region (Figure 2.3). Therefore, if the SWIR region of the spectrum is omitted, and the rest of the spectrum is preserved, a successful prediction of SOM can still be expected because the VNIR region is the most important region for C calibrations.



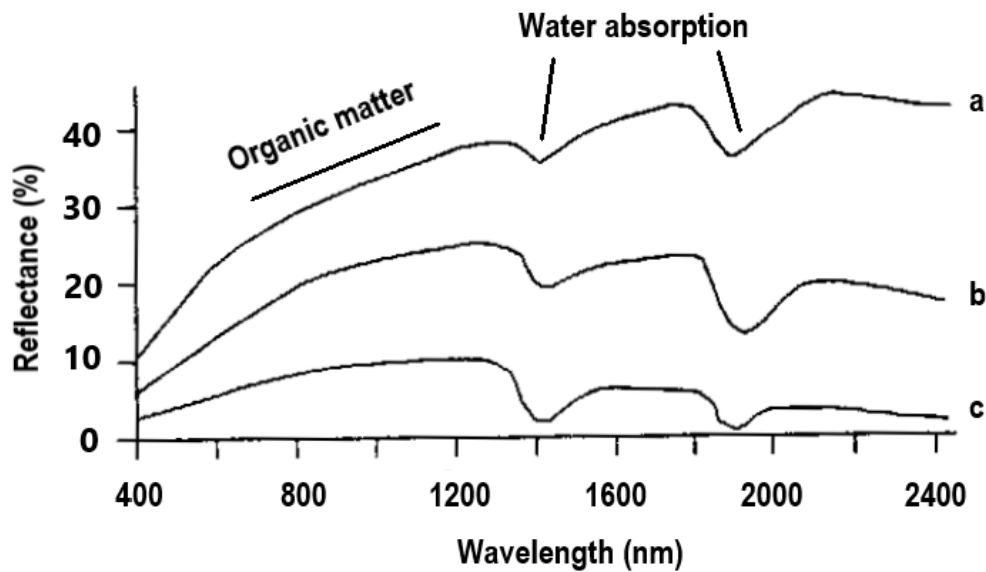


Figure 2.3. Soil reflectance curves as a function of water content, (a) 5%, (b) 20%, and (c) 40% water content. Adapted according to: Ben-dor et al., 2008b and Stoner and Baumgardner, 1981

#### 2.3.4. The potential of remote sensing in research of post-fire SOM

The usual methods of studying post-fire spatio-temporal variability of SOM is traditionally done via extensive soil sampling, coupled with laboratory wet chemical methods, such as the Walkley-Black and the dry combustion method (Walkley and Black, 1934; HRN ISO 10694). These methods are time-consuming and labour-intensive, and require the use of expensive laboratory equipment. In addition, these methods can only be used to measure SOM content and other soil properties of a limited number of samples. Considering the limitations of traditional methods, there are many advantages of using hyperspectral soil reflectance data obtained proximally, such as simultaneous measurements of various soil properties of interest in a short period of time, which facilitate monitoring of the soil status and considerably reduce costs. The above-mentioned method uses hundreds of continuous spectral bands with high resolution, however for spatially extensive and frequent soil mapping campaigns such methods are not economically sustainable (Gholizadeh et al., 2018a).

By utilising multispectral data from satellite sensors, it is possible to achieve economically feasible extensive and continuous soil mapping objectives. As already mentioned in chapter 2.3.1., multispectral instruments measure and record a smaller number of wavelengths, usually referred to as bands (Figure 2.4).

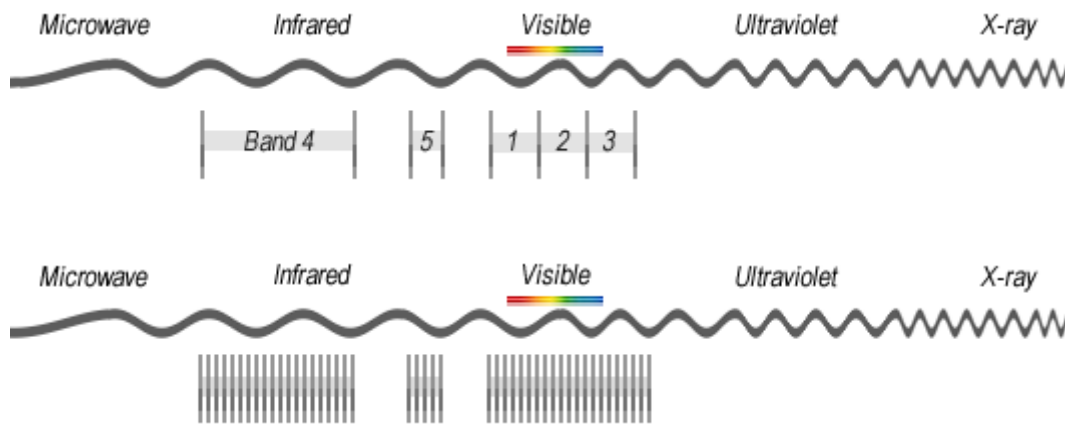


Figure 2.4. The difference between multispectral and hyperspectral sensors; source: GISGeography (downloaded from: <https://gisgeography.com>; 11.11.2022)

The acquired data provides information at a planetary scale and can be used, modified and adapted by users interested in environmental monitoring, such as crop growth, land use, disaster risk assessment, and urban development (Tarpanelli et al., 2022; Krtalić et al., 2021; Varghese et al., 2021; Hunt et al., 2019; Novelli et al., 2019; Pesaresi et al., 2016).

This information can also be used to monitor the recovery of SOM and other soil properties after wildfire. Furthermore, it can be used in monitoring the effects of wildfire in difficult-to-access areas. This is important because the effects of wildfire can be more severe in remote areas. Finally, spaceborne sensors can be used to measure the post-fire recovery over time. This is important because the recovery of SOM after wildfire can take years (see chapter 2.1.). Therefore, the main advantages of multispectral spaceborn over proximal hyperspectral sensors are the possibility of monitoring of the soil status on a regional and global scale, high revisit time, data reduction and rationalisation of costs.

In the recent years, multispectral data provided by Sentinel-2 mission has successfully been used in wildfire detection and severity assessment, modelling post-fire SOM, as well as post-fire vegetation recovery with great accuracy of up to 95% (Liu et al., 2022a; De Simone et al., 2020; Lasaponara et al., 2020; Rosero-Vlasova et al., 2018).

However, spaceborne sensors such as the one equipped on Sentinel-2 have the ability to obtain data on various soil properties on a global scale in a short period of time, provided the images are cloud-free and obtained when the soil is bare. Specifically, Sentinel-2 carries an optical sensor that records the reflectance of smaller  $\lambda$  that cannot penetrate the objects closest to the sensor, such as atmospheric obstacles (eg. clouds) or, in their absence, surface obstacles (eg. layer of vegetation). This prevents data collection of the soil pixels, unless the images are free of clouds and vegetation. Radar sensors record data obtained via scattering

of larger  $\lambda$  (in the microwave spectrum) capable of penetrating such obstacles. For example, Sentinel-1 mission is equipped with a synthetic aperture radar (SAR) instrument that records EM waves in the so called C-band almost entirely unaffected by atmospheric changes, whilst Sentinel-2 optical sensor is much more influenced by atmospheric water vapour (for more information see Plank, 2014). This major restricting factor of Sentinel-2 unables us to effectively monitor the long-term post-fire soil status considering that vegetation regrowth will take place at some point in the future, unabling the acquisition of bare soil pixels from such images.

Luckily, in recent years researchers have successfully fused data obtained from multiple sensor types in order to enhance the retrieval of various soil property data. For example, Amazirh et al. (2018) combined Sentinel-1 microwave and Landsat-7/8 VNIR-SWIR data to reduce RMSE in soil moisture calibration models in a semi-arid region in Morocco from  $0.16 \text{ m}^3 \text{ m}^{-3}$  (Sentinel-1 only) to  $0.03 \text{ m}^3 \text{ m}^{-3}$  (combined Sentinel-1 and Landsat-7/8). Arjasakusuma et al. (2022) combined Sentinel-1 and Sentinel-2 data to successfully improve mapping of magnitude and impacts of 2019's fire events in South Sumatra Province, Indonesia, and demonstrated the combination yielded the best accuracy of classification of burned areas ranging from 91.8% to 95.8%.

## 2.4. Geostatistical methods of SOM monitoring

Geostatistics is the application of statistics that focuses on the analysis and interpretation of spatial data, emphasising the incorporation of spatial relationships and variability into statistical models (Li and Heap, 2008). It is used to estimate the values of parameters at unobserved locations. In other words, geostatistical methods can be used to interpolate values at unsampled locations, and describe and measure spatial continuity inherent in natural phenomena through spatial interpolation. This greatly improves the understanding of the underlying patterns and processes of soil degradation, often induced by intensive agricultural practices but also environmental hazards, such as wildfires (Brevik et al., 2016).

Spatial patterns of soil properties are observed using the experimental semivariograms that depict the spatial autocorrelation of the measured sample points which can be described in the following formula:

$$y(h) = \frac{1}{2N(h)} \sum_{i=1}^{N(h)} [Z(x_i) - Z(x_i + h)]^2,$$

where  $y(h)$  is the semivariance at a given distance  $h$ ,  $Z(x_i)$  is the value of the variable  $Z$  at point  $x_i$ , and  $N(h)$  is the number of pairs of sample points separated by the lag distance  $h$  (Isaaks and Srivastava, 1989).

The semivariogram has certain characteristics that are commonly used to describe it: the range, sill and nugget (Figure 2.5). The distance where the model first flattens out is known as the range, showing at which distance  $h$  the measured points are spatially autocorrelated.

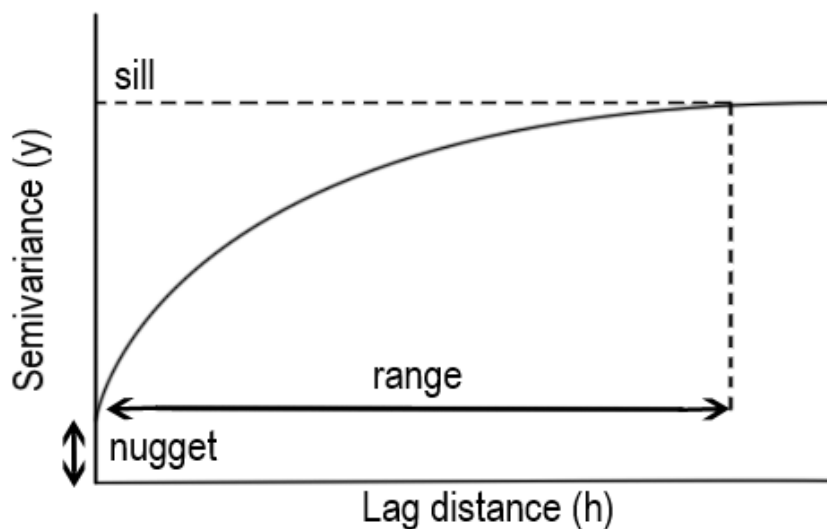


Figure 2.5. Semivariogram example. Adapted according to: Biswas and Cheng, 2013

Theoretically, at zero distance the semivariogram value is 0. However, the semivariogram often exhibits a nugget effect, which is attributed to spatial variations observed at distances smaller than the sampling interval and/or measurement errors (Shukla et al., 2020). Therefore, variations of the target variable at distances smaller than the sampling distances will appear as part of the nugget effect. Furthermore, in some cases, due to large small-scale variability of the target variable and insufficient sampling intensity, a phenomenon known as pure nugget effect could appear. The consequence of the pure nugget effect is a flat surface semivariogram, which indicates total lack of spatial continuity which disables further interpolations (Shukla et al., 2020). In terms of research, the presence of a pure nugget effect may suggest that additional sampling is needed at smaller scales in order to fully capture the variability of the target variable. This could involve increasing the density of sampling points or using higher resolution measurements to capture spatial variation at smaller scales (Goovaerts, 1997).

Finally, the sill is the value that the semivariogram model attains at the range (the value on the y-axis), and partial sill (PSill) is the sill minus the nugget. The spatial dependence of the soil properties is usually evaluated using nugget to sill ratio. According to Cambardella et al. (1994), if the ratio is <25% the variable has strong, between 25% and 75% moderate, and if it is >75% the variable has a weak spatial dependence.

Moreover, spatial variation is often not the same in all directions. This spatial behaviour is known as anisotropy, and such models reach the sill more rapidly in some directions than others, as opposed to isotropic models that reach the sill in all directions simultaneously (Spiliopoulos et al., 2011). Anisotropy is a common phenomenon observed in nature, where the spatial variability of a property or phenomenon differs depending on the direction or orientation in which it is measured. There are several reasons why anisotropy may occur in nature, such as human activity, geological and biological processes. Biological systems such as plant roots can create anisotropic patterns in soil properties by altering the structure and composition of the soil in different directions, while human activities such as land use changes, infrastructure development, and pollution can also create anisotropic patterns in environmental properties by altering the landscape in different ways (Germer and Braun, 2015; Peng and Horn, 2008).

Wildfires can also alter the structure and composition of soils in several ways, leading to directional variations in soil properties (Srivastava et al., 2018; Lorente et al., 2013). For example, by breaking down soil aggregates and creating soil crusts, the anisotropic patterns in soil porosity, water infiltration, and nutrient availability could occur (Srivastava et al., 2018; Widomski et al., 2013). Additionally, wildfires can cause rapid decomposition of SOM, leading to directional variations in its contents, as well as soil microbial activity (Lorente et al., 2013).

Anisotropy can have a significant impact on the way in which these phenomena are modelled, both in terms of the accuracy of the models and the computational efficiency, and should be taken into account in geostatistical modelling. With the usage of anisotropic variograms, which take into account the directional dependence of the variance of the variable being modelled, the accuracy of the chosen interpolation method can be greatly improved, as demonstrated by Oliveira et al. (2022), Zhang et al. (2012) and Ecker and Gelfand (2003).

One of the most widely used spatial interpolation methods for estimating soil properties is kriging (Webster and Oliver, 2007). Kriging is a linear unbiased predictor that covers a range of least-squares methods with great predictive power that is able to minimise the estimation error variation (Worsham et al., 2010). According to Webster and Oliver (2007), ordinary kriging (OK) is the most used type of kriging. It predicts the values of unknown points by calculating weights of the surrounding known values, and it requires a dense sampling grid to model local variations of soil properties (Bodaghabadi, 2018). Kriging methods have been successfully used in the past to model and map different soil properties, such as SOM (Rahmani et al., 2022; Hu et al., 2019; Bogunović et al., 2017;), soil pH (Armanto et al., 2022; Zhang et al., 2022; Bogunović et al., 2014), soil EC (Sahbeni and Székely, 2022; Samieifard et al., 2021; Zare et al., 2021) and many other soil properties of interest, such as plant available phosphorus (P) and potassium (K) (Kazmierczak et al., 2022; Behera et al., 2016).

Because SOM can be highly spatially variable, often the use of auxiliary data is used to improve SOM predictions at unsampled locations (Pouladi et al. 2019). The method that incorporates auxiliary data, also known as ordinary cokriging (OCK) assumes the existence of coregionalization, as well as inter-variable correlation between auxiliary variables (covariates) and the target variable (Mirzaee et al., 2016). According to Webster and Oliver (2007) it has proven useful when soil properties that are cheaper to measure (such as soil pH or EC) or obtain (such as freely available remotely sensed data) can be used to predict other soil properties that are more expensive to measure (such as SOM). Models like OCK often display a smaller spatial error and a stronger interdependence of the collected spatial data. The use of auxiliary data has been studied extensively in recent research. For example, Pouladi et al., (2019) used spectral indices (such as NDVI - Normalised Difference Vegetation Index and SAVI - Soil-Adjusted Vegetation Index) derived from freely available remotely sensed data as covariates to improve SOM predictions in the Jutland peninsula in Denmark. Similarly, Gholizadeh et al. (2018b) used 18 different spectral indices derived from remotely sensed data (via laboratory spectroradiometer measurements and Sentinel-2 data retrieval) to successfully improve mapping of SOC in different agricultural regions of the Czech Republic. Furthermore, Adhikari and Hartemink (2017) and Martinez et al. (2009) found soil EC as auxiliary data useful

for the spatial estimation of SOC in Central Sands, Wisconsin and in southwest Spain, respectively. Moreover, Jiang et al. (2022) conclude that quantitative soil variables as covariates have a more significant impact on the final interpolations than environmental variables (such as elevation, precipitation etc.).

Recent research is also implementing the use of auxiliary data and more complex geostatistical methods in an effort to improve land management strategies and mitigate risks and impact of natural disasters, including wildfires. For example, Lin et al. (2021) used OCK for deriving a reliable map of surface fuel loading in north central Taiwan, similar to Bright et al. (2022) who found random forest (RF), a multivariate method that is often compared to advanced multivariate cokriging (Hengl et al., 2018) useful for fuel load mapping on the Kaibab Plateau in northern Arizona, USA. However, research implementing such advanced geostatistical techniques in the research of wildfire impacts of soil properties is still scarce (Efthimiou et al., 2020; Dindaroglu et al. 2021).

In conclusion, although spatial mapping of SOM has been frequently investigated, space-time dynamics and mapping of post-fire SOM via more complex geostatistical techniques that implement the use of auxiliary data is not yet widely represented in international literature. Therefore, one of the objectives of this study is to compare the accuracy and precision of univariate (OK) with multivariate (OCK) spatial models in mapping SOM in the two-year post-fire period, which will provide valuable insights in the post-fire direction of SOM recovery in the Mediterranean environment.

### 3. MATERIALS AND METHODS

#### 3.1. Location and climate conditions

The study was conducted in Zadar County, Croatia (44° 05' N; 15° 22' E; 72 m a.s.l). The study area was located within a 2 km radius of Zadar airport. The climate is Mediterranean (Csa) according to the Köppen-Geiger classification (Kottek et al., 2006) with an average annual temperature of 14.9 °C and precipitation of 879.2 mm (Figure 3.1). Most of the vegetation in the area consists of *Quercus pubescens* Willd., *Pinus halpensis* Mill., *Pinus pinaster* Ait., *Pinus pinea* L. and *Juniperus communis* L. The soil type is chromic Cambisol (IUSS Working group WRB, 2015). The soil texture is silt loam (USDA soil texture classification system). These soils are characterised by their stable aggregate structure, which allows high permeability and good drainage, as well as high content of weatherable minerals, such as feldspars and ferromagnesian (Husnjak, 2014; Chesworth et al., 2008). The general soil properties of the studied area are shown in Table 3.1.

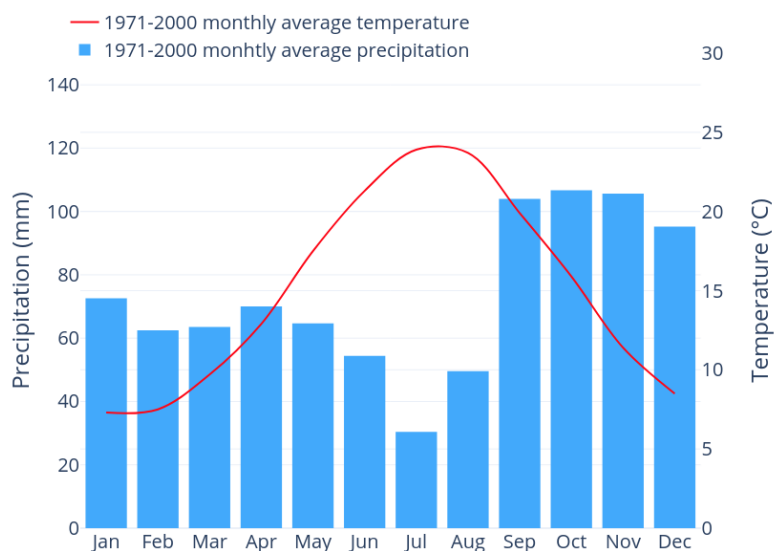


Figure 3.1. Meteorological data of the study location based on the 30-year average.

Source: Zaninović et al., 2008

Table 3.1. General soil properties (0-10 cm) of the study area

Mechanical composition			pH	SOM	EC	CaCO <sub>3</sub>
Sand (%)	Silt (%)	Clay (%)	(-log[H <sup>+</sup> ])	(%)	(μS/cm)	(%)
22.26	55.4	22.34	6.5	3.2	2.0	1.90



## 3.2. Experimental design

The wildfire affected approximately 13.5 ha of a mixed forest of *Quercus pubescens* Willd. and *Juniperus communis* L. on 15<sup>th</sup> August 2019. The severity of the fire was medium to high, as determined by visual inspection of burned vegetation and ash characteristics (Pereira et al., 2018). The experimental set-up was established according to the characteristics of the burned area, following the methodology described in Pereira et al. (2018): (I) - three categories of sampling areas were defined; C – control (unaffected by fire); MS – medium severity (where foliage and tree trunks were partially burned and soil was covered with black ash); HS – high severity (sites where foliage and tree trunks were completely burned and soil was covered with white ash); (II) - 120 soil samples were collected in total according to severity category (each category contained 40 samples). Finally, each category was subdivided according to the two vegetation species, i.e., each of the three severity categories contained 26 sample areas under *Quercus pubescens* Willd. and 14 sample areas under *Juniperus communis* L. (Figure 3.2). Prior to the soil sampling procedure 7 days post-fire, the ash layer on the surface was removed with a soft brush, in order to avoid the contamination of the samples and subsequent false results. Afterward, during the subsequent soil samplings, there was no need for removal of surface ash because it had already been incorporated into the soil profile via precipitation.

Soil samples were collected at a depth of 0-3 cm with a spade and each sampling point was georeferenced using Trimble GeoXH handheld device (GeoExplorer® 6000 series, Trimble GmbH, Raunheim, Germany), and marked with a marking bar. The final experimental design is shown in Figure 3.3. The categorical random sampling procedure led to a randomised sampling grid, where individual points (samples) were on average ~20 m apart (minimal distance between points was 5.4 m and maximal 54.1 m). The markers allowed for periodic soil sampling at the same microsite at seven days (0 MAF), 3 months (3 MAF), 6 months (6 MAF), 9 months (9 MAF), 12 months (12 MAF), 15 months (15 MAF), 18 months (18 MAF), 21 months (21 MAF) and 24 months (24 MAF) post-wildfire within a radius of approximately 0.5 m of the marker (Figure 3.4). A brief summary of the sampling campaign is provided in Table 3.2 and Figure 3.5 shows wildfire affected land seven days post-fire. During each sampling campaign, the collection of 120 soil samples was planned, resulting in a total of 1,080 samples.



Figure 3.2. Sample division according to wildfire severity and vegetation type. A total of 120 samples were divided equally into control samples (C) and two wildfire categories: medium severity (MS) and high severity (HS). Each of the three severity categories was further subdivided into samples collected under *Quercus pubescens* Willd (Q) and *Juniperus communis* L. (J)

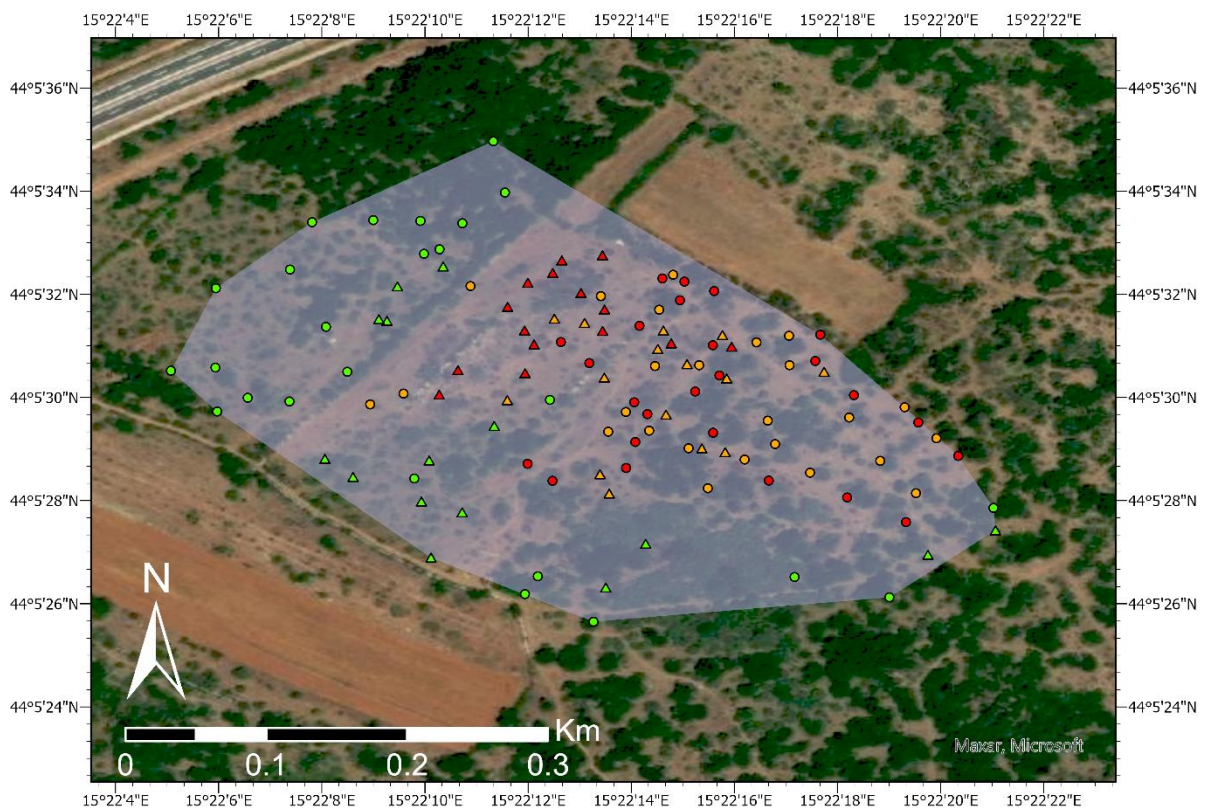


Figure 3.3. Study area and experimental design. Different shapes denote vegetation species (circles indicate samples under *Quercus pubescens* Willd.; triangles indicate samples under *Juniperus communis* L.) and different colours denote wildfire severity (green - C; orange - MS; red - HS)





Figure 3.4. Soil samples collected at three-month intervals at 120 marked locations, each time at a different part of the marked circle within a radius of approximately 0.5 m from the marker



Table 3.2. Summary of the sampling campaign with corresponding dates.

Sampling repetition number	Months after fire	Sampling date
I	0 MAF	22 <sup>nd</sup> August 2019
II	3 MAF	25 <sup>th</sup> November 2019
III	6 MAF	28 <sup>th</sup> February 2020
IV	9 MAF	28 <sup>th</sup> May 2020
V	12 MAF	25 <sup>th</sup> August 2020
VI	15 MAF	27 <sup>th</sup> November 2020
VII	18 MAF	3 <sup>rd</sup> March 2021
VIII	21 MAF	25 <sup>th</sup> May 2021
IX	24 MAF	26 <sup>th</sup> August 2021



Figure 3.5. Wildfire affected land photographed on 22<sup>nd</sup> August 2019

### 3.3. Laboratory analysis

#### 3.3.1. Chemical and physical analysis

Per each sampling campaign, 60 air-dried, ground and sieved (<2 mm) samples were separated for chemical analysis, while the remainder of 60 samples were not subjected to chemical analysis. Soil pH, electrical conductivity (EC), carbonates (CaCO<sub>3</sub>) and total carbon (TC) content were determined using standard analytical methods (Table 3.3).

Table 3.3. Summary of the analytical laboratory methods used in the study

Variable	Units	Method	Reference
pH	-log[H <sup>+</sup> ]	Electrometric (1:2.5 H <sub>2</sub> O solution)	HRN ISO 10390: 2005
Electrical conductivity	μS/cm	Electrometric	HRN ISO 11265: 2004
Carbonates	%	Volumetric	HRN ISO 10693: 2004
Total carbon content	%	Dry combustion	HRN ISO 10694: 2004

Soil pH and EC were determined electrometrically, using Beckman's φ 72 pH meter, in H<sub>2</sub>O (1:2.5), and HACH-CO150 conductometer (300-1900 μS), respectively. CaCO<sub>3</sub> content was determined by volumetric Scheibler calcimeter and TC by dry combustion using a vario MACRO CHNS analyzer (Elementar Analysensysteme GmbH, Langenselbold, Germany). SOM was calculated by multiplying the remainder of the difference between TC and CaCO<sub>3</sub> with a factor 1.724. To minimise laboratory expenses, half of the total collected samples were analysed, while the remaining 50% were estimated using the most effective SOM prediction model.

#### 3.3.2. Measurement of soil reflectance

Measurement of soil spectral reflectance in laboratory conditions was performed on all air-dried, ground and sieved (<2 mm) samples (N=120 for each sampling campaign). The measurements were carried out using a portable spectroradiometer (FieldSpec®3, ASD Inc., Boulder, USA) with a wavelength range of 350 - 1050 nm, a sampling interval of 1.4 nm and a spectral resolution of 3 nm with simultaneous recording of 700 wavelengths. Individual soil samples were placed in 1.5 cm petri dishes and recorded at a fixed distance of 0.5 cm using a vertically mounted manual optical probe (Figure 3.6). Prior to initial readings, the device was calibrated using a white calibration plate (Spectralon®, Labsphere, North Sutton, USA), and

white reference measurements were repeated every 10-15 minutes, as per manufacturer's instructions. The frequency at which the radiation is absorbed gives a reduced reflected signal, which is registered in the detector as a percentage of reflectance (% R). Each sample's reflectance measurement was taken by averaging 3 consecutive scans to reduce the noise in the spectral signal. A total of 1,080 soil spectral reflectance curves were recorded.

In order to compare the accuracy and precision of laboratory and in-situ obtained soil spectra models, soil reflectance was additionally measured on field-moist samples prior to grounding and sieving procedure on two occasions: 25th November 2019 (3 MAF) and 27th November 2020 (15 MAF). In order to determine the soil moisture percentage for soil samples taken on these two occasions, the following formula was used:

$$\text{soil moisture (\%)} = \frac{\text{weight of field moist soil (g)} - \text{weight of oven dry soil (g)}}{\text{weight of oven dry soil (g)}} * 100$$



Figure 3.6. Laboratory measurement of soil reflectance on air dried samples using FieldSpec®3 spectroradiometer

### 3.4. Satellite imagery acquisition and processing

Two cloud-free Sentinel-2 images (level-2A processing) of the survey location were downloaded from Copernicus Open Access Hub (<https://scihub.copernicus.eu/>) according to the closest dates of field sampling, namely 31<sup>st</sup> August and 5<sup>th</sup> September 2019. Sentinel-2 is a European Space Agency satellite mission equipped with a multispectral optical imaging instrument that collects data from thirteen (13) spectral bands: four VNIR bands at 10 m, six

VNIR and SWIR bands at 20 m and three bands at 60 m spatial resolution focused towards cloud screening and atmospheric correction (Table 3.4).

Table 3.4. Information on Sentinel-2 wavelengths and bandwidths (Source: <https://sentinel.esa.int>)

Spatial Resolution (m)	Band Number	S2A		S2B	
		Central Wavelength (nm)	Bandwidth (nm)	Central Wavelength (nm)	Bandwidth (nm)
10	2	492.4	66	492.1	66
	3	559.8	36	559.0	36
	4	664.6	31	664.9	31
	8	832.8	106	832.9	106
20	5	704.1	15	703.8	16
	6	740.5	15	739.1	15
	7	782.8	20	779.7	20
	8a	864.7	21	864.0	22
	11	1613.7	91	1610.4	94
	12	2202.4	175	2185.7	185
60	1	442.7	21	442.2	21
	9	945.1	20	943.2	21
	10	1373.5	31	1376.9	30

The full mission contains twin satellites (Sentinel-2A and Sentinel-2B) flying in the same orbit but phased at 180°, which allows a high revisit frequency of 5 days at the Equator. The level 2A images are atmospherically corrected from level-1C Top of the Atmosphere (ToA) to Bottom of Atmosphere (BoA) reflectance using Sen2cor processor (Main-Knorn et al., 2017). All of the image processing, visualisation and analysis was performed using freely available software developed by European Space Agency (ESA), SNAP-Sentinel Application Platform (<http://step.esa.int>). The software enables the extraction of multispectral data from atmospherically corrected image pixels, as is shown in Figure 3.7.



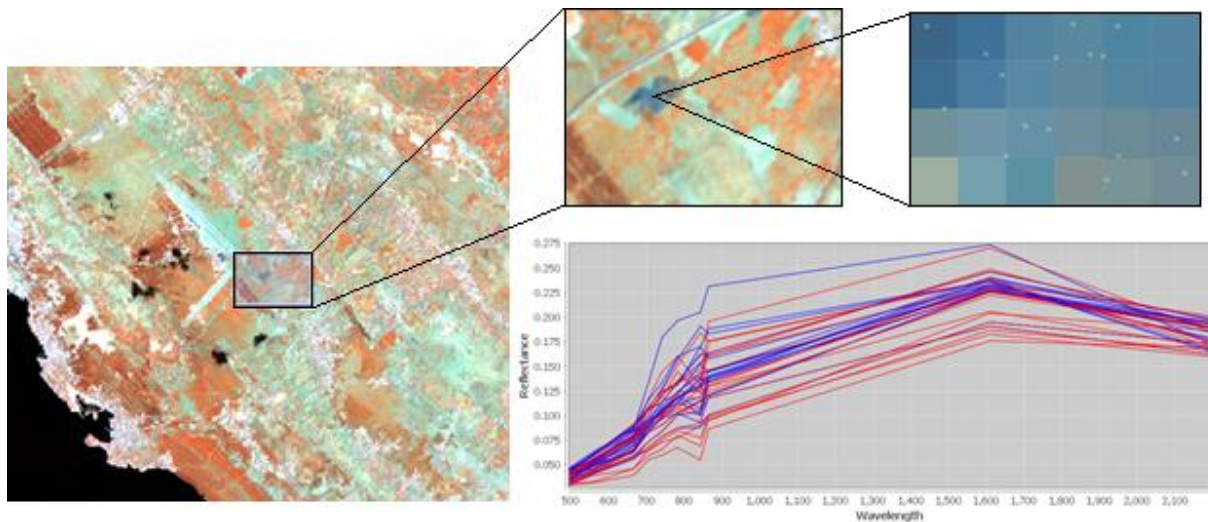


Figure 3.7. Sentinel-2 image and multispectral reflectance curves obtained from image pixels

Due to the large data volume of the images, which hinders the computing and analysis time, the images were first subsetting to the smaller area of interest. Eight VNIR and two SWIR (Short-Wave Infrared) bands with spatial resolution of 20 and 10 m were selected, and bands B1, B9 and B10 were omitted from the study because of their coarser 60 m resolution. The details of each band selected for the study are shown in Table 3.5. Subsequently, the images were resampled to uniform spatial resolution of 10 m using the nearest neighbour resampling. Some of the georeferenced sample points were uploaded to the resulting images and the reflectance values overlapping with the pixels extracted (N=28). Thereby, we generated two separate datasets with reflectance values obtained from two different sources (FieldSpec®3 hyperspectral and Sentinel-2 multispectral) for further model comparison.

Table 3.5. Summary description of the multispectral bands used in the study

Band	Spatial Resolution (m)	Spectral range (nm)	Central wavelength (nm)	Description
B2	10	458–523	490	Blue
B3	10	543–578	560	Green
B4	10	650–680	665	Red
B5	20	698–713	705	VNIR
B6	20	733–748	740	VNIR
B7	20	773–793	783	VNIR
B8	10	785–900	842	VNIR
B8a	20	855–875	865	VNIR
B11	20	1565–1655	1610	SWIR
B12	20	2100–2280	2190	SWIR



## 3.5. Statistical analysis and predictive modelling

### 3.5.1. Descriptive statistics and variability of soil properties after the wildfire

Before the statistical analysis was carried out, the collected data were checked for normality visually using Q-Q plots and histograms, and statistically using Kolmogorov-Smirnov test. The data was transformed when needed to meet the normality criterion in further statistical analysis using several techniques: logarithmic, Box-Cox and Yeo-Johnson transformations (McGrath et al., 2004; Yeo and Johnson, 2000; Box and Cox, 1964). Z-scores were subsequently calculated in order to detect outliers, which were removed if the score exceeded 3 standard deviations (Kannan et al., 2015). Once the normalised data were obtained, a factorial ANOVA was used to determine the percentage of variation attributable to each of the factors: fire severity, time and vegetation type. Tukey's HSD test was applied where significant differences were observed ( $p < 0.05$ ). Where data normality could not be achieved, a non-parametric Kruskal-Wallis analysis was applied and multiple comparison of mean ranks for all groups was applied where significant differences were observed ( $p < 0.05$ ).

The analysis was performed in the R 3.6.2 environment (R Core Team, 2021) using ggbiplot (v0.55), plyr (v1.8.5) and car (v3.0-6) packages, and Statistica 12.0 software (StatSoft, Inc., 2013). Graphs were created using Plotly Chart Studio (Plotly Technologies Inc., 2015).

### 3.5.2. Spectral data analysis and model development

Raw spectral reflectance data was used in all model developments, and spectral bands from 350 to 409 nm were removed due to large noise effect. If needed, for improvement of the signal-to-noise ratio, transformations of the original spectra were performed using first and second derivatives, as well as Savitzky-Golay filter using a second-order polynomial for derivation and smoothing (Nawar and Mouazen, 2017; Ben-Dor et al., 1997).

For the development of calibration and validation models for the prediction of SOM content based on VNIR spectral reflection two models were compared. First, multivariate linear partial least squares regression (PLSR), and second, non-linear neural networks (ANN). The independent (predictor, x-variable) input was the raw reflectance data in the range from 410-1050 nm, and the dependent (y-variable) input was the SOM content. The datasets were split in two parts: calibration (50%) and validation (50%).

Spectral data were subjected to principal component analysis (PCA) prior to ANN modelling due to its computationally demanding processing time. PCA is a technique that can be used

to reduce the dimensionality of a large number of spectral variables. PCs are computed as linear combinations of the spectral data that explain the most variance that are not mutually correlated. The first PC is the combination that accounts for the largest amount of variance in the sample, and each of the next PCs explain progressively smaller variance, until only those individual PCs that capture more than 0.1% of the variance in the data set are calculated and retained (Ringnér, 2008). In this study, PCA was applied to all of the 641 spectral variables (wavelengths), and the PC scores obtained via PCA analysis were used as input variables in the ANN modelling procedure.

For comparison of the accuracy and precision of prediction models described in Objective 3 (see Chapter 1.1.), the subsets of the original collected dataset (N=1080) were defined as follows:

1. In order to compare the accuracy and precision of linear and non-linear hyperspectral prediction models, reflectance data for the entire reflectance dataset collected over the 2-year study period was subjected to predictive SOM modelling (N=1080). Afterwards, this dataset was split according to the N of the sampling periods (0-24 MAF) and each model was compared (N=120).

2. In order to compare the accuracy and precision of hyperspectral prediction models using laboratory and in-situ measurements, reflectance data collected on 25th November 2019 (3 MAF) and 27th November 2020 (15 MAF) was used (N=240). On these two occasions the same soil samples were measured in field-moist and air dry state.

3. For comparison of the accuracy and precision of hyperspectral and multispectral (Sentinel-2) reflectance prediction models, partial reflectance data collected in the immediate post-fire period (0 MAF) was used (N = 28).

The original spectral data measured by spectroscopy and satellite imaging was processed by pre-treatment and transformation methods in ViewSpec Pro 4.07 software (ASD Inc., USA). Analysis of spectral data and SOM content (%) was performed using statistical analysis methods in the Unscrambler 9.7 spectral data analysis software tool (CAMO Software AS., Norway) and in the statistical package Statistica 12.0 (StatSoft, Inc., USA).

Models were tested for reliability and prediction ability using full cross-validation (each individual sample was used to test model estimates based on all other samples). The best performing models were used to predict the samples with undetermined SOM (N = 60). For the purpose of analysing the accuracy and performance of the model, the following was used:

coefficient of determination ( $R^2$ ), root mean square error (RMSE), and ratio of performance to deviation (RPD). Significance values for the entire statistical analysis will be performed for an error probability level of  $p < 0.05$ . RMSE is defined as:

$$RMSE = \sqrt{\frac{\sum_{s=0}^n (Os - Ps)^2}{n}},$$

where  $O_s$  and  $P_s$  are the observed and predicted values of SOM, and  $n$  is the number of samples. Models with the highest  $R^2$  and the lowest RMSE were considered as the best to predict post-fire SOM. RPD was calculated as the ratio between standard deviation (SD) of the reference SOM content against the root mean squared error of prediction ( $RMSE_p$ ), and evaluated according to the classification system shown in Table 3.6. According to Gholizadeh et al. (2018b) poor models can be used in differentiation between high and low values, however they cannot be used for quantitative predictions. Quantitative predictions are possible at RPD values greater than 1.8. A step-by-step illustration of the overall modelling process is shown in Figure 3.8.

Table 3.6. Classification system for model accuracy assessment determined by ratio of performance to deviation (RPD) value

RPD value	Classification of the model
< 1.0	very poor
1.0 < RPD < 1.4	poor
1.4 < RPD < 1.8	fair
1.8 < RPD < 2.0	good
2.0 < RPD < 2.5	very good
> 2.5	excellent

Source: Gholizadeh et al. (2018b)

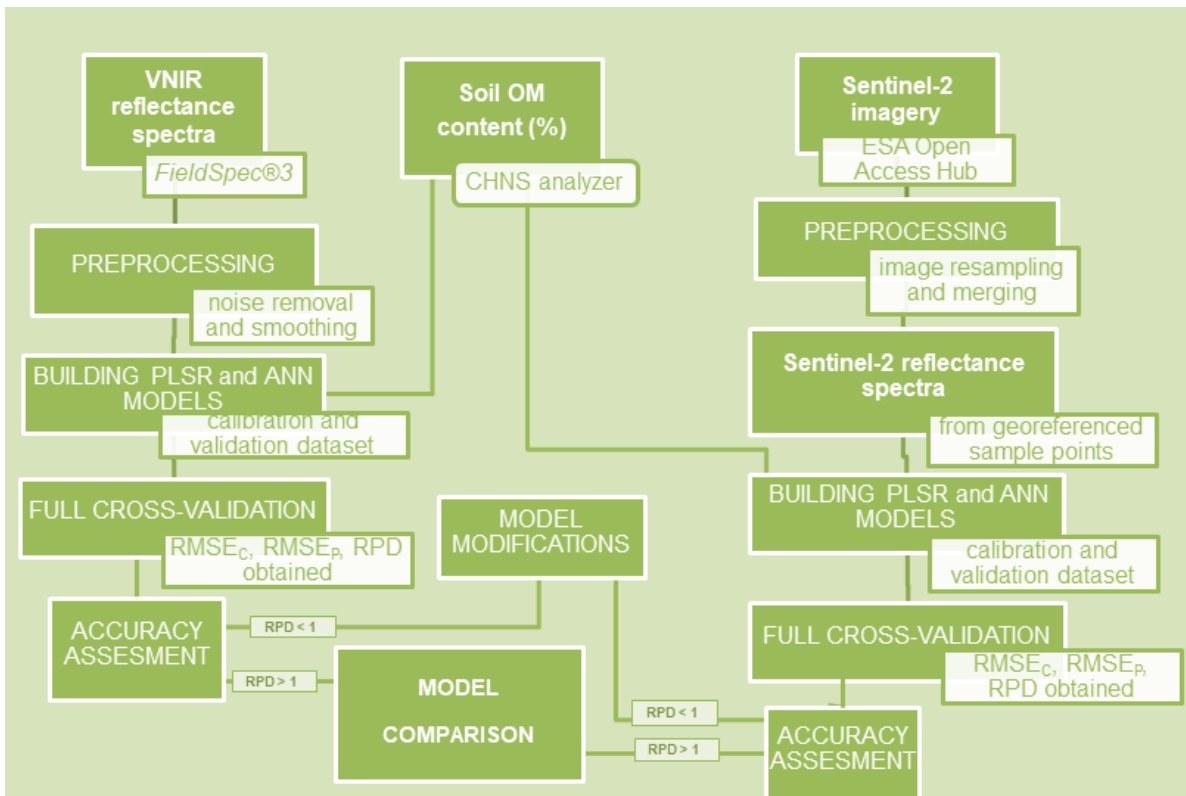


Figure 3.8. Schematic overview of spectral modelling procedure for comparison of hyperspectral and multispectral datasets. The procedure is similar when building models to compare in-situ and laboratory datasets

### 3.6. Geostatistical univariate and multivariate modelling and mapping

Geostatistical mapping was performed using ArcGis Pro 2.6.0 (ESRI, 2020). Spatial connectivity of collected SOM data was tested for anisotropy using directional semivariograms, and spatial dependence was assessed using the nugget/sill ratio.

Afterwards, the values for non-sampled sites were evaluated using two different interpolation methods. For univariate interpolation, ordinary kriging (OK) was used, and for multivariate interpolation, ordinary cokriging (OCK) was used. The covariates used were soil pH, EC, CaCO<sub>3</sub> content and average reflectance value calculated from 410-1050 nm wavelengths obtained with a proximal sensor. Furthermore, for the 0 MAF exclusively, the satellite sensor band that exhibited the highest correlation with SOM was utilised as a covariate. Anisotropy was taken into account for acquisition of the best fitted semivariogram models. In each interpolation, a maximum of 5 neighbours were included, and weights were assigned in a search neighbourhood divided into 4 sectors with 45° offsets. The accuracy of the variograms and the generated maps was evaluated using the root mean square error (RMSE) after cross-validation. The relative improvement (RI) in RMSE was used to measure the improvement on the prediction accuracy of OCK over the OK method, which was calculated using the following formula:

$$RI (\%) = \frac{RMSE_{OK} - RMSE_{OCK}}{RMSE_{OK}} * 100$$

## 4. RESULTS

### 4.1. Meteorological observations

Extreme meteorological conditions were recorded in all years studied (2019-2021), as shown in Figure 4.1. In 2019, 224.5 mm more annual precipitation was recorded than the 30-year average (1971-2000), and the month of November recorded an extreme 183 mm above-average precipitation (Table 4.1). Therefore, 2019 was assessed as „very wet“ by the Croatian Meteorological and Hydrological Service (DHMZ, data freely available at: <https://meteo.hr/>).

July of 2019 alone received 38.5 mm of precipitation more than average (Table 4.1), which influenced the moisture content of the vegetation and soil, ultimately causing the decrease in both wildfire number and severity in the area (Croatian Fire Brigade, 2022).

Although roughly average annual precipitation was recorded in 2020 and 2021, the values show considerable month-to-month variability and a period of prolonged drought in the winter and spring months, followed by extreme precipitation in the fall (November 2019 and October 2020). Similarly, average annual temperatures remained around 15 °C during the study years, although above-average temperatures were consistently recorded during the summer months. For example, August was 2.1, 1.9, and 1.2 °C above 30-year average temperatures in 2019, 2020, and 2021, respectively.

In view of the fact that ash produced by the wildfire is highly mobile, and is quickly redistributed and incorporated into the soil via wind and water (Pereira et al., 2019), it is important to mention that the first major precipitation events were recorded approximately 30 days post-fire, on 24<sup>th</sup> and 26<sup>th</sup> of September 2019, with 19.1 and 44.9 mm of rain, respectively.

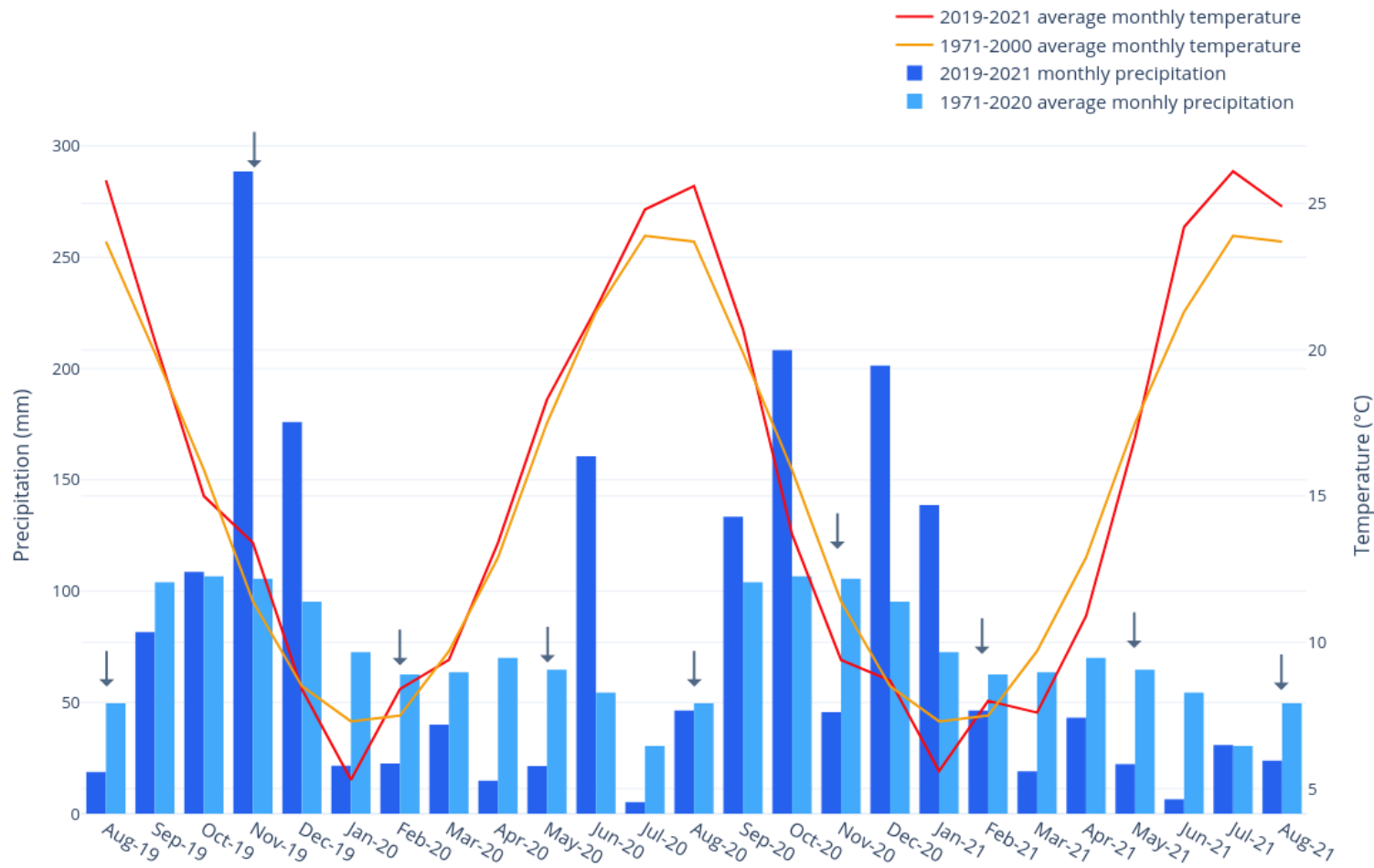


Figure 4.1. Monthly precipitation and temperature during the studied years in comparison with the 30-year average (1971-2020). The arrows indicate the dates on which sampling campaigns were carried out. *Graph data source: Croatian Meteorological and Hydrological Service (DHMZ)*

Table 4.1. Meteorological data in the studied years and their deviation from the 30-year average

	2019	2020	2021	1971-2000	Difference 2019	Difference 2020	Difference 2021
<b>Temperature, °C</b>							
January	4.5	5.3	5.6	7.3	-2.8	-2.0	-1.7
February	7.6	8.4	8.0	7.5	+0.1	+0.9	+0.5
March	10.5	9.4	7.6	9.7	+0.8	-0.3	-2.1
April	13.7	13.4	10.9	12.9	+0.8	+0.5	-2.0
May	14.9	18.3	17.0	17.5	-2.6	+0.8	-0.5
June	24.9	21.4	24.2	21.3	+3.6	+0.1	+2.9
July	25.5	24.8	26.1	23.9	+1.6	+0.9	+2.2
August	25.8	25.6	24.9	23.7	+2.1	+1.9	+1.2
September	20.3	20.7	20.6	19.9	+0.4	+0.8	+0.7
October	15.0	13.7	16.1	15.9	-0.9	-2.2	+0.2
November	13.4	9.4	12	11.4	+2.0	-2.0	+0.6
December	8.4	8.7	8.5	8.5	-0.1	+0.2	+0.0
<b>Average</b>	<b>15.4</b>	<b>14.9</b>	<b>15.1</b>	<b>15.0</b>	<b>+0.4</b>	<b>-0.03</b>	<b>+0.17</b>
<b>Precipitation, mm</b>							
January	87.1	21.6	138.7	72.6	+14.5	-51.0	+66.1
February	13.9	22.5	46.4	62.5	-48.6	-40.0	-16.1
March	30.7	40.0	19.0	63.5	-32.8	-23.5	-44.5
April	104.0	14.8	43.1	70	+34.0	-55.2	-26.9
May	118.6	21.4	22.2	64.7	+53.9	-43.3	-42.5
June	6.9	160.7	6.5	54.4	-47.5	+106.3	-47.9
July	68.9	5.2	30.8	30.4	+38.5	-25.2	+0.4
August	18.8	46.3	23.8	49.6	-30.8	-3.3	-25.8
September	81.6	133.4	78.4	104	-22.4	+29.4	-25.6
October	108.6	208.3	139.7	106.7	+1.9	+101.6	+33.0
November	288.6	45.6	175.9	105.6	+183.0	-60.0	+70.3
December	176.0	201.3	123.8	95.2	+80.8	+106.1	+28.6
<b>Total</b>	<b>1103.7</b>	<b>921.1</b>	<b>848.3</b>	<b>879.2</b>	<b>+224.5</b>	<b>+41.9</b>	<b>-30.9</b>

Table data source: Croatian Meteorological and Hydrological Service (DHMZ)



## 4.2. Field observations of post-fire vegetation recovery and visual soil status report

As previously stated, Mediterranean localities are well adapted to wildfire, and the good aggregate structure of the soil of the studied area (chromic Cambisol) allows high permeability and good drainage and high content of weatherable minerals that provide the nutrients needed for resprouting. Additionally, the terrain is flat, which neutralises the danger of post-fire soil erosion by water and runoff.

With that in mind, this chapter briefly describes the key on-site post-fire occurrences in hopes to improve and clarify the temporal evolution of SOM content and other soil properties as measured via laboratory analysis, chemometric methods and observed via remote sensing, and discussed in the following chapters. A visual overview of the field work and the initial post-fire soil status is shown in Figure 4.2.

By visually monitoring the vegetation recovery on the study site, it can be stated that a regrowth of vegetation in MS occurred as early as 3 MAF. The majority of MS areas affected by the fire in that timeframe exhibited native grass regrowth, mixed with other perennial plant species, such as ferns and creepers. On the other hand, HS samples did not follow this trend and were still mostly bare.

In the following vegetation season of 2020, namely on 6 and 9 MAF, MS samples continued to exhibit vegetation regrowth in the form of native grasses, which seemed to start to suppress all other vegetation species that started growing while the soil surface was stripped of vegetation following the wildfire (Figure 4.2.b and 4.2.c). During this time, vegetation started resprouting in HS areas, and consisted mostly of ferns and procumbent/creeper species, but the soil surrounding them was still exposed (Figures 4.3.c and 4.4.c). Vigorous resprouting at the base of the burned *Quercus p. Willd.* was observed in both MS and HS areas (see upper right corner of Figure 4.3.c), while resprouting of the *Juniperus c. L.* was spotted mostly in HS areas where there was no competition with other species (see upper left corner of Figure 4.5.a).

By the 21 and 24 MAF sampling period, MS areas were visually much more comparable to C, while soil in HS areas was still rather exposed (Figures 4.6 and 4.7). Furthermore, the long-term presence of charred material was observed in HS areas throughout the study period (Figure 4.5), while in MS it appeared to be less abundant and more readily incorporated into the soil profile (compare Figure 4.4.b and 4.4.c).

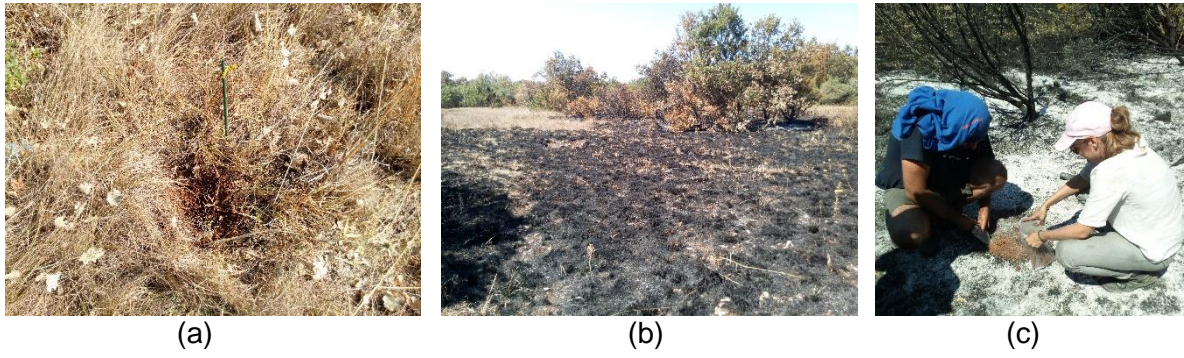


Figure 4.2. Soil condition on 22<sup>nd</sup> August 2019 (7 days post-wildfire): a) control, b) medium severity, c) high severity

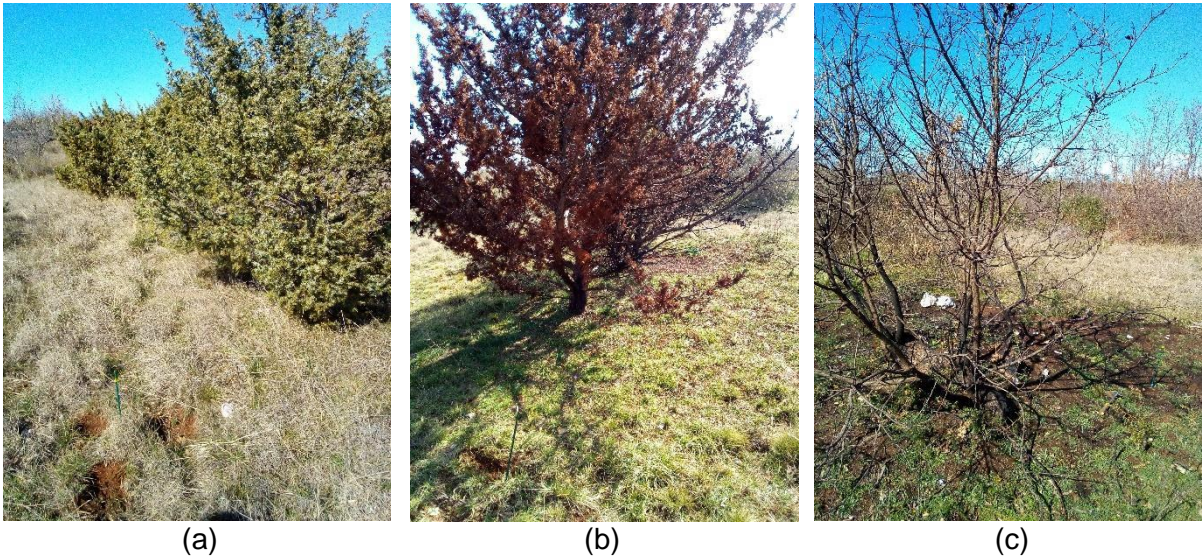


Figure 4.3. Soil condition on 28<sup>th</sup> February 2020 (6 months post-wildfire): a) control, b) medium severity, c) high severity



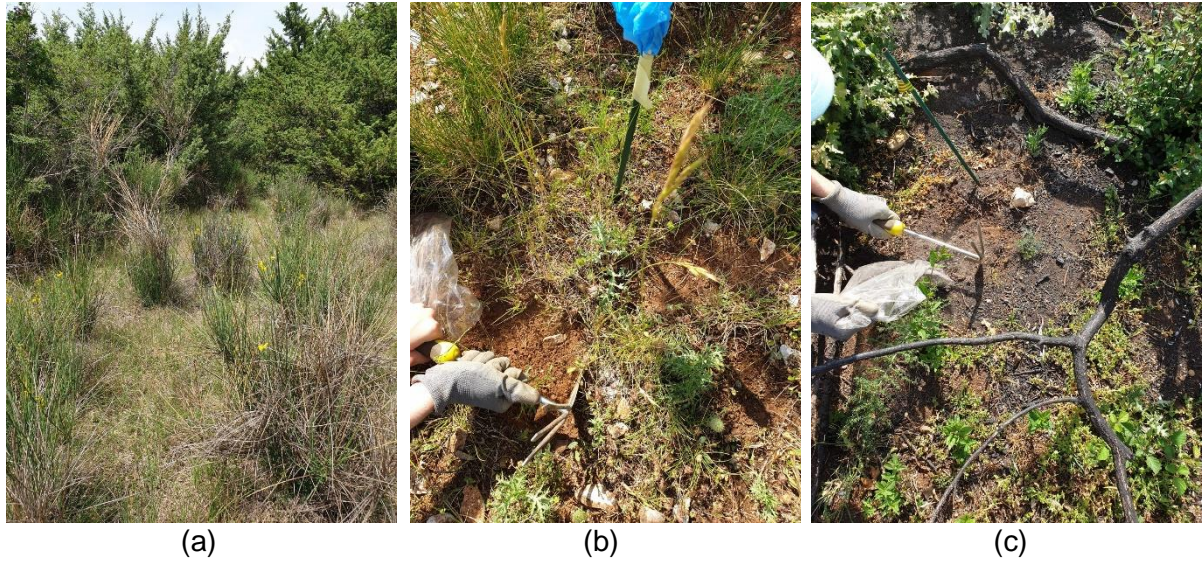


Figure 4.4. Soil condition on 28<sup>th</sup> May 2020 (9 months post-wildfire): a) control, b) medium severity, c) high severity



Figure 4.5. Charred material on the surface of the HS sampling area photographed on: a) 28<sup>th</sup> February 2020 (6 months post-wildfire), and b) 03<sup>rd</sup> March 2021 (18 months post-wildfire)





(a)

(b)

(c)

Figure 4.6. Soil condition on 25<sup>th</sup> May 2021 (21 months post-wildfire): a) control, b) medium severity, c) high severity



(a)

(b)

(c)

Figure 4.7. Soil condition on 26<sup>th</sup> August 2021 (24 months post-wildfire): a) control, b) medium severity, c) high severity

### 4.3. Soil organic matter content after the wildfire

Throughout the 2-year sampling period, the plan was to collect 120 soil samples per campaign. However, at certain C sampling sites, the unexpectedly dense vegetation at 21 MAF and 24 MAF impeded access to the area, thus preventing sample collection. Consequently, only 1,074 samples were collected out of the intended 1,080 samples.

In order to check the normality of the collected SOM data normal Q-Q plot and histogram were created (Figure 4.8). Additionally, a Kolmogorov-Smirnov test was performed (N=537). The results of the test showed that the distribution of SOM content does not conform to normally distributed data (K-S d = 0.16, p-value < 0.001). After the Box-Cox transformation the Z-scores were calculated and 2 outliers were detected and removed from further analysis. In the context of detecting outliers, Z scores can be used to identify data points that deviate significantly from the average. Normal Gaussian distribution was achieved after transformation (Figure 4.8), and this dataset was used for further analysis.

Overall SOM content during the study period and according to the wildfire severity and vegetation type are presented in Table 4.2. Both the standard deviation (SD) and coefficient of variation (CV) indicate moderate variability in the data set (according to Zhang et al., 2007), especially in the immediate post-fire period (SD = 4.49, CV = 0.53) and at the end of the two-year study (SD = 6.58, CV = 0.55). The average SOM content varied from 6.9 to 11.89% throughout the study period. The overall lowest content of 3.72% was recorded 21 months after wildfire in HS samples and under *Quercus pubescens* Willd. while the highest content of 33.19% was recorded 24 months after wildfire in C samples under the same vegetation type.

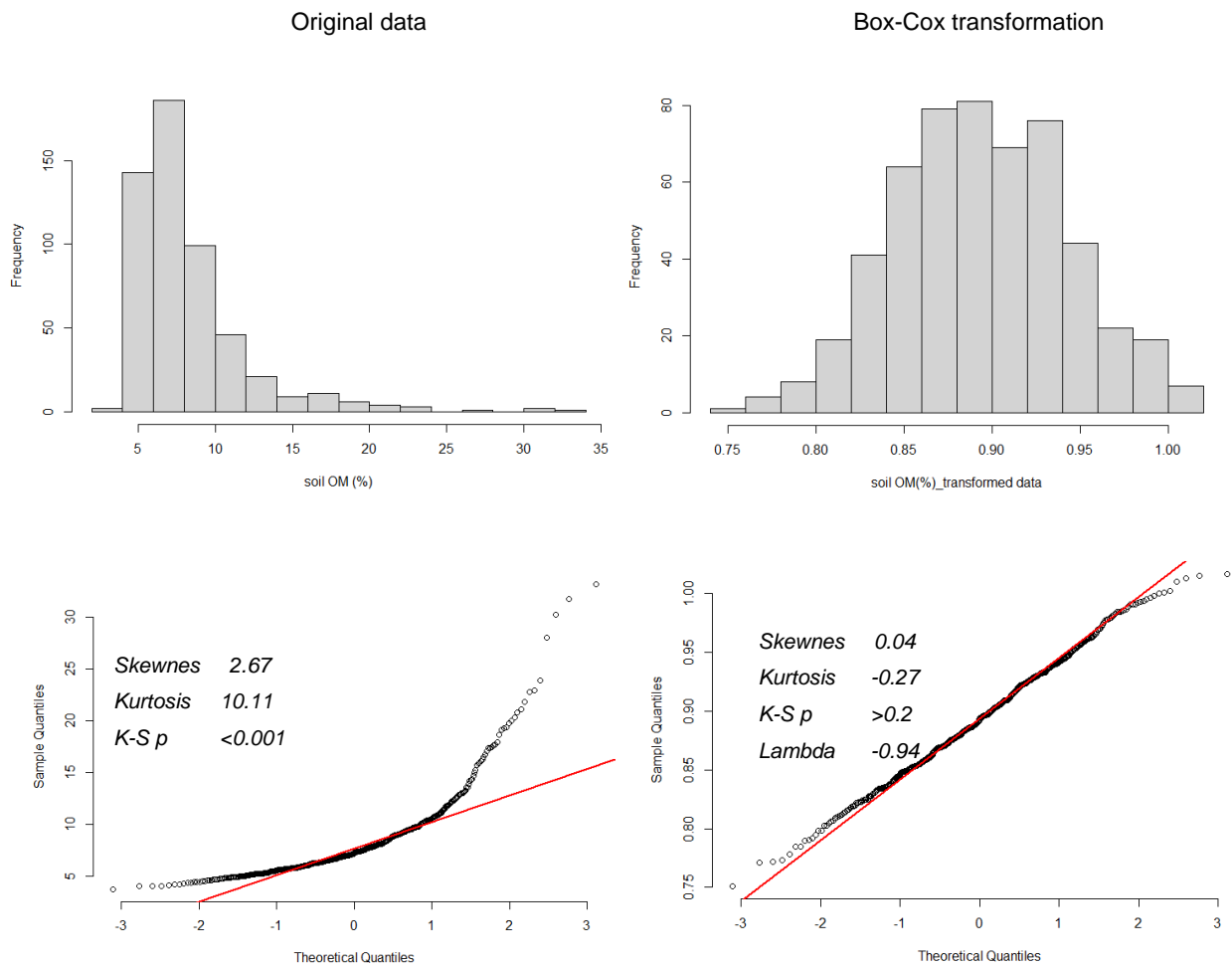


Figure 4.8. Histogram and Q-Q plot for SOM content before and after transformation (N=537)

Table 4.2. Descriptive statistics of SOM content (%) for nine sampling times, three wildfire severity levels and two vegetation types

	Sampling time									Wildfire severity			Vegetation	
	0 MAF	3 MAF	6 MAF	9 MAF	12 MAF	15 MAF	18 MAF	21 MAF	24 MAF	C	MS	HS	<i>Quercus p.</i>	<i>Juniperus c.</i>
N	60	60	60	60	60	60	60	56	59	178	179	178	348	187
Mean	8.54	7.30	7.92	7.42	6.90	7.38	7.80	7.01	11.89	7.55	7.31	9.19	8.94	7.04
Min	4.68	4.52	4.21	4.01	4.44	4.38	4.03	3.72	4.99	4.01	4.00	3.72	3.72	4.00
Max	23.89	20.34	22.80	17.92	12.93	15.94	16.07	21.85	33.19	33.19	22.96	31.76	33.19	27.99
SD	4.49	2.81	3.28	2.65	2.13	2.37	2.51	3.20	6.58	3.58	2.80	4.64	3.97	3.33
CV	0.53	0.38	0.41	0.36	0.31	0.32	0.32	0.46	0.55	0.47	0.38	0.50	0.44	0.47

MAF – Months after fire; C – Control; MS – Medium severity; HS – High severity; SD – Standard deviation; CV – Coefficient of variation

Factorial analysis of variance revealed that the content in SOM varied significantly over time, and according to the severity of wildfire and vegetation type (Table 4.3). High severity wildfire caused an overall 21.72% increase in average SOM content, while medium severity wildfire did not cause a significant change compared to unburned samples (Table 4.3). In addition, SOM content was significantly higher under *Quercus p.* than *Juniperus c.* throughout the study period. The interaction between wildfire *severity x time* factors was significant, while all other interactions between factors were not significant.

Table 4.3. Results of the factorial ANOVA and the mean values for the content of the SOM depending on the severity of the wildfire, time, vegetation and their interactions

	SOM (%)	N
T	*	
FS	*	
V	*	
T x FS	*	
T x V	n.s.	
FS x V	n.s.	
FS x V x T	n.s.	
<b>Time-Since-Fire</b>		
0 MAF	8.54 ± 0.45 b	60
3 MAF	7.30 ± 0.45 b	60
6 MAF	7.92 ± 0.45 b	60
9 MAF	7.42 ± 0.45 b	60
12 MAF	6.90 ± 0.45 b	60
15 MAF	7.38 ± 0.45 b	60
18 MAF	7.80 ± 0.45 b	60
21 MAF	7.01 ± 0.48 c	56
24 MAF	11.89 ± 0.45 a	59
<b>Fire severity</b>		
C	7.55 ± 0.26 b	178
MS	7.31 ± 0.26 b	179
HS	9.19 ± 0.26 a	178
<b>Vegetation</b>		
<i>Quercus p.</i>	8.94 ± 0.18 a	348
<i>Juniperus c.</i>	7.04 ± 0.24 b	187

Abbreviations: FS – Fire severity; V - Vegetation; T- Time; C – Control; MS – Medium severity; HS – High severity; MAF – Months after fire. \* – Significant difference at  $p < 0.05$ ; n.s. not significant at  $p < 0.05$ . Different letters represent significant ( $p < 0.05$ ) differences between fire severity, sampling time and vegetation. Values following  $\pm$  indicate standard deviation.

In the first 15 MAF, HS showed significant increase compared to C (Figure 4.9). The initial average (0 MAF) SOM content in C samples was 7.09%, and measured content in severely burned areas (0 MAF-HS) was 10.5%, which is a 48.1% increase. During the next five sampling periods (3, 6, 9, 12 and 15 MAF) the average SOM content in HS was 34.88%, 46.97%, 43.65%, 14.89% and 20.7% higher than content measured in C samples. In the following period (18, and 21 MAF) the content of SOM was higher in HS compared to C, although not significantly. The SOM content in MS showed an 8.68% increase in the immediate post-fire period (0 MAF) compared to C, which is notably lower than the increase observed in HS. No significant change compared to C was recorded during the 3, 6, 12, 15, 18 and 21 MAF. On the final sampling date (24 MAF), MS showed 29.97% decrease in average SOM content compared to C, while there was no significant difference between C and HS samples.



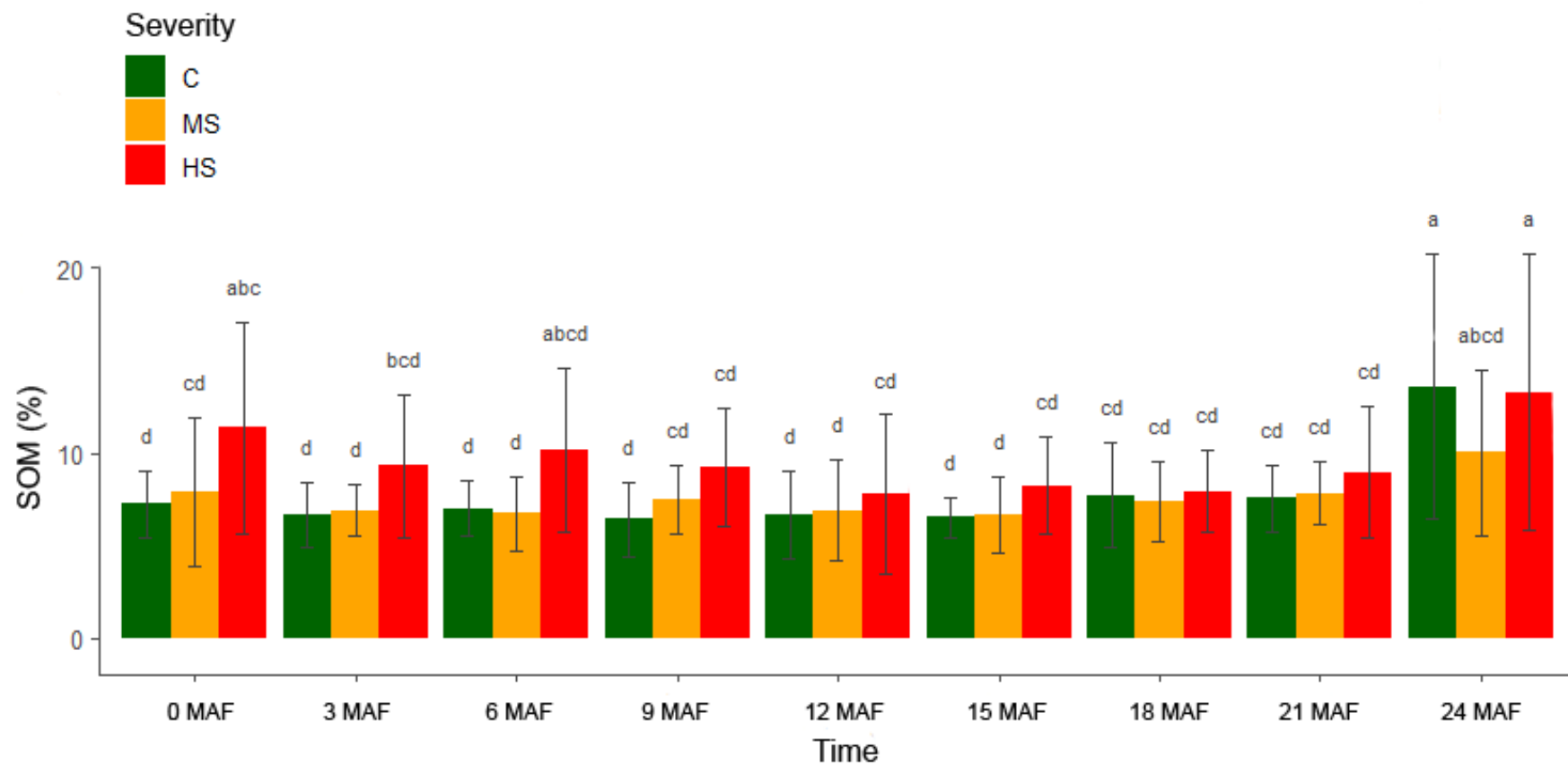
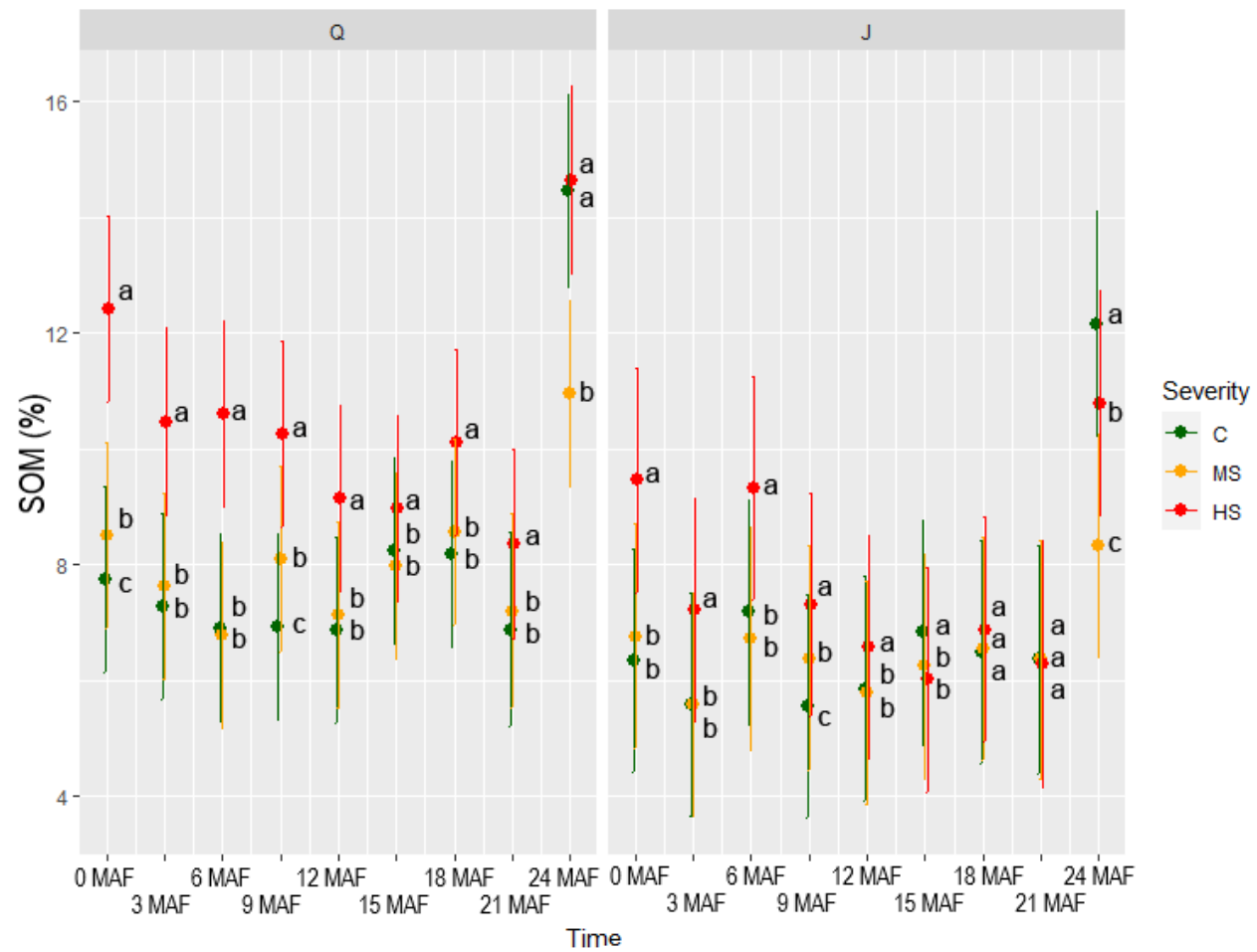


Figure 4.9. Mean SOM content (%) according to the interaction of the wildfire severity and time-since-fire factors. Whiskers represent standard deviation. Different letters indicate significant ( $p < 0.05$ ) differences between wildfire severity and time-since-fire.

In Figure 4.10. the average SOM content (%) according to the interaction of the wildfire severity, time-since-fire and vegetation factors is shown. As can be seen from the graph, the higher content was recorded under *Quercus p.* species in C, MS and HS samples. Moreover, higher SOM content compared to C persisted in Q-HS samples almost throughout the study period, while in J-HS samples it was higher during the first 15 months post-fire. At 24 MAF, lower content of SOM was observed in Q-MS and J-MS compared to both Q-HS and Q-C.



Abbreviations: C – Control; MS – Medium severity; HS – High severity; MAF – Months after fire; Q – *Quercus p.*; J – *Juniperus c.*

Figure 4.10. Mean SOM content (%) according to the interaction of the wildfire severity, time-since-fire and vegetation factors. Whiskers represent 95% confidence intervals. Different letters indicate significant ( $p < 0.05$ ) differences between wildfire severities on each given date

#### 4.4. Other soil properties after the wildfire

The results of statistical normality check showed that the distribution of soil pH conforms to normally distributed data (K-S  $d = 0.06$ ,  $p\text{-value} = 0.001$ ), while EC (K-S  $d = 0.22$ ,  $p\text{-value} < 0.001$ ) and  $\text{CaCO}_3$  (K-S  $d = 0.35$ ,  $p\text{-value} < 0.001$ ) required transformations. Several transformation techniques were attempted: logarithmic, and more powerful Box-Cox and Yeo-Johnson transformations (McGrath et al., 2004; Yeo and Johnson, 2000; Box and Cox, 1964). Box-Cox transformation of EC data achieved the most satisfactory Gaussian curve, although data normality was not achieved in its entirety (Figure 4.11). The  $\text{CaCO}_3$  dataset contained zero values, and seeing how Box-Cox transformation is only valid for positive  $x$ , the zero values were arbitrarily replaced with a positive constant, as proposed in Bellego and Pape (2019). This approach, however, also did not produce satisfactory results and a normal Gaussian distribution, and so a decision was made to use the original data in further analysis. The justification for this approach was explained by Raymaekers and Rousseeuw (2021) who argue that normality should fit the central part of the data, which is true in the case of  $\text{CaCO}_3$  dataset (Figure 4.12).

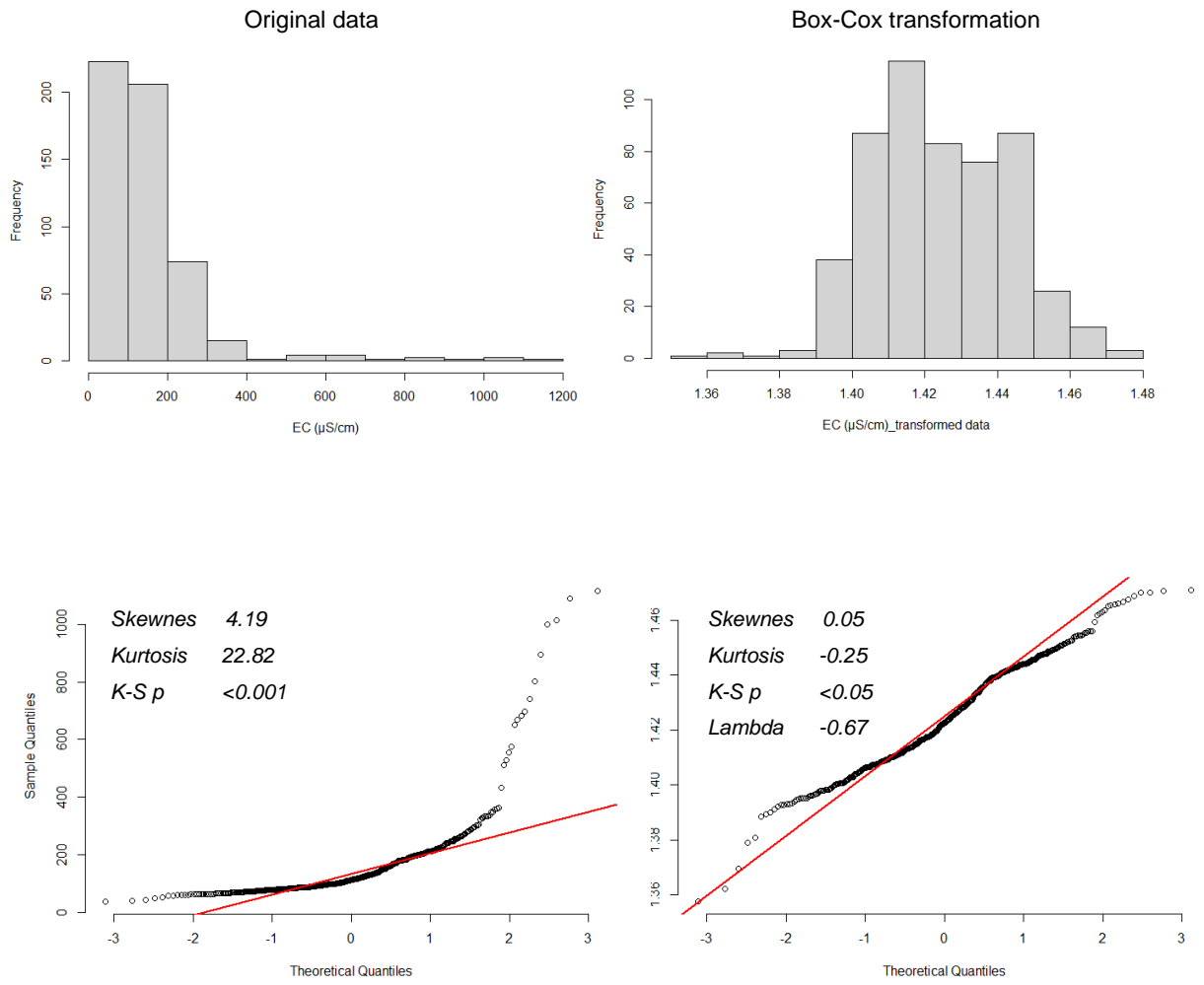


Figure 4.11. Histogram and Q-Q plot for soil EC data before and after transformation (N=535)

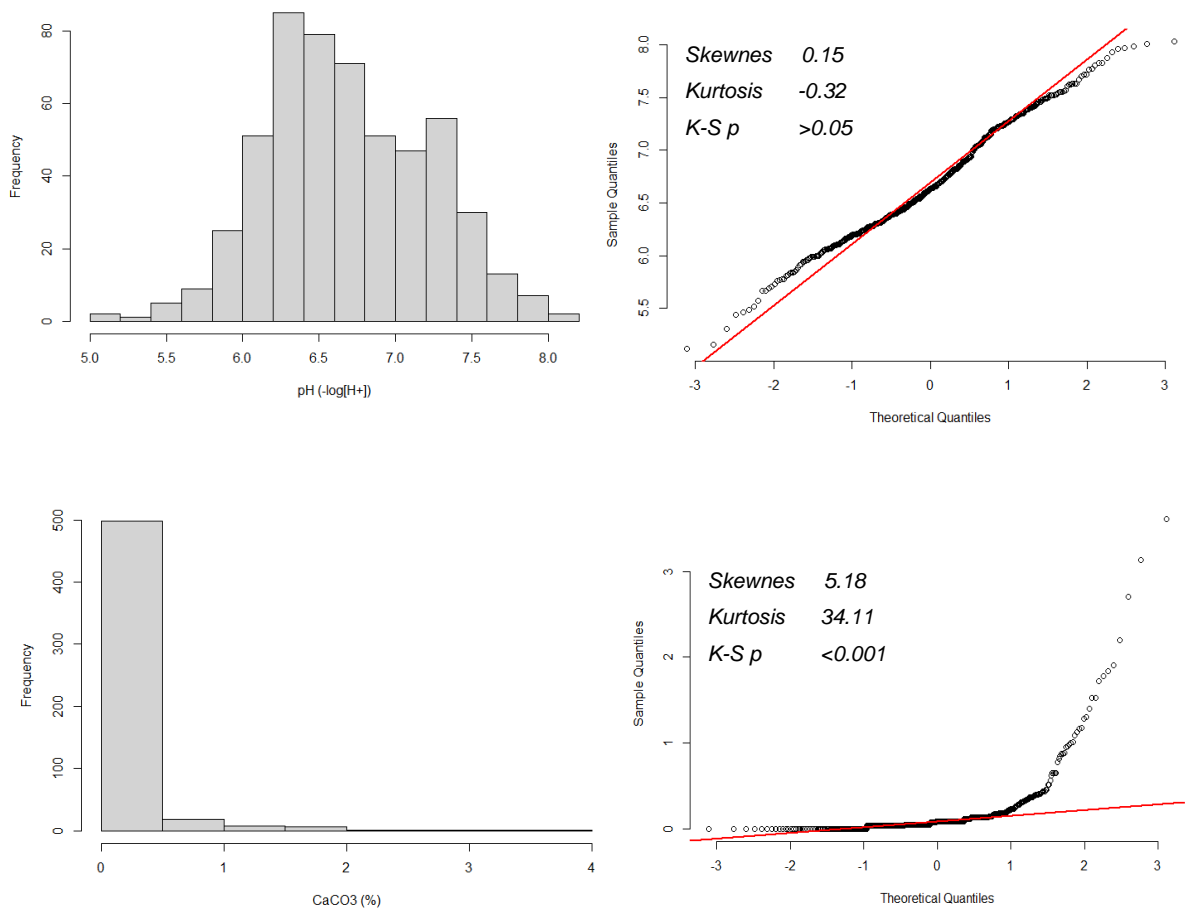


Figure 4.12. Histogram and Q-Q plot for soil pH and CaCO<sub>3</sub> data (N=535)

Overall data for soil pH, EC and CaCO<sub>3</sub> content during the study period and according to the wildfire severity and vegetation type are presented in Table 4.4. The variability data for soil pH showed that CV ranged from 0.53 to 0.82 throughout the study period, which indicates moderate variability (according to Zhang et al., 2007). Soil EC data also showed moderate variability, except on 0 and 15 MAF, when CV was 0.92 and 0.96, respectively. Soil CaCO<sub>3</sub> content data was highly variable, with CV values ranging from 1.07 to 2.44 throughout the study period. Throughout the study period the average soil pH, EC and CaCO<sub>3</sub> varied from 6.55 to 7.11, 117.4 to 283.4  $\mu\text{S}/\text{cm}$ , and 0.07 to 0.37%, respectively. The higher values were recorded in the first 6 months post-wildfire, and from then on the declining trend was observed for these soil properties. The overall lowest pH value was 5.12, recorded in C samples, 18 MAF and under *Quercus p.* vegetation, while the highest was 8.03 recorded in HS samples, 6

MAF and under the same vegetation type. The overall significantly higher pH values in MS and HS compared to C persisted throughout the study period in both vegetation types (Figure 4.13). Similarly, the overall lowest EC value was 38.7  $\mu\text{S}/\text{cm}$  also recorded in C samples, 18 MAF and under *Quercus p.* vegetation, while the highest was 1115  $\mu\text{S}/\text{cm}$  recorded in HS samples, 6 MAF and under *Juniperus c.* vegetation. The overall significantly higher EC values in HS persisted in the first 12 MAF period in both vegetation types, while in the following period (12-24 MAF) it started to decrease, but was still significantly higher than C. There was no significant difference between MS and C samples in both vegetation types throughout the study period (Figure 4.14).

Throughout the study period, most of the soil samples contained no carbonates, and in C samples the content varied from 0 to 0.38%, in MS samples it varied from 0 to 0.44%, while in HS samples it varied from 0 to 3.61%. The overall significantly higher  $\text{CaCO}_3$  content in HS persisted in the first 12 MAF period in both vegetation types, while there was no significant difference between MS and C samples in both vegetation types (Figure 4.15), which is similar to the movement of the average EC values throughout the study period.

Factorial analysis of variance revealed that the content in soil pH and EC varied significantly over time, and according to the severity of wildfire and vegetation type, while soil  $\text{CaCO}_3$  content varied significantly over time and according to severity, but not to vegetation type (Table 4.5). Wildfire caused an increase in soil pH in both MS and HS compared to C, while samples collected under *Juniperus c.* had significantly higher pH values than those collected under *Quercus p.* Furthermore, soil EC and  $\text{CaCO}_3$  content were significantly higher in HS compared to C and MS throughout the study, while samples collected under *Quercus p.* had significantly higher EC values than those collected under *Juniperus c.* It is also visible from Table 4.5 that no significant differences were observed in  $\text{CaCO}_3$  content in respect to different vegetation types.

Table 4.4. Descriptive statistics of soil pH, EC and CaCO<sub>3</sub> content for nine sampling times, three wildfire severity levels and two vegetation types

	Time									Wildfire severity			Vegetation	
	0 MAF	3 MAF	6 MAF	9 MAF	12 MAF	15 MAF	18 MAF	21 MAF	24 MAF	C	MS	HS	<i>Quercus p.</i>	<i>Juniperus c.</i>
pH														
N	60	60	60	60	60	60	60	56	59	178	179	178	348	187
Mean	6.89	6.83	7.11	6.75	6.69	6.64	6.33	6.35	6.55	6.30	6.56	7.20	6.66	6.73
Min	6.12	6.12	6.47	6.06	5.78	5.67	5.12	5.31	5.44	5.12	5.77	5.57	5.12	5.16
Max	7.77	7.63	8.03	7.54	7.72	7.52	7.23	7.39	7.57	7.12	7.76	8.03	8.03	8.01
SD	0.37	0.47	0.50	0.41	0.50	0.49	0.47	0.50	0.52	0.36	0.32	0.40	0.50	0.57
CV	0.05	0.07	0.07	0.06	0.07	0.07	0.07	0.08	0.08	0.06	0.05	0.06	0.07	0.08
EC (µS/cm)														
N	60	60	60	60	60	60	60	56	59	178	179	178	348	187
Mean	283.40	143.33	163.79	136.35	125.91	129.27	117.44	126.53	149.39	112.70	112.81	233.79	162.38	135.62
Min	40.90	68.60	62.80	44.70	59.30	52.20	38.70	60.00	65.30	38.70	59.30	65.10	38.70	40.90
Max	1089.00	349.00	1115.00	304.00	329.00	1013.00	225.00	335.00	333.00	1013.00	668.00	1115.00	1089.00	1115.00
SD	261.47	73.23	143.83	66.99	63.79	124.24	45.07	58.51	67.88	107.13	66.45	154.91	136.60	109.80
CV	0.92	0.52	0.88	0.49	0.51	0.96	0.38	0.46	0.45	0.95	0.59	0.66	0.84	0.81
CaCO <sub>3</sub> (%)														
N	60	60	60	60	60	60	60	56	59	178	179	178	348	187
Mean	0.15	0.37	0.34	0.14	0.13	0.10	0.07	0.13	0.12	0.06	0.06	0.39	0.18	0.16
Min	0.00	0.00	0.04	0.00	0.00	0.00	0.00	0.00	0.00	0.00	0.00	0.00	0.00	0.00
Max	0.87	3.61	3.13	1.01	1.30	0.44	0.95	1.28	1.84	0.38	0.44	3.61	3.61	2.20
SD	0.19	0.67	0.59	0.15	0.24	0.11	0.15	0.18	0.30	0.05	0.06	0.55	0.39	0.30
CV	1.27	1.78	1.73	1.07	1.87	1.07	2.25	1.39	2.44	0.85	0.93	1.40	2.15	1.84

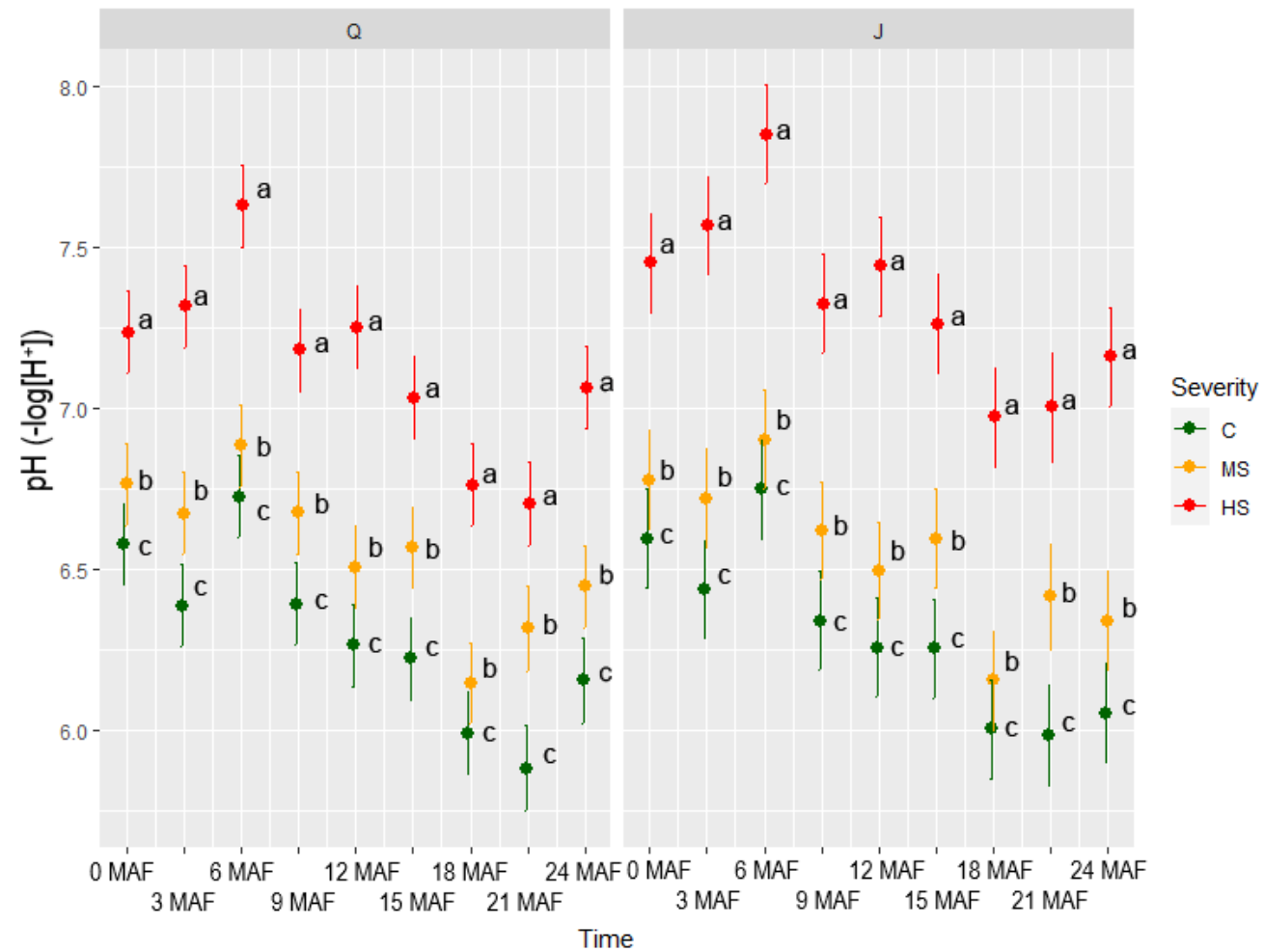
MAF – Months after fire; C – Control; MS – Medium severity; HS – High severity; SD – Standard deviation; CV – Coefficient of variation



Table 4.5. Factorial ANOVA results and mean values for soil pH, EC and CaCO<sub>3</sub> content according to fire severity, time, vegetation, and their interactions

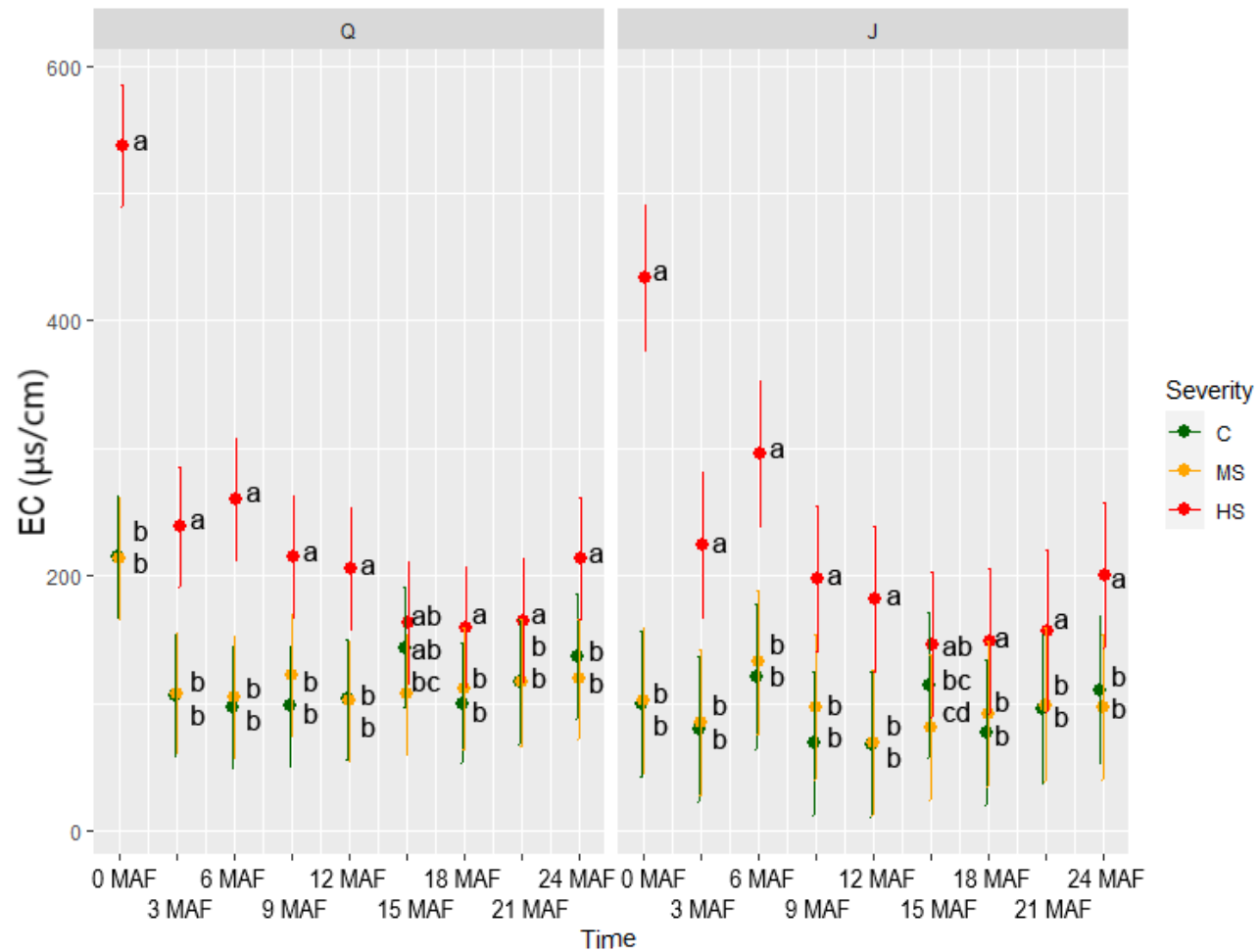
	pH	EC (μS/cm)	CaCO <sub>3</sub> (%)
T	*	*	*
FS	*	*	*
V	*	*	n.s.
T × FS	n.s.	*	-
T × V	n.s.	n.s.	-
FS × V	*	*	-
FS × V × T	n.s.	n.s.	-
<b>Time-Since-Fire</b>			
0 MAF	6.90 ± 0.04 b	266.87 ± 13.37 a	0.15 ± 0.04 b
3 MAF	6.85 ± 0.04 b	144.11 ± 13.37 b	0.37 ± 0.04 a
6 MAF	7.12 ± 0.04 a	168.12 ± 13.37 b	0.33 ± 0.04 a
9 MAF	6.76 ± 0.04 b	132.77 ± 13.37 b	0.14 ± 0.04 b
12 MAF	6.70 ± 0.04 c	121.37 ± 13.37 b	0.12 ± 0.04 b
15 MAF	6.66 ± 0.04 c	125.54 ± 13.37 b	0.11 ± 0.04 b
18 MAF	6.34 ± 0.04 c	114.74 ± 13.37 b	0.07 ± 0.04 b
21 MAF	6.39 ± 0.04 c	125.79 ± 14.06 b	0.13 ± 0.04 b
24 MAF	6.54 ± 0.04 c	146.08 ± 13.44 b	0.12 ± 0.04 b
<b>Fire severity</b>			
C	6.29 ± 0.02 c	108.12 ± 7.75 b	0.06 ± 0.02 b
MS	6.56 ± 0.02 b	108.66 ± 7.73 b	0.06 ± 0.02 b
HS	7.24 ± 0.02 a	230.35 ± 7.83 a	0.38 ± 0.02 a
<b>Vegetation</b>			
<i>Quercus p.</i>	6.66 ± 0.01 b	162.06 ± 5.30 a	0.18 ± 0.02 a
<i>Juniperus c.</i>	6.73 ± 0.02 a	136.03 ± 7.24 b	0.16 ± 0.02 a

Abbreviations: FS – Fire severity; V - Vegetation; T- Time; C – Control; MS – Medium severity; HS – High severity; MAF – Months after fire. Significant differences at: p<0.05\*, n.s. not significant at p<0.05. Different letters represent significant (p<0.05) differences between fire severity, sampling time and vegetation. Values following ± indicate standard deviation.



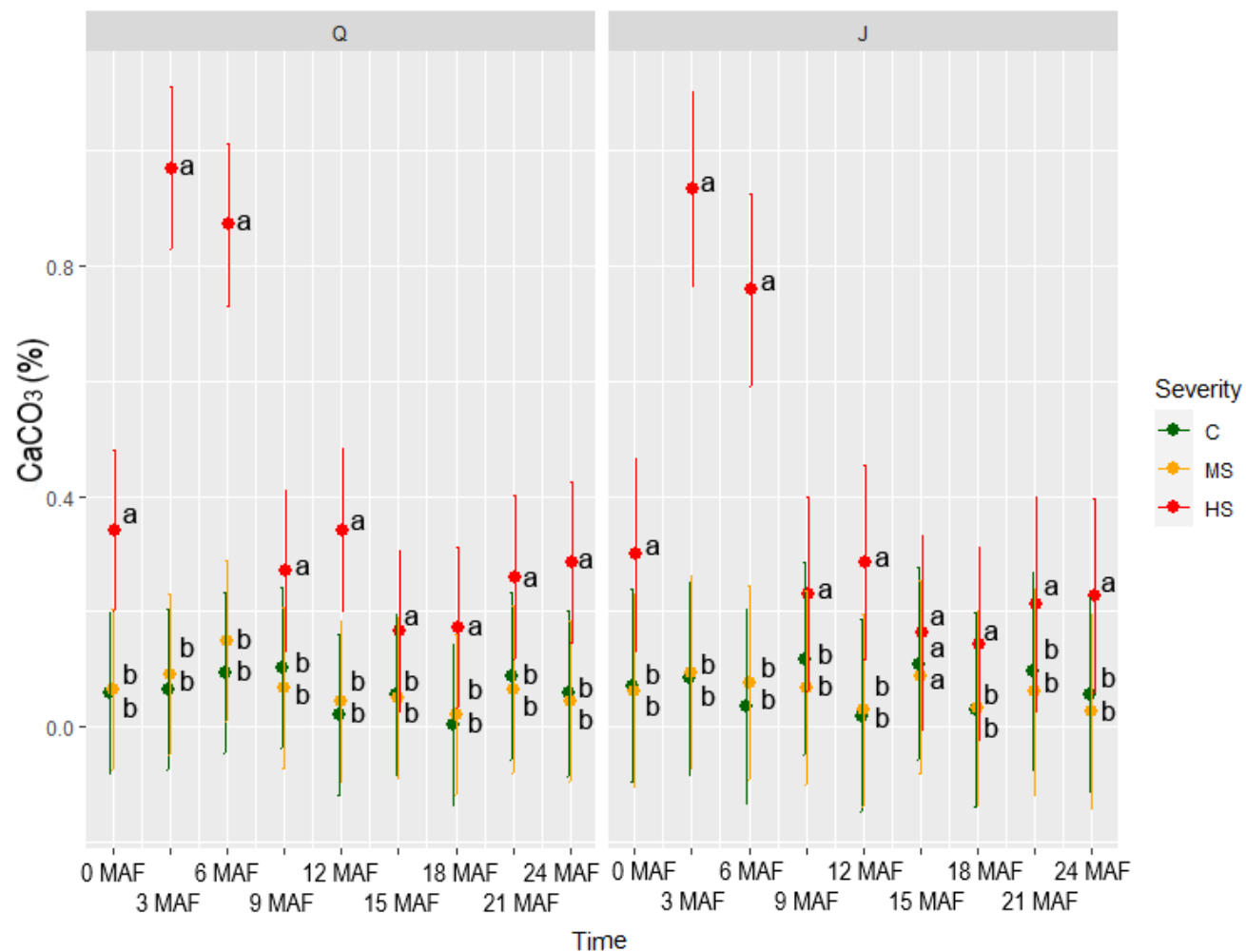
Abbreviations: C – Control; MS – Medium severity; HS – High severity; MAF – Months after fire; Q – *Quercus p.*; J – *Juniperus c.*

Figure 4.13. Mean soil pH values (-log[H<sup>+</sup>]) according to the interaction of the wildfire severity, time-since-fire and vegetation factors. Whiskers represent 95% confidence intervals. Different letters indicate significant (p < 0.05) differences between wildfire severities on each given date



Abbreviations: C – Control; MS – Medium severity; HS – High severity; MAF – Months after fire; Q – *Quercus p.*; J – *Juniperus c.*

Figure 4.14. Mean soil EC values (µS/cm) according to the interaction of the wildfire severity, time-since-fire and vegetation factors. Whiskers represent 95% confidence intervals. Different letters indicate significant ( $p < 0.05$ ) differences between wildfire severities on each given date



Abbreviations: C – Control; MS – Medium severity; HS – High severity; MAF – Months after fire; Q – *Quercus p.*; J – *Juniperus c.*

Figure 4.15. Mean soil CaCO<sub>3</sub> content (%) according to the interaction of the wildfire severity, time-since-fire and vegetation factors. Whiskers represent 95% confidence intervals. Different letters indicate significant ( $p < 0.05$ ) differences between wildfire severities on each given date

## 4.5. Description of soil spectral data

Average spectral data of three wildfire severities were grouped according to vegetation and sampling time. Figures 4.16 - 4.19 compare average reflectance of C, MS, and HS taken under *Juniperus c.* and *Quercus p.* at the beginning and the end of the study period (0 MAF and 24 MAF). Figures 4.20 - 4.25 compare each of the paired severity and vegetation categories (C-J, C-Q, MS-J, MS-Q, HS-J, and HS-Q) across the sampling times. Additionally, visual evaluation of the MS and HS samples taken at 0 MAF recorded with two different sensors (hyperspectral and multispectral) is shown in Figure 4.26.

Spectral bands from 350 to 409 nm removed from further analysis due to large noise effect can be seen best from the first derivative reflectance.

In the immediate post-fire period (0 MAF), the greatest spectral differences between C, MS, and HS groups were in the green/yellow to red (550 to 700 nm) region, especially in samples taken under *Quercus p.* vegetation (Figures 4.16 and 4.17). At the end of the study period (24 MAF), these spectral differences remained visible between C and HS group, however MS exhibited higher reflectance throughout the entire spectra, which was visible in both vegetation species (Figures 4.18 and 4.19).

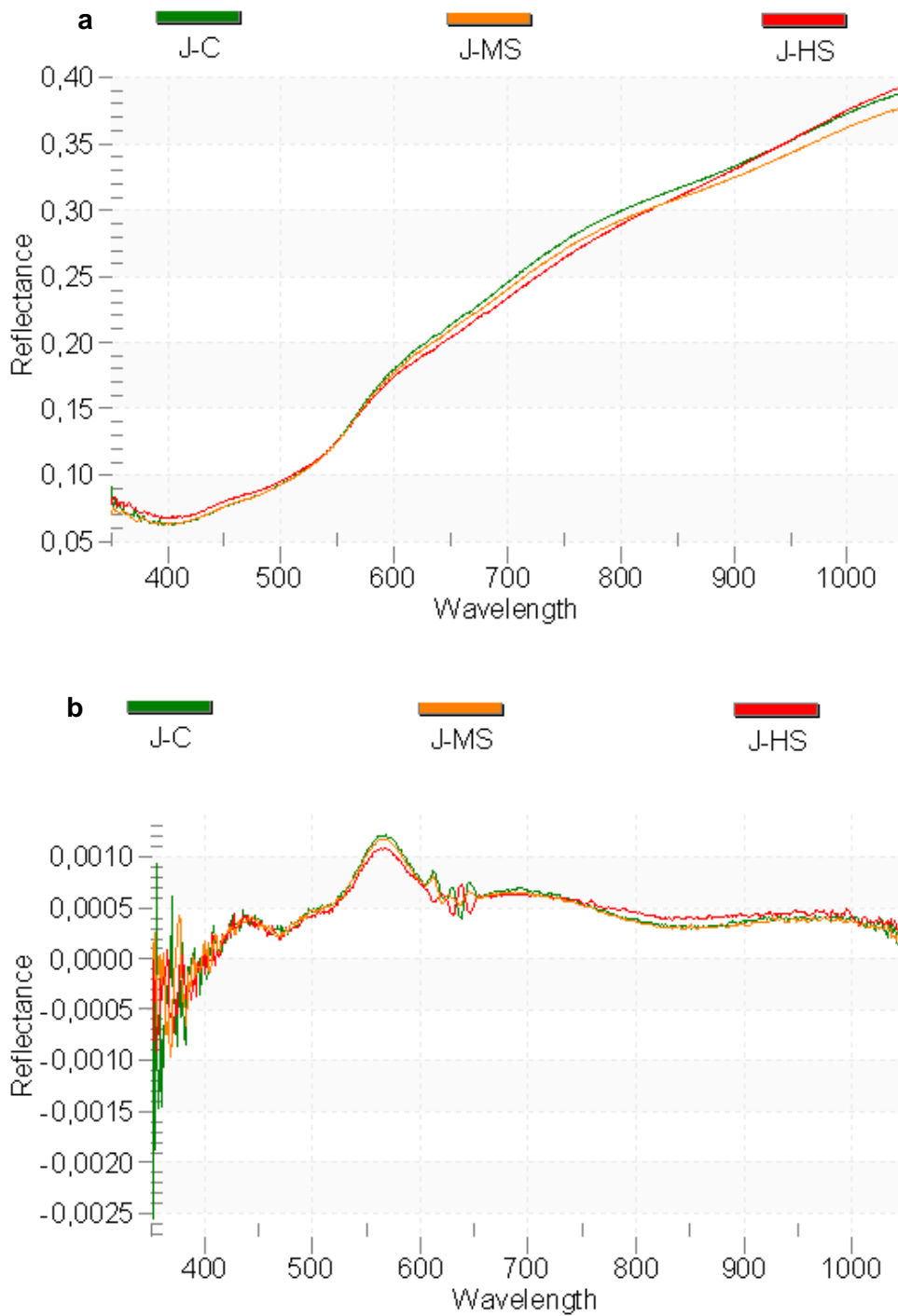


Figure 4.16. Average raw (a) and first derivative (b) reflectance for control, medium severity and high severity samples taken under *Juniperus c.* vegetation immediately post-fire on 22<sup>nd</sup> of August 2019 (N=42). Wavelengths are expressed in nm

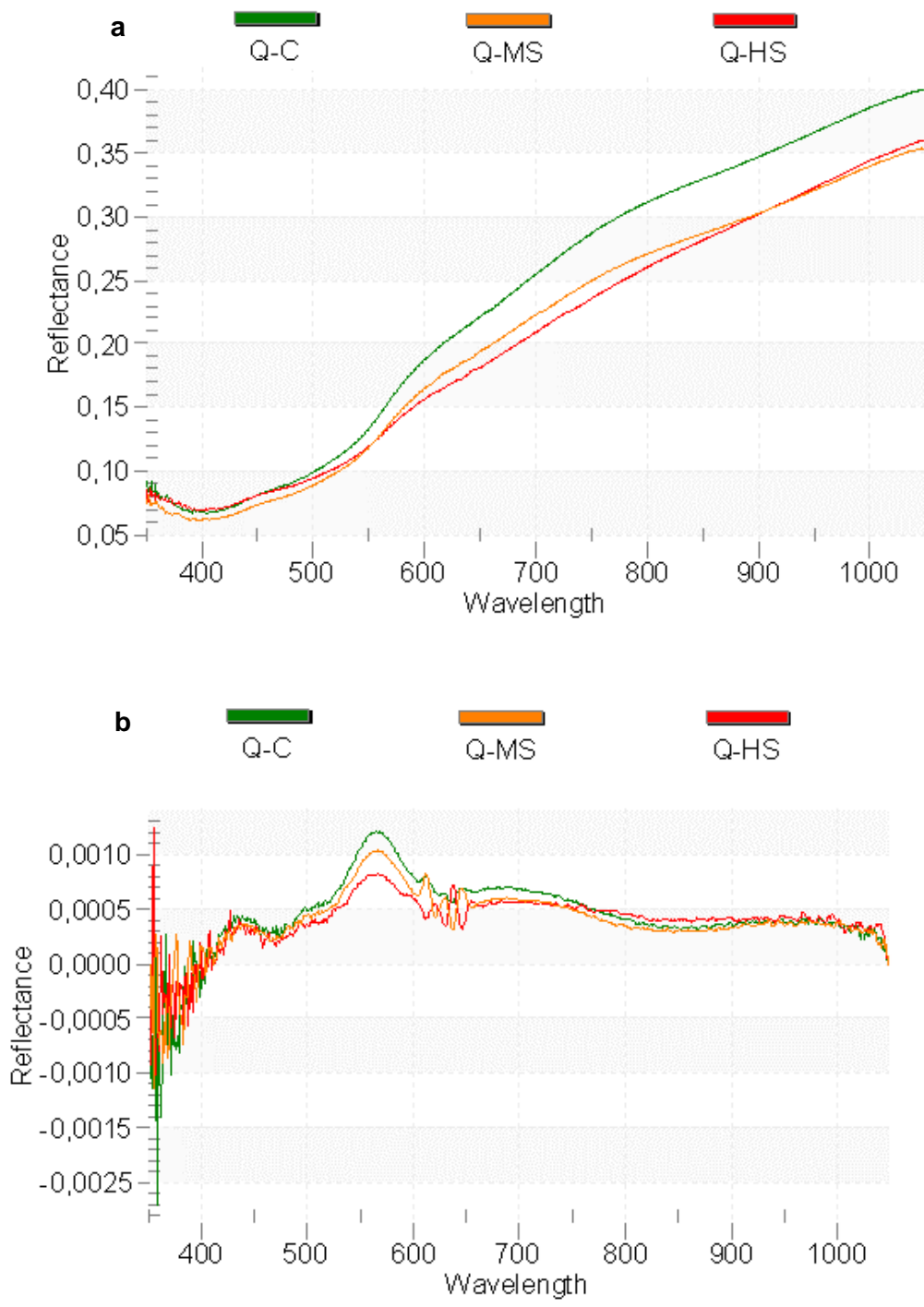


Figure 4.17. Average raw (a) and first derivative (b) reflectance for control, medium severity and high severity samples taken under *Quercus p.* vegetation immediately post-fire on 22<sup>nd</sup> of August 2019 (N=78). Wavelengths are expressed in nm

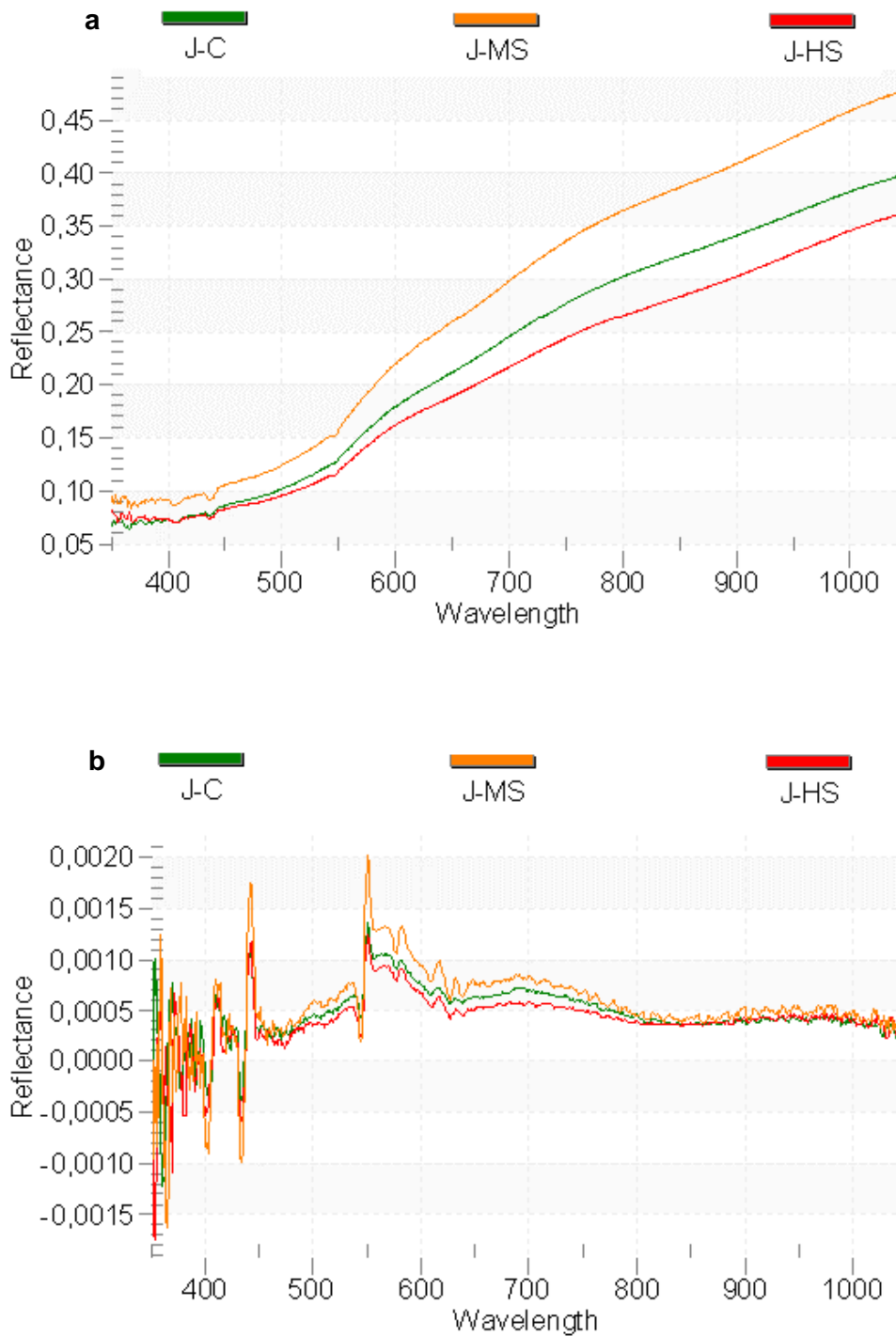


Figure 4.18. Average raw (a) and first derivative (b) reflectance for control, medium severity and high severity samples taken under *Juniperus c.* vegetation two years post-fire on 26<sup>th</sup> of August 2021 (N=42). Wavelengths are expressed in nm



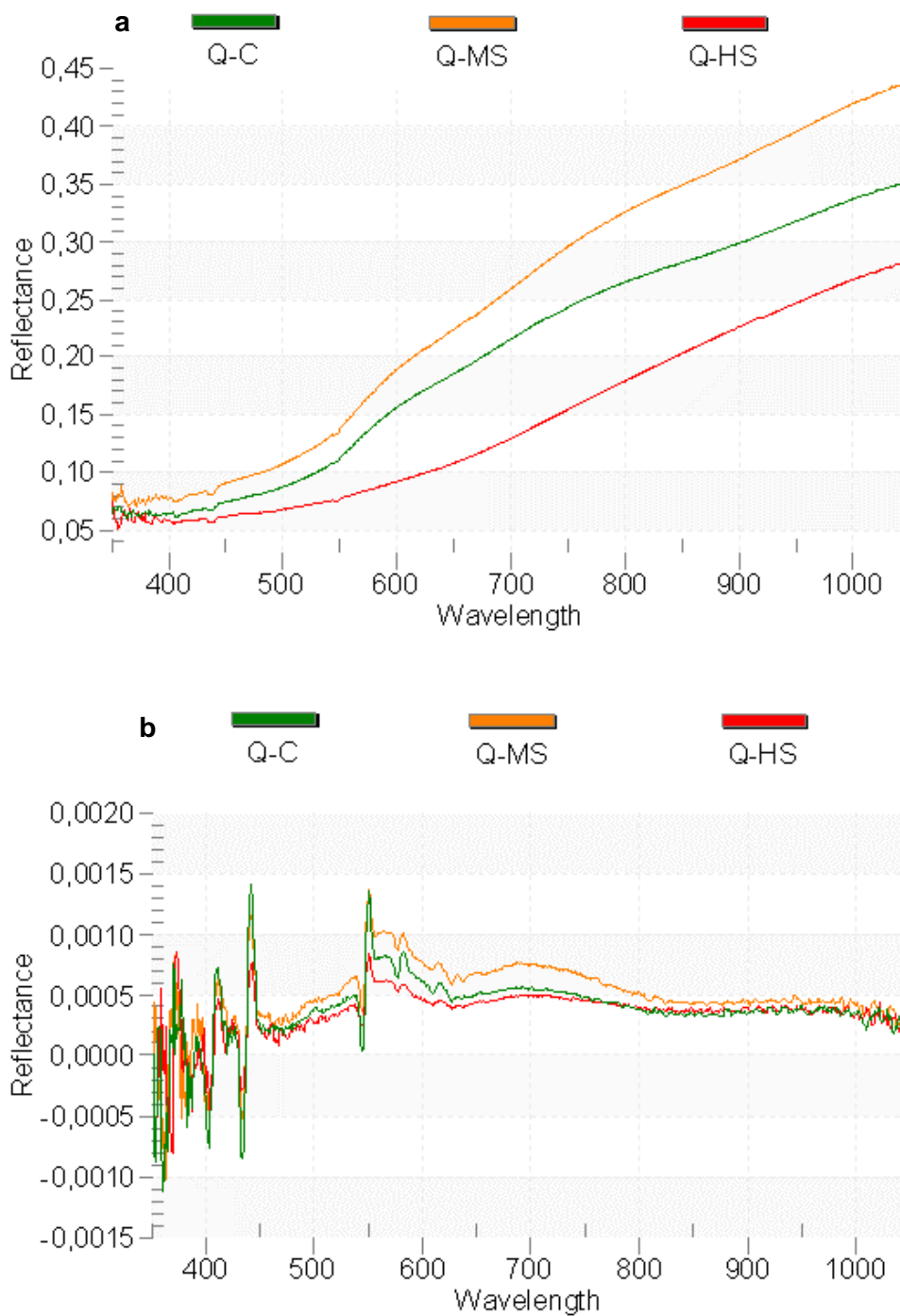


Figure 4.19. Average raw (a) and first derivative (b) reflectance for control, medium severity and high severity samples taken under *Quercus p.* vegetation two years post-fire on 26<sup>th</sup> of August 2021 (N=78). Wavelengths are expressed in nm

It can be seen from Figures 4.20 and 4.21 that the highest average reflectance in C was recorded as follows: 9 MAF > 21 MAF > 24 MAF for C-J group, and 21 MAF > 9 MAF > 24 MAF for C-Q group, i.e. in the months of May and August, while the lowest average reflectance was recorded as follows: 15 MAF > 3 MAF > 6 MAF in both C-J and C-Q group, i.e. in the months of February and November.

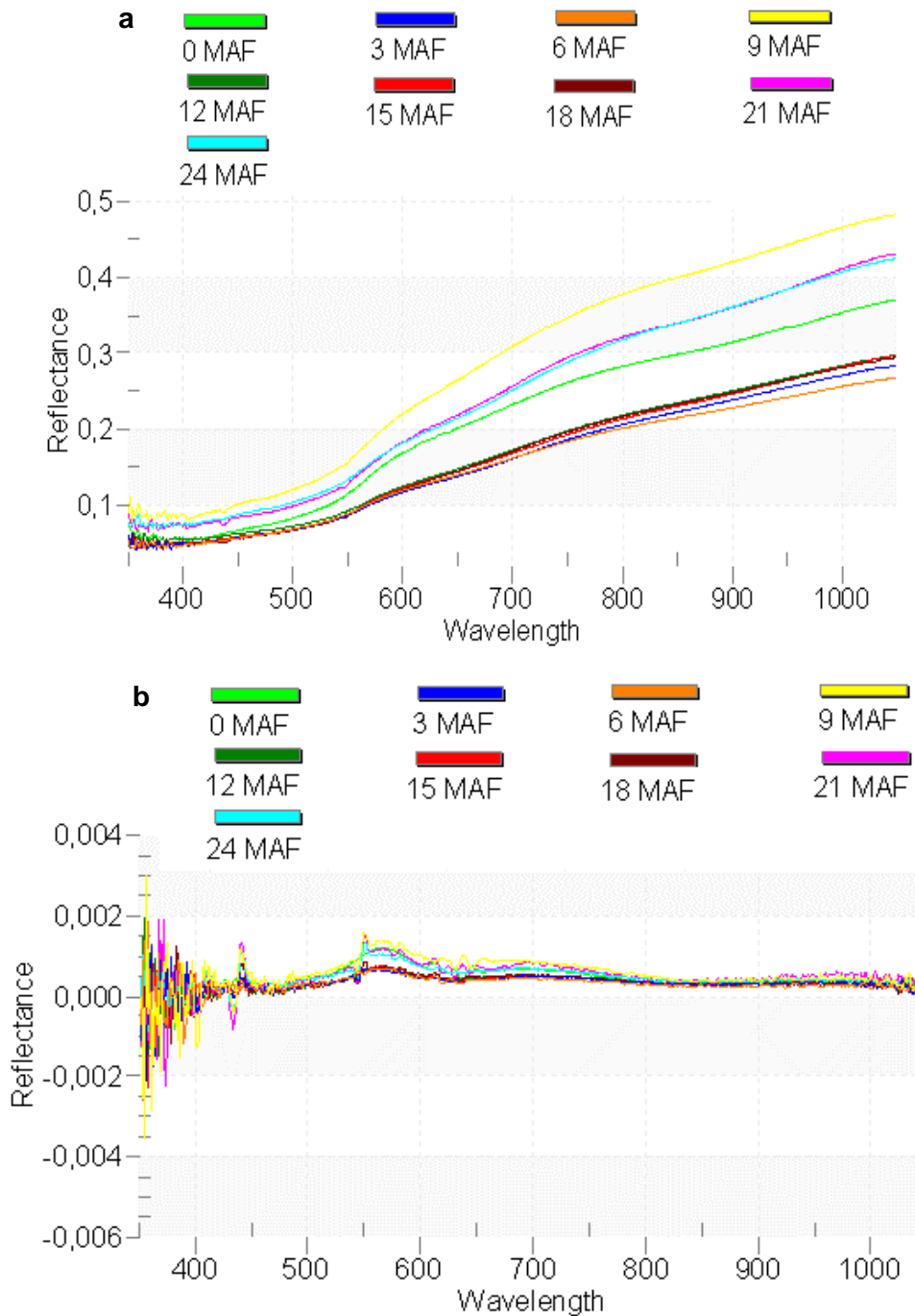


Figure 4.20. Average raw (a) and first derivative (b) reflectance for control samples taken under *Juniperus c.* vegetation during the study period. Wavelengths are expressed in nm

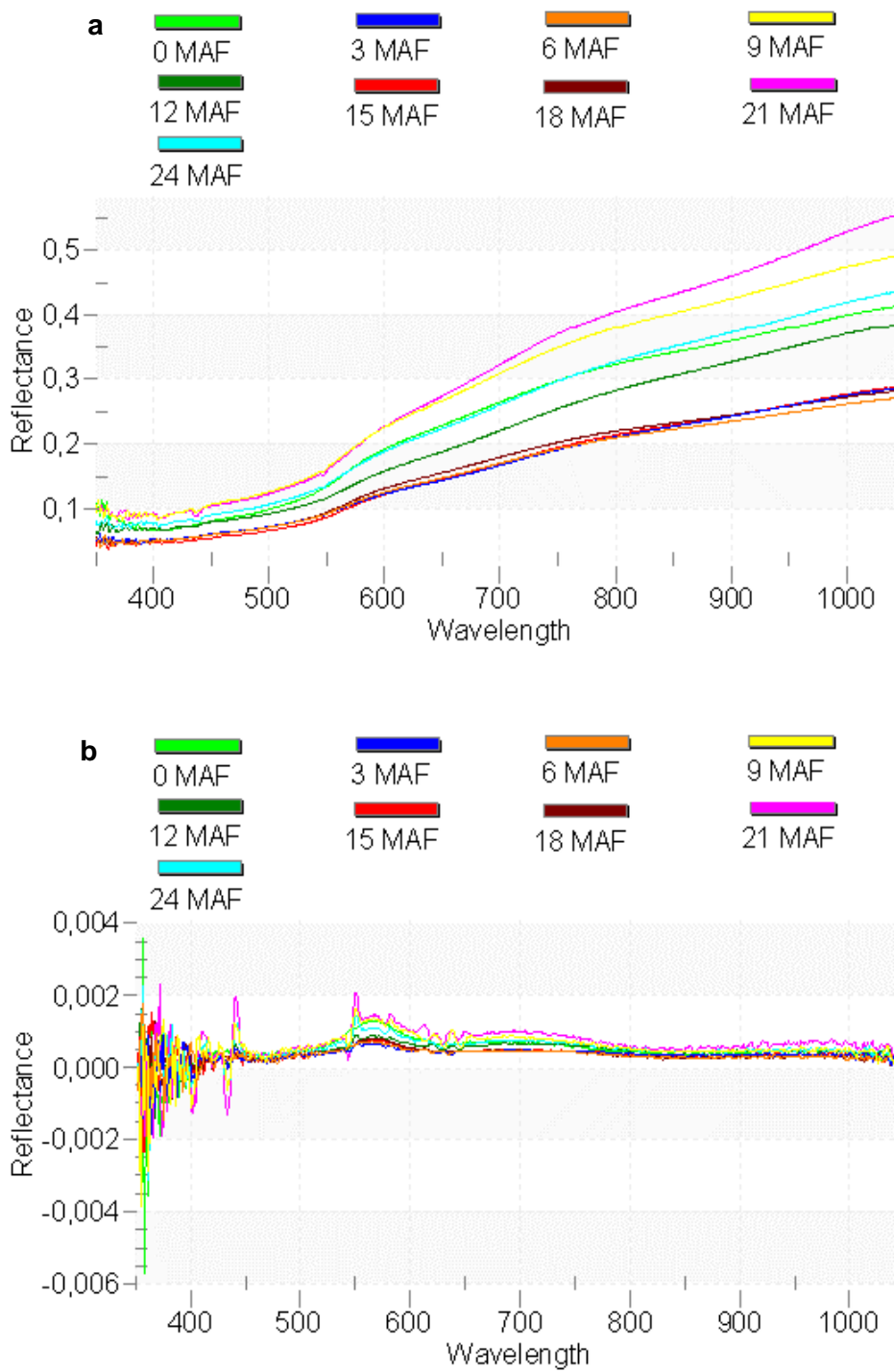


Figure 4.21. Average raw (a) and first derivative (b) reflectance for control samples taken under *Quercus p.* vegetation during the study period. Wavelengths are expressed in nm

Figures 4.22 and 4.23 show that the highest average reflectance in MS was recorded as follows: 24 MAF > 0 MAF > 9 MAF for MS-J group, and 9 MAF > 0 MAF > 24 MAF for MS-Q group, i.e. in the months of May and August (high spring and summer), while the lowest average reflectance was recorded as follows: 18 MAF > 6 MAF > 12 MAF in MS-J, i.e in the months of February, March and August (spring and summer) and 21 MAF > 18 MAF > 6 MAF in MS-Q group, i.e. in the months of February, March and May (early spring and spring).

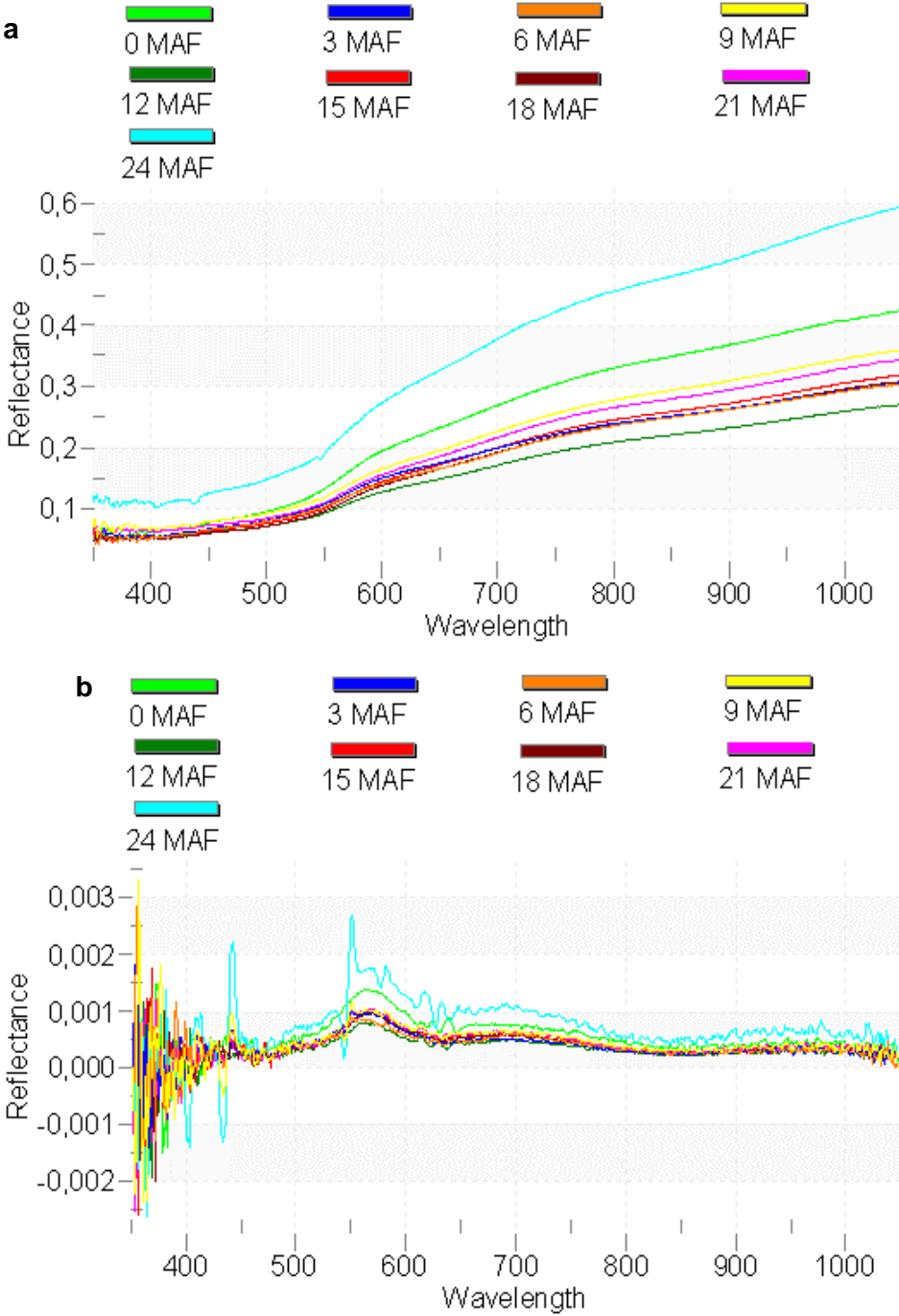


Figure 4.22. Average raw (a) and first derivative (b) reflectance for medium severity samples taken under *Juniperus c.* vegetation during the study period. Wavelengths are expressed in nm

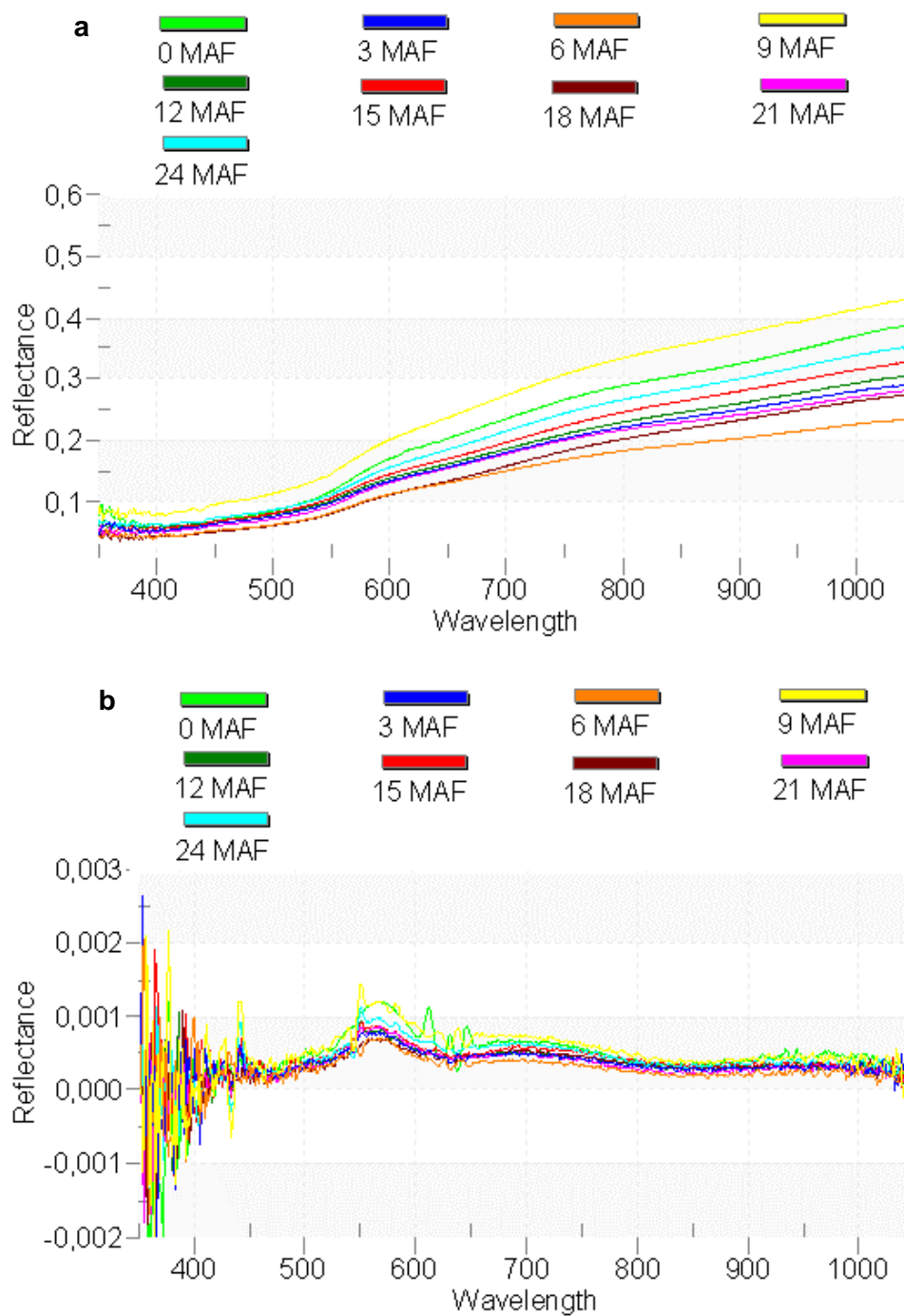


Figure 4.23. Average raw (a) and first derivative (b) reflectance for medium severity samples taken under *Quercus p.* vegetation during the study period. Wavelengths are expressed in nm

Figures 4.24 and 4.25 show that the highest average reflectance in HS was recorded as follows: 6 MAF > 15 MAF > 18 MAF for HS-J group, i.e. in the month of February, March, and November (early spring and autumn) and 18 MAF > 0 MAF > 21 MAF for HS-Q group, i.e. in the months of March, May and August (spring and summer), while the lowest average reflectance was recorded as follows: 9 MAF > 24 MAF > 12 MAF in HS-J, and 9 MAF > 12 MAF > 3 MAF in HS-Q group, i.e. in the months of May, August and November (spring, summer and autumn).

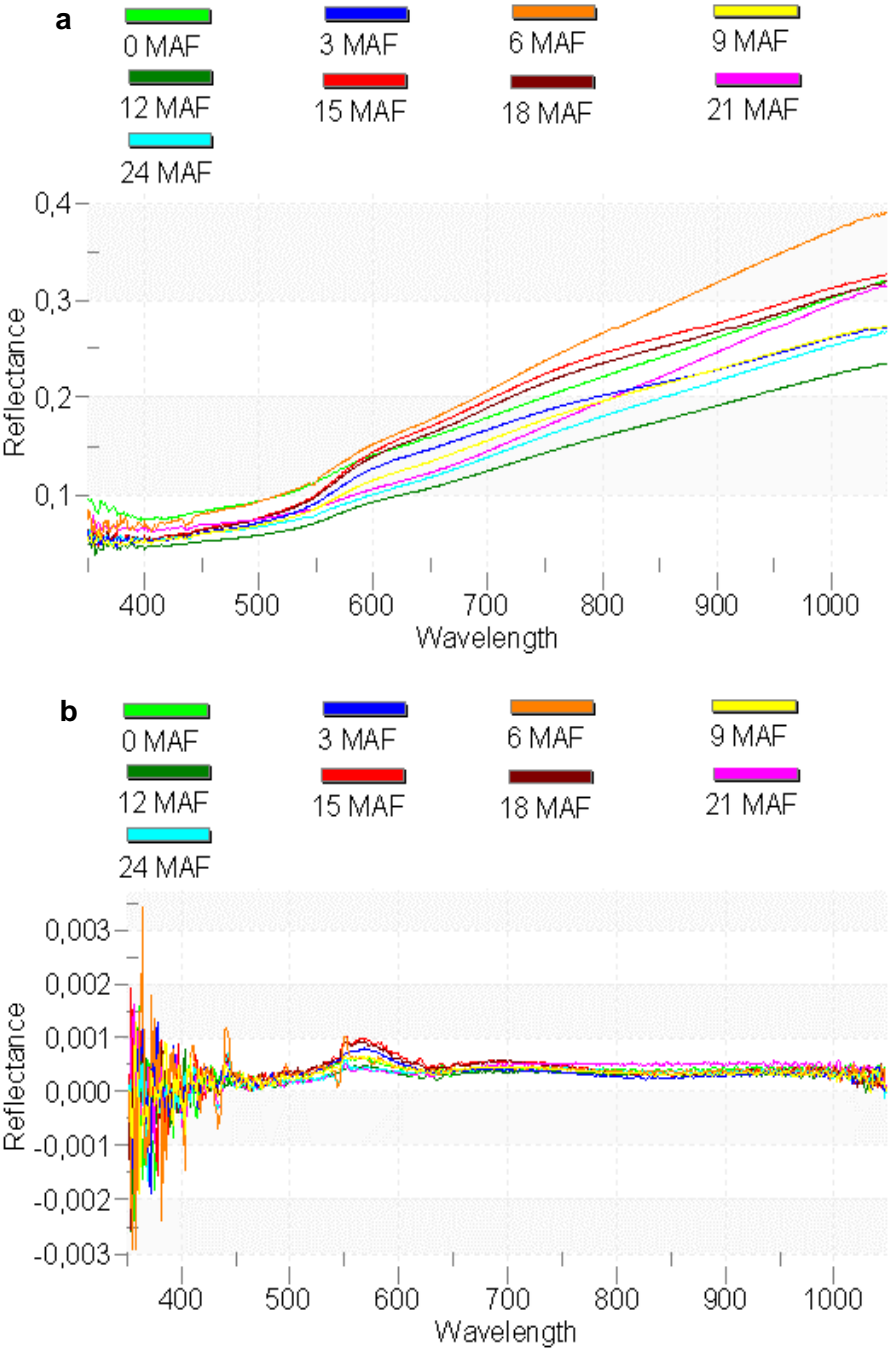


Figure 4.24. Average raw (a) and first derivative (b) reflectance for high severity samples taken under *Juniperus c.* vegetation during the study period. Wavelengths are expressed in nm

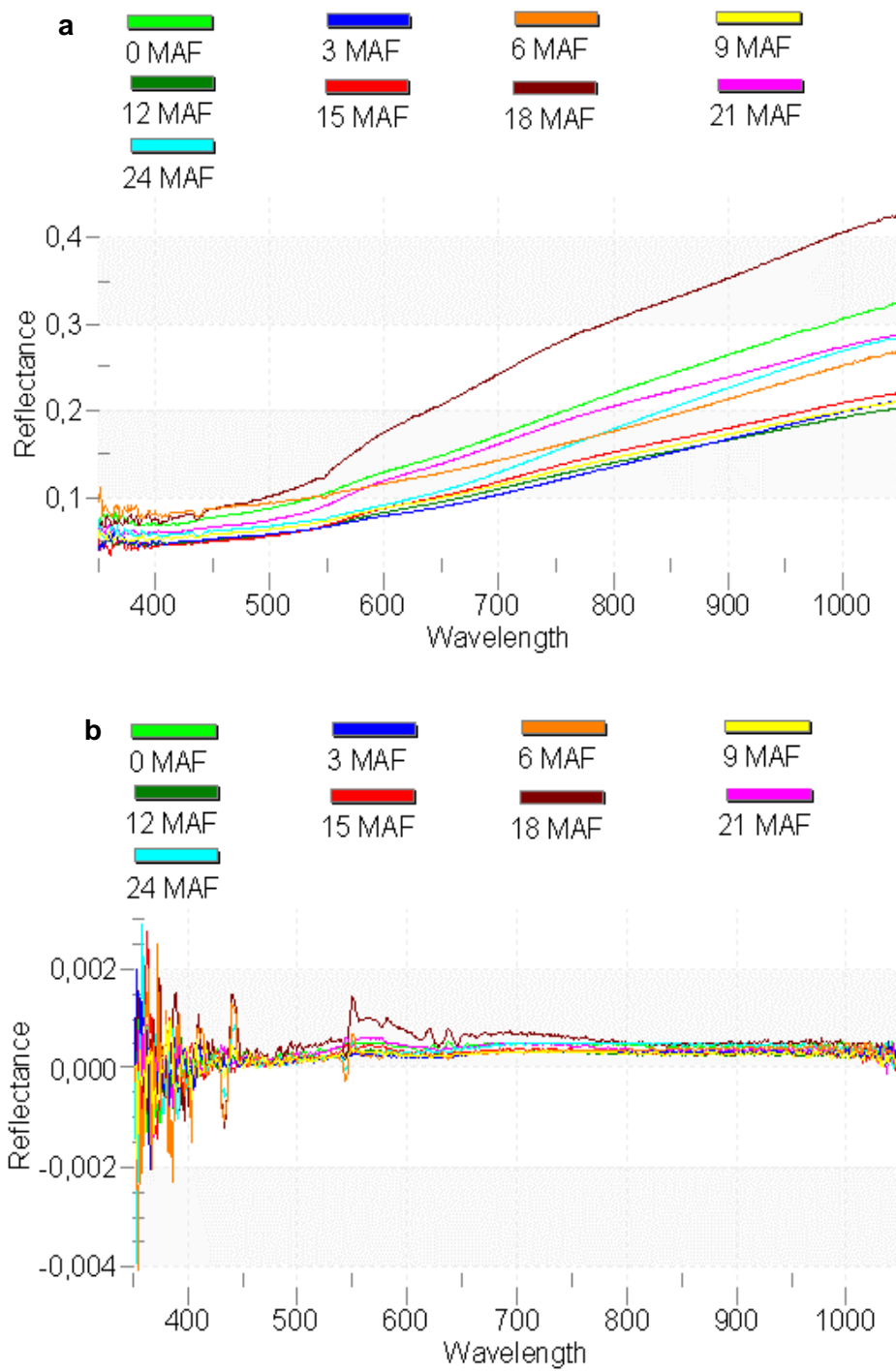


Figure 4.25. Average raw (a) and first derivative (b) reflectance for high severity samples taken under *Quercus p.* vegetation during the study period. Wavelengths are expressed in nm

Figure 4.26 shows average raw soil reflectance spectra in the immediate post-fire period measured for the same group of samples with two different sensors (FieldSpec®3 - hyperspectral and Sentinel-2 - multispectral). Sentinel-2 multispectral sensor detected lower reflectance of the HS samples compared to MS throughout the spectrum, while the hyperspectral sensor detected lower yellow/red reflectance and increased NIR reflectance in HS samples compared to MS.

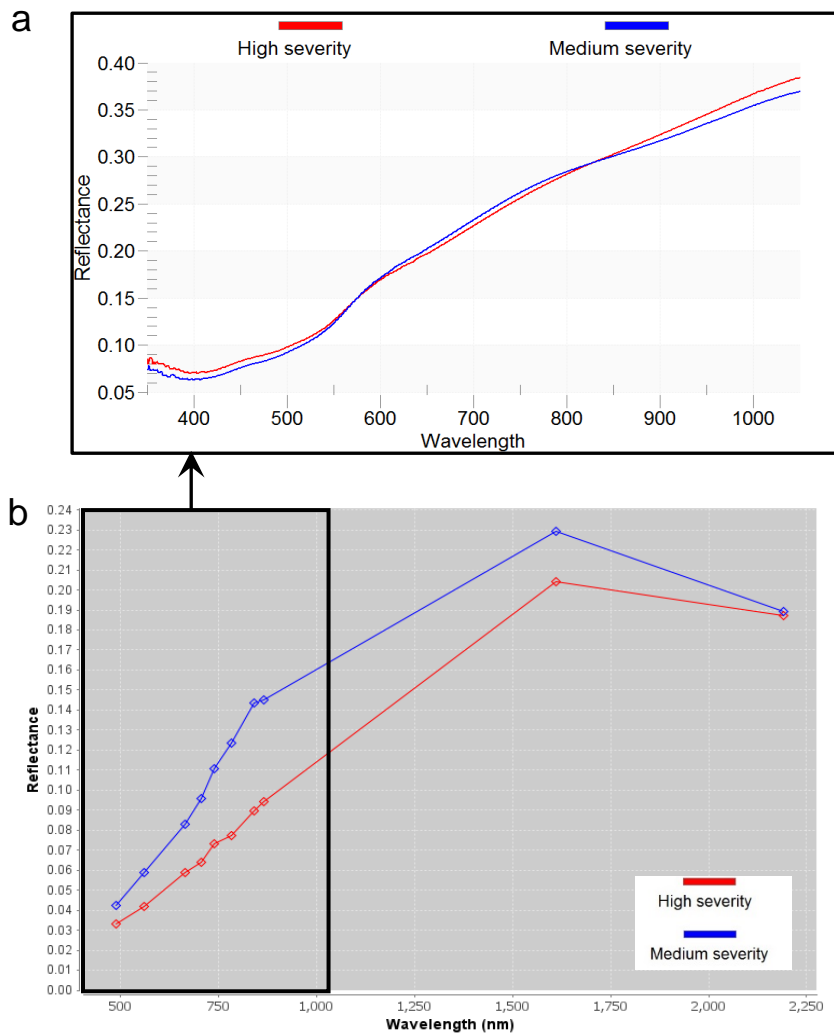


Figure 4.26. Comparative view of hyperspectral (a) and multispectral (b) reflectance data (N=28). Points on the graph below mark ten respective Sentinel-2 bands used in the study



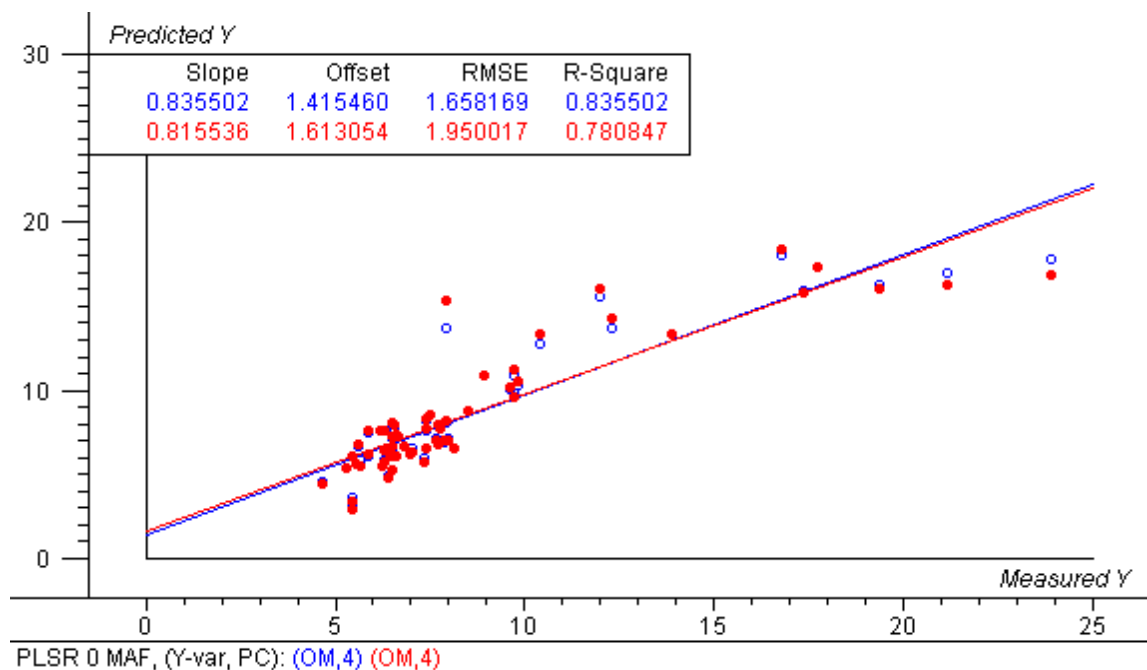
## 4.6. Linear (PLSR) and non-linear (ANN) modelling of post-fire SOM

### 4.6.1. Comparison of PLSR and ANN models

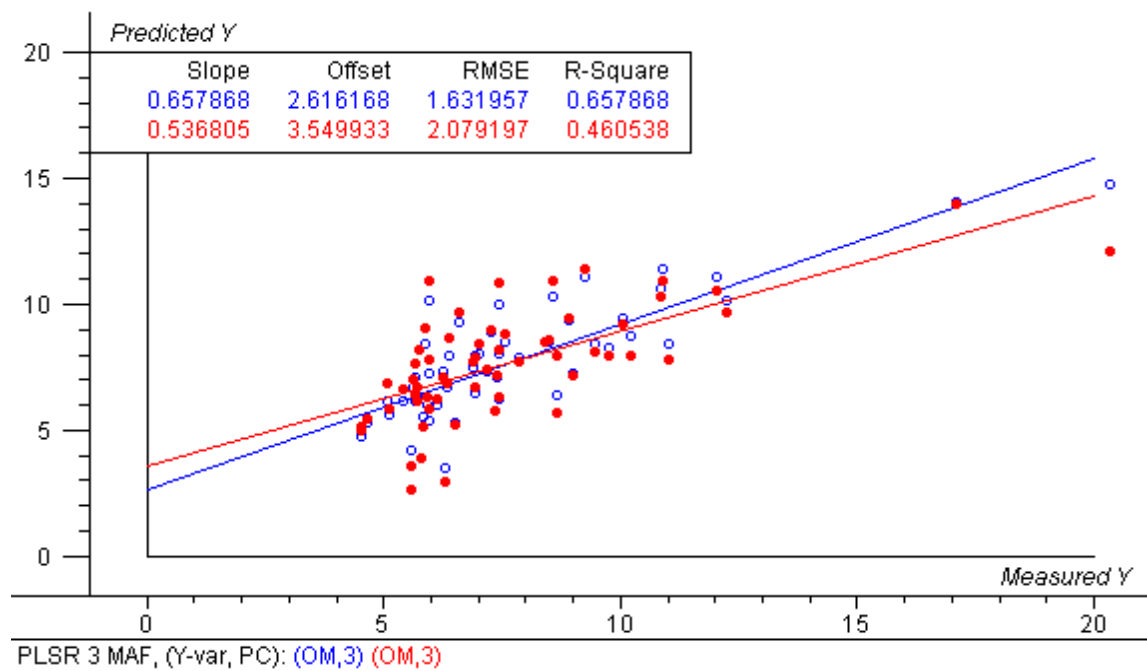
In order to compare the accuracy and precision of linear and non-linear hyperspectral prediction models, soil reflectance data for the entire reflectance dataset collected over the 2-year study period, as well as the subsets containing the data from each individual sampling period was subjected to predictive SOM modelling. Results of the partial least regression (PLSR) models calculated using spectral and SOM (%) data are shown in Figure 4.27. The independent (predictor, x-variable) input was the raw reflectance data in the range from 410-1050 nm, and the dependent (y-variable) input was the SOM content. At 3 MAF, transformations of the raw spectra were performed using the Savitzky-Golay filter which improved the model. The dataset was split in two parts: calibration (50%) and validation (50%). Overall, ten (10) PLSR models were obtained, nine (9) for each sampling period and one (1) for the entire 0-24 MAF dataset. At 0, 9 and 24 MAF outliers were detected and removed from further analysis.

In each PLSR model, three to five PCs were identified that represented the main structured information in the spectral dataset (Table 4.6), with first two components summarising the most variation in the data (PC1: 3-39% and PC2: 17-77%), as seen from the score plots in Figure 4.28. Residual variance for each model can be seen in the Appendix 1 (Figure 8.1).

PLSR models computed for each sampling time provided fair to very good predictions according to RPD, with values ranging from 1.62 (6 MAF) to 2.29 (21 MAF), with an exception at 3 MAF which produced a poor model (RPD = 1.35) (Table 4.6). The PLSR model computed for the entire dataset collected over the study period (0-24 MAF) provided fair predictions, with RPD value of 1.55 (Table 4.6).



● calibration ● validation



● calibration ● validation

Figure 4.27. PLSR models obtained from raw reflectance acquired at each individual sampling period as well as the entire reflectance dataset showing relationship between calibration and validation dataset

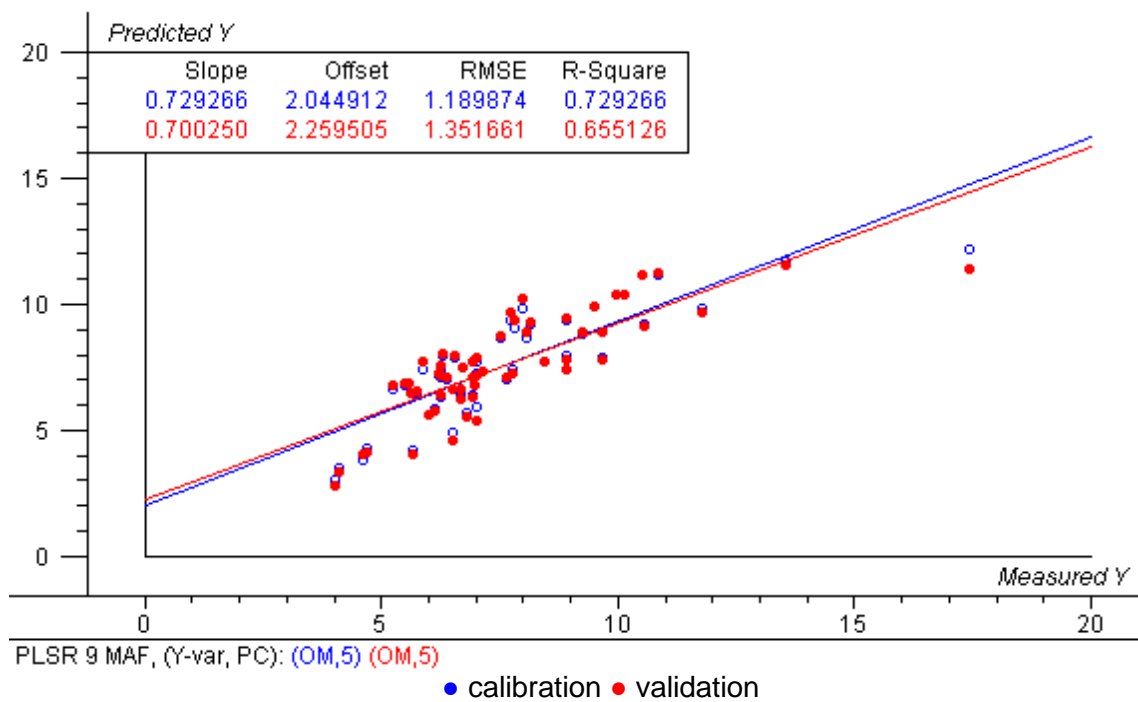
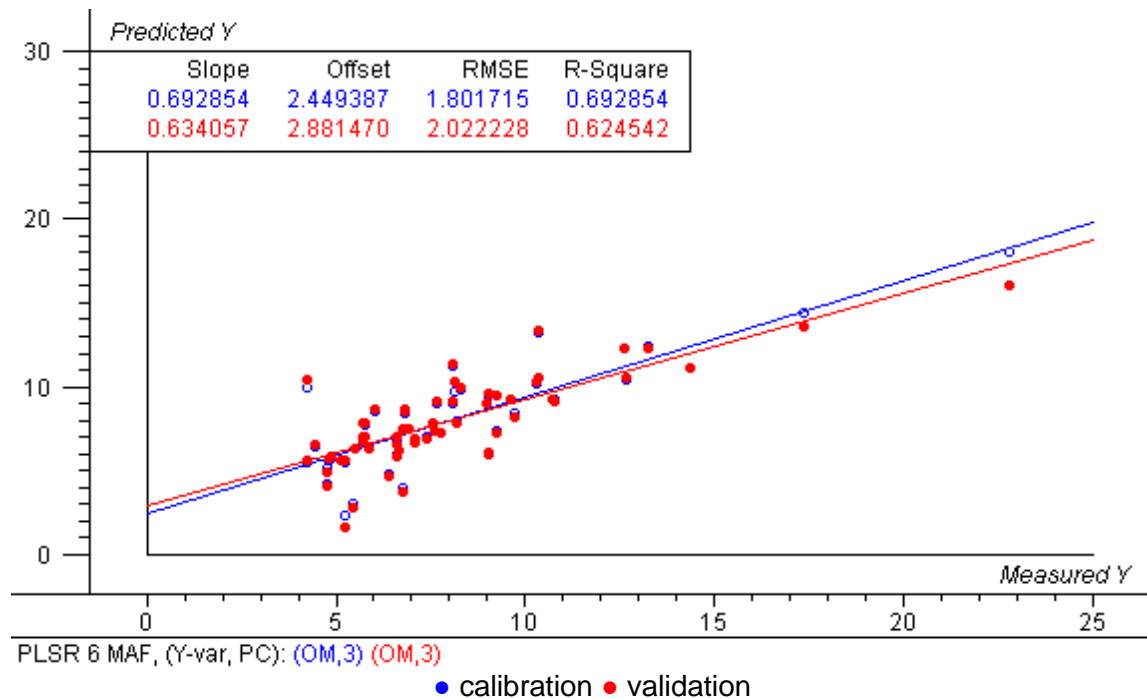


Figure 4.27. (continuation) PLSR models obtained from raw reflectance acquired at each individual sampling period as well as the entire reflectance dataset showing relationship between calibration and validation dataset

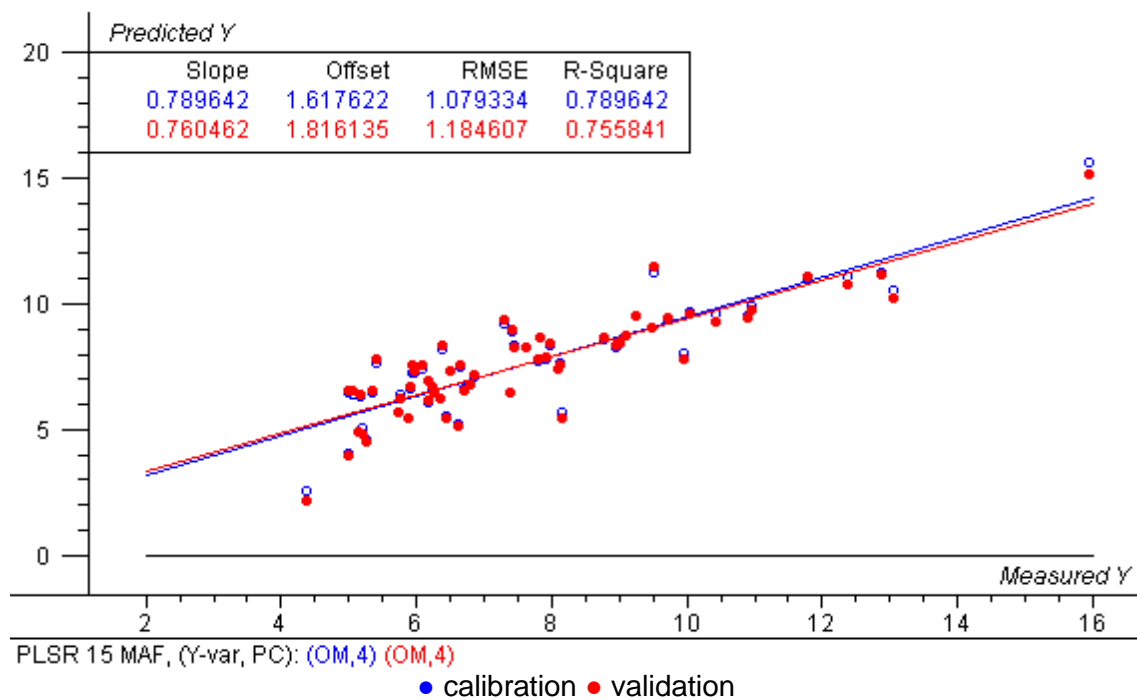
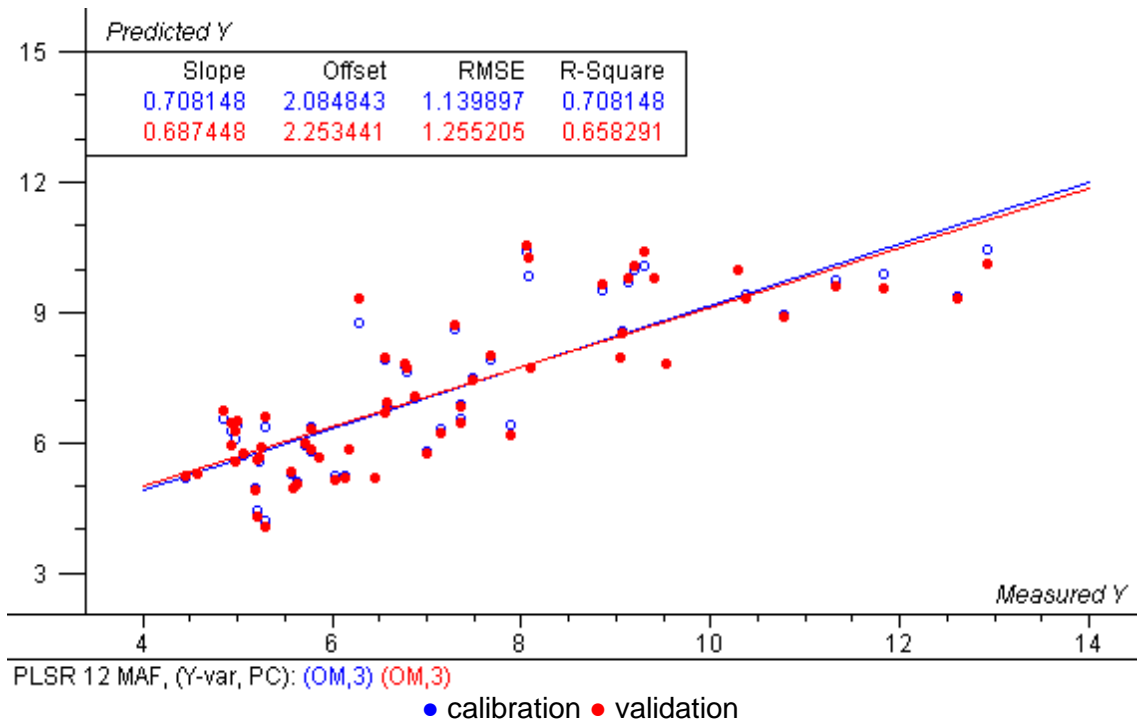
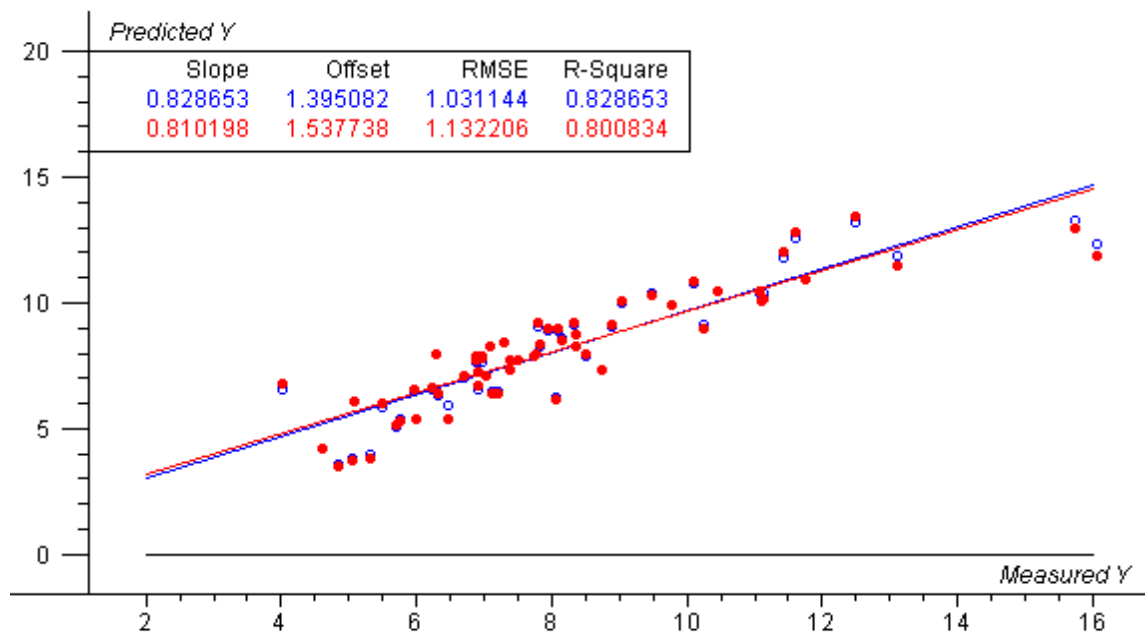


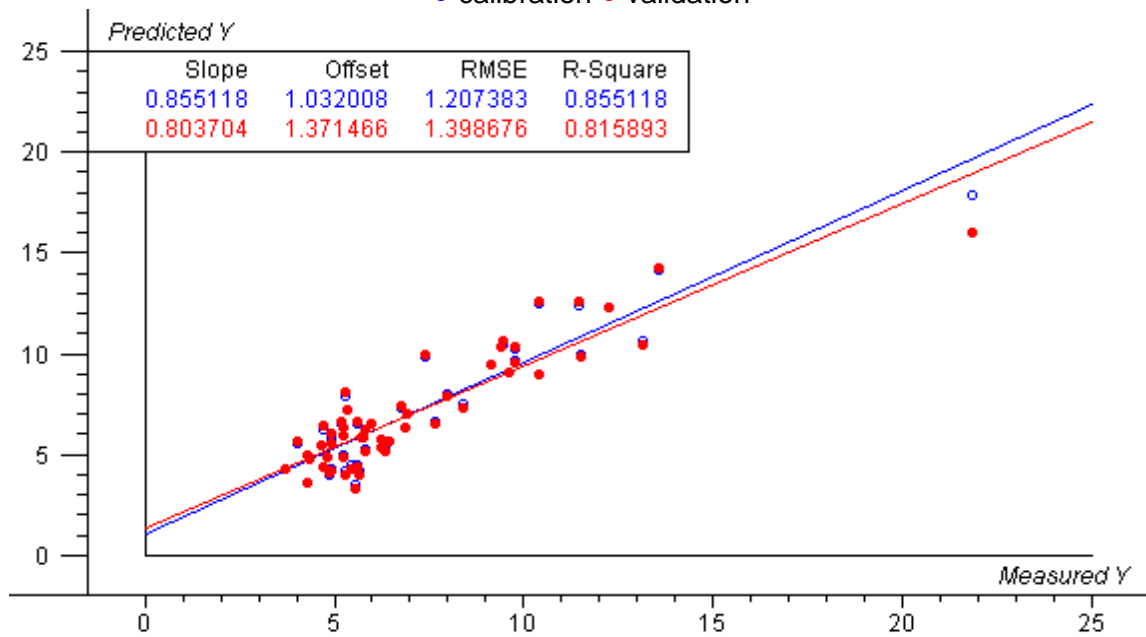
Figure 4.27. (continuation) PLSR models obtained from raw reflectance acquired at each individual sampling period as well as the entire reflectance dataset showing relationship between calibration and validation dataset



PLSR 18 MAF, (Y-var, PC): (OM,4) (OM,4)

● calibration ● validation

● calibration ● validation



PLSR 21 MAF, (Y-var, PC): (OM,3) (OM,3)

Figure 4.27. (continuation) PLSR models obtained from raw reflectance acquired at each individual sampling period as well as the entire reflectance dataset showing relationship between calibration and validation dataset

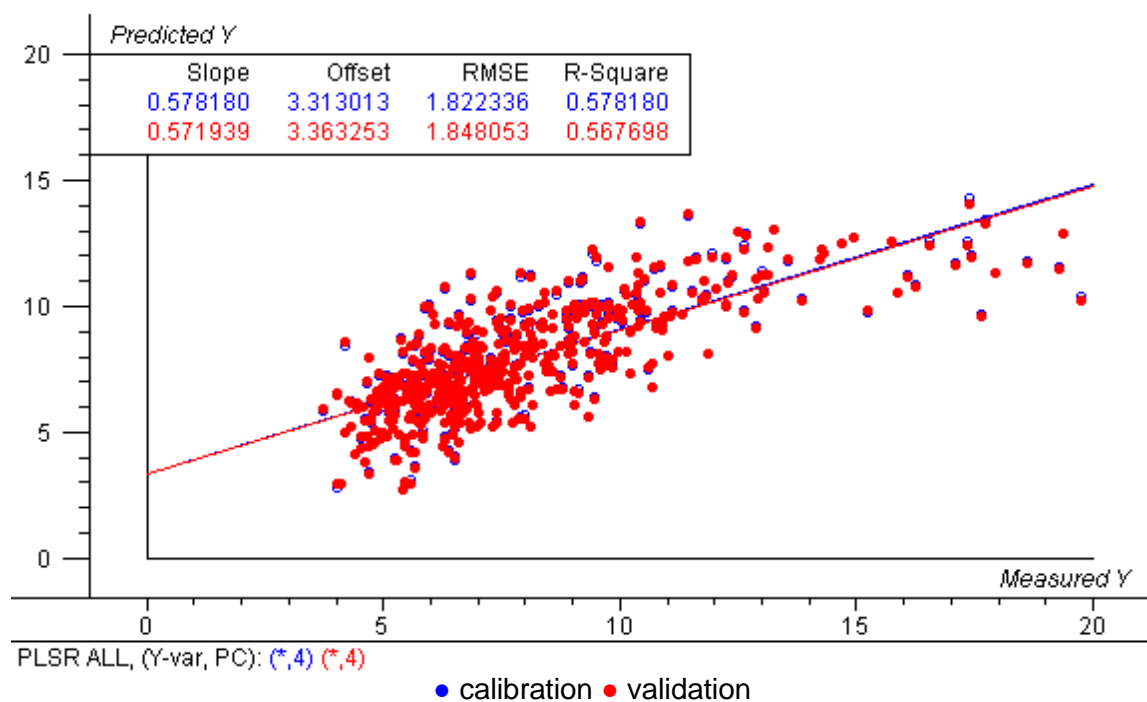
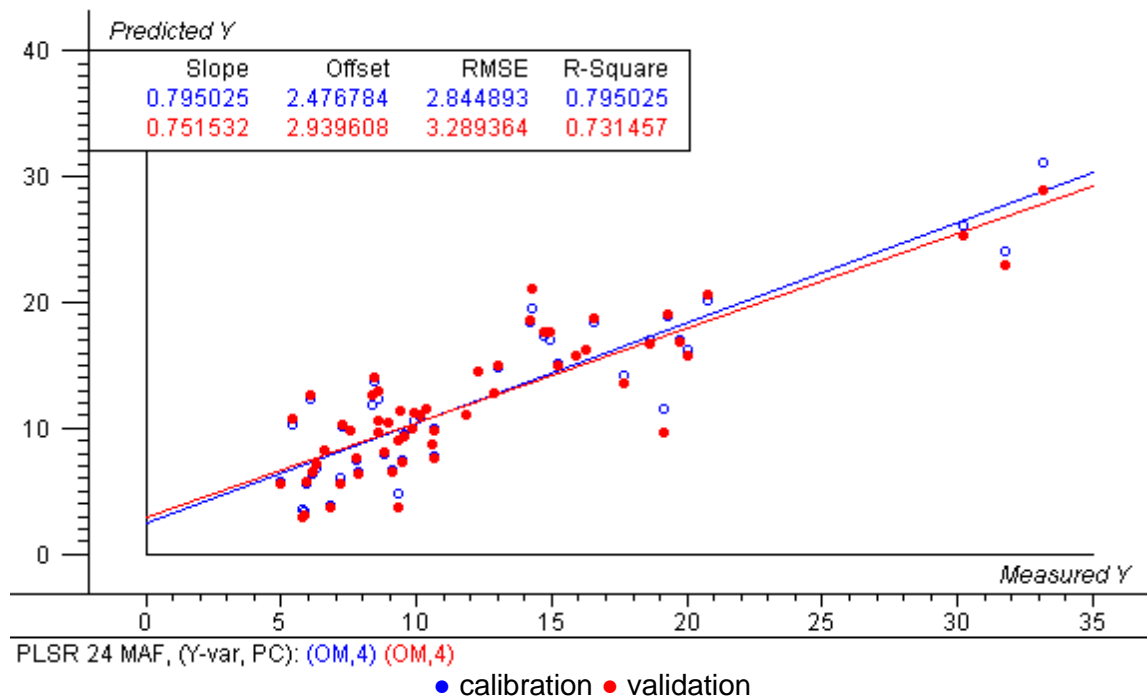


Figure 4.27. (continuation) PLSR models obtained from raw reflectance acquired at each individual sampling period as well as the entire reflectance dataset showing relationship between calibration and validation dataset

For ANN modelling, the input predictors (x-variables) were the PCA scores of raw reflectance data. Eleven (11) to eighteen (18) PCs summarised the most variation in the reflectance datasets (Table 4.6). The dataset was split in two parts: calibration (50%) and validation (50%). Overall, ten (10) ANN models were obtained, nine (9) for each sampling period and one (1) for the entire 0-24 MAF dataset. The outliers detected during PLSR modelling procedure were also removed from the ANN analysis.

By comparing the performance of linear and non-linear models, it became clear that ANN outperformed PLSR models, with RPD values ranging from 1.96 (9 MAF) to >2.5 (0, 3, 15, 18 and 24 MAF), which all fall in the category of very good and excellent models (Table 4.6). One exception was the model obtained at 21 MAF, when PLSR outperformed ANN with an RPD value of 2.29 (21 MAF ANN RPD=1.74).

Table 4.6. PLSR and ANN Model performance at each individual sampling period as well as the entire reflectance dataset

Dataset summary					Model performance						Unknown samples	
MIN	MAX	MEAN	SD	CV		NPC	RMSE <sub>C</sub>	RMSE <sub>P</sub>	R <sup>2</sup> <sub>C</sub>	R <sup>2</sup> <sub>P</sub>	RPD	Prediction deviation
<b>0 MAF (N=119)</b>												
4.68	23.89	8.60	4.12	0.48	PLSR	4	1.66	1.95	0.84	0.78	2.11	0.88
					ANN	11	0.41	0.82	0.99	0.96	>2.5	
<b>3 MAF (N=120)</b>												
4.52	20.34	7.65	2.81	0.37	PLSR	3	1.63	2.08	0.66	0.46	1.35	
					ANN	13	1.34	1.09	0.77	0.85	>2.5	1.01
<b>6 MAF (N=120)</b>												
4.21	22.80	7.97	3.28	0.41	PLSR	3	1.8	2.02	0.69	0.62	1.62	
					ANN	14	1.14	1.5	0.88	0.79	2.18	0.96
<b>9 MAF (N=120)</b>												
4.01	17.44	7.55	2.31	0.31	PLSR	5	1.19	1.35	0.73	0.66	1.71	
					ANN	13	0.95	1.18	0.83	0.74	1.96	1.1
<b>12 MAF (N=120)</b>												
4.44	12.93	7.14	2.13	0.30	PLSR	3	1.14	1.26	0.71	0.66	1.69	
					ANN	11	0.88	0.93	0.83	0.81	2.29	0.87
<b>15 MAF (N=120)</b>												
4.38	15.94	7.69	2.37	0.31	PLSR	4	1.08	1.18	0.79	0.76	2.01	
					ANN	14	0.82	0.34	0.88	0.98	>2.5	0.79
<b>18 MAF (N=120)</b>												
4.03	16.07	8.14	2.51	0.31	PLSR	4	1.03	1.13	0.83	0.8	2.22	
					ANN	13	0.5	0.94	0.96	0.86	>2.5	0.99
<b>21 MAF (N=120)</b>												
3.72	21.85	7.12	3.20	0.45	PLSR	3	1.21	1.4	0.86	0.82	2.29	1.16
					ANN	18	0.64	1.84	0.96	0.67	1.74	
<b>24 MAF (N=118)</b>												
4.99	33.19	12.08	6.34	0.52	PLSR	4	2.84	3.29	0.8	0.73	1.93	
					ANN	18	0.9	2	0.98	0.9	>2.5	0.89
<b>ALL MAF (N=1074)</b>												
3.72	33.19	8.33	3.86	0.46	PLSR	4	2.44	2.49	0.59	0.57	1.55	
					ANN	15	1.85	2.15	0.77	0.69	1.79	1.55

SD – Standard deviation; CV – Coefficient of variation; NPC – optimal number of principal components; RMSE<sub>C</sub> – Root mean square error of calibration; RMSE<sub>P</sub> – Root mean square error of prediction; R<sup>2</sup><sub>C</sub> – Coefficient of determination for calibration; R<sup>2</sup><sub>P</sub> – Coefficient of determination for validation; RPD – Ratio of performance to deviation. Prediction deviations are computed as a function of the model error, the sample leverage (a measure of how extreme an unknown data point is compared to the majority), and the sample residual variance.



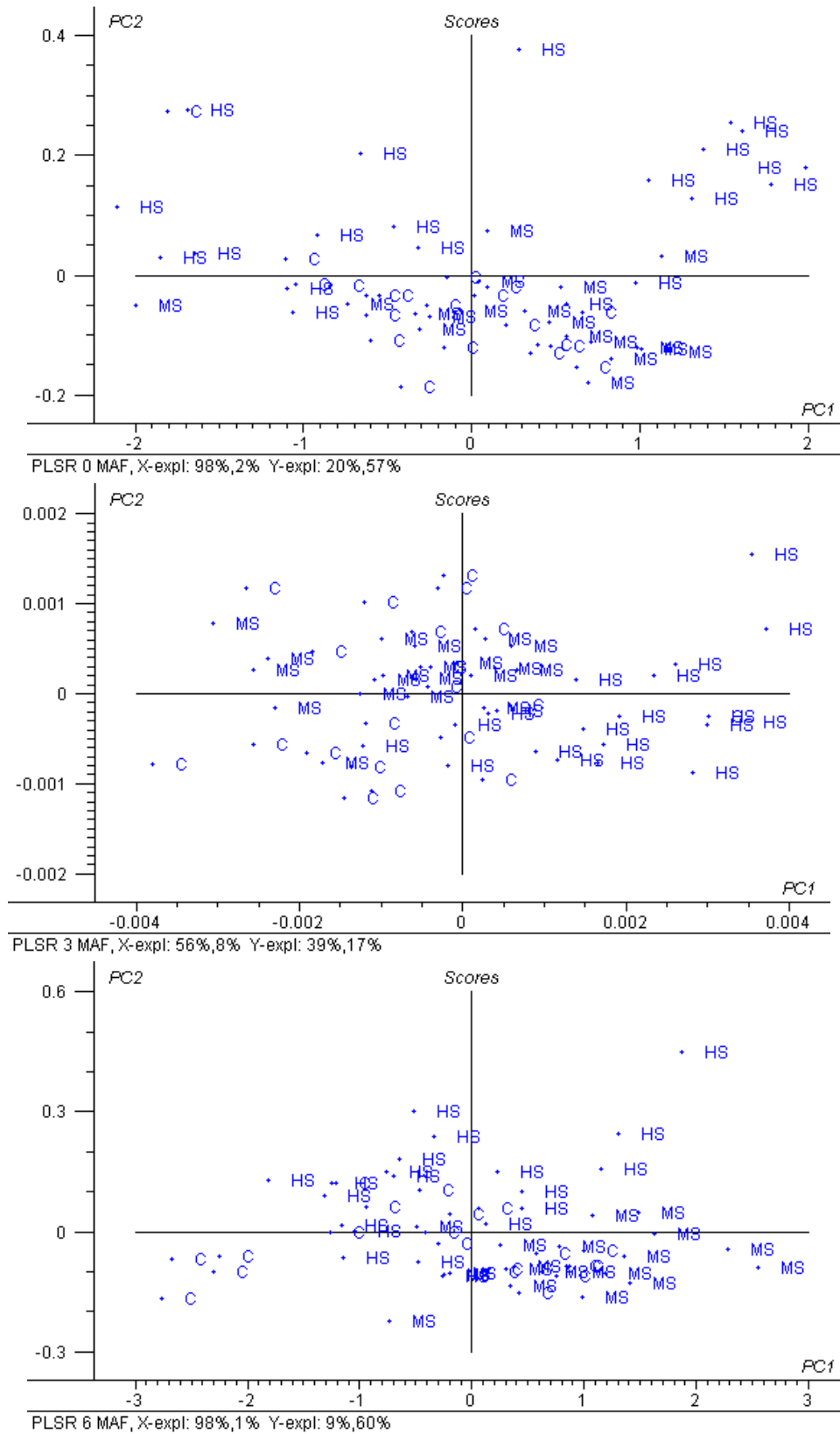


Figure 4.28. Score plots of PLSR models for the first 2 principal components explaining the most variance. Scores further out the scatter plot are extreme observations measured mostly in HS samples

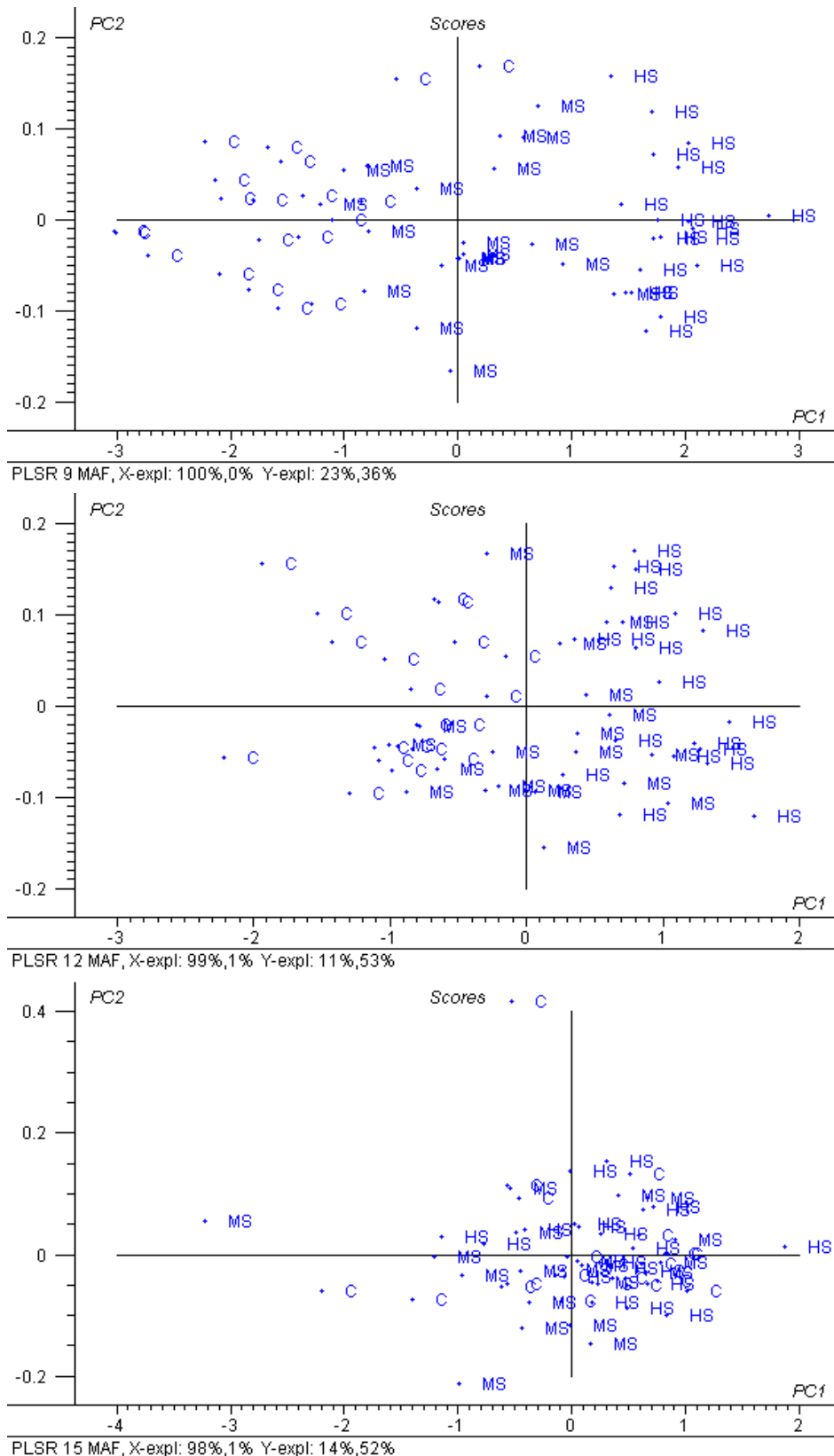


Figure 4.28. (continuation) Score plots of PLSR models for the first 2 principal components explaining the most variance. Scores further out the scatter plot are extreme observations measured mostly in HS samples

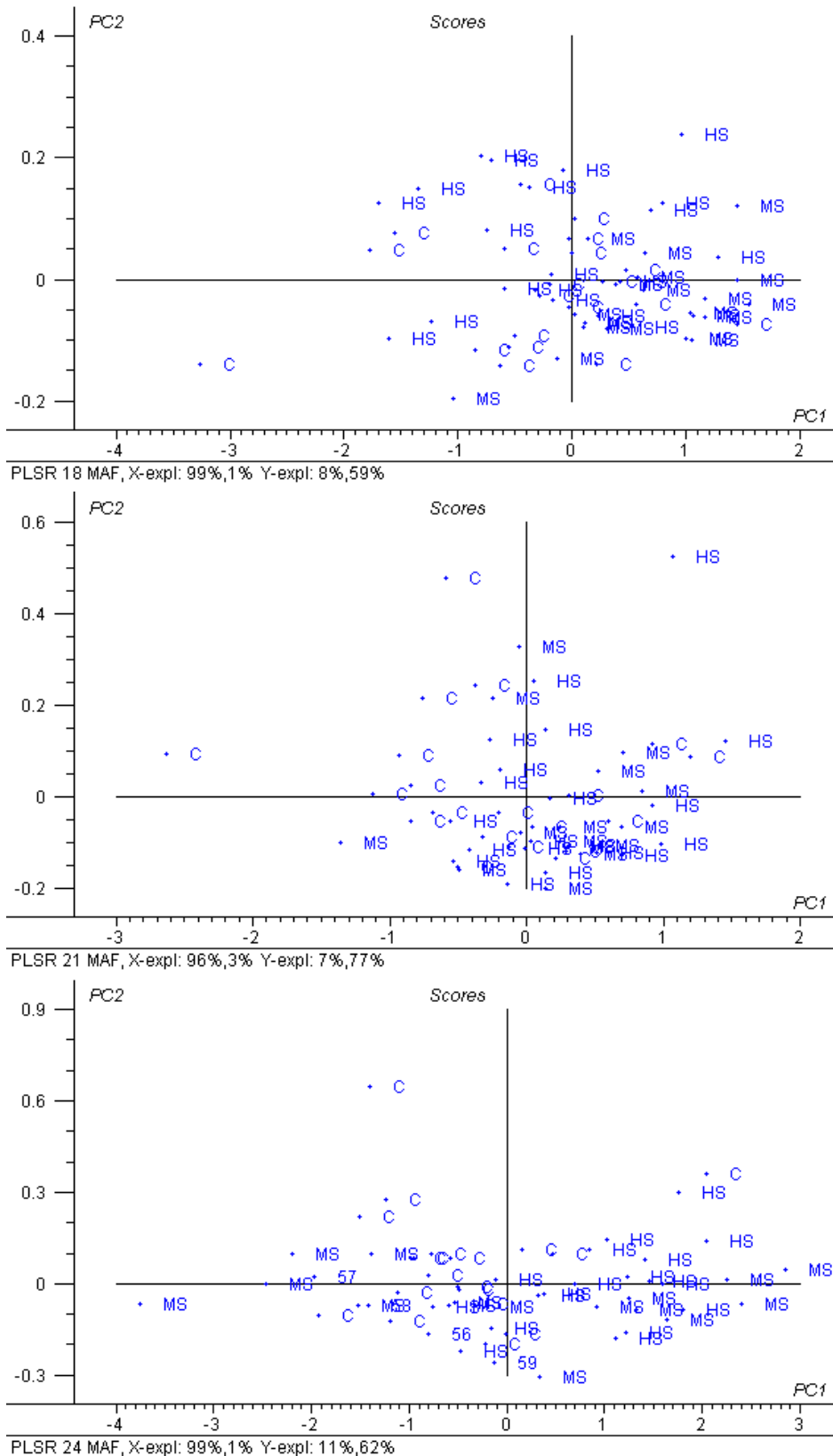


Figure 4.28. (continuation) Score plots of PLSR models for the first 2 principal components explaining the most variance. Scores further out the scatter plot are extreme observations measured mostly in HS samples

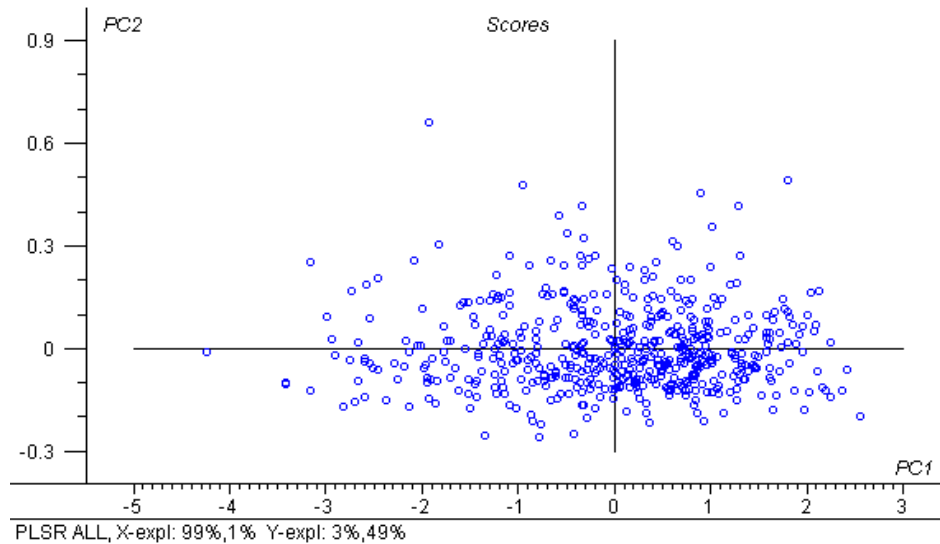


Figure 4.28. (continuation) Score plots of PLSR models for the first 2 principal components explaining the most variance. Scores further out the scatter plot are extreme observations measured mostly in HS samples

Figure 4.29 shows regression coefficients for the PCs that explained the most variance in the PLSR models and illustrates contributions of each spectral variable to the significant variation in the SOM data, detecting which spectral variables are most significant for predicting SOM content. Visible parts of the spectrum, namely 410 - ~550 nm and ~550 - ~620 nm, and NIR region > 1000 nm were identified as zones of major importance in all models.

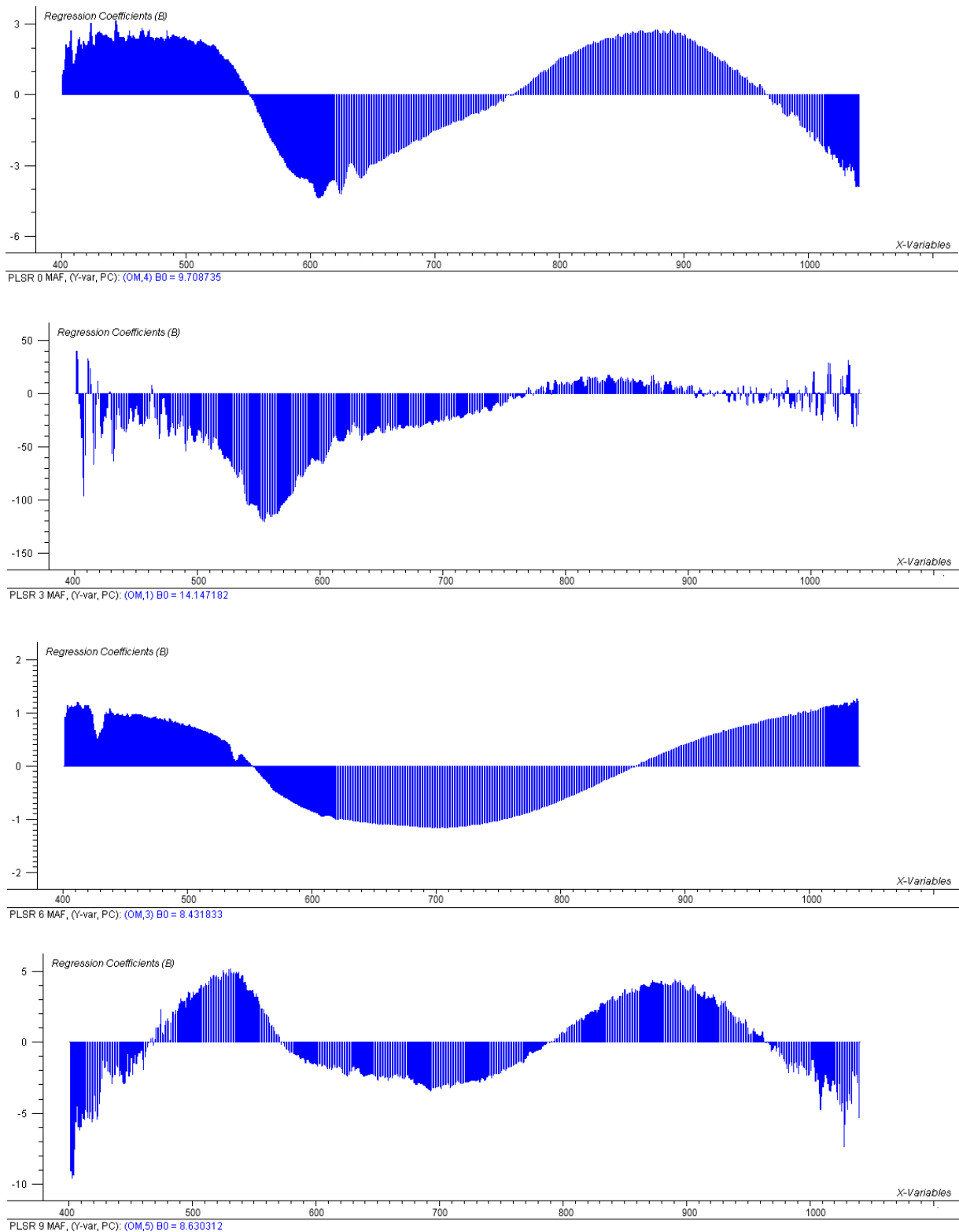


Figure 4.29. Variable importance projection for PLSR models calibrated at each sampling period to predict SOM content. Dark blue indicates statistically significant wavelengths (nm)

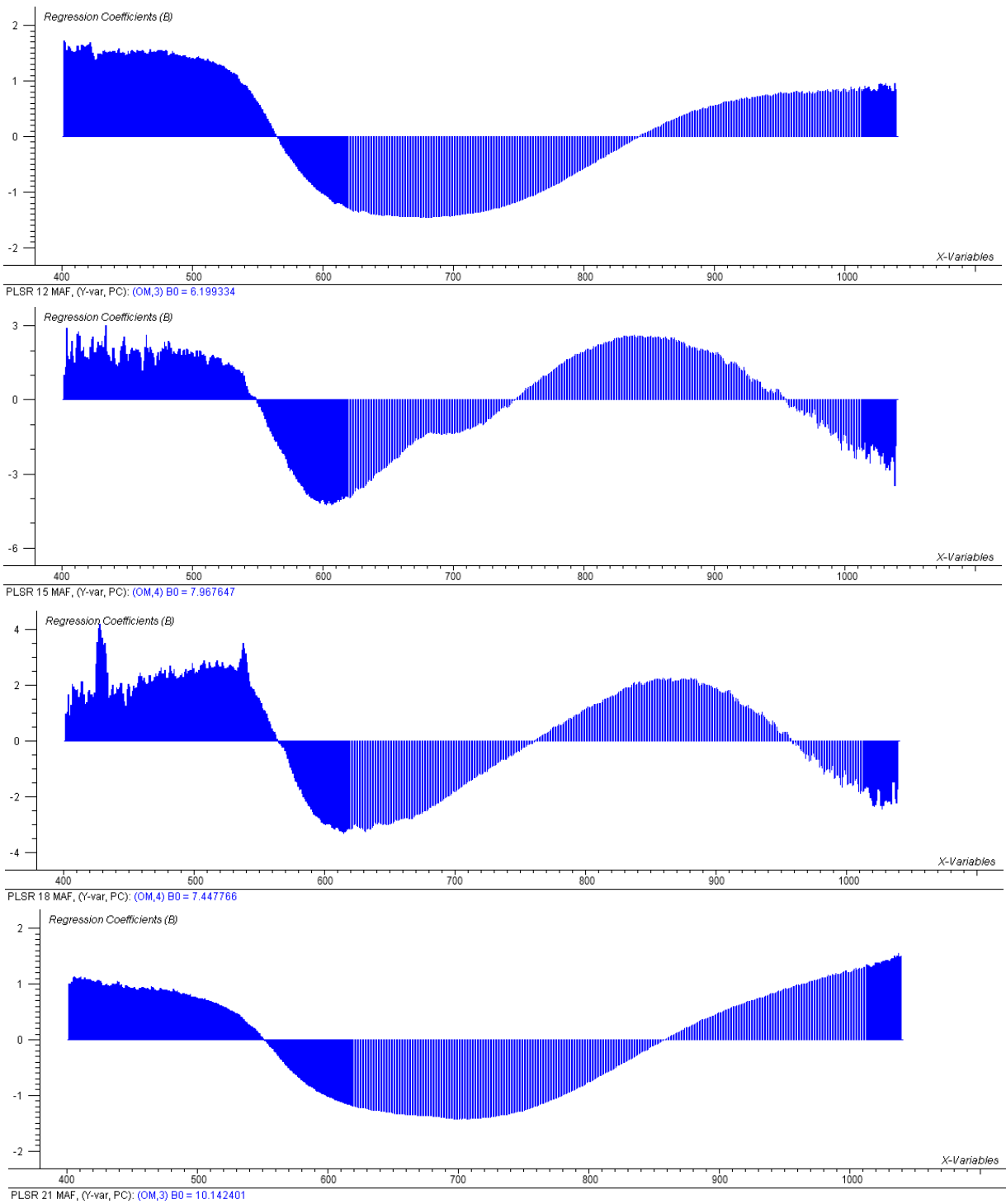


Figure 4.29. (continuation) Variable importance projection for PLSR models calibrated at each sampling period to predict SOM content. Dark blue indicates statistically significant wavelengths (nm)

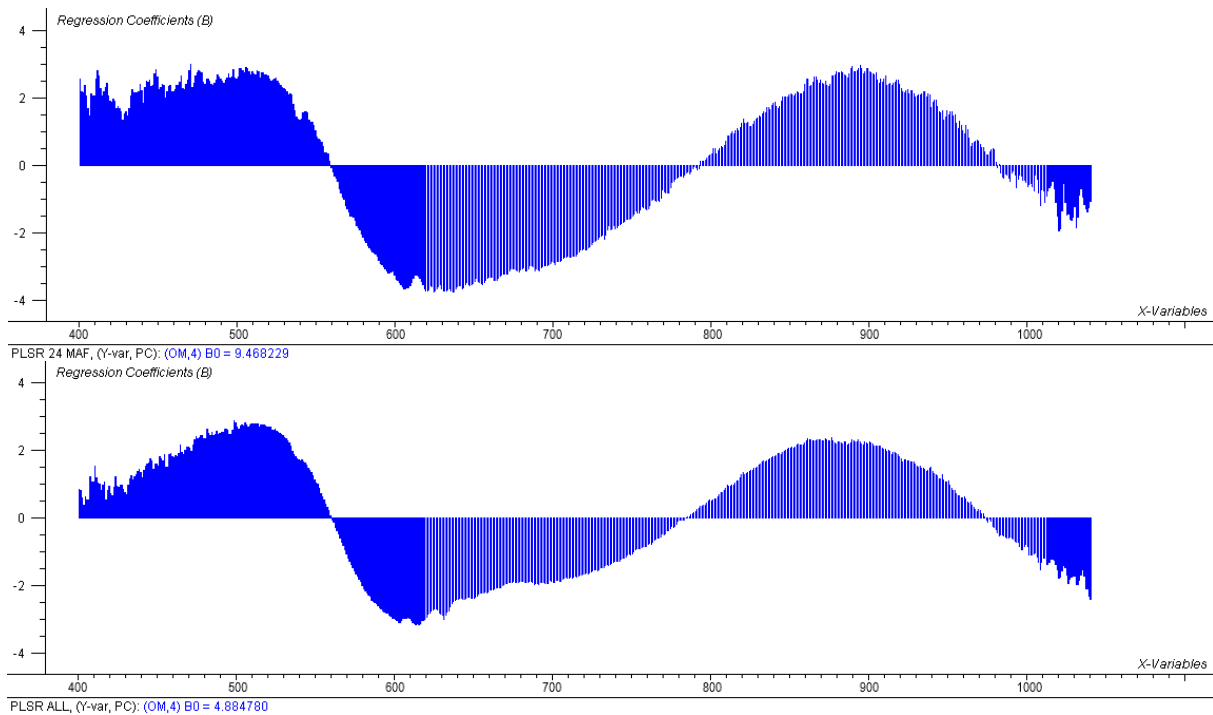


Figure 4.29. (continuation) Variable importance projection for PLSR models calibrated at each sampling period to predict SOM content. Dark blue indicates statistically significant wavelengths (nm)

#### 4.6.2. Comparison of models obtained from in-situ and laboratory reflectance measurements

The measured soil moisture on these two occasions is shown in Table 4.7, and was on average 37.3% and 22.9 %, respectively. Results of the partial least regression (PLSR) model calculated using spectral and SOM (%) data are shown in Figure 4.30. The independent (predictor) input was the raw reflectance data in the range from 410-1050 nm. The dataset was split in two parts: calibration (50%) and validation (50%).

Figure 4.30 shows the relationship between the measured and predicted SOM content in the calibration and validation datasets. Four PCs summarised the most variation in the laboratory VNIR dataset, and 6 PCs in-situ VNIR dataset. The PLSR model adequately predicted variations in SOM content in both laboratory and in-situ VNIR spectroscopy, with  $R^2_p=0.62$  and  $R^2_p=0.64$ , respectively. According to the RPD values (laboratory RPD=1.62; in-situ RPD=1.67), both models yielded fair models and may be used for further prediction for soil mapping purposes (Table 4.8).

Table 4.7. Average moisture (%) content of all soil samples taken 3 and 15 months after the wildfire (N=120)

	Time	
	3 MAF	15 MAF
N	60	60
Min	27.50	13.49
Max	53.85	31.45
Mean	37.33	22.88
SD	7.25	4.95
CV	0.19	0.22

SD – Standard deviation; CV – Coefficient of variation



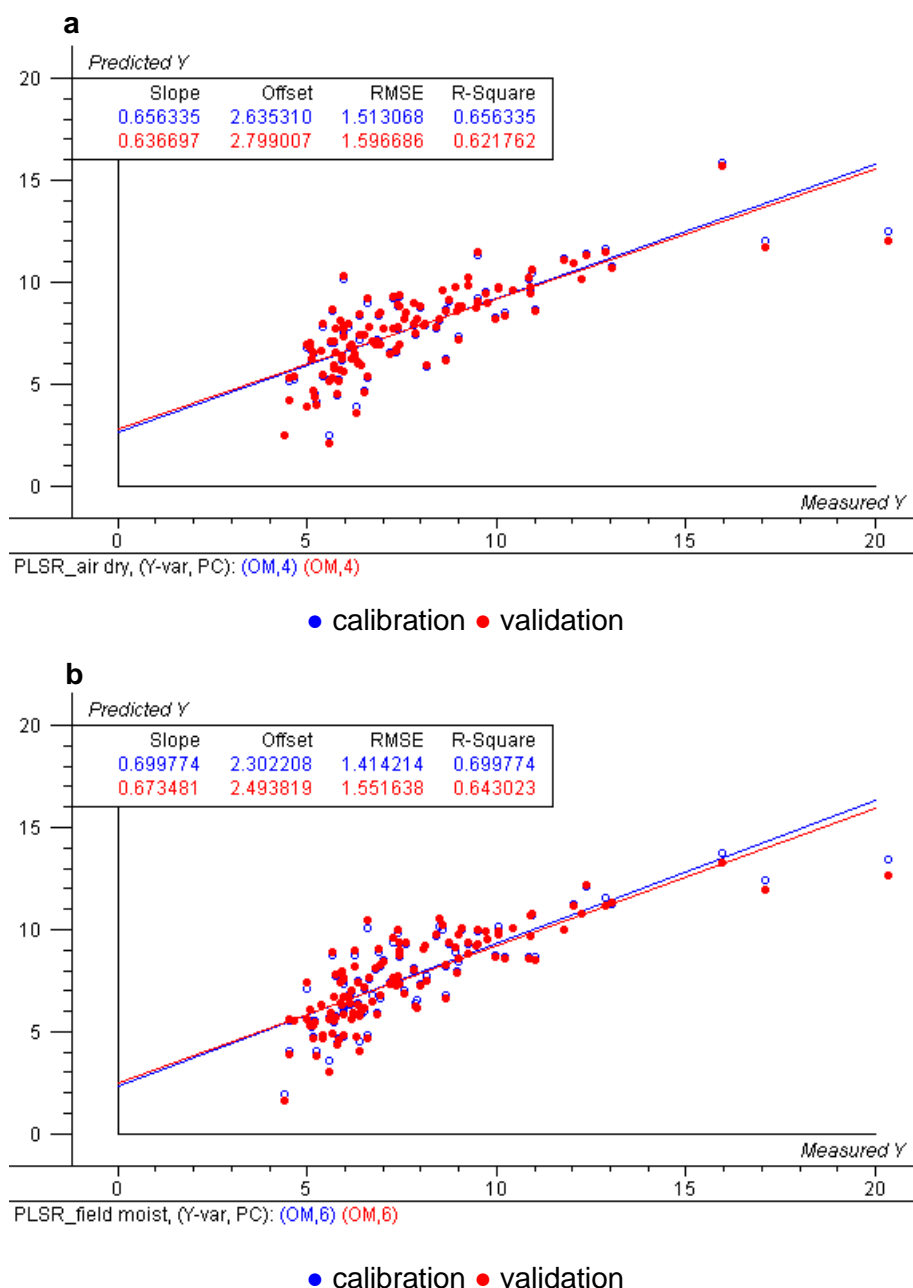


Figure 4.30. Results of the PLSR model showing relationship between predicted and observed SOM content (%) using **a**) laboratory and **b**) in-situ raw reflectance data

For ANN modelling, the input predictors were the PCA scores of raw reflectance data. Twenty-four (24) and twenty-seven (27) PCs summarised the most variation in the laboratory and in-situ VNIR dataset, respectively. ANN model adequately predicted variations in SOM content in both laboratory and in-situ VNIR spectroscopy with  $R^2_{p=}$  0.64 and  $R^2_{p=}$  0.72, respectively. According to the RPD values (laboratory RPD=1.67; in-situ RPD=1.75), both models performed better than PLSR models, and may be used for further prediction for soil mapping purposes, where large numbers of analyses are usually preferred (Table 4.8).

Table 4.8. Model performance of laboratory (air dry) and in situ (field moist) spectroscopy

Dataset summary					Model performance						
MIN	MAX	MEAN	SD	CV		NP C	RMSE <sub>C</sub>	RMSE <sub>P</sub>	R <sup>2</sup> <sub>C</sub>	R <sup>2</sup> <sub>P</sub>	RPD
<b>Laboratory VNIR (N=240)</b>											
4.38	20.34	7.67	2.59	0.3	PLSR	4	1.51	1.6	0.66	0.62	1.62
				4	ANN	24	1.24	1.55	0.77	0.64	1.67
<b>In-situ VNIR (N=240)</b>											
4.38	20.34	7.67	2.59	0.3	PLSR	6	1.41	1.55	0.7	0.64	1.67
				4	ANN	27	0.52	1.37	0.96	0.72	1.75

SD – Standard deviation; CV – Coefficient of variation; NPC – optimal number of principal components; RMSE<sub>C</sub> – Root mean square error of calibration; RMSE<sub>P</sub> – Root mean square error of prediction; R<sup>2</sup><sub>C</sub> – Coefficient of determination for calibration; R<sup>2</sup><sub>P</sub> – Coefficient of determination for validation; RPD – Ratio of performance to deviation

#### 4.6.3. Comparison of models obtained from laboratory (hyperspectral) and satellite (multispectral) reflectance measurements

Results of the partial least regression (PLSR) model calculated using spectral and SOM (%) data are shown in Figure 4.31. In the laboratory-based modelling using hyperspectral reflectance, the independent input (predictor) was the raw reflectance data spanning the range of 410-1050 nm. On the other hand, for the modelling utilising satellite-based reflectance, the inputs comprised eight VNIR bands and two SWIR bands extracted from the respective pixels of Sentinel-2 images (see table 3.4). The datasets were split in two parts: calibration (50%) and validation (50%).

Figure 4.31 shows the relationship between the measured and predicted SOM content in the calibration and validation datasets. Eight (8) PCs summarised the most variation in the laboratory VNIR dataset, and five (5) PCs Sentinel-2 dataset. The PLSR model adequately predicted variations in SOM content in VNIR spectroscopy, with  $R^2_p=0.58$ , however it was inadequate for the Sentinel-2 dataset with  $R^2_p=0.33$ . According to the RPD values, only laboratory calibrations provided a fair model (RPD=1.58), while Sentinel-2 calibrations produced a poor model (RPD=1.17) that can only distinguish between high and low SOM content (Table 4.9).

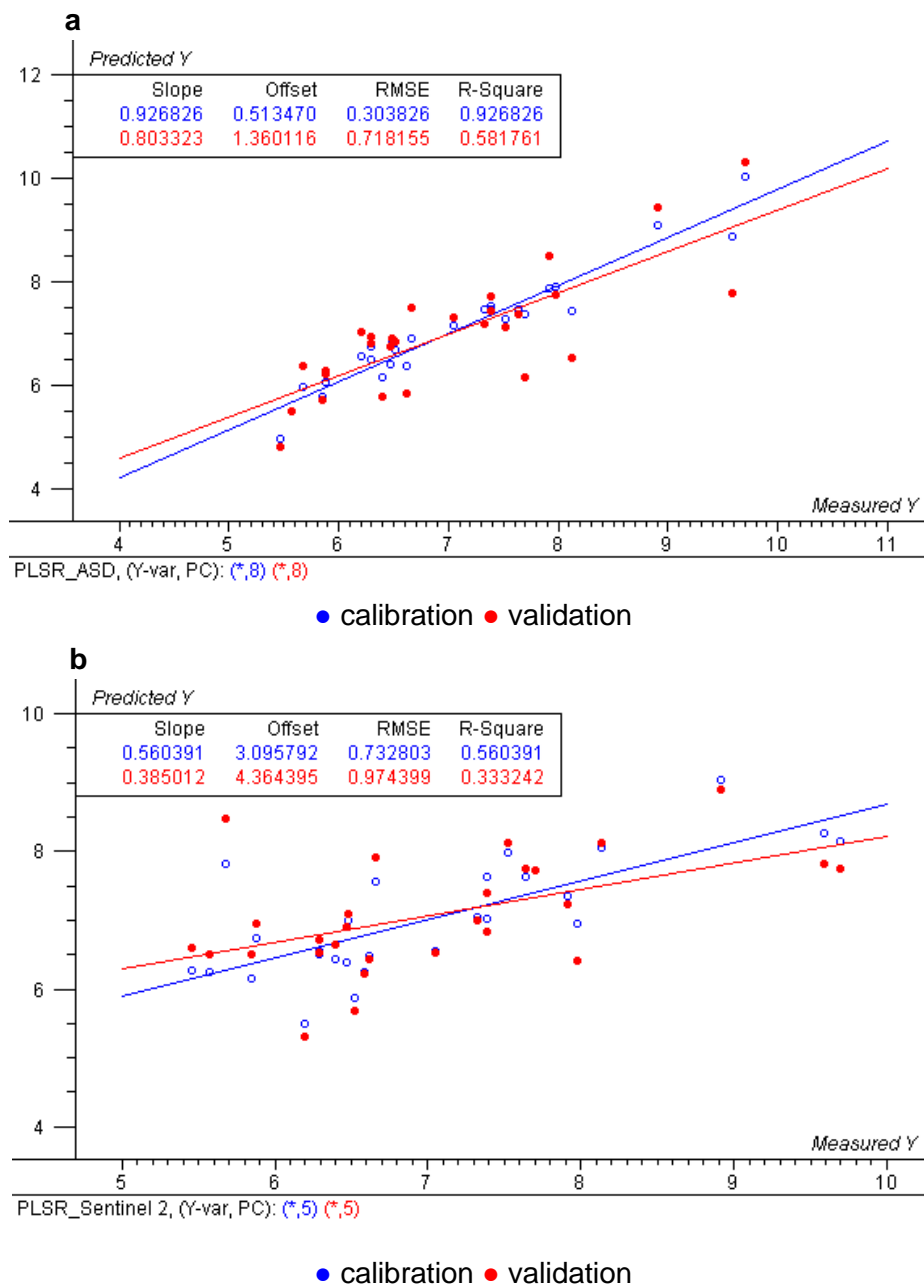


Figure 4.31. Results of the PLSR model showing relationship between predicted and observed SOM content (%) using **a**) laboratory hyperspectral and **b**) Sentinel-2 multispectral reflectance data (N=28)

For ANN modelling of the laboratory VNIR data, the input predictors were the PCA scores of raw reflectance data. Thirteen (13) PCs summarised the most variation in the dataset, and ANN model adequately predicted variations in SOM with  $R^2_p = 0.74$  and RPD= 1.97, indicating a good model.

PCA was not necessary for ANN modelling of the Sentinel-2 data, because it consisted of only 10 bands for 28 samples (as explained in chapter 3.4). The ANN model performed better than

the PLSR model for multispectral data, and adequately predicted variations in SOM with  $R^2_P=0.88$  and  $RPD=1.48$ , indicating a fair model (Table 4.9).

Table 4.9. Model performance of laboratory and Sentinel-2 reflectance data

Dataset summary					Model performance						
MIN	MAX	MEAN	SD	CV		NPC	RMSE <sub>C</sub>	RMSE <sub>P</sub>	R <sup>2</sup> <sub>C</sub>	R <sup>2</sup> <sub>P</sub>	RPD
<b>Laboratory VNIR</b>											
5.46	9.70	7.02	1.14	0.16	PLSR	8	0.3	0.72	0.93	0.58	1.58
					ANN	13	0.28	0.58	0.94	0.74	1.97
<b>Sentinel-2</b>											
5.46	9.70	7.02	1.14	0.16	PLSR	5	0.73	0.97	0.56	0.33	1.17
					ANN	-	0.77	0.77	0.88	0.88	1.48

SD – Standard deviation; CV – Coefficient of variation; NPC – optimal number of principal components; RMSE<sub>C</sub> – Root mean square error of calibration; RMSE<sub>P</sub> – Root mean square error of prediction; R<sup>2</sup><sub>C</sub> – Coefficient of determination for calibration; R<sup>2</sup><sub>P</sub> – Coefficient of determination for validation; RPD – Ratio of performance to deviation

Figure 4.32 shows regression coefficients for the PCs that explained the most variance in the PLSR models and illustrates contributions of each spectral variable to the significant variation in the SOM data. According to proximal-derived regression coefficients, peaks in the 410-700 nm can be identified as zones of major importance, while satellite derived regression coefficients show B8 and B11, recording wavelengths at 842 and 1610 nm, respectively, as spectral variables most significant for predicting SOM content.

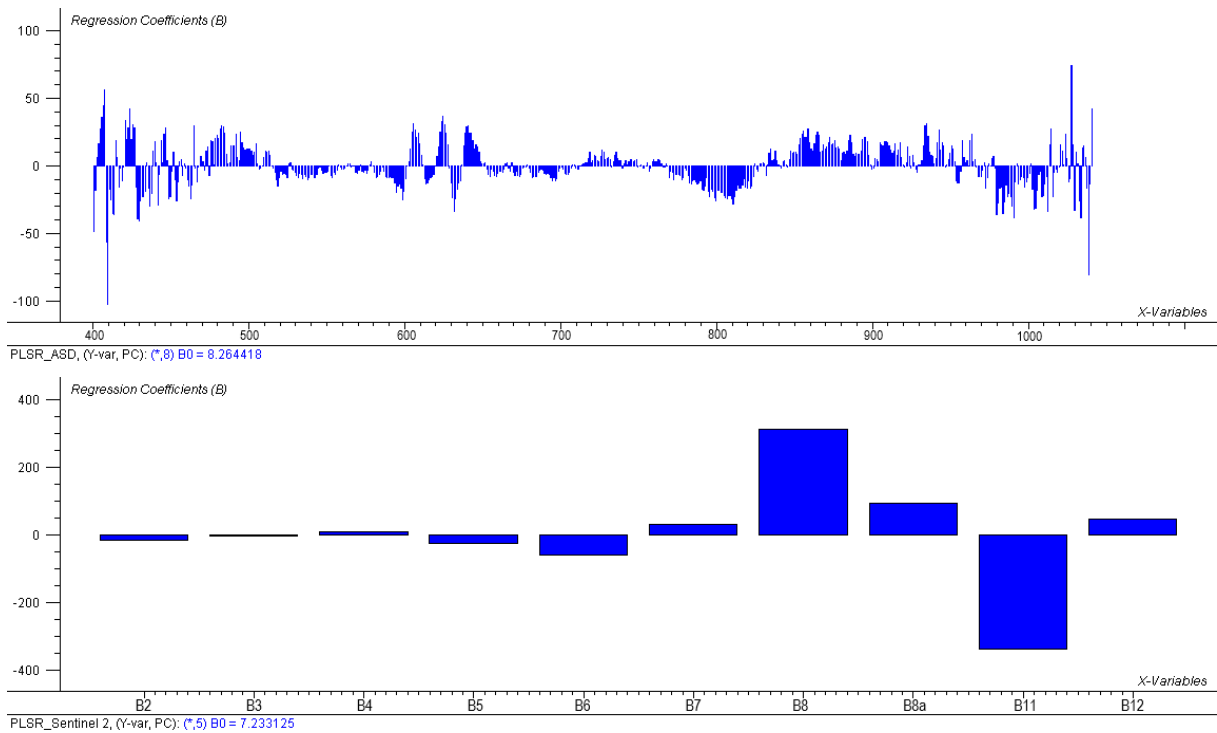


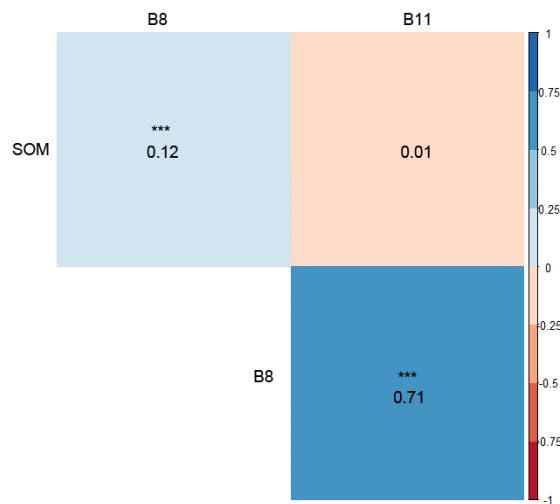
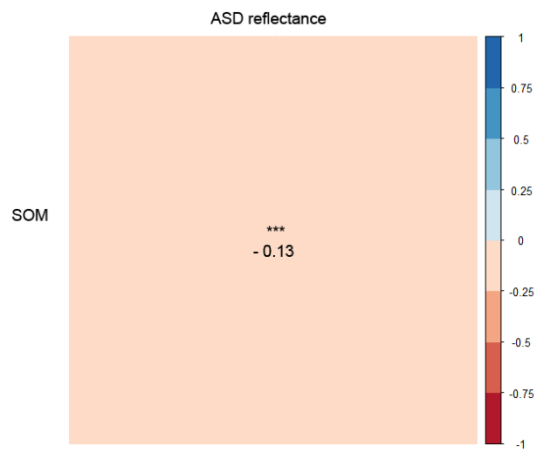
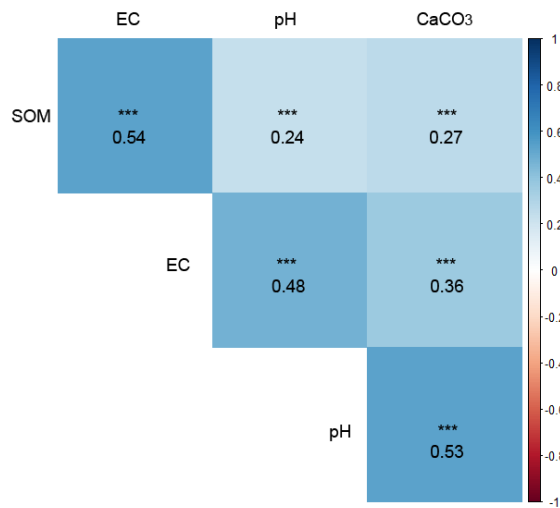
Figure 4.32. Variable importance projection for PLSR models calibrated from the same dataset at 0 MAF but measured with proximal (ASD) and satellite (Sentinel-2) sensors to predict SOM content. Dark blue indicates statistically significant wavelengths (nm)

## 4.7. Geostatistical univariate and multivariate modelling and mapping of SOM

Results of the descriptive parameters of SOM, soil pH, EC and CaCO<sub>3</sub> content are shown in Chapters 4.3 and 4.4. SOM, soil EC and CaCO<sub>3</sub> content showed non-normal distribution and were transformed, however due to inability of normalisation of the CaCO<sub>3</sub> data, the decision was made to use the original dataset in the analysis. Figure 4.33 shows the correlation matrix of the measured soil properties, along with the correlation matrix of average reflectance data and the two most significant Sentinel-2 bands (B8 and B11) for predicting SOM content (see Figure 4.32). Significant positive correlations were observed between soil pH, EC, and CaCO<sub>3</sub> content with SOM. Among these correlations, the strongest was found between SOM and EC (0.54), while the weakest was observed between SOM and soil pH (0.24). In contrast, the correlation coefficient for average reflectance data displayed a significant negative correlation with SOM, measuring -0.13. Regarding the Sentinel-2 bands, B8 exhibited a significant positive correlation with SOM (0.12), whereas B11 did not show a significant correlation. For this reason, only B8 was used as a covariate in the OCK method.

The variogram characteristics (nugget, sill, range) and best fit models for 0-24 MAF data is shown in Table 4.10. The pure nugget effect was recorded immediately post-fire (at 0 MAF) and at 15 MAF in OK method, and at 0, 9, 12 and 15 MAF in OCK method when using CaCO<sub>3</sub> as a covariate. Overall, a larger nugget was observed in all OK methods throughout the study period (0.89-28.4), compared to OCK (0.001-16.6). Nugget/Sill ratio in OK varied from 10% to 74%, indicating strong to moderate spatial dependence of SOM content. The ratio in OCK with EC as a covariate varied from <0.1% to 19%, which shows strong spatial dependence of SOM content. In the case of pH as a covariate, the ratio varied from 4% to 97%. This suggests a range of spatial dependence, from strong to weak, in relation to SOM content. For CaCO<sub>3</sub> as a covariate, the ratio spanned from 2.2% to 30%, indicating a range of spatial dependence from strong to moderate with respect to SOM content.

When average reflectance was used as a covariate, the ratio showed a range of 0.4% to 97%, implying a variety of spatial dependence levels, ranging from strong to weak, in relation to SOM content. Throughout the majority of the research period, the relative improvement (RI) of the prediction accuracy was best in OCK with EC as a covariate, and varied from 4% (observed at 15 MAF) to 27% (observed at 3 MAF). Only at 0 MAF and 15 MAF, the RI was best in OCK with average reflectance as a covariate, with respective values of 23% and 15%. Figure 4.34 shows the final post-fire SOM content maps obtained with the most accurate method for each specific sampling period.



\*\*\* Correlation is significant at the 0.05 level

Figure 4.33. Correlation matrix of the measured soil properties, average reflectance values measured with a proximal (ASD) sensor and two Sentinel-2 bands most significant for predicting SOM content



Table 4.10. Model parameters fitted for semivariogram of SOM and cross-semivariograms between SOM and selected covariables

Time	Method	Model	C <sub>0</sub>	C	Range (m)	C <sub>0</sub> /C <sub>0</sub> +C (%)	Spatial dependence	RMSE	RI (%)
0 MAF	OK	Gauss	19.13	0	74.34	-	no	1.01	
	OCK_EC	Exp	0.03	723.3	18.98	<0.1	strong	0.83	+17.8
	OCK_pH	Stable	0.5	0.59	19.28	46	moderate	0.83	+17.8
	OCK_CaCO <sub>3</sub>	Exp	0.04	0	74.34	-	no	1.01	0.0
	<b>OCK_Reflectance</b>	<b>Stable</b>	<b>0.001</b>	<b>0.05</b>	<b>18.98</b>	<b>2</b>	<b>strong</b>	<b>0.78</b>	<b>+22.8</b>
OCK_Sentinel	J-Bess	0.002	0.008	38.61	20	strong	0.98	+3.0	
3 MAF	OK	Gauss	6.68	2.29	423.1	74	moderate	1.07	
	OCK_EC	<b>Exp</b>	<b>0.5</b>	<b>121.76</b>	<b>18.98</b>	<b>0.4</b>	<b>strong</b>	<b>0.78</b>	<b>+27.1</b>
	OCK_pH	Stable	0.43	0.45	26.6	49	moderate	0.91	+15.0
	OCK_CaCO <sub>3</sub>	Exp	0.04	0.61	18.98	6	strong	0.88	+17.8
	OCK_Reflectance	Stable	0.002	0.03	22.12	6	strong	0.87	+18.7
6 MAF	OK	Gauss	2.47	12.91	39.27	16	strong	1.01	
	OCK_EC	<b>Exp</b>	<b>2.3</b>	<b>349.58</b>	<b>23.31</b>	<b>1</b>	<b>strong</b>	<b>0.81</b>	<b>+19.8</b>
	OCK_pH	Stable	0.03	0.75	50.06	4	strong	0.89	+11.9
	OCK_CaCO <sub>3</sub>	J-Bess	0.03	1.32	37.66	2.2	strong	0.89	+11.9
	OCK_Reflectance	Sph	0.002	0.02	51.13	9	strong	0.88	+12.9
9 MAF	OK	Exp	0.89	7.87	42.72	10	strong	0.94	
	OCK_EC	<b>Exp</b>	<b>5.5</b>	<b>98.87</b>	<b>42.72</b>	<b>5</b>	<b>strong</b>	<b>0.8</b>	<b>+14.9</b>
	OCK_pH	Exp	0.006	0.47	19.28	1	strong	0.89	+5.3
	OCK_CaCO <sub>3</sub>	Exp	0.02	0	270.31	-	no	0.93	+1.1
	OCK_Reflectance	K-Bess	0.003	0.07	19.38	4.1	strong	0.92	+2.1
12 MAF	OK	Rat.Q.	2.38	3.86	46.73	38	moderate	0.93	
	OCK_EC	<b>K-Bess</b>	<b>16.6</b>	<b>70.76</b>	<b>48.22</b>	<b>19</b>	<b>strong</b>	<b>0.81</b>	<b>+12.9</b>
	OCK_pH	Exp	0.16	0.34	42.84	32	moderate	0.87	+6.5
	OCK_CaCO <sub>3</sub>	Exp	0.08	0	46.84	-	no	0.89	+4.3
	OCK_Reflectance	Stable	0.7	0.02	52.2	97	weak	0.89	+4.3
15 MAF	OK	Exp	3.92	0	423.1	-	no	1	
	OCK_EC	Stable	9.29	38.04	32.84	20	strong	0.96	+4.0
	OCK_pH	Stable	0.18	0.006	57.09	97	weak	0.98	+2.0
	OCK_CaCO <sub>3</sub>	Exp	0.01	0	38.06	-	no	0.99	+1.0
	<b>OCK_Reflectance</b>	<b>J-Bess</b>	<b>0.001</b>	<b>0.01</b>	<b>27.6</b>	<b>9</b>	<b>strong</b>	<b>0.85</b>	<b>+15.0</b>
18 MAF	OK	Exp	3.34	3.94	43.86	46	moderate	0.91	
	OCK_EC	<b>Stable</b>	<b>0.3</b>	<b>58.48</b>	<b>52.2</b>	<b>1</b>	<b>strong</b>	<b>0.81</b>	<b>+11.0</b>
	OCK_pH	Stable	0.03	0.26	42.72	10	strong	0.87	+4.4
	OCK_CaCO <sub>3</sub>	Sph	0.004	0.15	42.95	3	strong	0.82	+9.9
	OCK_Reflectance	Sph	0.003	0.02	44.1	13	strong	0.89	+2.2
21 MAF	OK	Rat.Q.	2.69	9.72	73.46	22	strong	0.85	
	OCK_EC	<b>Stable</b>	<b>5.12</b>	<b>1205</b>	<b>104.24</b>	<b>0.4</b>	<b>strong</b>	<b>0.72</b>	<b>+15.3</b>
	OCK_pH	Stable	0.04	0.53	47.29	7	strong	0.84	+1.2
	OCK_CaCO <sub>3</sub>	Exp	0.03	0.07	49.97	30	moderate	0.84	+1.2
	OCK_Reflectance	Exp	0.001	0.004	74.57	20	strong	0.83	+2.4
24 MAF	OK	Rat.Q.	28.4	22.53	403.63	56	moderate	1.08	
	OCK_EC	<b>Stable</b>	<b>0.5</b>	<b>256.04</b>	<b>28.99</b>	<b>0.2</b>	<b>strong</b>	<b>0.88</b>	<b>+18.5</b>
	OCK_pH	Stable	0.21	0.37	19.84	36	moderate	0.98	+9.3
	OCK_CaCO <sub>3</sub>	J-Bess	0.05	0.34	56.37	13	strong	1.01	+6.5
	OCK_Reflectance	J-Bess	0.003	0.007	63.71	30	moderate	1.02	+5.6

C<sub>0</sub> – Nugget; C – Partial Sill; C<sub>0</sub>/C<sub>0</sub>+C – Nugget/Sill ratio; RMSE – Root mean square error; RI – Relative improvement; OK – Ordinary kriging; OCK – Ordinary cokriging; Gauss – Gaussian model; Exp – Exponential model; J-Bess – J-Bessel model; Sph – Spherical model; K-Bess – K-Bessel model; Rat.Q. – Rational Quadratic model

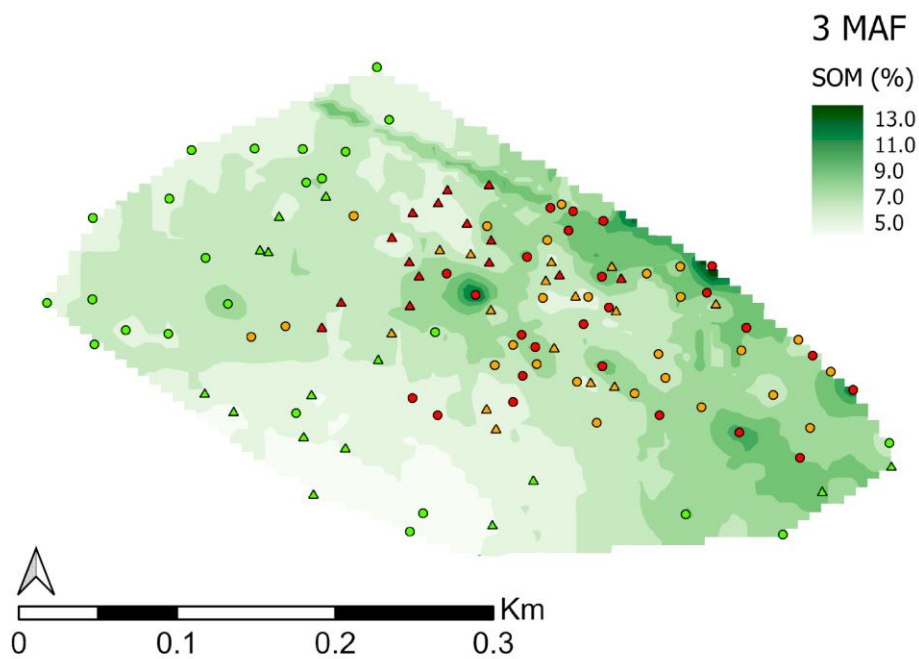
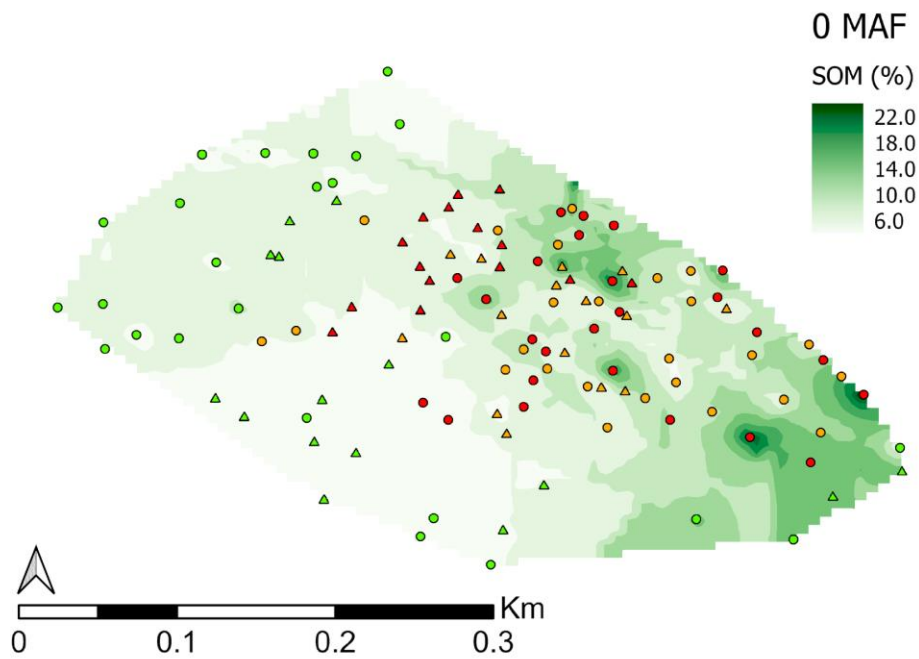


Figure 4.34. Post-fire soil organic matter (SOM) content maps for the 2-year study period (0-24 months after fire MAF). Different shapes denote vegetation species (circles indicate samples under *Quercus pubescens* Willd.; triangles indicate samples under *Juniperus communis* L.) and different colours denote wildfire severity (green - C; orange - MS; red - HS)

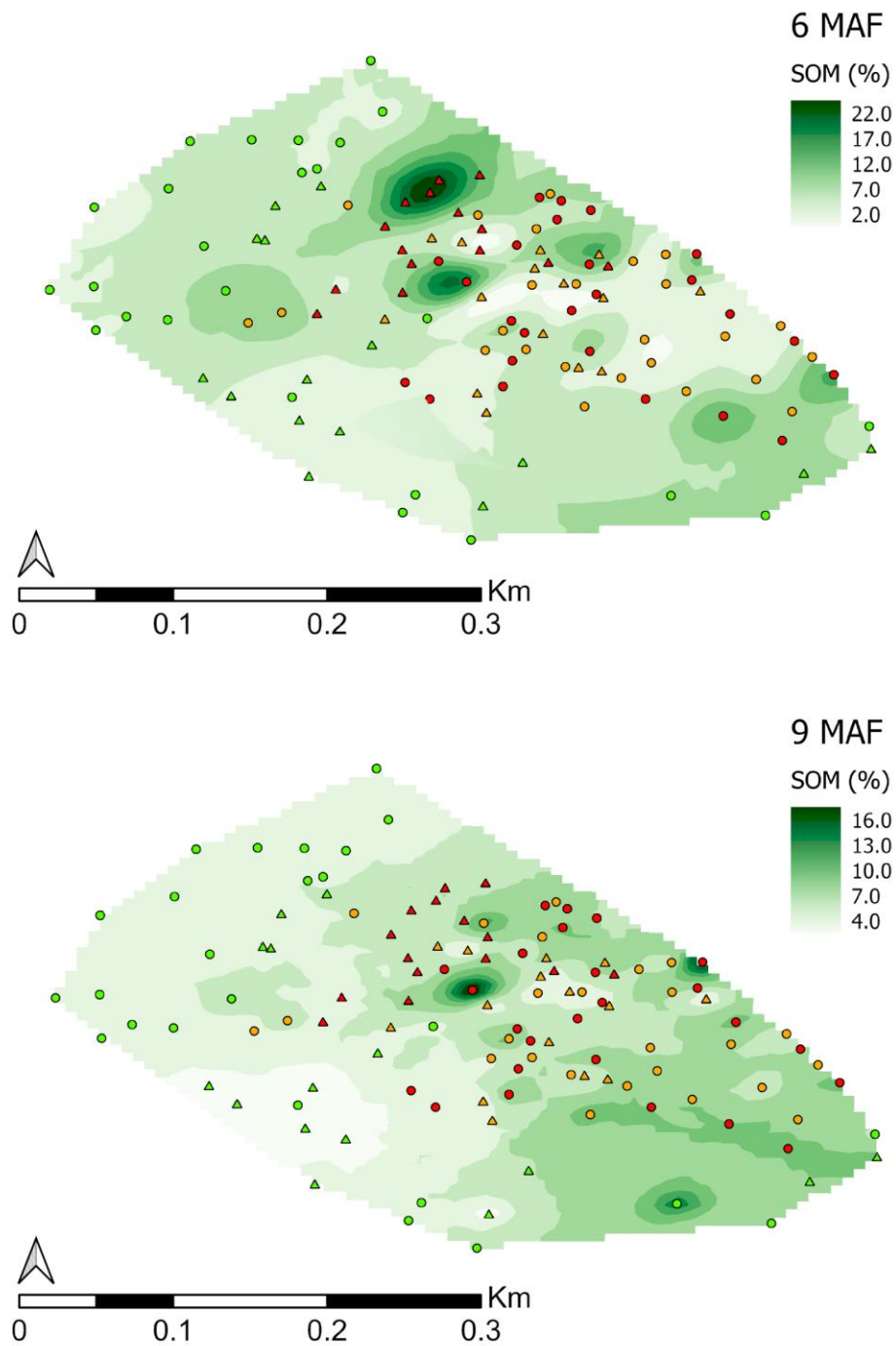


Figure 4.34. (continuation) Post-fire soil organic matter (SOM) content maps for the 2-year study period (0-24 months after fire MAF). Different shapes denote vegetation species (circles indicate samples under *Quercus pubescens* Willd.; triangles indicate samples under *Juniperus communis* L.) and different colours denote wildfire severity (green - C; orange - MS; red - HS)

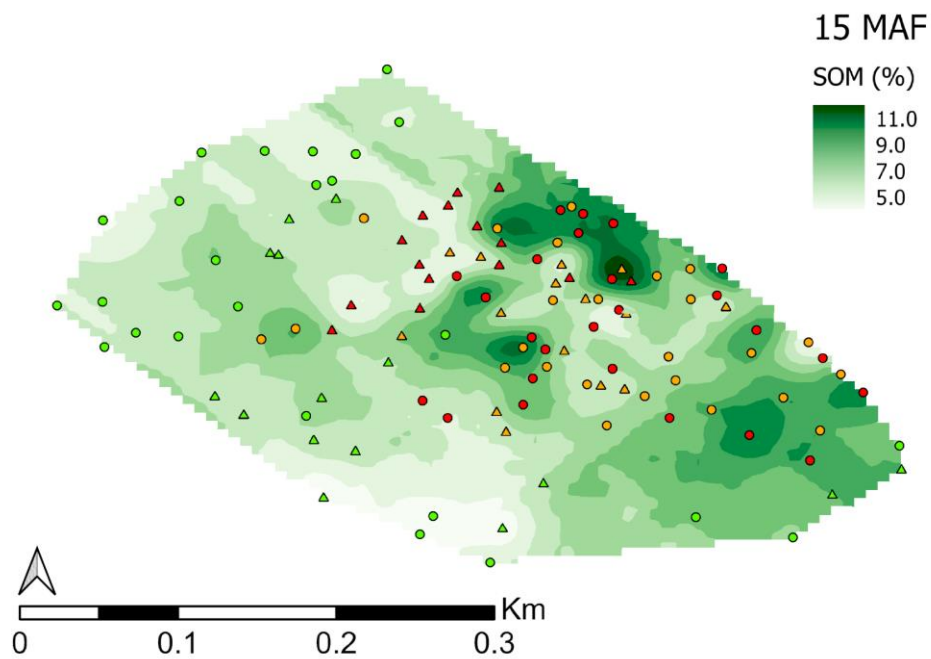
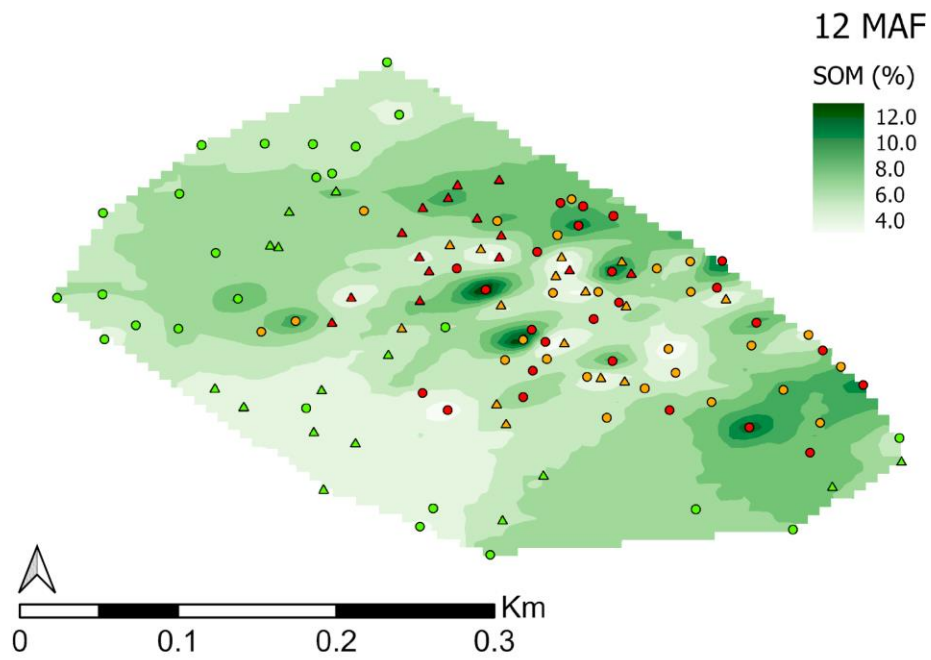


Figure 4.34. (continuation) Post-fire soil organic matter (SOM) content maps for the 2-year study period (0-24 months after fire MAF). Different shapes denote vegetation species (circles indicate samples under *Quercus pubescens* Willd.; triangles indicate samples under *Juniperus communis* L.) and different colours denote wildfire severity (green - C; orange - MS; red - HS)

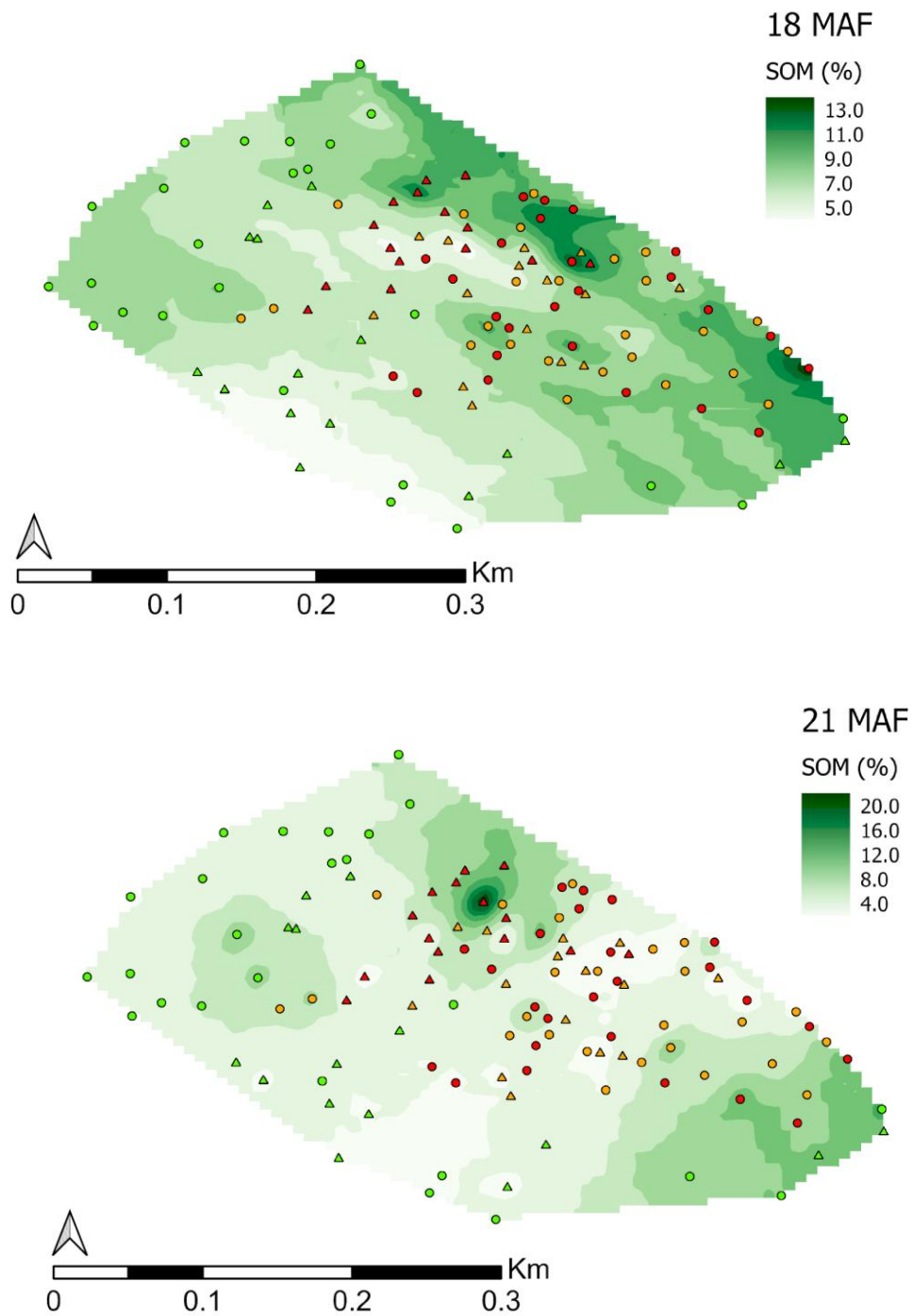


Figure 4.34. (continuation) Post-fire soil organic matter (SOM) content maps for the 2-year study period (0-24 months after fire MAF). Different shapes denote vegetation species (circles indicate samples under *Quercus pubescens* Willd.; triangles indicate samples under *Juniperus communis* L.) and different colours denote wildfire severity (green - C; orange - MS; red - HS)

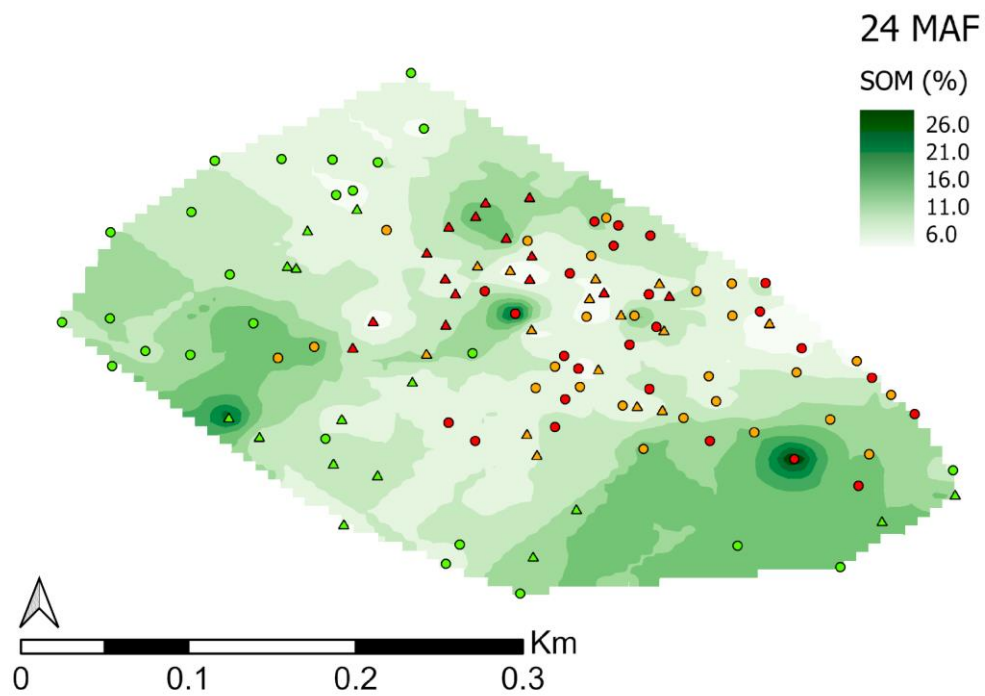


Figure 4.34. (continuation) Post-fire soil organic matter (SOM) content maps for the 2-year study period (0-24 months after fire MAF). Different shapes denote vegetation species (circles indicate samples under *Quercus pubescens* Willd.; triangles indicate samples under *Juniperus communis* L.) and different colours denote wildfire severity (green - C; orange - MS; red - HS)

## 5. DISCUSSION

### 5.1. Soil organic matter content after the wildfire

The first objective of this study was to monitor the temporal distribution of SOM content after a wildfire. A significant increase in SOM content in the HS samples compared to MS and C was recorded in the first 9 MAF (by 35 to 48%), which indicated that incorporation of burned material (ash, charred foliage and bark, dead roots, burned grass-bed) into the soil profile occurred. The SOM content in MS increased significantly (by ~9%) in the immediate post-fire period (0 MAF), and was higher than in C in the following post-fire period (although not significantly), suggesting that the incorporation of burned material occurred, but was not as pronounced as in HS. These findings are consistent with previous studies that have shown that wildfires can result in the incorporation of burned material into the soil, leading to an increase in SOM content (Ping et al., 2022; Šestak et al., 2022; Francos et al., 2018b). In the following period of 12-21 MAF the SOM content in HS was still elevated compared to C, although not significantly (see Figure 4.8), probably because of an onset of slow vegetation regrowth and recovery, which was first observed in HS in the study field in the spring following the wildfire (6 MAF). However, as discussed in chapter 4.2., during the entire 2-year study the vegetation recuperation in HS was slower than in MS, which certainly caused reduced nutrient demand and uptake. This probably resulted in the accumulation of soil nutrients, as well as SOM.

No change in SOM content was observed in MS compared to C throughout the study period, with the exception of 0 MAF and 24 MAF. At 24 MAF a significantly lower content was recorded in MS compared to C, indicating intensive and ongoing vegetation regeneration in these areas affected by a wildfire of medium severity, as also supported via visual observations of post-fire vegetation recovery of the wildfire affected area.

Intensive post-fire vegetation recovery was also observed by Fuentes-Ramirez et al. (2022) who measured plant species richness and plant abundance following a 2015 wildfire in the south-central area of Chile. They reported the increase in species richness of 93% in MS, and 70% in HS areas in the third year after the wildfire, as well as an increase in species mean abundance per hectare throughout the 3-year study period.

Similarly, Arroyo-Vargas et al. (2019) observed that mean vegetation abundance tended to increase over time across the low, medium and high severity levels, but especially in low to medium severity.



In both MS-J and MS-Q, combustion of the organic material occurred at a lesser extent compared to HS-J and HS-Q, which caused a lower amount of ash produced by the wildfire and deposited on soil surface. This could explain why the increase of SOM content was less pronounced in MS compared to HS in both vegetation types. Additionally, the recuperation of vegetation on all MS sites was visible as early as 3 MAF, and in HS at 6 MAF a slow regrowth was visible. The intensive regrowth and regeneration of vegetation in MS would not be possible without increased nutrient uptake originating from ash accumulation and SOM mineralization, and this is probably what caused a significant decrease in SOM content at 24 MAF. This supports the previous studies that low and medium severity wildfires generally have a more neutral or even beneficial effect on ecosystem recovery compared to high severity wildfires (Yang et al., 2021; Pereira et al., 2017; Alcañiz et al., 2016; Inbar et al., 2014).

The increase of post-fire SOM was also reported by Muráňová and Šimanský (2015), who recorded a 24% increase in SOC content in HS in the immediate post-fire period. Interestingly, they reported the increase of the amount of post-fire SOC content, but at the same time its quality worsened due to deterioration of humic to fulvic acid ratio. Unfortunately, this study did not address the detailed breakdown and the nature of post-fire SOM, and is in this sense, limited to extrapolating some deductions based solely by measure of increase or decrease of SOM. Future studies should further investigate the nature of post-fire SOM in a sense of its quality, so as to confirm or deny the findings reported in this and other studies.

Contrary to Muráňová and Šimanský (2015), Moya et al. (2019) reported SOC decrease in high severity areas 3 years after a wildfire in a mountainous region of south-eastern Spain, but noticed its content was dependent on vegetation recovery i.e., in plant recovered areas SOC content was higher than in unrecovered areas. This could be explained by the fact that due to removal of vegetation the amount of fresh organic material (leaves and other rapidly decomposing plant parts rich in C) is reduced in the short-term, and increased as vegetation gradually recovers. This indicates that high severity wildfires cause a discontinuation of established SOC patterns in mountainous regions, where erosion prevents the retention of soil nutrients long enough for the recovery of vegetation to begin, and the absence of vegetation prevents the normalisation of the nutrients and SOM content in the soil. Similar observations were made in a study by Francos et al. (2018a) that observed post-fire SOM decrease and attributed it to post-fire vegetation consumption, and subsequent erosion and leaching processes. They observed that high severity wildfire is a long-term disturbance in sloped terrains because it triggered erosion processes that disabled vegetation recovery.

However, considering the terrain configuration and favourable initial soil properties in this study (Table 3.1), post-fire soil erosion did not occur, and favourable weather conditions (Figure 4.1) enabled vegetation recovery in both MS and HS, although at different rates. The absence of full vegetation recovery in HS during the study period was probably influenced by higher



temperature reaches of the wildfire rather than terrain configuration. The absence of erosion processes in the study field favoured the build up of SOM in HS, especially in the first 12 MAF (Figure 4.9), after which the SOM content decreased as vegetation recovered. Vegetation recovery in MS was observed as early as 3 MAF, probably due to the overall lower temperature reached during wildfire on these sites coupled with partial combustion of biomass, which resulted in more favourable conditions for vegetation recovery. Thus, an increase of SOM was observed in MS in the immediate post-fire period, and rather than accumulating, it served as a source of nutrients for vegetation resprouting and regrowth. Significant decrease of SOM in MS was observed compared to C at a period of intense vegetation regrowth, namely at 24 MAF.

The influence of vegetation species on post-wildfire SOM can vary based on several factors, including their ecological roles, physiology, and interactions with other organisms (Fultz et al., 2016; Pasta et al., 2016; Van Auken and Smeins, 2008; Iglesias et al., 1997). In this study there was no significant relationship between the severity of a wildfire and the type of vegetation present in the area affected by the wildfire. This suggests that the severity of the wildfire did not depend on the type of vegetation in the area. The results did indicate that the mean SOM content is higher in areas with *Quercus p.* than in those with *Juniperus c.*, with differences observed in C, MS, and especially HS. The higher SOM content in C-Q compared to C-J could suggest that *Quercus p.* is more effective in contributing to SOM formation than *Juniperus c.* Additionally, the higher SOM content in HS-Q compared to HS-J in the first 3 MAF (see Figure 4.10) could suggest that the decomposition of *Quercus p.* litter contributes more to SOM formation than *Juniperus c.*, particularly in the early stages after a wildfire.

Given that *Quercus p.* is a deciduous tree with broad leaves that can thrive in dry environments, and has the potential to enhance the development of mycorrhizal fungi - which are essential for both plant growth and SOM accumulation (Iannaccone et al., 2020) - it is plausible to suggest that in a situation following a wildfire, *Quercus p.* has a more prominent role in promoting soil fertility by stimulating soil microbial activity and the cycling of nutrients. On the other hand, *Juniperus c.* is a coniferous shrub that is well adapted to harsh and dry conditions but experiences significant seed mortality in the aftermath of wildfires and does not possess the capability to regenerate via resprouting (Blanco-Sacristán et al., 2023). However, *Juniperus c.* can influence SOM by increasing soil moisture retention, and it can also create microsites that support SOM accumulation by providing shelter and nutrients for other plant species (Blanco-Sacristán et al., 2023; Van Auken and Smeins, 2008; García et al., 1999).

In general, the influence of *Quercus p.* and *Juniperus c.* on post-wildfire SOM can be complementary. While *Quercus p.* can contribute to early-stage SOM formation, *Juniperus c.* can support long-term SOM accumulation by promoting soil stability and facilitating the growth

of other plant species. However, the exact nature and magnitude of these effects require further investigation to fully understand the role that each species plays in SOM dynamics, particularly in the context of post-wildfire ecosystems. Such research could help inform management strategies for restoring and maintaining healthy soils in areas affected by wildfires.

## 5.2. Other soil properties

Soil pH was significantly higher on both MS and HS than on C taken under both vegetation species during the entire study period. The increase in the immediate post-fire period (0 MAF), before the first precipitation event could primarily be attributed to the loss of organic acids and hydroxyl groups (-OH) during the oxidation process of burning (Heydari et al., 2017). In the following months, i.e. 3 and 6 MAF, and after the first precipitation events, pH values in HS were steadily increasing, which can be attributed to ash (rich in base cations) incorporation into the soil profile (Pereira et al., 2019; Alcañiz et al., 2018). At the same time, the vegetation was still scarce in HS in 6 MAF, the soil surface was exposed and there was no competition for nutrients, which ultimately led to pH values increasing in the 0-6 MAF period, with maximum values observed in 6 MAF (see Figure 4.12). In MS areas, soil pH was consistently higher than C, although not to such an extent as in HS. The peak pH values were also observed in 6 MAF, indicating the period in which ash was being incorporated into the soil profile enhanced by precipitation. Regrowth of vegetation in MS started as early as 3 MAF, and the soil surface was never as exposed as it was on HS areas, which indicates vegetation uptake of the nutrients released from ash. Furthermore, the soil surface was initially covered with less ash in MS, which also caused lower pH values in MS compared to HS.

Although pH values followed the same pattern in both vegetation species, a slightly lower overall pH was observed in *Quercus p.* samples. This could be linked with the relationship between increasing SOM content and a decrease in pH due to the release of organic acids following SOM decomposition, as described in Huang et al. (2009). In this study, *Quercus p.* samples had a higher average SOM content and consequently lower pH values.

Finally, it could be concluded that the first 6 months post-fire were characterised by intense base cation release enhanced by precipitation. In the following months, i.e. in the period from 9 to 24 MAF, the pH values started to drop in both MS and HS (in both vegetation species), although they remained higher than C during the entire study period, which agrees with previous studies such as Granged et al. (2011) and Litton and Santelices (2003) that observed high pH values for up to two years post-fire. According to Granged et al. (2011), several factors should be considered when studying the return of soil pH to pre-fire levels, including climate,

soil type, ash accumulation, erosion processes, but most importantly, the regrowth of vegetation. According to Antos et al. (2003), in their study area, soil pH remained high until the dominant conifer vegetation had returned to the site. Therefore, the decrease in pH values between 9 and 24 MAF in both MS and HS in this study, particularly noticeable in MS samples, can be attributed to the main driving force of vegetation regrowth.

Significantly higher EC values were observed in HS areas, especially in the immediate post-fire period (0 MAF), while MS was not significantly different compared to C, as observed under both vegetation species (Figure 4.14). The highest EC values were recorded at 0 MAF in HS in both vegetation species, indicating high levels of soluble elements, which originated from the burning of organic matter and started accumulating in the soil, as also observed by Certini (2005). As previously mentioned, the vegetation recuperation in HS areas was lagging behind in comparison to MS, and as a result nutrient uptake was diminished, which led to nutrient accumulation in the soil surface. The absence of vegetation recuperation in HS could have further been promoted by high EC values, which negatively affected plant germination (Moreno-Casasola, 2011).

By the next sampling period (3 MAF), an above average amount of precipitation occurred (see Figure 4.1), which caused increased ion leaching and decreased EC values in the entire area. This is most evident in the first 12 MAF, afterwards the EC values started to drop, possibly because of the onset of vegetation regrowth and uptake that has started to take place in HS areas as well. Similar results were observed by Pereira et al. (2017) and Muñoz-Rojas et al. (2016), who reported increased EC to be ephemeral and recorded its recovery to pre-fire levels within a year post-fire.

In the case of *Quercus p.* and *Juniperus c.* vegetation, one possible reason why soil EC might be higher under *Quercus p.* than under *Juniperus c.* could be related to differences in litter quality and decomposition rates. *Quercus* litter tends to have higher nutrient content and decomposes more quickly than *Juniperus* litter (Ayres et al., 2009). As a result, *Quercus p.* litter can release more dissolved ions into the soil, leading to a higher concentration of dissolved salts and a higher soil EC compared to *Juniperus c.* litter. Additionally, *Quercus p.* vegetation is typically associated with higher SOM content (as explained in chapter 5.1), which can also contribute to a higher soil EC. The higher SOM content can increase the cation exchange capacity of the soil, leading to a higher retention of cations in the soil solution, and consequently, a higher soil EC.

The initial increase in CaCO<sub>3</sub> content in HS areas was highest at 3 MAF. Afterwards it showed a declining trend throughout the study period (6-24 MAF), although it was still significantly higher compared to C and MS in both vegetation species. According to Goforth et al. (2005) the lighter ash colour produced by HS wildfires is due to an increase in the CaCO<sub>3</sub> content, which is characterised as highly hydrophilic and soluble in water. The increase could be

attributed to the fact that white ash from completely combusted organic matter contains more alkaline oxides, which react with atmospheric CO<sub>2</sub> and water vapour to form carbonates, as proposed by Goforth et al. (2005). Considering the soil type in the research area is Cambisol rich in weatherable minerals, it is not excluded that the high temperatures reached during the burning in HS were sufficient for the transformation of aluminosilicate minerals rich in calcium cations, such as feldspar. This explains the significantly higher content of carbonates in HS areas, and the absence of carbonates formation in MS samples. In MS areas, the temperatures reached during burning were simply not high enough for the transformation to occur. Similar results were reported by Pereira et al. (2012), who observed that CaCO<sub>3</sub> content increases with increasing fire severity, however this conclusion needs to be verified in future research. Furthermore, it would seem that the weather conditions, i.e. above-average precipitation and favourable temperatures in September and October of 2020 favoured the process of dissolution of the CaCO<sub>3</sub> formed during the wildfire, and the process was still ongoing 24 MAF as its content was still significantly higher compared to C and MS at that time. This is due to low solubility of CaCO<sub>3</sub> at high soil pH (Ulery et al., 1993).

### 5.3. Wildfire influence on soil reflectance

The objective of determining the relationship of spectral reflectance and SOM content can be discussed by visually comparing the spectral reflectance curves. Visual evaluation of reflectance spectra and its first derivatives in Figures 4.15 – 4.24 exhibit patterns of reflectance typical for soil (Ben-dor et al., 2008b). As shown in Figures 4.15 – 4.18 differences between two wildfire severities and control are obvious in both vegetation species. Specifically, HS samples had the highest average SOM content, and therefore lowest average reflectance throughout the study period, whereas C samples had the lowest average SOM content causing highest average reflectance (see Figure 4.8). According to Francos et al. (2021), the modelling of SOM in soils of low content (< 0.6%) may lead to inaccurate estimations. This challenge was not met in the present study, given how the researched soils were rich in SOM from the start, and the wildfire, although moderate to high in its severity, caused an additional increase of its content (contrary to some research that recorded SOM combustion at high severities, ex. Moya et al., 2019; Francos et al., 2018a, Otero et al., 2015). At 0 MAF, green/yellow to red reflectance region (550 to 700 nm) decreased in burned areas. Similar results were obtained by Šestak et al. (2022) who reported the decrease of soil reflectance following wildfire in the same reflectance region on burned samples from Mediterranean Croatia. These results support the fact that SOM differences explain reflectance variation in the VNIR spectral region, namely higher SOM content decreases reflectance and vice versa (Baumgardner et al., 1986).

According to Zheng et al. (2016) and Tian et al. (2013), SOM content correlates with reflectance in the range from 500-700 nm the most. These observations in research conducted on various soil types, and including this study, lead to a conclusion that 500-700 nm range carries the majority of information on SOM that could be useful in developing universal models for estimating SOM in different types of soils, including ones affected by wildfires.

Higher reflectance recorded at 24 MAF in MS samples compared to both C and HS supports the assumption of intensive vegetation regeneration during this period, favouring mineralization of SOM and nutrient uptake, as discussed previously in chapter 5.1., and observed in previous studies (Fuentes-Ramirez et al., 2022; Arroyo-Vargas et al., 2019).

Figures 4.19 – 4.24 illustrated the seasonality of SOM changes. In C-J and C-Q samples (Figures 4.19 and 4.20), average reflectance was highest in the spring and summer months, reflecting SOM decrease during this time of vegetation growth and development, taking up nutrients produced by SOM mineralization. On the contrary, average reflectance was lowest during the colder months of autumn and winter. According to Wuest (2014) seasonal variation of SOM occurs due to variations in temperature, soil moisture, and plant growth, and as much as 13% of C variability can be explained by seasonal variation. Therefore, during the colder months of the year lower temperatures and vegetation dormancy favour SOM build up. The average reflectance shown in Figures 4.21 – 4.24 could illustrate the disturbance in the established seasonal SOM patterns and ongoing ecosystem restoration in both MS and HS. This is emphasised by the fact that the lowest average reflectance was not recorded in the autumn/winter season as expected, but in the spring and summer months, indicating the absence of vegetation regrowth and SOM accumulation. Some exceptions to these observations were noted, particularly in the average reflectance of the MS samples, where high average reflectance in summer indicates nutrient uptake and intense vegetation regrowth, leading to depleted SOM content. In the past, studies have mostly focused on a particular aspect of wildfire effects on the environment, such as vegetation response or soil properties following wildfire. Only recently researchers have shifted their focus to holistically examine the post-fire environmental response (see Fuentes-Ramirez et al., 2022; Fernández-García et al., 2021; Kim et al., 2021; Huerta et al., 2020) and are advancing research by, for example, relating post-fire nutrient uptake by vegetation and post-fire nutrient variability. In this context, soil spectroscopy could be used in examining the temporal distribution of SOM following fire, thus proving to be a valuable tool in comprehensively exploring the effects of wildfire on environmental components. Further research is encouraged to gain detailed insight into post-fire environmental interactions and to improve post-fire environmental management strategies.

## 5.4. Linear (PLSR) and non-linear (ANN) modelling of post-fire SOM

### 5.4.1. PLSR vs. ANN models

The next objective of this study was to determine the relationship of spectral reflectance and soil organic matter content using linear and nonlinear calibration models. In order to complete this objective, the entire reflectance dataset collected over the 2-year study period, as well as the subsets containing the data from each individual sampling period was subjected to predictive SOM modelling. Overall, nine (9) of each PLSR and ANN and one (1) of each PLSR and ANN model for the entire 0-24 MAF dataset were calibrated, tested and validated to predict SOM content from the gathered reflectance data. Validation models with minimal root mean square error of prediction ( $RMSE_P$ ) and the highest coefficient of determination ( $R^2$ ) indicated highest model accuracy. To compare the performance of the obtained models, ratio of performance to deviation (RPD) was calculated.

In linear PLSR models, three to five PCs accounted for the most variation in spectral data, and The  $RMSE_P$  values ranged from 1.13 to 3.29%, while  $R^2$  between measured and predicted SOM content ranged from 0.46 to 0.82.

PLSR models computed for each sampling time provided fair to very good predictions (RPD= 1.62 to 2.29), with an exception at 3 MAF which produced a poor model (RPD = 1.35,  $RMSE_P$  = 2.08,  $R^2$  = 0.46). This was the only model that benefited from data smoothing procedure (Savitzky-Golay) that effectively preserved high frequency signal components and reduced noise (Savitzky and Golay, 1964). However, still a large part of the variation in the model remained unexplained. This is probably related to the complex wildfire impacts on SOM and the effects of intrinsic factors that occurred in the immediate post-fire period. Namely, the formation of char and  $CaCO_3$  could have affected the linear VNIR-SOM relationship and behaviour of spectral curves. Incidentally, the highest  $CaCO_3$  content was observed at 3 MAF, indicating the post-fire formation of new forms of C (Cofer et al., 1997) and an ongoing complex process of post-fire soil recovery observed in other studies (Pereira et al., 2019; Francos et al., 2018a; Prendergast-Miller et al., 2017). These studies observed that the process of post-fire soil recovery clearly shows a non-linear relationship, and this is why perhaps non-linear ANN models generally proved to be superior to PLSR models, as discussed below. As for the PLSR model obtained with the entire 0-24 MAF dataset, its accuracy and performance was inferior to individual models computed for each sampling period separately, with  $RMSE_P$  of 2.49,  $R^2$  of 0.57 between measured and predicted SOM content, and RPD value of 1.55 indicating a fair model. These results emphasise the benefit of data segmentation during the short-term post-wildfire monitoring that enables us to model specific features of post-fire SOM

dynamics. It would seem beneficial for post-fire SOM monitoring to use models computed according to the specific stages of SOM dynamics, ie. to compute models segmented by the rate of soil regeneration and/or seasonal criteria, that take into account the speed and seasonality of soil changes. However, in order to reduce costs, a generalised model based on all available data could prove useful, if only to detect the direction of SOM recovery.

For ANN modelling, eleven (11) to eighteen (18) PCs summarised the most variation in the reflectance datasets. By comparing the RPD performance the results showed that ANN outperformed PLSR models, with RPD values ranging from 1.74 to >2.5. The lowest performing model was obtained at 21 MAF, with an RPD value of 1.74, which still indicates a good model capable of quantitative SOM prediction. These results confirm that learning non-linear ANN algorithms are able to correlate complex spectral information with the target variable, especially in the conditions of complex post-fire SOM dynamics. Similar results were obtained by Viscarra Rossel and Behrens (2010) who compared multiple data mining techniques, including PLSR and ANN for calibrating VNIR reflectance spectra to SOC, and confirmed the superiority of the ANN model that can detect complex non-linear interactions in the data. Furthermore, due to high computation power demand of ANN models, direct modelling using the entire VNIR spectra (641 wavelengths per sample) was not efficient. Therefore, the reduced data from the PCA analysis were used as input features in the form of PC scores, which resulted in satisfactory computational performance without losing important information on the reflectance – SOM relationship. In conclusion, non-linear models such as ANN should be used to estimate the field variability of SOM, especially in the complex conditions of post-fire soil dynamics.

Regression coefficients computed from PLSR models shown in Figure 4.28 identified the important spectral variables most responsible for SOM prediction. Visible parts of the spectrum, namely 410 - ~550 nm and ~550 - ~620 nm, and NIR region > 1000 nm were identified as zones of major importance in all models. According to Ben-Dor et al. (2008b), changes in the mineral components (such as iron oxide) appear in the visible part of the reflectance spectrum as a combination of overtones attributed to specific chemical groups and their structural configuration, which mainly affect the slope of the spectral curve. The soil type investigated in this study (Cambisol) is rich in Fe oxide goethite that interacts with SOM and clay minerals having a significant influence on soil aggregation processes (Durn et al., 2019). The 410 - ~550 nm and ~550 - ~620 nm region is therefore revealed as a zone in which the absorption features of iron oxides affected the spectral curve slope, and therefore affected the calibration of SOM models in this study.

Moreover, the > 1000 nm region could be significant for SOM modelling due to electronic transitions of goethite iron oxide at 920 nm, as proposed by Viscarra-Rossel and Behrens

(2010). Similar results have been reported in previous studies. Stevens et al. (2013) reported the high correlations between SOC content and reflectance around 540, 640 and 900 nm, and associated it to the absence or presence of iron oxides in the agricultural regions of Grand-Duchy of Luxembourg. More importantly, Šestak et al. (2022) reported peaks from 450 – 600 nm and 900 – 1050 nm as zones of major importance for modelling SOC content in burned soils of Mediterranean Croatia.

#### 5.4.2. In-situ vs. laboratory reflectance measurements

As stated in Chapter 1.1, to compare the accuracy and precision of hyperspectral prediction models using laboratory and in situ measurements, reflectance data collected on 3 MAF and 15 MAF were used. In this way, the same soil samples were measured in the most humid part of the year in a field-moist state. Measurements were repeated on the same soil samples after they were air-dried, ground, and sieved to compare the accuracy and precision of the soil spectra obtained in the laboratory and in the field.

The PLSR models calculated for each condition provided fair predictions (laboratory RPD=1.62; in situ RPD=1.67), while ANN models performed better (laboratory RPD=1.67; in situ RPD=1.75). Contrary to expectations, the models obtained with in situ data performed slightly better on SOM estimates. Stevens et al. (2008) conducted a similar study on agricultural soils and found a slight decrease in the accuracy of field-scale compared to laboratory measurements of soil C. However, the same study reports that the accuracy of both in situ and laboratory measurements is satisfactory and concludes that the number of samples needed to adequately model soil C variability ranges from 7 to 129. The models in this study were built with 240 samples, so the sampling intensity was found to be sufficient for successful SOM estimation. According to Ben-Dor et al. (2008b), soil moisture alters soil refractive properties most strongly in the SWIR region, typically around 1400 and 1900 nm, which was not included in this study because the ASD spectroradiometer measured the range of 350-1050 nm. Therefore, the wavelengths most sensitive to soil moisture were omitted from this study, which had a positive effect on the modelling procedure of the field-moist samples. Furthermore, in order to successfully acquire relevant spectral responses under field conditions, some general guidelines are usually followed, the most important of which is to obtain the measurements under constant weather conditions, ideally in absence of clouds that scatter solar irradiance and degrade the signal-to-noise ratio (Salisbury, 1998). The guidelines were followed in this study, and the field measurements were made on sunny days, which



allowed spectral data to be collected with a quality as similar as possible to spectral measurements made in the laboratory.

These results indicate that the reflectance data collected in the field is sufficient for successful post-fire SOM modelling, which has some implications for the operational costs of future research. It implies the possibility of measuring reflectance data in situ, and taking a reduced number of samples for detailed laboratory analysis, which would significantly reduce labour intensity and increase measurement intensity if needed for research purposes. Similar opinion was given in a recent study by Li et al. (2022), who discussed the cost-effectiveness of reflectance spectroscopy for estimating SOC, and concluded that VNIR spectroscopy is more cost-effective than the dry combustion method, especially for large numbers of samples. They also recommend skipping the grinding of the collected samples in order to reduce sample preparation time.

#### 5.4.3. Hyperspectral vs. multispectral reflectance measurements

One of the objectives of the study was to compare the accuracy and precision of hyperspectral and multispectral (satellite Sentinel-2) prediction models, and for that purpose a subset of reflectance data collected in the immediate post-fire period (0 MAF) was used (N=28, see Chapter 3.5.2). Due to the nature of optical sensors, data collection was not possible for later dates due to regrowth of vegetation, which obscured the bare soil pixels and disabled any further retrieval of spectral data.

According to the RPD values of the obtained PLSR models, laboratory calibrations provided a fair model (RPD=1.58), while Sentinel-2 calibrations produced a poor model (RPD=1.17). According to Gholizadeh et al. (2018b) models with RPD values between 1 and 1.4 could still be used to distinguish between high and low SOM content. The coefficients of determination ( $R^2$ ) were 0.58 and 0.33 for laboratory and Sentinel-2 PLSR validation models, respectively, indicating that 58% of the SOM variance could be explained by the variance of the VNIR hyperspectral, but only 33% could be explained by Sentinel-2 multispectral data.

On the other hand, ANN modelling showed significant improvements compared to PLSR. The RPD value calculated for the laboratory VNIR data was 1.97, indicating a good model, and 1.48 for Sentinel-2 data, indicating a fair model. According to  $R^2$  for laboratory and Sentinel-2 ANN models, 74% of the SOM variance could be explained by the variance of the VNIR hyperspectral and 88% could be explained by Sentinel-2 multispectral data. Considering the parameters used for evaluation of the accuracy and performance of models, the superiority of ANN comes into focus. These results further confirm that learning non-linear ANN algorithms can detect complex non-linear interactions in the post-fire soil environment.

Based on the given information, it is difficult to provide a direct answer to the question of the precision of satellites when used on a small area versus a large burned area. However, we can make some general observations regarding the use of Sentinel-2 data in this study.

It is worth noting that Sentinel-2 data has a spatial resolution of 10 metres, which can be considered relatively high for remote sensing applications. However, the precision of satellite data can be affected by various factors, such as atmospheric conditions, sensor noise, and calibration errors, among others. Therefore, it is important to carefully process and validate the satellite data to ensure their accuracy for the specific application. In this study, the ANN model trained with Sentinel-2 data achieved a fair RPD value of 1.48 and a strong  $R^2$  value of 0.88, indicating a reasonable accuracy for predicting SOM content in the post-fire soil environment. However, it is possible that the precision of the Sentinel-2 data may be affected by the relatively small area under study, which can limit the ability to capture fine-scale variations in the soil properties. On the other hand, the laboratory VNIR data used in this study may provide higher precision due to the controlled conditions and high spectral resolution of the instrument. However, the laboratory data may not fully capture the spectral variations present in the field data, and may not be representative of the actual post-fire soil status.

In summary, the use of laboratory data versus satellite data can have trade-offs in terms of precision and representativeness. However, the strong performance of the ANN model in this study suggests that it can effectively capture complex non-linear interactions in the post-fire soil environment, regardless of the data source.

Furthermore, because vegetation regrowth occurred in MS and covered the soil surface as early as 3 MAF, this study only obtained and analysed remotely sensed data for the immediate post-fire period (0 MAF). Nevertheless, the successful utilisation of ANN model with multispectral data indicates that Sentinel-2 remotely sensed data has significant potential for monitoring SOM in burned areas, as long as the soil remains devoid of vegetation.

Promising results were achieved in this study using ANN models and data extracted from 10 Sentinel-2 bands, however considering the results of recent studies, these models could benefit from calculating and including multiple spectral indices as continuous variables, because they are expected to improve the model prediction capability (Liu et al., 2022b; Gholizadeh et al., 2018b, Jin et al., 2016). For example, Gholizadeh et al. (2018b) calculated 18 different spectral soil and vegetation indices, extracted 10 Sentinel-2 bands and modelled SOC content using a non-linear modelling method (in this case Support Vector Machine Regression) in agricultural areas across Czech Republic. They reported RPD values of 1.6 – 1.92 at different study areas, indicating fairly successful prediction models. Most recently, Liu et al. (2022b) recognized the need for new bare soil spectral indices to improve model accuracy in SOC mapping of bare soil pixels, which would undoubtedly prove beneficial in post-fire soil

monitoring using satellite sensor data. They reported the successful development of new bare soil indices that improved model accuracy (using Sentinel-2 data and non-linear models), with  $R^2$  value of 0.81 in an agricultural area in southeast Iowa State, USA.

Furthermore, by analysing regression coefficients of the obtained Sentinel-2 models (Figure 4.31), this study observed that B11 (1565-1655 nm) correlates with SOM content the most, and consequently highly affects SOM predictions, followed by B8 and 8a in the VNIR region (785-900 nm). These results can be attributed mainly to the previously discussed absorption features typical for soil spectral curves (see Chapters 2.3.1. and 2.3.2.) in the VNIR-SWIR region. In a study by Gholizadeh et al. (2018b), spectral bands providing the strongest correlations with SOC were B4 and B5 (650–713 nm) followed by B11 and B12 (1565–2280 nm), which is somewhat similar to this study. This suggests the potential robustness of these bands in capturing variations in SOM particularly when considering various research conducted across many regions with distinct soil types while investigating the same phenomenon. As noted by Jin et al. (2016), different soil types can influence the sensitivity of satellite spectral bands to SOM content, and affect the way light interacts with the soil surface and is subsequently reflected back to the sensor. This inherent variability in soil characteristics across regions can result in divergent correlations between bands and SOM content, even when using similar remote sensing platforms and methodologies.

In conclusion, as discussed in Chapter 5.4.1., these results strongly suggest that the freely available Sentinel-2 imagery is a cost-effective and valuable source of information for environmental monitoring purposes, especially in cases where intense soil sampling and a large number of laboratory analyses are needed. Similar to proximal in situ data collection, downloading freely available Sentinel-2 data could significantly reduce operational costs of future research, even if the predictions are less accurate than traditional methods. Sentinel-2 images provide a large information database, with high revisit time, as well as spatial and spectral resolution adequate for SOM monitoring on a local, regional and global scale.

## 5.5. Geostatistical univariate and multivariate modelling and mapping

The final objectives of this study were to compare the accuracy and precision of univariate with multivariate spatial models, and to monitor spatial distribution of SOM content after a fire. For univariate interpolation, ordinary kriging (OK) was used, and for multivariate interpolation, ordinary cokriging (OCK) method was used, with soil pH, EC,  $\text{CaCO}_3$  content and average reflectance as covariates. For 0 MAF exclusively, B8 was utilised as a covariate. The hypothesis was that univariate spatial models show less spatial dependence than multivariate

ones, which was assessed by interpreting nugget/sill ratio of the calculated semivariograms and cross-semivariogram.

The pure nugget effect was recorded at 0 MAF and at 15 MAF in OK method, indicating spatial micro variability of SOM content caused by the effects of wildfire (Table 4.10). In cases of pure nugget effect, it is considered that interpolations of the target variables are not possible, due to the absence of statistical stationarity in the data. Pure nugget effect implies that the disturbance caused by the wildfire was significant, resulting in high variability at a small scale. Changes in spatial patterns of SOC following wildfire disturbance were also observed by Wang et al. (2019). To address this issue, a potential solution would be to increase the number of samples included in the model. By incorporating a larger number of samples, a more comprehensive representation of the spatial patterns and variability can be achieved.

However, many studies recognized that auxiliary information (covariates), can be included in geostatistical modelling approaches to account for the remaining spatial variation (Qin et al., 2022; Mirzaee et al., 2016; Lark, 2012). In this study, covariates that are more affordable and easier to measure (soil pH, EC and  $\text{CaCO}_3$ ), as well as collected average reflectance data and freely available Sentinel-2 data were used in OCK interpolations of SOM content. All of the covariates reduced nugget effects ( $C_0 - \text{OK} = 0.89-28.4$ ,  $C_0 - \text{OCK} = 0.001-16.6$ ) and RMSE ( $\text{OK}_{\text{RMSE}} = 0.85-1.08$ ,  $\text{OCK}_{\text{RMSE}} = 0.72-1.02$ ) throughout the study period.

The reduced nugget effect indicates that by incorporating covariates, the OCK model can capture and account for some of the variability that would otherwise contribute to the nugget effect in OK.

Spatial dependence increased the most in OCK with soil EC as a covariate (OCK\_EC). It varied from <0.1% to 19%, which shows strong spatial dependence of SOM content compared to OK ( $\text{OK}_{\text{nugget/sill}} = 10-74\%$ ). Strong spatial dependence observed in OCK\_EC indicates a high degree of spatial correlation in the data and suggests that the EC covariate used in cokriging had effectively captured most of the remaining variation in the primary SOM variable. The strong spatial dependence is supported by the significant correlations observed between SOM and soil EC. Among all soil properties correlations, the strongest was found between SOM and EC (0.54), while the weakest was observed between SOM and soil pH (0.24).

In the case of pH as a covariate (OCK\_pH), the spatial dependence varied from 4% to 97%, which suggests a strong to weak spatial dependence. The weak spatial dependence observed in OCK\_pH at 15 MAF could be explained by extrinsic factors, such as weather conditions (Cambardella et al., 1994). Namely, prior to soil sampling on 15 MAF, extreme precipitation was recorded in the study area, which may have influenced the overall spatial dependence observed in the dataset.

For  $\text{CaCO}_3$  as a covariate (OCK\_ $\text{CaCO}_3$ ) similar results were observed. The spatial dependence spanned from 2.2% to 30%, indicating a range of spatial dependence from strong

to moderate with respect to SOM content. However, at 0, 12 and 15 MAF a pure nugget effect was recorded in OCK\_CaCO<sub>3</sub> cross-semivariogram, indicating that there may be unexplained variability in SOM content that is not related to the CaCO<sub>3</sub> covariate. For this reason, it is recommended that alternative covariates that may better capture the spatial patterns and reduce the nugget effect be considered in SOM mapping using OCK method.

Average reflectance as a covariate for SOM mapping (OCK\_Reflectance) increased spatial dependence from 0.4% to 97%. However, weak spatial dependence was observed at 12 MAF, indicating extrinsic factors influencing the overall spatial dependence observed in the dataset. In this case, the extrinsic factors could be extreme weather conditions and/or vegetation growth supported by nutrient uptake influencing the spatial dependence of soil properties during the time of the soil sampling at 12 MAF.

Furthermore, OCK with B8 as a covariate (OCK\_Sentinel) showed strong spatial dependence (20%) at 0 MAF. This result showed that Sentinel-2 data can provide useful information to improve SOM mapping. The strong spatial dependence is supported by the significant correlation observed between SOM and B8 (0.12). The potential for improving the quality of SOM mapping is significant as the availability of satellite imagery with higher spatial resolution continues to increase.

Based on the relative improvement (RI) results of OCK method, EC would be the most suitable covariate to improve the accuracy of SOM modelling in this study. Throughout the majority of the research period, the RI of the prediction accuracy was best in OCK\_EC, and varied from 4% (observed at 15 MAF) to 27% (observed at 3 MAF). Only at 0 MAF and 15 MAF, the RI was best in OCK\_Reflectance, with respective values of 23% and 15%.

It is important to consider other factors and conduct a comprehensive analysis before concluding on the most suitable covariate for improving the accuracy of SOM content modelling. While EC shows promising results in terms of RI, the interplay of various covariates and their impact on different aspects of SOM dynamics should be thoroughly examined. Further research and experimentation are necessary to validate the robustness of EC as a covariate and to ensure its applicability across diverse soil types and environmental conditions.

The best improvements in OCK compared to the OK method were observed at 0 MAF and 3 MAF, which is probably due to higher SOM variability in the first 3 MAF. The use of auxiliary data in this time frame particularly reduced spatial error when using the OCK method. Ranges calculated for OCK\_EC throughout the study period varied from 18.98 m (0 and 3 MAF) to 104.24 m (21 MAF), indicating a fairly dense sampling grid is necessary in order to cover all of the post-fire SOM content variability. In this study, the randomised sampling procedure led to an uneven sampling grid, where some points were closer together, while others further apart. However, the mean distance between sampling points was 19.89 m, with minimal distance

between points of 5.43 m and maximal 54.1 m (see Chapter 3.2.), which leads to a conclusion that a fairly sufficient number of samples was acquired for this study.

Moreover, the selection of the covariates proved successful under the conditions of consistent environmental variables such as slope and soil type in this study area. Similar results were confirmed by Jiang et al. (2022) who compared various spatial interpolation methods performance in different spatial scales in Sanjiang plain in northeast China. They concluded that on a larger spatial scale, qualitative environmental variables such as elevation and soil type can improve prediction accuracy; however, on a small scale where such variables are often consistent, quantitative variables are more useful as auxiliary information.

The data acquired and analysed in this study provided short-term information on wildfire effects on SOM content on a local scale and provided some valuable insights into the direction of SOM recovery in the Mediterranean environment. Long-term studies (10-30 years) are encouraged for developing models that monitor the effects on SOM and to fully understand the spatial and temporal change in soil quality.

## 6. CONCLUSIONS

The aim of this study was to monitor the spatio-temporal changes of post-fire soil quality using soil spectroscopy, remote sensing and geostatistic methods, which has so far not been done in the pedological and climatic conditions of Mediterranean Croatia.

- HS wildfires led to a 21.72% increase in average SOM content, while MS wildfires showed no significant change compared to unburned samples. The intensive vegetation regrowth in MS was likely facilitated by increased nutrient uptake from SOM mineralization, explaining the significantly lower SOM content in MS compared to HS. This supports previous studies suggesting low severity wildfires benefit ecosystem recovery.
- The spectral reflectance analysis revealed that soil reflectance is significantly affected by variations in SOM content resulting from different wildfire severities. The greatest spectral differences between C, MS and HS were found in green/yellow to red (500-700 nm) region. This suggests that this region carries the majority of information on SOM that could be useful in developing universal models for estimating SOM in soils affected by wildfires.
- The results of this study emphasise the advantage of data segmentation in short-term post-wildfire monitoring, allowing the modelling of specific features of post-fire SOM dynamics. While using models tailored to specific stages of SOM regeneration and seasonal criteria may be beneficial, a cost-effective approach could involve a generalised model based on all available data, with ANN models being recommended in such cases.
- The identified important spectral variables most responsible for SOM prediction were in the visible part of the spectrum. Namely 410 - ~550 nm and ~550 - ~620 nm, and NIR region > 1000 nm contributed most to computation of principal components that carry most of the variation in spectral data, and those spectral regions were highly correlated with post-fire SOM content.
- Contrary to expectations, in situ data performed slightly better than laboratory data for SOM estimates when used in models. This is attributed to the exclusion of the SWIR

region sensitive to soil moisture (1400 and 1900 nm) from the study and the developed models, which had a positive effect on the modelling procedure of the field-moist samples. Furthermore, if the general guidelines for in-situ measurements are followed (constant weather conditions, ideally no clouds), the data collected will be of sufficient quality for successful post-fire SOM modelling. This could reduce the labour intensity and increase measurement intensity if needed for research purposes.

- Promising results were achieved in this study using ANN models and multispectral data, though these models could benefit from calculating and including multiple spectral indices as continuous variables, as suggested by some recent studies. These results strongly suggest that the freely available Sentinel-2 imagery represents a valuable source of information for environmental monitoring purposes, especially in the conditions of complex post-fire SOM dynamics where intense soil sampling and a large number of laboratory analyses are needed.
- According to the relative improvement (RI) outcomes from the OCK spatial model, EC proved to be the optimal covariate for improving the accuracy of SOM modelling. Over the majority of the study period, the RI of prediction accuracy in OCK\_EC ranged from 4% to 27%.
- The data acquired and analysed in this study provided short-term information on wildfire effects on SOM content on a local scale and provided some valuable insights into the direction of SOM recovery in the Mediterranean environment. Long-term studies (10-30 years) are encouraged for developing models that monitor the effects on SOM and to fully understand the spatial and temporal change in soil quality.



## 7. REFERENCES

- Adeline K.R.M., Gomez C., Gorretta N., Roger J.-M. (2017). Predictive ability of soil properties to spectral degradation from laboratory Vis-NIR spectroscopy data. *Geoderma* 288: 143–153. doi:
- Adhikari K., Hartemink A.E. (2017). Soil organic carbon increases under intensive agriculture in the Central Sands, Wisconsin, USA. *Geoderma Regional* 10: 115–125. doi:[10.1016/j.geodrs.2017.07.003](https://doi.org/10.1016/j.geodrs.2017.07.003)
- Agbeshie A.A., Abugre S., Atta-Darkwa T., Awuah R. (2022). A review of the effects of forest fire on soil properties. *J For Res.* doi:[10.1007/s11676-022-01475-4](https://doi.org/10.1007/s11676-022-01475-4)
- Aizat A. M., Roslan M. K., Sulaiman W. N. A., Karam, D. S. (2014). The relationship between soil pH and selected soil properties in 48 years logged-over forest. *International journal of environmental sciences*, 4 (6): 1129-1140. doi:10.6088/ijes.2014040600004
- Alcañiz M., Outeiro L., Francos M., Farguell J., Úbeda X. (2016). Long-term dynamics of soil chemical properties after a prescribed fire in a Mediterranean forest (Montgrí Massif, Catalonia, Spain). *Science of The Total Environment* 572: 1329–1335. doi:[10.1016/j.scitotenv.2016.01.115](https://doi.org/10.1016/j.scitotenv.2016.01.115)
- Alcañiz M., Outeiro L., Francos M., Úbeda X. (2018). Effects of prescribed fires on soil properties: A review. *Science of The Total Environment* 613–614: 944–957. doi:[10.1016/j.scitotenv.2017.09.144](https://doi.org/10.1016/j.scitotenv.2017.09.144)
- Ali E., Cramer W., Carnicer J., Georgopoulou E., Hilmi N.J.M., Le Cozannet G., Lionello P. (2022). Cross-Chapter Paper 4: Mediterranean Region. In: *Climate Change 2022: Impacts, Adaptation, and Vulnerability. Contribution of Working Group II to the Sixth Assessment Report of the Intergovernmental Panel on Climate Change* (Pörtner H.O., Roberts D.C., Tignor M., Poloczanska E.S., Mintenbeck K., Alegría A., Craig M., Langsdorf S., Lösschke S., Möller V., Okem A., Rama B., eds), Cambridge University Press. in Press.
- Amazirh A., Merlin O., Er-Raki S., Gao Q., Rivalland V., Malbeteau Y., Khabba S., Escorihuela M.J. (2018). Retrieving surface soil moisture at high spatio-temporal resolution from a synergy between Sentinel-1 radar and Landsat thermal data: A study case over bare soil. *Remote Sensing of Environment* 211: 321–337. doi:[10.1016/j.rse.2018.04.013](https://doi.org/10.1016/j.rse.2018.04.013)
- Antos J.A., Halpern C.B., Miller R.E., Cromack K., Halaj M.G. (2003). Temporal and spatial changes in soil carbon and nitrogen after clearcutting and burning of an old-growth Douglas-Fir forest. USDA, Research Paper 555, Pacific Northwest Research Station, Portland, OR.

- Arjasakusuma S., Kusuma S.S., Vetrira Y., Prasasti I., Arief R. (2022). Monthly Burned-Area Mapping using Multi-Sensor Integration of Sentinel-1 and Sentinel-2 and machine learning: Case Study of 2019's fire events in South Sumatra Province, Indonesia. *Remote Sensing Applications: Society and Environment* 27: 100790. doi:[10.1016/j.rsase.2022.100790](https://doi.org/10.1016/j.rsase.2022.100790)
- Armanto M.E., Zuhdi M., Setiabudidaya D., Ngudiantoro N., Wildayana E., Hermawan A., Imanudin M.S. (2022). Deciphering Spatial Variability and Kriging Mapping for Soil pH and Groundwater Levels. *J Lahan Suboptimal* 11 (2): 187–196. doi:[10.36706/jlso.11.2.2022.577](https://doi.org/10.36706/jlso.11.2.2022.577)
- Arroyo-Vargas P., Fuentes-Ramírez A., Muys B., Pauchard A. (2019). Impacts of fire severity and cattle grazing on early plant dynamics in old-growth Araucaria-Nothofagus forests. *For Ecosyst* 6 (1): 44. doi:[10.1186/s40663-019-0202-2](https://doi.org/10.1186/s40663-019-0202-2)
- Arshad M.A., Martin S. (2002). Identifying critical limits for soil quality indicators in agro-ecosystems. *Agriculture, Ecosystems & Environment* 88 (2): 153–160. doi:[10.1016/S0167-8809\(01\)00252-3](https://doi.org/10.1016/S0167-8809(01)00252-3)
- Ayres E., Steltzer H., Simmons B. L., Simpson R. T., Steinweg J. M., Wallenstein M. D., Wall D. H. (2009). Home-field advantage accelerates leaf litter decomposition in forests. *Soil Biology and Biochemistry*, 41 (3): 606–610. doi: [10.1016/j.soilbio.2008.12.022](https://doi.org/10.1016/j.soilbio.2008.12.022)
- Bach H., Mauser W. (1994). Modelling and model verification of the spectral reflectance of soils under varying moisture conditions. In: *Proceedings of IGARSS '94 – 1994 IEEE International Geoscience and Remote Sensing Symposium, Presented at the IGARSS '94 – 1994 IEEE International Geoscience and Remote Sensing Symposium, IEEE, Pasadena, CA, USA*, pp. 2354–2356. doi:[10.1109/IGARSS.1994.399735](https://doi.org/10.1109/IGARSS.1994.399735)
- Baumgardner M.F., Silva L.F., Biehl L.L., Stoner E.R. (1986). Reflectance Properties of Soils. In: *Advances in Agronomy*, Elsevier, pp. 1–44. doi:[10.1016/S0065-2113\(08\)60672-0](https://doi.org/10.1016/S0065-2113(08)60672-0)
- Behera S.K., Suresh K., Rao B.N., Mathur R.K., Shukla A.K., Manorama K., Ramachandrudu K., Harinarayana P., Prakash C. (2016). Spatial variability of some soil properties varies in oil palm (*Elaeis guineensis* Jacq.) plantations of west coastal area of India. *Solid Earth* 7 (3): 979–993. doi:[10.5194/se-7-979-2016](https://doi.org/10.5194/se-7-979-2016)
- Bellégo C. and Pape L. (2019) Dealing with Logs and Zeros in Regression Models, *CREST Série des Documents de Travail* No. 2019-13. available at: <https://EconPapers.repec.org/RePEc:arx:papers:2203.11820> [accessed 4<sup>th</sup> November 2022]
- Ben-Dor E., Heller D., Chudnovsky A. (2008a). A Novel Method of Classifying Soil Profiles in the Field using Optical Means. *Soil Sci Soc Am J* 72 (4): 1113–1123. doi:[10.2136/sssai2006.0059](https://doi.org/10.2136/sssai2006.0059)
- Ben-Dor E., Inbar Y., Chen Y. (1997). The reflectance spectra of organic matter in the visible near-infrared and short wave infrared region (400–2500 nm) during a controlled decomposition

- process. *Remote Sensing of Environment* 61 (1): 1–15. doi:[10.1016/S0034-4257\(96\)00120-4](https://doi.org/10.1016/S0034-4257(96)00120-4)
- Ben-Dor E., Taylor R.G., Hill J., Demattê J.A.M., Whiting M.L., Chabrilat S., Sommer S. (2008b). Imaging Spectrometry for Soil Applications. In: *Advances in Agronomy*, Elsevier, pp. 321–392. doi:[10.1016/S0065-2113\(07\)00008-9](https://doi.org/10.1016/S0065-2113(07)00008-9)
- Biswas A., Cheng B. (2013). Model Averaging for Semivariogram Model Parameters. In: *Advances in Agrophysical Research* (Grundas S., Stanisaw A., ed.), InTech, London, United Kingdom, pp. 81-96. doi: 10.5772/52339
- Blanco-Sacristán J., Guirado E., Molina-Pardo J.L., Cabello J., Giménez-Luque E., Alcaraz-Segura D. (2023) Remote Sensing-Based Monitoring of Postfire Recovery of Persistent Shrubs: The Case of *Juniperus communis* in Sierra Nevada (Spain). *Fire* 6 (1):4. doi:[10.3390/fire6010004](https://doi.org/10.3390/fire6010004)
- Bodí M.B., Martin D.A., Balfour V.N., Santín C., Doerr S.H., Pereira P., Cerdà A., Mataix-Solera J. (2014). Wildland fire ash: Production, composition and eco-hydro-geomorphic effects. *Earth-Science Reviews* 130: 103–127. doi:[10.1016/j.earscirev.2013.12.007](https://doi.org/10.1016/j.earscirev.2013.12.007)
- Bogunović I., Mesić M., Zgorelec Z., Jurišić A., Bilandžija D. (2014). Spatial variation of soil nutrients on sandy-loam soil. *Soil and Tillage Research* 144: 174–183. doi:[10.1016/j.still.2014.07.020](https://doi.org/10.1016/j.still.2014.07.020)
- Bogunović I., Pereira P., Brevik E.C. (2017). Spatial distribution of soil chemical properties in an organic farm in Croatia. *Science of The Total Environment* 584–585: 535–545. doi:[10.1016/j.scitotenv.2017.01.062](https://doi.org/10.1016/j.scitotenv.2017.01.062)
- Bogunović I., Trevisani S., Pereira P., Vukadinovic V. (2018). Mapping soil organic matter in the Baranja region (Croatia): Geological and anthropic forcing parameters. *Science of The Total Environment* 643: 335–345. doi:[10.1016/j.scitotenv.2018.06.193](https://doi.org/10.1016/j.scitotenv.2018.06.193)
- Boisramé G., Thompson S., Collins B., Stephens S. (2017). Managed Wildfire Effects on Forest Resilience and Water in the Sierra Nevada. *Ecosystems* 20 (4): 717–732. doi:[10.1007/s10021-016-0048-1](https://doi.org/10.1007/s10021-016-0048-1)
- Bonilla C.A., Pastén P.A., Pizarro G.E., González V.I., Carkovic A.B., Céspedes R.A. (2014). Forest Fires and Soil Erosion Effects on Soil Organic Carbon in the Serrano River Basin (Chilean Patagonia). In: *Soil Carbon* (Hartemink A.E., McSweeney K., eds), Springer International Publishing, Cham, pp. 229–237. doi:[10.1007/978-3-319-04084-4\\_24](https://doi.org/10.1007/978-3-319-04084-4_24)
- Box G.E.P., Cox D.R. (1964). An Analysis of Transformations. *Journal of the Royal Statistical Society: Series B (Methodological)* 26 (2): 211–243. doi:[10.1111/j.2517-6161.1964.tb00553.x](https://doi.org/10.1111/j.2517-6161.1964.tb00553.x)
- Brevik E.C., Calzolari C., Miller B.A., Pereira P., Kabala C., Baumgarten A., Jordán A. (2016). Soil mapping, classification, and pedologic modelling: History and future directions. *Geoderma* 264: 256–274. doi:[10.1016/j.geoderma.2015.05.017](https://doi.org/10.1016/j.geoderma.2015.05.017)

- Bright B.C., Hudak A.T., McCarley T.R., Spannuth A., Sánchez-López N., Ottmar R.D., Soja A.J. (2022). Multitemporal lidar captures heterogeneity in fuel loads and consumption on the Kaibab Plateau. *fire ecol* 18 (1): 18. doi:[10.1186/s42408-022-00142-7](https://doi.org/10.1186/s42408-022-00142-7)
- Bruckner M. Z. (2012). Water and Soil Characterization, pH and Electrical Conductivity. In: *Microbial Life Educational Resources*. Montana. Montana State University Bozeman, pp. 15–36.
- Bruno T.J., Svoronos P.D.N. (2005). *CRC Handbook of Fundamental Spectroscopic Correlation Charts*, 0 Edition. CRC Press. doi:[10.1201/9780849332500](https://doi.org/10.1201/9780849332500)
- Cambardella C.A., Moorman T.B., Novak J.M., Parkin T.B., Karlen D.L., Turco R.F., Konopka A.E. (1994). Field-Scale Variability of Soil Properties in Central Iowa Soils. *Soil Science Society of America Journal* 58 (5): 1501–1511. doi:[10.2136/sssaj1994.03615995005800050033x](https://doi.org/10.2136/sssaj1994.03615995005800050033x)
- Carrión-Paladines V., Hinojosa M.B., Jiménez Álvarez L., Reyes-Bueno F., Correa Quezada L., García-Ruiz R. (2022). Effects of the Severity of Wildfires on Some Physical-Chemical Soil Properties in a Humid Montane Shrublands Ecosystem in Southern Ecuador. *Fire* 5 (3): 66. doi:[10.3390/fire5030066](https://doi.org/10.3390/fire5030066)
- Certini G. (2005). Effects of fire on properties of forest soils: a review. *Oecologia* 143 (1): 1–10. doi:[10.1007/s00442-004-1788-8](https://doi.org/10.1007/s00442-004-1788-8)
- Chesworth W., Camps Arbostain M., Macías F., Spaargaren O., Spaargaren O. (2008). Cambisols. In: *Encyclopedia of Soil Science, Encyclopedia of Earth Sciences Series* (Chesworth W., ed), Springer Netherlands, Dordrecht, pp. 80–81. doi:[10.1007/978-1-4020-3995-9\\_85](https://doi.org/10.1007/978-1-4020-3995-9_85)
- Cofer W.R., Koutzenogii K.P., Kokorin A., Ezcurra A. (1997). Biomass Burning Emissions and the Atmosphere. In: *Sediment Records of Biomass Burning and Global Change* (Clark J.S., Cachier H., Goldammer J.G., Stocks B., eds), Springer Berlin Heidelberg, Berlin, Heidelberg, pp. 189–206. doi:[10.1007/978-3-642-59171-6\\_9](https://doi.org/10.1007/978-3-642-59171-6_9)
- Cozzolino D., Morón A. (2006). Potential of near-infrared reflectance spectroscopy and chemometrics to predict soil organic carbon fractions. *Soil and Tillage Research* 85 (1–2): 78–85. doi:[10.1016/j.still.2004.12.006](https://doi.org/10.1016/j.still.2004.12.006)
- Croatian fire brigade (2022). Statistical report of the State's Fire Operations Center 193 with an overview of fire data for 2022. Available at: <https://hvz.gov.hr/> [accessed 31<sup>st</sup> March 2022]
- Daniel K.W., Tripathi N.K., Honda K., Apisit E. (2004). Analysis of VNIR (400–1100 nm) spectral signatures for estimation of soil organic matter in tropical soils of Thailand. *International Journal of Remote Sensing* 25 (3): 643–652. doi:[10.1080/0143116031000139944](https://doi.org/10.1080/0143116031000139944)
- Daughtry C.S.T. (2001). Discriminating Crop Residues from Soil by Shortwave Infrared Reflectance. *Agronomy Journal* 93 (1): 125–131. doi:[10.2134/agronj2001.931125x](https://doi.org/10.2134/agronj2001.931125x)

- De Simone W., Di Musciano M., Di Cecco V., Ferella G., Frattaroli A.R. (2020). The potentiality of Sentinel-2 to assess the effect of fire events on Mediterranean mountain vegetation. *Plant Sociology* 57: 11–22. doi:[10.3897/pls2020571/02](https://doi.org/10.3897/pls2020571/02)
- DeBano L. F., Neary D. G., Ffolliott, P. F. (1998). *Fire effects on ecosystems*. John Wiley & Sons, New York, USA, pp. 1-13
- Delač D., Kisić I., Bogunović I., Pereira, P. (2021). Temporal impacts of pile burning on vegetation regrowth and soil properties in a Mediterranean environment (Croatia). *Science of The Total Environment* 799: 149318. doi:[10.1016/j.scitotenv.2021.149318](https://doi.org/10.1016/j.scitotenv.2021.149318)
- Delač D., Kisić I., Pereira P. (2022). Temporal Impact of Mulch Treatments (*Pinus halepensis* Mill. and *Olea europaea* L.) on Soil Properties after Wildfire Disturbance in Mediterranean Croatia. *Agronomy* 12 (10): 2484. doi:[10.3390/agronomy12102484](https://doi.org/10.3390/agronomy12102484)
- DHMZ – Croatian Meteorological and Hydrological Service (2013). Sixth National Communication of the Republic of Croatia under the United Nation Framework Convention on the Climate Change (UNFCCC). Available at: [https://klima.hr/razno/publikacije/NIKIP6\\_DHMZ.pdf](https://klima.hr/razno/publikacije/NIKIP6_DHMZ.pdf) [accessed 07 April 2022]
- Dijkstra F. A., Geibe C., Holmström S., Lundström U. S., Van Breemen N. (2001). The effect of organic acids on base cation leaching from the forest floor under six North American tree species. *European Journal of Soil Science* 52 (2): 205-214. doi: [10.1046/j.1365-2389.2001.00369.x](https://doi.org/10.1046/j.1365-2389.2001.00369.x)
- Dindaroglu T., Babur E., Yakupoglu T., Rodrigo-Comino J., Cerdà A. (2021). Evaluation of geomorphometric characteristics and soil properties after a wildfire using Sentinel-2 MSI imagery for future fire-safe forest. *Fire Safety Journal* 122: 103318. doi:[10.1016/j.firesaf.2021.103318](https://doi.org/10.1016/j.firesaf.2021.103318)
- Dlapa P., Bodí M.B., Mataix-Solera J., Cerdà A., Doerr S.H. (2013). FT-IR spectroscopy reveals that ash water repellency is highly dependent on ash chemical composition. *CATENA* 108: 35–43. doi:[10.1016/j.catena.2012.02.011](https://doi.org/10.1016/j.catena.2012.02.011)
- Dlapa P., Bodí M.B., Mataix-Solera J., Cerdà A., Doerr S.H. (2015). Organic matter and wettability characteristics of wildfire ash from Mediterranean conifer forests. *CATENA* 135: 369–376. doi:[10.1016/j.catena.2014.06.018](https://doi.org/10.1016/j.catena.2014.06.018)
- dos Santos U.J., Demattê J.A. de M., Menezes R.S.C., Dotto A.C., Guimarães C.C.B., Alves B.J.R., Primo D.C., Sampaio E.V. de S.B. (2020). Predicting carbon and nitrogen by visible near-infrared (Vis-NIR) and mid-infrared (MIR) spectroscopy in soils of Northeast Brazil. *Geoderma Regional* 23: e00333. doi:[10.1016/j.geodrs.2020.e00333](https://doi.org/10.1016/j.geodrs.2020.e00333)
- Doufexi M., Gamvroula D.E., Alexakis D.E. (2022). Elements' Content in Stream Sediment and Wildfire Ash of Suburban Areas in West Attica (Greece). *Water* 14 (3): 310. doi:[10.3390/w14030310](https://doi.org/10.3390/w14030310)

- Dove N.C., Safford H.D., Bohlman G.N., Estes B.L., Hart S.C. (2020). High-severity wildfire leads to multi-decadal impacts on soil biogeochemistry in mixed-conifer forests. *Ecol Appl* 30 (4). doi:[10.1002/eap.2072](https://doi.org/10.1002/eap.2072)
- Durn G., Škapin S.D., Vdović N., Rennert T., Ottner F., Ružičić S., Cukrov N., Sondi I. (2019). Impact of iron oxides and soil organic matter on the surface physicochemical properties and aggregation of Terra Rossa and Calcocambisol subsoil horizons from Istria (Croatia). *CATENA* 183: 104184. doi:[10.1016/j.catena.2019.104184](https://doi.org/10.1016/j.catena.2019.104184)
- Echigo T., Kimata M., Kyono A., Shimizu M., Hatta T. (2005). Re-investigation of the crystal structure of whewellite [Ca(C<sub>2</sub>O<sub>4</sub>)·H<sub>2</sub>O] and the dehydration mechanism of caoxite [Ca(C<sub>2</sub>O<sub>4</sub>)·3H<sub>2</sub>O]. *Mineral mag* 69 (1): 77–88. doi:[10.1180/0026461056910235](https://doi.org/10.1180/0026461056910235)
- Ecker M.D. and Gelfand A.E. (2003). Spatial modelling and prediction under stationary non-geometric range anisotropy. *Environmental and Ecological Statistics* 10 (2): 165–178. doi:[10.1023/A:1023600123559](https://doi.org/10.1023/A:1023600123559)
- Efthimiou N., Psomiadis E., Panagos P. (2020). Fire severity and soil erosion susceptibility mapping using multi-temporal Earth Observation data: The case of Mati fatal wildfire in Eastern Attica, Greece. *CATENA* 187: 104320. doi:[10.1016/j.catena.2019.104320](https://doi.org/10.1016/j.catena.2019.104320)
- Fernández C., Vega J.A., Fonturbel T., Pérez-Gorostiaga P., Jiménez E., Madrigal J. (2007). Effects of wildfire, salvage logging and slash treatments on soil degradation. *Land Degrad Dev* 18 (6): 591–607. doi:[10.1002/ldr.797](https://doi.org/10.1002/ldr.797)
- Fernández-García V., Marcos E., Huerta S., Calvo L. (2021). Soil-vegetation relationships in Mediterranean forests after fire. *For Ecosyst* 8 (1): 18. doi:[10.1186/s40663-021-00295-y](https://doi.org/10.1186/s40663-021-00295-y)
- Ferreira C.S.S., Seifollahi-Aghmiuni S., Destouni G., Ghajarnia N., Kalantari Z. (2022). Soil degradation in the European Mediterranean region: Processes, status and consequences. *Science of The Total Environment* 805: 150106. doi:[10.1016/j.scitotenv.2021.150106](https://doi.org/10.1016/j.scitotenv.2021.150106)
- Fidêncio P.H., Poppi R.J., de Andrade J.C., Cantarella H. (2002). Determination of organic matter in soil using near-infrared spectroscopy and partial least squares regression. *Communications in Soil Science and Plant Analysis* 33 (9–10): 1607–1615. doi:[10.1081/CSS-120004302](https://doi.org/10.1081/CSS-120004302)
- Flannigan M.D., Stocks B.J., Wotton B.M. (2000). Climate change and forest fires. *Science of The Total Environment* 262 (3): 221–229. doi:[10.1016/S0048-9697\(00\)00524-6](https://doi.org/10.1016/S0048-9697(00)00524-6)
- Francos M., Úbeda X., Pereira P., Alcañiz M. (2018a). Long-term impact of wildfire on soils exposed to different fire severities. A case study in Cadiretes Massif (NE Iberian Peninsula). *Science of the Total Environment* 615: 664–671. doi:[10.1016/j.scitotenv.2017.09.311](https://doi.org/10.1016/j.scitotenv.2017.09.311)



- Francos M., Pereira P., Mataix-Solera J., Arcenegui V., Alcañiz M., Úbeda X. (2018b). How clear-cutting affects fire severity and soil properties in a Mediterranean ecosystem. *Journal of Environmental Management* 206: 625–632. doi:[10.1016/j.jenvman.2017.11.011](https://doi.org/10.1016/j.jenvman.2017.11.011)
- Francos M., Pereira P., Úbeda X. (2019). Mapping impact of intense rainfall on a high-severity burned area using principal component analysis. *CIG* 45 (2): 601–621. doi:[10.18172/cig.3516](https://doi.org/10.18172/cig.3516)
- Francos N., Ogen Y., Ben-Dor E. (2021). Spectral Assessment of Organic Matter with Different Composition Using Reflectance Spectroscopy. *Remote Sensing* 13 (8): 1549. doi:[10.3390/rs13081549](https://doi.org/10.3390/rs13081549)
- Fuentes-Ramirez A., Almonacid-Muñoz L., Muñoz-Gómez N., Moloney K.A. (2022). Spatio-Temporal Variation in Soil Nutrients and Plant Recovery across a Fire-Severity Gradient in Old-Growth Araucaria-Nothofagus Forests of South-Central Chile. *Forests* 13 (3): 448. doi:[10.3390/f13030448](https://doi.org/10.3390/f13030448)
- Fultz L. M., Moore-Kucera J., Dathe J., Davinic M., Perry G., Wester D., Rideout-Hanzak, S. (2016). Forest wildfire and grassland prescribed fire effects on soil biogeochemical processes and microbial communities: Two case studies in the semi-arid Southwest. *Applied Soil Ecology* 99: 118-128. doi:[10.1016/j.apsoil.2015.10.023](https://doi.org/10.1016/j.apsoil.2015.10.023)
- García D., Zamora R., Hódar J. A., Gómez, J. M. (1999). Age structure of *Juniperus communis* L. in the Iberian peninsula: conservation of remnant populations in Mediterranean mountains. *Biological Conservation*, 87 (2): 215-220. doi:10.1016/S0006-3207(98)00059-7
- Germer K., Braun J. (2015). Determination of anisotropic saturated hydraulic conductivity of a odellings slope soil. *Soil Science Society of America Journal* 79 (6): 1528-1536. doi:[10.2136/sssaj2015.02.0071](https://doi.org/10.2136/sssaj2015.02.0071)
- Gholizadeh, A., Saberioon, M., Ben-Dor, E., Borůvka, L. (2018a). Monitoring of selected soil contaminants using proximal and remote sensing techniques: Background, state-of-the-art and future perspectives. *Critical reviews in environmental science and technology* 48 (3): 243-278.
- Gholizadeh, A., Žižala, D., Saberioon, M., Borůvka, L. (2018b). Soil organic carbon and texture retrieving and mapping using proximal, airborne and Sentinel-2 spectral imaging. *Remote Sens. Environ.* 2018, 218, 89–103
- Goforth B.R., Graham R.C., Hubbert K.R., Zanner C.W., Minnich R.A. (2005). Spatial distribution and properties of ash and thermally altered soils after high-severity forest fire, southern California. *Int J Wildland Fire* 14 (4): 343. doi:[10.1071/WF05038](https://doi.org/10.1071/WF05038)
- González-Pérez J.A., González-Vila F.J., Almendros G., Knicker H. (2004). The effect of fire on soil organic matter—a review. *Environment International* 30 (6): 855–870. doi:[10.1016/j.envint.2004.02.003](https://doi.org/10.1016/j.envint.2004.02.003)

- González-Teruel J.D., Jones S.B., Soto-Valles F., Torres-Sánchez R., Lebron I., Friedman S.P., Robinson D.A. (2020). Dielectric Spectroscopy and Application of Mixing Models Describing Dielectric Dispersion in Clay Minerals and Clayey Soils. *Sensors* 20 (22): 6678. doi:[10.3390/s20226678](https://doi.org/10.3390/s20226678)
- Goovaerts, P. (1997). *Geostatistics for natural resources evaluation*. Oxford University Press, pp 101-106, 177.
- Granged A.J.P., Zavala L.M., Jordán A., Bárcenas-Moreno G. (2011). Post-fire evolution of soil properties and vegetation cover in a Mediterranean heathland after experimental burning: A 3-year study. *Geoderma* 164 (1–2): 85–94. doi:[10.1016/j.geoderma.2011.05.017](https://doi.org/10.1016/j.geoderma.2011.05.017)
- Grillakis M., Voulgarakis A., Rovithakis A., Seiradakis K.D., Koutroulis A., Field R.D., Kasoar M., Papadopoulos A., Lazaridis M. (2022). Climate drivers of global wildfire burned area. *Environmental Research Letters* 17 (4): 045021. doi:[10.1088/1748-9326/ac5fa1](https://doi.org/10.1088/1748-9326/ac5fa1)
- Heaton L., Fullen M.A., Bhattacharyya R. (2016). Critical Analysis of the van Bemmelen Conversion Factor used to Convert Soil Organic Matter Data to Soil Organic Carbon Data: Comparative Analyses in a UK Loamy Sand Soil. *EspacoAberto* 6 (1): 35–44. doi:[10.36403/espacoaberto.2016.5244](https://doi.org/10.36403/espacoaberto.2016.5244)
- Hebel C.L., Smith J.E., Cromack K. (2009). Invasive plant species and soil microbial response to wildfire burn severity in the Cascade Range of Oregon. *Applied Soil Ecology* 42 (2): 150–159. doi:[10.1016/j.apsoil.2009.03.004](https://doi.org/10.1016/j.apsoil.2009.03.004)
- Heim W., Thomas A., Berner I., Korschefsky T., Hölzel N., Kamp J. (2022). Anthropogenic fire patterns affect niche breadth and niche overlap in sympatric songbird species. *Science of The Total Environment* 155160. doi:[10.1016/j.scitotenv.2022.155160](https://doi.org/10.1016/j.scitotenv.2022.155160)
- Heitner C., Dimmel D., Schmidt J.A. (2010). *Lignin and lignans: advances in chemistry*. CRS Press, Boca Raton, pp. 683.
- Hengl T., Nussbaum M., Wright M.N., Heuvelink G.B.M., Gräler B. (2018). Random forest as a generic framework for predictive modelling of spatial and spatio-temporal variables. *PeerJ* 6: e5518. doi:[10.7717/peerj.5518](https://doi.org/10.7717/peerj.5518)
- Henig-Sever N., Poliakov D., Broza M. (2001). A novel method for estimation of wild fire intensity based on ash pH and soil microarthropod community. *Pedobiologia* 45 (2): 98–106. doi:[10.1078/0031-4056-00072](https://doi.org/10.1078/0031-4056-00072)
- Heydari M., Rostamy A., Najafi F., Dey D.C. (2017). Effect of fire severity on physical and biochemical soil properties in Zagros oak (*Quercus brantii* Lindl.) forests in Iran. *J For Res* 28 (1): 95–104. doi:[10.1007/s11676-016-0299-x](https://doi.org/10.1007/s11676-016-0299-x)
- Ho L. C. (1976). Variation in the Carbon/Dry Matter Ratio in Plant Material. *Annals of Botany*, 40(165), 163–165. Available at: <http://www.jstor.org/stable/42753403> [accessed 5<sup>th</sup> July 2022]



- Hrelja I, Šestak I, Bogunović I. (2020). Wildfire Impacts on Soil Physical and Chemical Properties – A Short Review of Recent Studies. *Agriculturae Conspectus Scientificus* 85 (4): 293-301. Available at: <https://hrcak.srce.hr/245967>
- Hrelja I., Šestak I., Delač D., Pereira P., Bogunović I. (2022). Soil Chemical Properties and Trace Elements after Wildfire in Mediterranean Croatia: Effect of Severity, Vegetation Type and Time-Since-Fire. *Agronomy* 12 (7): 1515. doi:[10.3390/agronomy12071515](https://doi.org/10.3390/agronomy12071515)
- Hu B., Zhou Q., He C., Duan L., Li W., Zhang G., Ji W., Peng J., Xie H. (2021). Spatial variability and potential controls of soil organic matter in the Eastern Dongting Lake Plain in southern China. *J Soils Sediments* 21 (8): 2791–2804. doi:[10.1007/s11368-021-02906-1](https://doi.org/10.1007/s11368-021-02906-1)
- Huang Y., Wu L., Yu J. (2009). Relationships between soil organic matter content (SOM) and pH in topsoil of zonal soils in China. *Acta Pedologica Sinica* 2009, 46 (5): 851-860.
- Huerta S., Fernández-García V., Calvo L., Marcos E. (2020). Soil Resistance to Burn Severity in Different Forest Ecosystems in the Framework of a Wildfire. *Forests* 11 (7): 773. doi:[10.3390/f11070773](https://doi.org/10.3390/f11070773)
- Hunt M.L., Blackburn G.A., Carrasco L., Redhead J.W., Rowland C.S. (2019). High resolution wheat yield mapping using Sentinel-2. *Remote Sensing of Environment* 233: 111410. doi:[10.1016/j.rse.2019.111410](https://doi.org/10.1016/j.rse.2019.111410)
- Husnjak, S. (2014). Soil systematics of Croatia. University textbook, University of Croatia publishing house, Zagreb. [in croatian]
- Iannaccone M., Di Santo P., Buhagiar J. A., Paura B., Coccozza C. (2020). Enhancement of sprouting and rooting of *Quercus pubescens* by benzylaminopurine and Indole-butyric acid in micropropagation. *Fresenius Environmental Bulletin*, 29 (11): 10287-10293.
- Iglesias T., Cala V., Gonzalez J. (1997). Mineralogical and chemical modifications in soils affected by a forest fire in the Mediterranean area. *Science of the Total Environment* 204 (1): 89-96. doi:[10.1016/S0048-9697\(97\)00173-3](https://doi.org/10.1016/S0048-9697(97)00173-3)
- Inbar A., Lado M., Sternberg M., Tenau H., Ben-Hur M. (2014). Forest fire effects on soil chemical and physicochemical properties, infiltration, runoff, and erosion in a semiarid Mediterranean region. *Geoderma* 221–222: 131–138. doi:[10.1016/j.geoderma.2014.01.015](https://doi.org/10.1016/j.geoderma.2014.01.015)
- IPCC (2022). *Climate Change 2022: Impacts, Adaptation, and Vulnerability. Contribution of Working Group II to the Sixth Assessment Report of the Intergovernmental Panel on Climate Change* (Pörtner H.-O., Roberts D.C., Tignor M., Poloczanska E.S., Mintenbeck K., Alegría A., Craig M., Langsdorf S., Lösschke S., Möller V., Okem A., Rama B., eds), Cambridge University Press. In Press.
- IUSS Working Group WRB. 2015. World Reference Base for Soil Resources 2014, update 2015 International soil classification system for naming soils and creating legends for soil maps. World Soil Resources Reports No. 106. FAO, Rome.

- Isaaks E. H., Srivastava, M. R. (1989). *Applied geostatistics*. Oxford University, London.
- Jhariya M.K., Raj A. (2014). Effects of wildfires on flora, fauna and physico-chemical properties of soil-An overview. *JANS* 6 (2): 887–897. doi:[10.31018/jans.v6i2.550](https://doi.org/10.31018/jans.v6i2.550)
- Jalal M. A. F., Read D. J. (1983). The organic acid composition of Calluna heathland soil with special reference to phyto-and fungitoxicity: I. Isolation and identification of organic acids. *Plant and Soil* 70: 257-272. doi: 10.1007/BF02374785
- Jiang B., Xu W., Zhang D., Nie F., Sun Q. (2022). Contrasting multiple deterministic interpolation responses to different spatial scale in prediction soil organic carbon: A case study in Mollisols regions. *Ecological Indicators* 134: 108472. doi:[10.1016/j.ecolind.2021.108472](https://doi.org/10.1016/j.ecolind.2021.108472)
- Jiménez-González M.A., De la Rosa J.M., Jiménez-Morillo N.T., Almendros G., González-Pérez J.A., Knicker H. (2016). Post-fire recovery of soil organic matter in a Cambisol from typical Mediterranean forest in Southwestern Spain. *Science of The Total Environment* 572: 1414–1421. doi:[10.1016/j.scitotenv.2016.02.134](https://doi.org/10.1016/j.scitotenv.2016.02.134)
- Jiménez-Pinilla P., Mataix-Solera J., Arcenegui V., Delgado R., Martín-García J.M., Lozano E., Martínez-Zavala L., Jordán A. (2016). Advances in the knowledge of how heating can affect aggregate stability in Mediterranean soils: a XDR and SEM-EDX approach. *CATENA* 147: 315–324. doi:[10.1016/j.catena.2016.07.036](https://doi.org/10.1016/j.catena.2016.07.036)
- Jin X., Du J., Liu H., Wang Z., Song K. (2016). Remote estimation of soil organic matter content in the Sanjiang Plain, Northeast China: The optimal band algorithm versus the GRA-ANN model. *Agricultural and Forest Meteorology* 218–219: 250–260. doi:[10.1016/j.agrformet.2015.12.062](https://doi.org/10.1016/j.agrformet.2015.12.062)
- Jordán A., Zavala L.M., Mataix-Solera J., Nava A., Alanis A. (2011). Effect of fire severity on water repellency and aggregate stability on Mexican Volcanic soils. *Catena* 84: 136-147. doi: [10.1016/j.catena.2010.10.007](https://doi.org/10.1016/j.catena.2010.10.007)
- Jordán A., Gordillo-Rivero Á.J., García-Moreno J., Zavala L.M., Granged A.J.P., Gil J., Neto-Paixão H.M. (2014). Post-fire evolution of water repellency and aggregate stability in Mediterranean calcareous soils: a 6-year study. *Catena* 118: 115-123. doi:[10.1016/j.catena.2014.02.001](https://doi.org/10.1016/j.catena.2014.02.001)
- Kazeev K., Vilкова V., Shkhatpatsev A., Bykhalova O., Rudenok Y., Nizhelskiy M., Kolesnikov S., Minkina T., Sushkova S., Mandzhieva S., Rajput V.D. (2022). Consequences of the catastrophic wildfire in 2020 for the soil cover of the Utrish State Nature Reserve. *Sains Tanah J Soil Sci Agroclimatology* 19 (1): 52. doi:[10.20961/stjssa.v19i1.58709](https://doi.org/10.20961/stjssa.v19i1.58709)
- Kazmierczak R., Balarezo Giarola N.F., Carpinelli S., Biasso Riferite F., Brant Dias S.H., Bürkner dos Santos J., Ferreira da Fonseca A. (2022). Spatial Variability of Phosphorus and Potassium Contents - Effect of Long-Term in Soil Tillage Systems. *SSRN Journal*. doi:[10.2139/ssrn.4119522](https://doi.org/10.2139/ssrn.4119522)

- Keiluweit M., Nico P.S., Johnson M.G., Kleber M. (2010). Dynamic Molecular Structure of Plant Biomass-Derived Black Carbon (Biochar). *Environ Sci Technol* 44 (4): 1247–1253. doi:[10.1021/es9031419](https://doi.org/10.1021/es9031419)
- Kesselmeier J., Bode K., Hofmann U., Müller H., Schäfer L., Wolf A., Torres L. (1997). Emission of short chained organic acids, aldehydes and monoterpenes from *Quercus ilex* L. and *Pinus pinea* L. in relation to physiological activities, carbon budget and emission algorithms. *Atmospheric Environment* 31: 119-133. doi: [10.1016/S1352-2310\(97\)00079-4](https://doi.org/10.1016/S1352-2310(97)00079-4)
- Khviyuzov S., Bogolitsyn K., Volkov A., Kuposov G., Gusakova M. (2020). Features of frequency dependence of electrical conductivity and dielectric properties in lignins from conifers and deciduous trees. *Holzforschung* 74 (12): 1113–1122. doi:[10.1515/hf-2019-0149](https://doi.org/10.1515/hf-2019-0149)
- Kim Y., Kim C.-G., Lee K.S., Choung Y. (2021). Effects of Post-Fire Vegetation Recovery on Soil Erosion in Vulnerable Montane Regions in a Monsoon Climate: A Decade of Monitoring. *J Plant Biol* 64 (2): 123–133. doi:[10.1007/s12374-020-09283-1](https://doi.org/10.1007/s12374-020-09283-1)
- Kisić I., Bogunović I., Delač D., Barčić D. (2023). Open space fires in the Republic of Croatia - occurrence, frequency and suppression. *Hrvatske vode* 31 (124): 117-126.
- Knicker H., Almendros G., González-Vila F.J., Martin F., Lüdemann H.-D. (1996). <sup>13</sup>C- and <sup>15</sup>N-NMR spectroscopic examination of the transformation of organic nitrogen in plant biomass during thermal treatment. *Soil Biology and Biochemistry* 28 (8): 1053–1060. doi:[10.1016/0038-0717\(96\)00078-8](https://doi.org/10.1016/0038-0717(96)00078-8)
- Kottek M., Grieser J., Beck C., Rudolf B., Rubel F. (2006). World map of the Köppen-Geiger climate classification updated. *Meteorologische Zeitschrift* 15 (3): 259-263.
- Krtalić A., Linardić D., Pernar, R. (2021). Framework for spatial and temporal monitoring of urban forest and vegetation conditions: Case study Zagreb, Croatia. *Sustainability* 13 (11): 6055. doi:[10.3390/su13116055](https://doi.org/10.3390/su13116055)
- Kutiel P., Inbar M. (1993). Fire impacts on soil nutrients and soil erosion in a Mediterranean pine forest plantation. *CATENA* 20 (1–2): 129–139. doi:[10.1016/0341-8162\(93\)90033-L](https://doi.org/10.1016/0341-8162(93)90033-L)
- Lambers H., Mougél C., Jaillard B., Hinsinger P. (2009). Plant-microbe-soil interactions in the rhizosphere: an evolutionary perspective. *Plant and Soil* 321: 83–115. doi:[10.1007/s11104-009-0042-x](https://doi.org/10.1007/s11104-009-0042-x)
- Lark R.M. (2012). Distinguishing spatially correlated random variation in soil from a ‘pure nugget’ process. *Geoderma* 185–186: 102–109. doi:[10.1016/j.geoderma.2012.03.029](https://doi.org/10.1016/j.geoderma.2012.03.029)
- Lasaponara R., Proto A.M., Aromando A., Cardettini G., Varela V., Danese M. (2020). On the Mapping of Burned Areas and Burn Severity Using Self Organizing Map and Sentinel-2 Data. *IEEE Geosci Remote Sensing Lett* 17 (5): 854–858. doi:[10.1109/LGRS.2019.2934503](https://doi.org/10.1109/LGRS.2019.2934503)
- Li J., Heap A.D. (2008). A Review of Spatial Interpolation Methods for Environmental Scientists. *Geoscience Australia, Canberra, Australia. Record 2008/23.*

- Li S., Viscarra Rossel R.A., Webster R. (2022). The cost-effectiveness of reflectance spectroscopy for estimating soil organic carbon. *European J Soil Science* 73 (1). doi:[10.1111/ejss.13202](https://doi.org/10.1111/ejss.13202)
- Lillesand, T.M., Kiefer, R.W., Chipman, J.W. (2004). *Remote sensing and image interpretation*. 5th ed. John Wiley & Sons, New York.
- Lin C., Ma S.-E., Huang L.-P., Chen C.-I., Lin P.-T., Yang Z.-K., Lin K.-T. (2021). Generating a Baseline Map of Surface Fuel Loading Using Stratified Random Sampling Inventory Data through Cokriging and Multiple Linear Regression Methods. *Remote Sensing* 13 (8): 1561. doi:[10.3390/rs13081561](https://doi.org/10.3390/rs13081561)
- Lin Y., Mei L., Wei Q., Li B., Zhang P., Sun S., Cui G. (2022). *Leymus chinensis* resists degraded soil stress by modulating root exudate components to attract beneficial microorganisms. *Frontiers in microbiology* 13: 951838. doi: [10.3389/fmicb.2022.951838](https://doi.org/10.3389/fmicb.2022.951838)
- Litton C. M., Santelices R. (2003). Effect of wildfire on soil physical and chemical properties in a *Nothofagus glauca* forest, Chile. *Revista Chilena de Historia Natural* 76 (4): 529-542.
- Liu Q., Fu B., Chen Z., Chen Li, Liu L., Peng W., Liang Y., Chen Lin. (2022a). Evaluating Effects of Post-Fire Climate and Burn Severity on the Early-Term Regeneration of Forest and Shrub Communities in the San Gabriel Mountains of California from Sentinel-2(MSI) Images. *Forests* 13 (7): 1060. doi:[10.3390/f13071060](https://doi.org/10.3390/f13071060)
- Liu Q., He L., Guo L., Wang M., Deng D., Lv P., Wang R., Jia Z., Hu Z., Wu G., Shi T. (2022b). Digital mapping of soil organic carbon density using newly developed bare soil spectral indices and deep neural network. *CATENA* 219: 106603. doi:[10.1016/j.catena.2022.106603](https://doi.org/10.1016/j.catena.2022.106603)
- Liu S., An N., Yang J., Dong S., Wang C., Yin Y. (2015). Prediction of soil organic matter variability associated with different land use types in mountainous landscape in southwestern Yunnan province, China. *CATENA* 133: 137–144. doi:[10.1016/j.catena.2015.05.010](https://doi.org/10.1016/j.catena.2015.05.010)
- Lobell D.B., Asner G.P. (2002). Moisture Effects on Soil Reflectance. *Soil Sci Soc Am j* 66 (3): 722–727. doi:[10.2136/sssaj2002.7220](https://doi.org/10.2136/sssaj2002.7220)
- Lorente M., Parsons W. F., McIntire E. J., Munson, A. D. (2013). Wildfire and forest harvest disturbances in the boreal forest leave different long-lasting spatial signatures. *Plant and soil* 364: 39-54. doi:[10.1007/s11104-012-1331-3](https://doi.org/10.1007/s11104-012-1331-3)
- Ma W., Tang S., Dengzeng Z., Zhang D., Zhang T., Ma X. (2022). Root exudates contribute to belowground ecosystem hotspots: a review. *Frontiers in Microbiology* 13: 937940. doi: [10.3389/fmicb.2022.937940](https://doi.org/10.3389/fmicb.2022.937940)
- Majder-Lopatka, M., Szulc, W., Rutkowska, B., Ptasiński, D., Kazberuk, W. (2019). Influence of fire on selected physico-chemical properties of forest soil. *Soil Science Annual* 70 (1): 39-43. doi: 10.2478/ssa-2019-0005

- Martín A., Díaz-Raviña M., Carballas T. (2012). Short- and medium-term evolution of soil properties in Atlantic forest ecosystems affected by wildfires. *Land Degrad Dev* 23 (5): 427–439. doi:[10.1002/ldr.1078](https://doi.org/10.1002/ldr.1078)
- Martinez G., Vanderlinden K., Ordóñez R., Muriel J.L. (2009). Can Apparent Electrical Conductivity Improve the Spatial Characterization of Soil Organic Carbon? *Vadose Zone Journal* 8 (3): 586–593. doi:[10.2136/vzj2008.0123](https://doi.org/10.2136/vzj2008.0123)
- Mastrolonardo G., Certini G., Krebs R., Forte C., Egli M. (2013). Effects of fire on soil organic matter quality along an altitudinal sequence on Mt. Etna, Sicily. *CATENA* 110: 133–145. doi:[10.1016/j.catena.2013.05.017](https://doi.org/10.1016/j.catena.2013.05.017)
- McBeath A.V., Smernik R.J., Krull E.S. (2013). A demonstration of the high variability of chars produced from wood in bushfires. *Organic Geochemistry* 55: 38–44. doi:[10.1016/j.orggeochem.2012.11.006](https://doi.org/10.1016/j.orggeochem.2012.11.006)
- McGrath D., Zhang C., Carton O.T. (2004). Geostatistical analyses and hazard assessment on soil lead in Silvermines area, Ireland. *Environmental Pollution* 127 (2): 239–248. doi:[10.1016/j.envpol.2003.07.002](https://doi.org/10.1016/j.envpol.2003.07.002)
- Mayer M., Prescott C. E., Abaker W. E., Augusto L., Cécillon L., Ferreira G. W., Vesterdal, L. (2020). Tamm Review: Influence of forest management activities on soil organic carbon stocks: A knowledge synthesis. *Forest Ecology and Management* 466, 118127. doi:[10.1016/j.foreco.2020.118127](https://doi.org/10.1016/j.foreco.2020.118127)
- Merino A., Chávez-Vergara B., Salgado J., Fonturbel M.T., García-Oliva F., Vega J.A. (2015). Variability in the composition of charred litter generated by wildfire in different ecosystems. *CATENA* 133: 52–63. doi:[10.1016/j.catena.2015.04.016](https://doi.org/10.1016/j.catena.2015.04.016)
- Merino A., Fonturbel M.T., Fernández C., Chávez-Vergara B., García-Oliva F., Vega J.A. (2018). Inferring changes in soil organic matter in post-wildfire soil burn severity levels in a temperate climate. *Science of The Total Environment* 627: 622–632. doi:[10.1016/j.scitotenv.2018.01.189](https://doi.org/10.1016/j.scitotenv.2018.01.189)
- Miller C. E. (2001). Chemical principles of near-infrared technology. In: *Near-Infrared Technology in the Agricultural and Food Industries* (Williams P. and Norris K., eds.), The American Association of Cereal Chemists Inc., St. Paul, MN, pp. 19–37.
- Mirzaee S., Ghorbani-Dashtaki S., Mohammadi J., Asadi H., Asadzadeh F. (2016). Spatial variability of soil organic matter using remote sensing data. *CATENA* 145: 118–127. doi:[10.1016/j.catena.2016.05.023](https://doi.org/10.1016/j.catena.2016.05.023)
- Mmolawa K., Or D. (2000). Root zone solute dynamics under drip irrigation: A review. *Plant and soil* 222 (1-2): 163-190. doi: 10.1023/A:1004756832038
- Moreno-Casasola P. (2008). Dunes. In: *Encyclopedia of Ecology* (Jorgensen S.E., Fath B., eds), Amsterdam, Elsevier Ltd, pp. 971–976. doi:10.1016/B978-008045405-4.00328-1

- Moya D., González-De Vega S., Lozano E., García-Orenes F., Mataix-Solera J., Lucas-Borja M.E., de las Heras J. (2019). The burn severity and plant recovery relationship affect the biological and chemical soil properties of *Pinus halepensis* Mill. stands in the short and mid-terms after wildfire. *Journal of Environmental Management* 235: 250–256. doi:[10.1016/j.jenvman.2019.01.029](https://doi.org/10.1016/j.jenvman.2019.01.029)
- Munns R. (2002). Comparative physiology of salt and water stress. *Plant, cell & environment* 25 (2): 239-250. doi:[10.1046/j.0016-8025.2001.00808.x](https://doi.org/10.1046/j.0016-8025.2001.00808.x)
- Muráňová K., Šimanský, V. (2015). The effect of different severity of fire on soil organic matter and aggregates stability. *Acta fytotechnica et zootechnica* 2015, 18 (1): 1-5. doi:[10.15414/afz.2015.18.01.01-05](https://doi.org/10.15414/afz.2015.18.01.01-05)
- Nave L.E., Vance E.D., Swanston C.W., Curtis P.S. (2011). Fire effects on temperate forest soil C and N storage. *Ecological Applications* 21 (4): 1189–1201. doi:[10.1890/10-0660.1](https://doi.org/10.1890/10-0660.1)
- Nawar S., Mouazen A.M. (2017). Predictive performance of mobile vis-near infrared spectroscopy for key soil properties at different geographical scales by using spiking and data mining techniques. *CATENA* 151: 118–129. doi:[10.1016/j.catena.2016.12.014](https://doi.org/10.1016/j.catena.2016.12.014)
- Neary D.G., Klopatek C.C., DeBano L.F., Ffolliott P.F. (1999). Fire effects on belowground sustainability: a review and synthesis. *Forest Ecology and Management* 122 (1–2): 51–71. doi:[10.1016/S0378-1127\(99\)00032-8](https://doi.org/10.1016/S0378-1127(99)00032-8)
- Nocentini C., Certini G., Knicker H., Francioso O., Rumpel C. (2010). Nature and reactivity of charcoal produced and added to soil during wildfire are particle-size dependent. *Organic Geochemistry* 41 (7): 682–689. doi:[10.1016/j.orggeochem.2010.03.010](https://doi.org/10.1016/j.orggeochem.2010.03.010)
- Novelli F., Spiegel H., Sandén T., Vuolo F. (2019). Assimilation of Sentinel-2 Leaf Area Index Data into a Physically-Based Crop Growth Model for Yield Estimation. *Agronomy* 9 (5): 255. doi:[10.3390/agronomy9050255](https://doi.org/10.3390/agronomy9050255)
- Oliveira A.L.G., Lima J.P., Brasco T.L., Amaral L.R. (2022). The importance of modelling the effects of trend and anisotropy on soil fertility maps. *Computers and Electronics in Agriculture* 196: 106877. doi:[10.1016/j.compag.2022.106877](https://doi.org/10.1016/j.compag.2022.106877)
- Orumaa A., Agan A., Anslan S., Drenkhan T., Drenkhan R., Kauer K., Köster K., Tedersoo L., Metslaid M. (2022). Long-term effects of forest fires on fungal community and soil properties along a hemiboreal Scots pine forest fire chronosequence. *Science of The Total Environment* 851: 158173. doi:[10.1016/j.scitotenv.2022.158173](https://doi.org/10.1016/j.scitotenv.2022.158173)
- Otero M., Santos D., Barros A.C., Calapez P., Maia P., Keizer J.J., Esteves V.I., Lillebø A.I. (2015). Soil properties, phosphorus fractions and sorption after wildfire in north-central Portugal. *Geoderma Regional* 5: 86–95. doi:[10.1016/j.geodrs.2015.04.003](https://doi.org/10.1016/j.geodrs.2015.04.003)
- Oxford Reference. Beer-Lambert law. Retrieved 7 Oct. 2022, from <https://www.oxfordreference.com/view/10.1093/oi/authority.20110803095455747>.



- Parro K., Köster K., Jögiste K., Seglinš K., Sims A., Stanturf J.A., Metslaid M. (2019). Impact of post-fire management on soil respiration, carbon and nitrogen content in a managed hemiboreal forest. *Journal of Environmental Management* 233: 371–377. doi:[10.1016/j.jenvman.2018.12.050](https://doi.org/10.1016/j.jenvman.2018.12.050)
- Pasta S., De Rigo D., Caudullo G. (2016). *Quercus pubescens* in Europe: distribution, habitat, usage and threats. *European Atlas of forest tree species*, pp. 156-157. Available at: [https://forest.jrc.ec.europa.eu/media/atlas/Quercus\\_pubescens.pdf](https://forest.jrc.ec.europa.eu/media/atlas/Quercus_pubescens.pdf) [accessed 6th April 2023]
- Pathak H., Rao D.L.N. (1998). Carbon and nitrogen mineralization from added organic matter in saline and alkali soils. *Soil Biology and Biochemistry* 30 (6): 695–702. doi:[10.1016/S0038-0717\(97\)00208-3](https://doi.org/10.1016/S0038-0717(97)00208-3)
- Paula S., Pausas J.G. (2008). Burning seeds: germinative response to heat treatments in relation to resprouting ability: Post-fire germination and resprouting. *Journal of Ecology* 96 (3): 543–552. doi:[10.1111/j.1365-2745.2008.01359.x](https://doi.org/10.1111/j.1365-2745.2008.01359.x)
- Pausas J.G., Keeley J.E. (2019). Wildfires as an ecosystem service. *Front Ecol Environ* 17 (5): 289–295. doi:[10.1002/fee.2044](https://doi.org/10.1002/fee.2044)
- Pausas J.G., Llovet J., Rodrigo A., Vallejo R. (2008). Are wildfires a disaster in the Mediterranean basin? – A review. *Int. J. Wildland Fire* 17, 713-723. doi:[10.1071/WF07151](https://doi.org/10.1071/WF07151)
- Pavlek K., Bišćević F., Furčić P., Grđan A., Gugić V., Malešić N., Moharić P., Vragović V., Fuerst-Bjeliš B., Cvitanović M. (2017). Spatial patterns and drivers of fire occurrence in a Mediterranean environment: a case study of southern Croatia. *Geografisk Tidsskrift-Danish Journal of Geography* 117 (1): 22–35. doi:[10.1080/00167223.2016.1266272](https://doi.org/10.1080/00167223.2016.1266272)
- Peng X., Horn, R. (2008). Time-dependent, anisotropic pore structure and soil strength in a 10-year period after intensive tractor wheeling under conservation and conventional tillage. *Journal of Plant Nutrition and Soil Science* 171 (6): 936-944. doi:[10.1002/jpln.200700084](https://doi.org/10.1002/jpln.200700084)
- Pereira P., Brevik E. C., Bogunović I., Estebanz-Sánchez F. (2019). Ash and soils. A twin relationship in fire-affected areas. In: *Fire effects on soil properties* (Pereira P., Mataix-Solera J., Úbeda X., Reind G. and Cerdà A., eds), Leiden, Netherlands, CSIRO Publishing, pp. 39-67.
- Pereira P., Cerda A., Martin D., Úbeda X., Depellegrin D., Novara A., Martínez-Murillo J.F., Brevik E.C., Menshov O., Comino J.R., Miesel J. (2017). Short-term low-severity spring grassland fire impacts on soil extractable elements and soil ratios in Lithuania. *Science of The Total Environment* 578: 469–475. doi:[10.1016/j.scitotenv.2016.10.210](https://doi.org/10.1016/j.scitotenv.2016.10.210)
- Pereira P., Úbeda X., Martin D.A. (2012). Fire severity effects on ash chemical composition and water-extractable elements. *Geoderma* 191: 105–114. doi:[10.1016/j.geoderma.2012.02.005](https://doi.org/10.1016/j.geoderma.2012.02.005)

- Pesaresi M., Corbane C., Julea A., Florczyk A., Syrris V., Soille P. (2016). Assessment of the Added-Value of Sentinel-2 for Detecting Built-up Areas. *Remote Sensing* 8 (4): 299. doi:[10.3390/rs8040299](https://doi.org/10.3390/rs8040299)
- Ping X., Chang Y., Liu M., Hu Y., Huang W., Shi S., Jia Y., Li D. (2022). Carbon Emission and Redistribution among Forest Carbon Pools, and Change in Soil Nutrient Content after Different Severities of Forest Fires in Northeast China. *Forests* 13 (1): 110. doi:[10.3390/f13010110](https://doi.org/10.3390/f13010110)
- Plank S. (2014). Rapid Damage Assessment by Means of Multi-Temporal SAR — A Comprehensive Review and Outlook to Sentinel-1. *Remote Sensing* 6 (6): 4870–4906. doi:[10.3390/rs6064870](https://doi.org/10.3390/rs6064870)
- Plante A.F., Fernández J.M., Leifeld J. (2009). Application of thermal analysis techniques in soil science. *Geoderma* 153 (1–2): 1–10. doi:[10.1016/j.geoderma.2009.08.016](https://doi.org/10.1016/j.geoderma.2009.08.016)
- Pouladi N., Møller A.B., Tabatabai S., Greve M.H. (2019). Mapping soil organic matter contents at field level with Cubist, Random Forest and kriging. *Geoderma* 342: 85–92. doi:[10.1016/j.geoderma.2019.02.019](https://doi.org/10.1016/j.geoderma.2019.02.019)
- Prendergast-Miller M.T., de Menezes A.B., Macdonald L.M., Toscas P., Bissett A., Baker G., Farrell M., Richardson A.E., Wark T., Thrall P.H. (2017). Wildfire impact: Natural experiment reveals differential short-term changes in soil microbial communities. *Soil Biology and Biochemistry* 109: 1–13. doi:[10.1016/j.soilbio.2017.01.027](https://doi.org/10.1016/j.soilbio.2017.01.027)
- Qiao P., Lei M., Yang S., Yang J., Guo G., Zhou X. (2018). Comparing ordinary kriging and inverse distance weighting for soil as pollution in Beijing. *Environ Sci Pollut Res* 25 (16): 15597–15608. doi:[10.1007/s11356-018-1552-y](https://doi.org/10.1007/s11356-018-1552-y)
- Qin F., Guo C., Liu D., Xu S., Wang S. (2022). A comparison of ordinary kriging, regression kriging and REML-EBLUP for mapping soil organic matter on a regional scale. *Arab J Geosci* 15 (12): 1120. doi:[10.1007/s12517-022-10008-6](https://doi.org/10.1007/s12517-022-10008-6)
- Rahman M.M., Tsukamoto J., Rahman Md. Motiur, Yoneyama A., Mostafa K.M. (2013). Lignin and its effects on litter decomposition in forest ecosystems. *Chemistry and Ecology* 29 (6): 540–553. doi:[10.1080/02757540.2013.790380](https://doi.org/10.1080/02757540.2013.790380)
- Rahmani S.R., Ackerson J.P., Schulze D., Adhikari K., Libohova Z. (2022). Digital Mapping of Soil Organic Matter and Cation Exchange Capacity in a Low Relief Landscape Using LiDAR Data. *Agronomy* 12 (6): 1338. doi:[10.3390/agronomy12061338](https://doi.org/10.3390/agronomy12061338)
- Raymaekers J., Rousseeuw P.J. (2021). Transforming variables to central normality. *Mach Learn.* doi:[10.1007/s10994-021-05960-5](https://doi.org/10.1007/s10994-021-05960-5)
- Ringnér M. (2008). What is principal component analysis? *Nat Biotechnol* 26 (3): 303–304. doi:[10.1038/nbt0308-303](https://doi.org/10.1038/nbt0308-303)



- Rodriguez C., Guo J. (2020). Wildfire impacts on soil physical properties: 2016 Erskine fire, California, Presented at the 116th Annual GSA Cordilleran Section Meeting - 2020, p. 347323. doi:[10.1130/abs/2020CD-347323](https://doi.org/10.1130/abs/2020CD-347323)
- Rosero-Vlasova O.A., Vlassova L., Pérez-Cabello F., Montorio R., Nadal-Romero E. (2018). Modelling soil organic matter and texture from satellite data in areas affected by wildfires and cropland abandonment in Aragón, Northern Spain. *J Appl Rem Sens* 12 (04): 1. doi:[10.1117/1.JRS.12.042803](https://doi.org/10.1117/1.JRS.12.042803)
- Ruffault J., Moron V., Trigo R.M., Curt T. (2016). Objective identification of multiple large fire climatologies: an application to a Mediterranean ecosystem. *Environ Res Lett* 11 (7): 075006. doi:[10.1088/1748-9326/11/7/075006](https://doi.org/10.1088/1748-9326/11/7/075006)
- Sahbeni G., Székely B. (2022). Spatial modelling of soil salinity using kriging interpolation techniques: A study case in the Great Hungarian Plain. *EURASIAN JOURNAL OF SOIL SCIENCE (EJSS)* 11 (2): 102–112. doi:[10.18393/ejss.1013432](https://doi.org/10.18393/ejss.1013432)
- Salisbury J.W. (1998). *Spectral Measurements Field Guide: Defense Technical Information Center, Fort Belvoir, VA.* doi:[10.21236/ADA362374](https://doi.org/10.21236/ADA362374)
- Samieifard R., Heidari A., Drohan P. J. (2021). Assessment of Some Kriging Methods For Mapping The Soil Electrical Conductivity: Case Study Of Southeastern Coast Of Caspian Sea Of Iran. *Journal of Global Ecology and Environment*, 13 (1): 12-21.
- Santín C, Doerr S. (2019) Carbon. In: *Fire effects on soil properties* (Pereira P., Mataix-Solera J., Úbeda X., Reind G. and Cerdà A., eds), Leiden, Netherlands, CSIRO Publishing, pp.115-128.
- Santín C., Doerr S.H. (2016). Fire effects on soils: the human dimension. *Phil Trans R Soc B* 371 (1696): 20150171. doi:[10.1098/rstb.2015.0171](https://doi.org/10.1098/rstb.2015.0171)
- Santín C., Doerr S.H., Kane E.S., Masiello C.A., Ohlson M., de la Rosa J.M., Preston C.M., Dittmar T. (2016a). Towards a global assessment of pyrogenic carbon from vegetation fires. *Glob Change Biol* 22 (1): 76–91. doi:[10.1111/gcb.12985](https://doi.org/10.1111/gcb.12985)
- Santín C., Doerr S.H., Merino A., Bryant R., Loader N.J. (2016b). Forest floor chemical transformations in a boreal forest fire and their correlations with temperature and heating duration. *Geoderma* 264: 71–80. doi:[10.1016/j.geoderma.2015.09.021](https://doi.org/10.1016/j.geoderma.2015.09.021)
- Santín C., Doerr S.H., Shakesby R.A., Bryant R., Sheridan G.J., Lane P.N.J., Smith H.G., Bell T.L. (2012). Carbon loads, forms and sequestration potential within ash deposits produced by wildfire: new insights from the 2009 'Black Saturday' fires, Australia. *Eur J Forest Res* 131 (4): 1245–1253. doi:[10.1007/s10342-012-0595-8](https://doi.org/10.1007/s10342-012-0595-8)
- Savitzky Abraham., Golay M.J.E. (1964). Smoothing and Differentiation of Data by Simplified Least Squares Procedures. *Anal Chem* 36 (8): 1627–1639. doi:[10.1021/ac60214a047](https://doi.org/10.1021/ac60214a047)

- Schmerbeck J., Fiener P. (2015). Wildfires, Ecosystem Services, and Biodiversity in Tropical Dry Forest in India. *Environmental Management* 56 (2): 355–372. doi:[10.1007/s00267-015-0502-4](https://doi.org/10.1007/s00267-015-0502-4)
- Semella S., Hutengs C., Seidel M., Ulrich M., Schneider B., Ortner M., Thiele-Bruhn S., Ludwig B., Vohland M. (2022). Accuracy and Reproducibility of Laboratory Diffuse Reflectance Measurements with Portable VNIR and MIR Spectrometers for Predictive Soil Organic Carbon Modeling. *Sensors* 22 (7): 2749. doi:[10.3390/s22072749](https://doi.org/10.3390/s22072749)
- Šestak I., Pereira P., Telak L.J., Perčin A., Hrelja I., Bogunović I. (2022). Soil Chemical Properties and Fire Severity Assessment Using VNIR Proximal Spectroscopy in Fire-Affected Abandoned Orchard of Mediterranean Croatia. *Agronomy* 12 (1): 129. doi:[10.3390/agronomy12010129](https://doi.org/10.3390/agronomy12010129)
- Shakesby R.A. (2011). Post-wildfire soil erosion in the Mediterranean: Review and future research directions. *Earth-Science Reviews* 105 (3–4): 71–100. doi:[10.1016/j.earscirev.2011.01.001](https://doi.org/10.1016/j.earscirev.2011.01.001)
- Sheridan G., Lane P., Nyman P. (2018). Erosion. In: *Fire Effects on Soil Properties* (Pereira P., Mataix-Solera J., Úbeda X., Rein G., Cerdà A., eds), CSIRO Publishing, Clayton South, Australia, pp. 89-113.
- Shoshany M., Goldshleger N., Chudnovsky A. (2013). Monitoring of agricultural soil degradation by remote-sensing methods: a review. *International Journal of Remote Sensing* 34 (17): 6152–6181. doi:[10.1080/01431161.2013.793872](https://doi.org/10.1080/01431161.2013.793872)
- Shukla K., Kumar P., Mann G.S., Khare M. (2020). Mapping spatial distribution of particulate matter using Kriging and Inverse Distance Weighting at supersites of megacity Delhi. *Sustainable Cities and Society* 54: 101997. doi:[10.1016/j.scs.2019.101997](https://doi.org/10.1016/j.scs.2019.101997)
- Singh D., Prasanna R., Sharma V., Rajawat M. V. S., Nishanth S., Saxena A. K. (2020). Prospecting plant–microbe interactions for enhancing nutrient availability and grain biofortification. In *Wheat and Barley Grain Biofortification* (pp. 203-228). Woodhead Publishing, Sawston, Cambridge. doi: [10.1016/B978-0-12-818444-8.00008-0](https://doi.org/10.1016/B978-0-12-818444-8.00008-0)
- Smith J.L., Doran J.W. (2015). Measurement and Use of pH and Electrical Conductivity for Soil Quality Analysis. In: *SSSA Special Publications* (Doran J.W., Jones A.J., eds), Soil Science Society of America, Madison, WI, USA, pp. 169–185. doi:[10.2136/sssaspecpub49.c10](https://doi.org/10.2136/sssaspecpub49.c10)
- Somers B., Gysels V., Verstraeten W.W., Delalieux S., Coppin P. (2010). Modelling moisture-induced soil reflectance changes in cultivated sandy soils: a case study in citrus orchards. *European Journal of Soil Science* 61 (6): 1091–1105. doi:[10.1111/j.1365-2389.2010.01305.x](https://doi.org/10.1111/j.1365-2389.2010.01305.x)
- Sosulski F. W., Patterson J. K., Law A. G. (1960). The Lignin Content of Grass Strains<sup>1</sup>. *Agronomy Journal*, 52 (3): 130-134. doi:[10.2134/agronj1960.0002196200](https://doi.org/10.2134/agronj1960.0002196200)

- Soucémariadin L.N., Quideau S.A., MacKenzie M.D., Bernard G.M., Wasylishen R.E. (2013). Laboratory charring conditions affect black carbon properties: A case study from Quebec black spruce forests. *Organic Geochemistry* 62: 46–55. doi:[10.1016/j.orggeochem.2013.07.005](https://doi.org/10.1016/j.orggeochem.2013.07.005)
- Spiliopoulos I., Hristopulos D.T., Petrakis M.P., Chorti A. (2011). A multigrid method for the estimation of geometric anisotropy in environmental data from sensor networks. *Computers & Geosciences* 37 (3): 320–330. doi:[10.1016/j.cageo.2010.06.007](https://doi.org/10.1016/j.cageo.2010.06.007)
- Srivastava A., Wu J. Q., Elliot W. J., Brooks E. S., Flanagan D. C. (2018). A simulation study to estimate effects of wildfire and forest management on hydrology and sediment in a forested watershed, northwestern US. *Transactions of the ASABE*, 61 (5): 1579-1601. doi: 10.13031/trans.12326
- Stavi I. (2019). Wildfires in Grasslands and Shrublands: A Review of Impacts on Vegetation, Soil, Hydrology, and Geomorphology. *Water* 11 (5): 1042. doi:[10.3390/w11051042](https://doi.org/10.3390/w11051042)
- Stenberg B., Viscarra Rossel R.A., Mouazen A.M., Wetterlind J. (2010). Visible and Near Infrared Spectroscopy in Soil Science. In: *Advances in Agronomy*, Elsevier, pp. 163–215. doi:[10.1016/S0065-2113\(10\)07005-7](https://doi.org/10.1016/S0065-2113(10)07005-7)
- Stevens A., Nocita M., Tóth G., Montanarella L., van Wesemael B. (2013). Prediction of Soil Organic Carbon at the European Scale by Visible and Near InfraRed Reflectance Spectroscopy. *PLoS ONE* 8 (6): e66409. doi:[10.1371/journal.pone.0066409](https://doi.org/10.1371/journal.pone.0066409)
- Stevens A., van Wesemael B., Bartholomeus H., Rosillon D., Tychon B., Ben-Dor E. (2008). Laboratory, field and airborne spectroscopy for monitoring organic carbon content in agricultural soils. *Geoderma* 144 (1–2): 395–404. doi:[10.1016/j.geoderma.2007.12.009](https://doi.org/10.1016/j.geoderma.2007.12.009)
- Stoner E.R., Baumgardner M.F. (1981). Characteristic Variations in Reflectance of Surface Soils. *Soil Science Soc of Amer J* 45 (6): 1161–1165. doi:[10.2136/sssaj1981.03615995004500060031x](https://doi.org/10.2136/sssaj1981.03615995004500060031x)
- Tarpanelli A., Mondini A.C., Camici S. (2022). Effectiveness of Sentinel-1 and Sentinel-2 for flood detection assessment in Europe. *Nat Hazards Earth Syst Sci* 22 (8): 2473–2489. doi:[10.5194/nhess-22-2473-2022](https://doi.org/10.5194/nhess-22-2473-2022)
- Tavakkoli E., Rengasamy P., Smith E., McDonald G. K. (2015). The effect of cation–anion interactions on soil pH and solubility of organic carbon. *European Journal of Soil Science* 66 (6): 1054-1062. doi: [10.1111/ejss.12294](https://doi.org/10.1111/ejss.12294)
- Tian Y., Zhang J., Yao X., Cao W., Zhu Y. (2013). Laboratory assessment of three quantitative methods for estimating the organic matter content of soils in China based on visible/near-infrared reflectance spectra. *Geoderma* 202–203: 161–170. doi:[10.1016/j.geoderma.2013.03.018](https://doi.org/10.1016/j.geoderma.2013.03.018)

- Tripathi A., Tiwari R.K. (2022). Synergetic utilization of sentinel-1 SAR and sentinel-2 optical remote sensing data for surface soil moisture estimation for Rupnagar, Punjab, India. *Geocarto International* 37 (8): 2215–2236. doi:[10.1080/10106049.2020.1815865](https://doi.org/10.1080/10106049.2020.1815865)
- Turco M., Llasat M.-C., von Hardenberg J., Provenzale A. (2014). Climate change impacts on wildfires in a Mediterranean environment. *Climatic Change* 125 (3–4): 369–380. doi:[10.1007/s10584-014-1183-3](https://doi.org/10.1007/s10584-014-1183-3)
- Úbeda X., Pereira P., Outeiro L., Martin D.A. (2009). Effects of fire temperature on the physical and chemical characteristics of the ash from two plots of cork oak (*Quercus suber*). *Land Degrad Dev* 20 (6): 589–608. doi:[10.1002/ldr.930](https://doi.org/10.1002/ldr.930)
- Ulery A. L., Graham R. C., Amrhein C. (1993). Wood-Ash Composition And Soil Ph Following Intense Burning. *Soil Science*, 156 (5): 358–364. doi: 10.1097/00010694-199311000-00008
- Van Auken O.W., Smeins F. (2008). Western North American Juniperus Communities: Patterns and Causes of Distribution and Abundance. In: *Western North American Juniperus Communities* (Van Auken O.W., ed). *Ecological Studies*, vol 196. Springer, New York, NY. [https://doi.org/10.1007/978-0-387-34003-6\\_1](https://doi.org/10.1007/978-0-387-34003-6_1)
- Varghese D., Radulović M., Stojković S., Crnojević V. (2021). Reviewing the Potential of Sentinel-2 in Assessing the Drought. *Remote Sensing* 13 (17): 3355. doi:[10.3390/rs13173355](https://doi.org/10.3390/rs13173355)
- Vaudour E., Gomez C., Fouad Y., Lagacherie P. (2019). Sentinel-2 image capacities to predict common topsoil properties of temperate and Mediterranean agroecosystems. *Remote Sensing of Environment* 223: 21–33. doi:[10.1016/j.rse.2019.01.006](https://doi.org/10.1016/j.rse.2019.01.006)
- Verma S., Jayakumar S. (2012). Impact of forest fire on physical, chemical and biological properties of soil: A review. *Proceedings of the International Academy of Ecology and Environmental Sciences*, 2 (3): 168.
- Verma S., Jayakumar S. (2015). Post-fire regeneration dynamics of tree species in a tropical dry deciduous forest, Western Ghats, India. *Forest Ecology and Management* 341: 75–82. doi:[10.1016/j.foreco.2015.01.005](https://doi.org/10.1016/j.foreco.2015.01.005)
- Viscarra Rossel R.A., Behrens T. (2010). Using data mining to model and interpret soil diffuse reflectance spectra. *Geoderma* 158 (1–2): 46–54. doi:[10.1016/j.geoderma.2009.12.025](https://doi.org/10.1016/j.geoderma.2009.12.025)
- Viscarra Rossel R.A., Walvoort D.J.J., McBratney A.B., Janik L.J., Skjemstad J.O. (2006). Visible, near infrared, mid infrared or combined diffuse reflectance spectroscopy for simultaneous assessment of various soil properties. *Geoderma* 131 (1–2): 59–75. doi:[10.1016/j.geoderma.2005.03.007](https://doi.org/10.1016/j.geoderma.2005.03.007)
- Vukomanović J., Steelman T. (2019). A Systematic Review of Relationships Between Mountain Wildfire and Ecosystem Services. *Landscape Ecol* 34 (5): 1179–1194. doi:[10.1007/s10980-019-00832-9](https://doi.org/10.1007/s10980-019-00832-9)

- Wang G., Li J., Ravi S., Theiling B.P., Sankey J.B. (2019). Fire changes the spatial distribution and sources of soil organic carbon in a grassland-shrubland transition zone. *Plant Soil* 435 (1–2): 309–321. doi:[10.1007/s11104-018-3895-z](https://doi.org/10.1007/s11104-018-3895-z)
- Webster R. and Oliver M. A. (2007). Local Estimation or Prediction: Kriging. In: *Geostatistics for environmental scientists*. West Sussex, England, John Wiley & Sons. pp.153-194. Available at: <https://planninginsights.co.in/data/ebook/1622466729.pdf> [accessed 23rd November 2022]
- Widomski M. K., Iwanek M., Stepniewski W. (2013). Implementing anisotropy ratio to modeling of water flow in layered soil. *Soil Science Society of America Journal*, 77 (1): 8-18. doi:[10.2136/sssaj2012.0142](https://doi.org/10.2136/sssaj2012.0142)
- Wong V. N., Dalal R. C., Greene R. S. (2009). Carbon dynamics of sodic and saline soils following gypsum and organic material additions: a laboratory incubation. *Applied Soil Ecology* 41 (1): 29-40. doi: [10.1016/j.apsoil.2008.08.006](https://doi.org/10.1016/j.apsoil.2008.08.006)
- Worsham L., Markewitz D., Nibbelink N. (2010). Incorporating Spatial Dependence into Estimates of Soil Carbon Contents under Different Land Covers. *Soil Sci Soc Am J* 74 (2): 635–646. doi:[10.2136/sssaj2008.0412](https://doi.org/10.2136/sssaj2008.0412)
- Wuest S. (2014). Seasonal Variation in Soil Organic Carbon. *Soil Science Society of America Journal* 78 (4): 1442–1447. doi:[10.2136/sssaj2013.10.0447](https://doi.org/10.2136/sssaj2013.10.0447)
- Xue L., Li Q., Chen H. (2014). Effects of a Wildfire on Selected Physical, Chemical and Biochemical Soil Properties in a *Pinus massoniana* Forest in South China. *Forests* 5 (12): 2947–2966. doi:[10.3390/f5122947](https://doi.org/10.3390/f5122947)
- Yang Y., Hu X., Cao X., Jin T., Wang Y. (2021). Medium-Term Effects of Different Wildfire Severities on Soil Properties: a Case Study of Hengduan Mountains, southwestern China. In *IOP Conference Series: Earth and Environmental Science* (Vol. 861, No. 6, p. 062021). IOP Publishing.
- Yeo I.K., Johnson R.A. (2000). A new family of power transformations to improve normality or symmetry. *Biometrika* 87 (4): 954–959. doi:[10.1093/biomet/87.4.954](https://doi.org/10.1093/biomet/87.4.954)
- Yousaf B., Liu G., Wang R., Abbas Q., Imtiaz M., Liu R. (2017). Investigating the biochar effects on C-mineralization and sequestration of carbon in soil compared with conventional amendments using the stable isotope ( $\delta^{13}\text{C}$ ) approach. *GCB Bioenergy* 9 (6): 1085–1099. doi:[10.1111/gcbb.12401](https://doi.org/10.1111/gcbb.12401)
- Yue C., Ciais P., Zhu D., Wang T., Peng S.S., Piao S.L. (2016). How have past fire disturbances contributed to the current carbon balance of boreal ecosystems? *Biogeosciences* 13 (3): 675–690. doi:[10.5194/bg-13-675-2016](https://doi.org/10.5194/bg-13-675-2016)
- Zare S., Abtahi A., Fallah Shamsi S.R., Lagacherie P. (2021). Combining laboratory measurements and proximal soil sensing data in digital soil mapping approaches. *CATENA* 207: 105702. doi:[10.1016/j.catena.2021.105702](https://doi.org/10.1016/j.catena.2021.105702)

- Zavala L.M., De Celis R., Jordán A. (2014). How wildfires affect soil properties. A brief review. *CIG* 40 (2): 311–332. doi:[10.18172/cig.2522](https://doi.org/10.18172/cig.2522)
- Zhang S., Huang Y., Shen C., Ye H., Du Y. (2012). Spatial prediction of soil organic matter using terrain indices and categorical variables as auxiliary information. *Geoderma* 171–172: 35–43. doi:[10.1016/j.geoderma.2011.07.012](https://doi.org/10.1016/j.geoderma.2011.07.012)
- Zhang X.-Y., Sui Y.-Y., Zhang X.-D., Meng K., Herbert S.J. (2007). Spatial Variability of Nutrient Properties in Black Soil of Northeast China. *Pedosphere* 17 (1): 19–29. doi:[10.1016/S1002-0160\(07\)60003-4](https://doi.org/10.1016/S1002-0160(07)60003-4)
- Zhang Y., Duan M., Li S., Zhang X., Song X., Cui D. (2022). Rational Sampling Numbers of Soil pH for Spatial Variation: A Case Study from Yellow River Delta in China. *Applied Sciences* 12 (13): 6376. doi:[10.3390/app12136376](https://doi.org/10.3390/app12136376)
- Zheng G., Ryu D., Jiao C., Hong C. (2016). Estimation of Organic Matter Content in Coastal Soil Using Reflectance Spectroscopy. *Pedosphere* 26 (1): 130–136. doi:[10.1016/S1002-0160\(15\)60029-7](https://doi.org/10.1016/S1002-0160(15)60029-7)
- Zovko M., Romić D., Colombo C., Di Iorio E., Romić M., Buttafuoco G., Castrignanò, A. (2018). A geostatistical Vis-NIR spectroscopy index to assess the incipient soil salinization in the Neretva River valley, Croatia. *Geoderma* 332: 60-72. doi:[10.1016/j.geoderma.2018.07.005](https://doi.org/10.1016/j.geoderma.2018.07.005)



# CURRICULUM VITAE

Iva Hrelja was born on September 5, 1991 in Zagreb. In 2016, she completed her graduate studies in Agroecology at the Faculty of Agriculture, University of Zagreb. From 2017 to 2019, she was employed as an expert associate at the Department of General Agronomy, and from 2019 to 2023 as an assistant on the project "Erosion and soil degradation in Croatia" funded by the Croatian Science Foundation. She has authored five scientific papers of a1 category, three of a2 category, and two of a3 category. She is also the author of 12 abstracts presented at international conferences. Her scientific interests are remote sensing, precision agriculture and soil chemistry. She has improved her skills at numerous courses and workshops in the field of remote sensing and geostatistics and is a member of the Croatian Soil Science Society and European Geosciences Union.

## Scientific papers in journals:

- Bogunović, I., **Hrelja, I.**, Kisić, I., Dugan, I., Krevh, V., Defterdarović, J., Filipović, V., Filipović, L., Pereira, P.. Straw Mulch Effect on Soil and Water Loss in Different Growth Phases of Maize Sown on Stagnosols in Croatia. *Land*, 12 (2023), 4; 1-14. doi: 10.3390/land12040765
- **Hrelja, I.**, Šestak, I., Delač, D., Pereira, P., Bogunović, I. Soil Chemical Properties and Trace Elements after Wildfire in Mediterranean Croatia: Effect of Severity, Vegetation Type and Time-Since-Fire. *Agronomy*, 12 (2022), 7; 1515, 16 doi:10.3390/agronomy12071515
- **Hrelja, I.**, Stipaničev, D., Repec, S., Perčin, A., Mesić, M., Šestak, I., Zgorelec, Ž. Comprehensive analysis of nitrates, sulphates and agrochemicals in leachates from an intensive agriculture area - A case study in Croatia. *Journal of Central European agriculture*, 23 (2022), 1; 138-153 doi:10.5513/JCEA01/23.1.3361
- Šestak, I., Bilandžija, N., Perčin, A., Fadljević, I., **Hrelja, I.**, Zgorelec, Ž. Assessment of the Impact of Soil Contamination with Cadmium and Mercury on Leaf Nitrogen Content and Miscanthus Yield Applying Proximal Spectroscopy. *Agronomy*, 12 (2022), 2; 255, 14 doi:10.3390/agronomy12020255
- Šestak, I., Pereira, P., Telak, L.J., Perčin, A., **Hrelja, I.**, Bogunović, I. Soil Chemical Properties and Fire Severity Assessment Using VNIR Proximal Spectroscopy in Fire-Affected Abandoned Orchard of Mediterranean Croatia. *Agronomy*, 12 (2022), 1; 1-20 doi:10.3390/agronomy12010129
- Šestak, I., Vitezica, L., **Hrelja, I.** (2022). Analysis of Climate Change in Croatia Based on Calculation of Temperature Thresholds. *ACS - Agriculturae Conspectus Scientificus*, 87 (2022),4; 295-302. (<https://www.bib.irb.hr/1238539>)
- **Hrelja, I.**, Šestak, I., Bogunović, I. Wildfire Impacts on Soil Physical and Chemical Properties - A Short Review of Recent Studies. *ACS - Agriculturae conspectus scientificus*, 85 (2020), 4; 293-301. (<https://www.bib.irb.hr/1090790>)
- **Hrelja, I.**, Zgorelec, Ž., Kisić, I. Environmental Pollution and Ecosystem Surveys in Rijeka-Bakar, Croatia - A Review. *ACS - Agriculturae conspectus scientificus*, 85 (2020), 1; 9-17. (<https://www.bib.irb.hr/1054685>)

#### Scientific papers in conference proceedings:

- **Hrelja, I.**, Šestak, I., Perčin, A., Bogunović, I. Mapping of soil chemical properties immediately after fire in Mediterranean Croatia. 56th Croatian and 16th International Symposium on Agriculture: proceedings. Vodice, Croatia, 2021. pp. 85-89. (<https://www.bib.irb.hr/1142601>)
- Jantol, A., Gavrilović, A., Mašek, T., Fabek Uher, S., Petek, M., Perčin, A., **Hrelja, I.**, Zgorelec, Ž. Mogućnost primjene izmeta šturka (*Gryllus assimilis* Fab.) kao poboljšivača tla. 57th Croatian and 17th International Symposium on Agriculture: proceedings. Majić, I., Antunović, Z. (eds). Vodice, Croatia, 2022. pp. 76-80. (<https://www.bib.irb.hr/1202298>)

#### Abstracts in conference proceedings:

- Zgorelec, Ž., Vitezica, L., Galić, M., **Hrelja, I.**, Perčin, A., Kisić, I., Jakovljević, I., Pehnek, G. The quality of urban soils and their potential for use in Maksimirska Street in the city of Zagreb. 11th Symposium with International Participation Book of Abstracts. Beograd: University of Belgrade Faculty of Agriculture, 2023. pp. 74-75.
- Bogunović, I., **Hrelja, I.**, Kisić, I., Dugan, I., Krevh, V., Defterdarović, J., Filipović, V., Filipović, L., Pereira, P.. Straw Mulch Effect on Soil and Water Loss in Different Growth Phases of Maize Sown on Stagnosols in Croatia. EGU General Assembly 2023, Vienna, Austria, 2023. doi: 10.5194/egusphere-egu23-5996
- Bogunović, I., Dugan, I., Telak, L.J., **Hrelja, I.**, Perčin, A., Šestak, I., Pereira, P. Soil erosion and degradation in Croatia - SEDCRO. Book of abstracts – 14th Congress of the Croatian Society of Soil Science “Soil degradation - challenge in agricultural production”. Popović, B., Zebec, V., Perčin, A. (eds). Osijek: Croatian Society of Soil Science, 2022. pp. 18-19. (<https://www.bib.irb.hr/1225051>)
- Bogunović, I., Telak, L.J., **Hrelja, I.**, Kisić, I., Dugan, I., Krevh, V., Pereira, P. Straw mulch effect on soil and water losses in different growth phases of Maize sown on Pseudogley in Croatia. 57th Croatian and 17th International Symposium on Agriculture: proceedings. Majić, I., Antunović, Z. (eds). Vodice, Croatia, 2022. pp. 4-4. (<https://www.bib.irb.hr/1202013>)
- **Hrelja, I.**, Šestak, I., Bogunović, I. Satellite sensors in monitoring the impact of wildfire on soil quality. Book of abstracts – Biotechnical PhD days 2022. Kos, B., Ivanković, A., Beljo Lučić, R., Novak, J., Rumbak, I., Balbino, S. (eds). University of Zagreb Faculty of Food Technology and Biotechnology, 2022. pp. 74-75. (<https://www.bib.irb.hr/1218785>)
- **Hrelja, I.**, Šestak, I., Pereira, P., Bogunović, I. Changes in soil texture after wildfire: effect of severity, vegetation type and time-since-fire in Mediterranean environment. Book of abstracts – 14th Congress of the Croatian Society of Soil Science “Soil degradation - challenge in agricultural production”. Popović, B., Zebec, V., Perčin, A. (eds). Osijek: Croatian Society of Soil Science, 2022. pp. 37-38. (<https://www.bib.irb.hr/1215660>)
- Zgorelec, Ž., Abramović, R., Kisić, I., Galić, M., **Hrelja, I.**, Šprem, N. Content and spatial variability of metals in the soil of the Luža shooting range. Book of abstracts – 14th Congress of the Croatian Society Of Soil Science “Soil degradation - challenge in agricultural production”. Popović, B., Zebec, V., Perčin, A. (eds). Osijek: Croatian Society Of Soil Science, 2022. pp. 93-94
- Dugan, I., Telak, L.J., **Hrelja, I.**, Kisić, I., Bogunović, I. Straw mulch impact on soil properties and initial soil erosion processes in the maize field. EGU General Assembly 2021, Online, Vienna, Austria, 2021. EGU21-2538, 1 doi:10.5194/egusphere-egu21-2538



- **Hrelja, I.**, Šestak, I., Bogunović, I. Estimation of soil organic matter using proximal and satellite sensors after a wildfire in Mediterranean Croatia. EGU General Assembly 2021, Online, Vienna, Austria, 2021. 3896, 1 doi:<https://doi.org/10.5194/egusphere-egu21-3896>
- **Hrelja, I.**, Šestak, I., Pereira, P., Perčin, A., Telak, L.J., Bogunović, I. Diffuse reflectance spectroscopy and model analysis for assessing fire affected soil chemical properties in Croatia. CASEE Conference 2021 Book of Abstracts. Prague, Czech Republic, 2021. pp. 11-12. (<https://www.bib.irb.hr/1130987>)
- Zgorelec, Ž., Rinkovec, J., Pehcec, G., Mesić, M., Kisić, I., Bogunović, I., Perčin, A., Šestak, I., Bilandžija, D., Galić, M., **Hrelja, I.** Concentrations of Pt, Pd and Rh in the air, soil and vegetation of the city of Zagreb. Air protection 2021. Pehcec, G. (ed). Zagreb: Croatian Air Protection Association, 2021.
- **Hrelja, I.**, Šestak, I., Perčin, A., Pereira, P., Bogunović, I. VNIR spectroscopy for assessment of post-fire impacts on soil properties using linear and non-linear calibration methods. EGU General Assembly 2020, Online, Vienna, Austria, 2020. doi:10.5194/egusphere-egu2020-974

## 8. APPENDIX

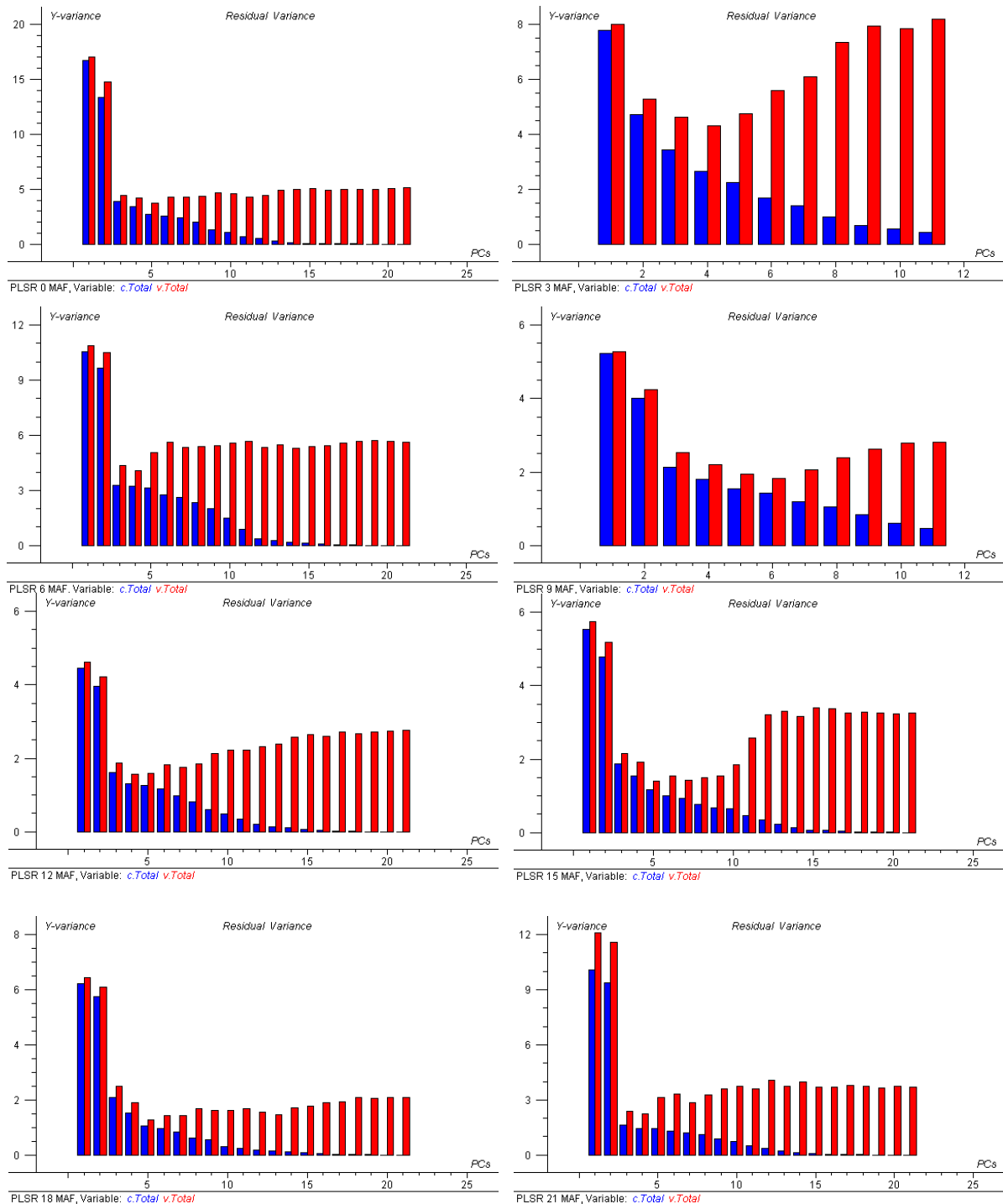


Figure 8.1. Residual variance of PLSR models acquired at each individual sampling period as well as the entire reflectance dataset

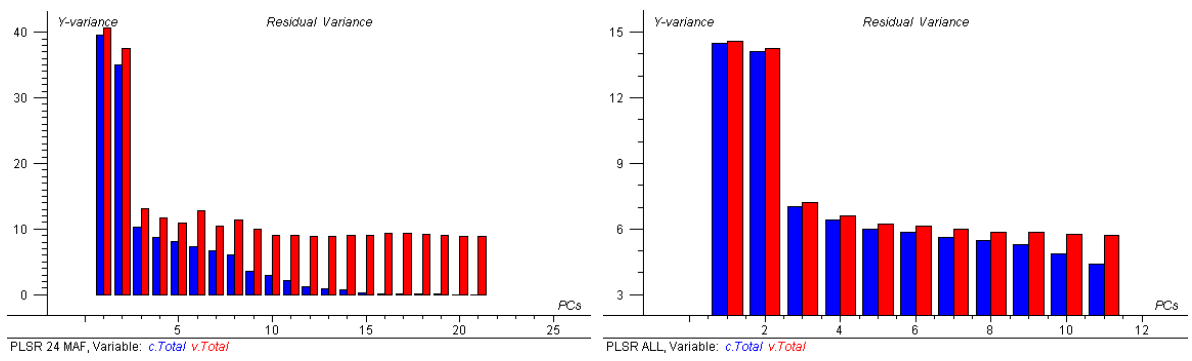


Figure 8.1. (continuation) Residual variance of PLSR models acquired at each individual sampling period as well as the entire reflectance dataset